Poznan University of Technology

Faculty of Chemical Technology

Institute of Chemistry and Technical Electrochemistry

Field of study: Chemical Technology

Paweł Jeżowski

LITHIUM-ION CAPACITORS BASED ON IN-SITU PRE-LITHIATION OF THE GRAPHITE ELECTRODE FROM A COMPOSITE POSITIVE ELECTRODE

Kondensator litowo-jonowy oparty na pre-litowaniu elektrody grafitowej z dodatniej elektrody kompozytowej

DOCTORAL DISSERTATION

Promoter:

prof. dr. hab. François Béguin

Poznań 2016

This thesis' research was supported by the ECOLCAP project funded in the frame of the Welcome program implemented by the Foundation for Polish Science (FNP) within the measure 1.2. "Strengthening the human resources potential of science", of the Innovative Economy operational program supported by European Union

Project leader: Professor **François Béguin**

Badania do niniejszej pracy prowadzone były przy wsparciu przez project ECOLCAP realizowany w ramach programu Welcome, finansowanego prze Fundację na rzecz Nauki Polskiej (FNP) zgodnie z działaniem 1.2. „Wzmocnienie potnecjału kadrowego nauki", programu operacyjnego Innowacyjna Gospodaraka wspieranego przez Unię Europejską

Kierwonik projektu: Profesor **François Béguin**

The French embassy in Poland and the French "Ministère des affaires étrangères et du développement international" as well as the Polish Ministry of Science and Higher Education in Poland are also greatly acknowledged for supporting this work within the framework of the PHC Polonium project 31438NH.

Coordinator from the Polish side: prof. dr hab. **Elżbieta Frąckowiak**

Coordinator from the French side: prof. **Thierry Brousse**

Szczegolne podziękowania dla Ambasady francuskiej w Polsce oraz francuskiego ministerstwa "Ministère des affaires étrangères et du développement international" jak i polskiego Ministerstwa Nauki i Szkolnictwa Wyższego za wsparcie tej pracy w ramach PHC Polonim projekt 31438NH.

Koordynator od strony polskiej: prof. dr hab. **Elżbieta Frąckowiak**

Koordynator od strony francuskiej: prof. **Thierry Brousse**

A part of the research work was supported by the LIDER project financed from National Center for Research and Development (NCBiR) LIDER/ 018/ 513/ L-4/ 12/ NCBR/ 201 “Electrochemical capacitor with high energy density and power operating in coupled redox pair solutions”

Project leader: dr inż. **Krzysztof Fic**

Część pracy badawczej zostało wsparte przez projekt LIDER finansowany przez Narodowe Centrum Badań i Rozwoju LIDER/ 018/ 513/ L-4/ 12/ NCBR/ 201 „Kondensator elektrochemiczny o wysokiej gęstości energii i mocy operujący w roztworach sprzężonych par redoks”

Kierwonik projektu: dr inż. **Krzysztof Fic**

I am grateful to my scientific supervisor and promoter of this thesis
prof. dr hab **François Béguin**
for all his time and efforts put into this work
and his endless ocean of patience during corrections
as I am "not a poet"

Sincere thanks to
Prof. **Thierry Brousse** and dr **Olivier Crosnier**
for having the opportunity to visit their research group in Nantes

I would also like to thank
prof. dr hab **Elżbieta Frąckowiak**
for the scientific consultations which broaden my knowledge

Many thanks to
dr eng **Krzysztof Fic**
for all his patience towards my "one question"
and his advices in the field of science

I would like to acknowledge:
prof. dr hab eng **Stanisław Błażewicz**
for high temperature treatment of multiwalled carbon nanotubes
dr eng **Mirosława Pawlyta**
for the high quality TEM images
Companies **Blue Solutions**, **Imerys**, **Kuraray**, **Superior Graphite**
for kindly supplying the materials used during this thesis

I would like also to mention all the persons who helped me during the preparation of this thesis: Agnieszka Brzózka, Camille Douard, Dominika Gastoł, Nicolas Goubard, Barbara Górska and Paula Ratajczak, as well as all the present and former members of the Power Sources group in Poznan University of Technology.

Last but not least, I would like to say thank you to my Mother, family and friends for supporting me during the time of this thesis preparation.

TABLE OF CONTENTS

INTRODUCTION 10

CHAPTER I

Literature review 16

I.1. Electrical double-layer capacitors (EDLCs) 16

I. 1.1. The electrical double-layer 16

I. 1.2. Energy storage in EDLCs 19

I. 1.3. Carbon electrode materials for EDLCs 22

I. 1.4. Electrolytes used in electrochemical capacitors 27

Conclusion 31

I. 2. Lithium-ion batteries (LIBs) 32

I. 2.1. Principle of LIB operation 32

I. 2.2. Cathode materials 34

I. 2.3. Anode material 39

I. 2.4. Electrolytes for LIBs 46

I. 2.5. Chemistry of S.E.I. formation on the lithium surface 47

I. 2.6. Chemistry of S.E.I. formation on the carbon surface 48

Conclusion 52

I. 3. Lithium-ion capacitors (LICs) 53

I. 3.1. Principle of energy storage in LICs 53

I. 3.2. Lithium sources for pre-lithiation of carbon anodes 56

Conclusion 61

CHAPTER II

Establishing the pre-lithiation conditions _____63

Introduction_____64

II. 1. Synthesis and structural characterization of $Li_{0.65}Ni_{1.35}O_2$_____65

II. 2. Electrochemical extraction of lithium ions from sacrificial metal oxide $Li_{0.65}Ni_{1.35}O_2$_____67

II. 3. Pre-lithiation of graphite with $Li_{0.65}Ni_{1.35}O_2$ in a full cell configuration_____68

II. 4. Modification of the procedure for graphite pre-lithiation with AC/$Li_{0.65}Ni_{1.35}O_2$ as lithium source _____70

II. 5. Adjustment of the operating voltage of the LIC with AC/LNiO positive electrode _____ 75

II. 6. Improvement of the positive electrode conductivity by introducing MWCNTs to the AC/$Li_{0.65}Ni_{1.35}O_2$ composite_____78

Conclusion_____81

CHAPTER III

Lithium rich transition metal oxides for improving the electrochemical performance_____83

Introduction_____84

III. 1. Synthesis and structural characterization of lithium metal oxides with high amount of lithium _____84

III. 2. Electrochemical performance of lithium zinc oxide_____ 87

III. 3. Ball milling of LZnO, LAlO and LZrO with various conductive agents to increase the amount of lithium extracted _____ 88

III. 4. LIC system with lithium zinc oxide as sacrificial lithium source_____ 95

Conclusion_____98

CHAPTER IV

Lithium rhenium oxide as a promising material for graphite pre-lithiation _____ 99

Introduction_____100

IV. 1. Synthesis and characterization of lithium rhenium oxide and of a composite Li_5ReO_6/AC electrode 100

IV. 2. Electrochemical irreversibility of lithium rhenium oxide Li_5ReO_6 102

IV. 3. *In-situ* XRD study of lithium extraction from lithium rhenium oxide Li_5ReO_6 103

IV. 4. Realization of a LIC cell with composite Li_5ReO_6/AC electrode 106

IV. 5. Cycle life of the LIC systems based on the positive Li_5ReO_6/AC composite electrode 111

Conclusion 114

CHAPTER V

Lithiated organic material as a "green" source of lithium 116

Introduction 117

V. 1. Synthesis and characterization of 3,4–dihydroxybenzonitrile dilithium salt (Li_2DHBCN) 117

V. 2. Preparation of composites electrodes including Li_2DHBCN 121

V. 3. Electrochemical lithium extraction from Li_2DHBCN 123

V. 4. Realization and performance of LIC cell where graphite is pre-lithiated with AC/Li_2DHBCN composite positive electrode 124

V. 5. Realization of a LIC pouch-cell prototype with Li_2DHBCN /AC composite positive electrode 131

Conclusion 136

GENERAL CONCLUSION 138

EXPERIMENTAL ANNEX 141

A. 1. Electrochemical techniques 142

A. 2. Characterization of the activated carbons used for positive electrode of LIC 146

A. 3. Characterization of graphite used for negative electrode of LIC 148

A. 4. Electrodes preparation _____150

A. 5. Electrochemical cell _____ 151

A. 6. Characterization of lithiated metal oxides _____153

A. 7. Techniques used for the characterization of lithiated organic compounds _____ 155

A. 8. Chemicals and materials presented in the main text_____155

REFERENCES _____ 157

SCIENTIFIC ACHIEVEMENTS _____ 171

ABSTRACT _____ 178

STRESZCZENIE _____ 182

INTRODUCTION

Since the discovery of the steam engine, the global world energy demand grows exponentially, while the use of fuels (coal, oil or gas) follows the same trend, and that of renewables (biomass, hydro, …) increases very slowly (Figure 1). According to one of the newest reports, the world use of oil and coal should reach a peak in 2025 [1]. Since these sources are limited, humankind needs to wisely consider how they should be distributed and more appropriately applied for other usages, as for example chemistry. It means that the next decades are crucial for educating the next generations to be more aware about environment protection and energy generation as well as its storage.

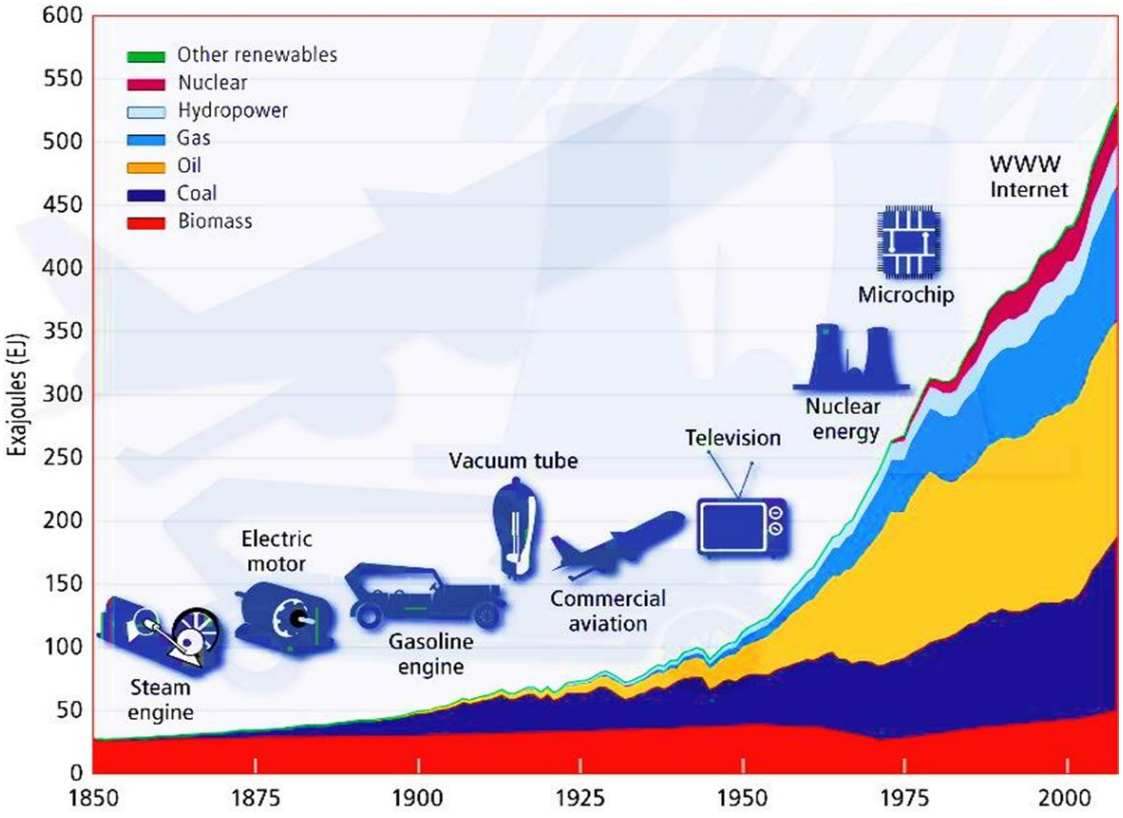

Figure 1 Evolution of usage of various energy sources since 1850 [2].

One of the most important tasks for European Union countries is to diverge from fossil fuels towards renewable energy sources such as sun, wind, water etc. Those sources can be considered as infinite and should be used to their highest extent in order to reduce the energy dependency on fossil fuels. Despite the fact that the energy coming from sun or wind can be harvested and transformed into electricity, it is not constant and depends on

day/night cycles as well as various factors such as climate, geolocalization and topography. Therefore, it would be necessary to store at least part of this energy when it is harvested and use it when needed. For that, electrical energy storage devices adapted to the amount of energy to be stored and power harvested should be developed and fabricated.

Since the discovery of electricity, scientists all around the world tried to build systems which could generate and/or accumulate electrical energy. The first historical mention about such device is dated back to the work of Alessandro Volta in 1800, who created the first electrochemical cell by connecting copper (positive electrode) and zinc plates (negative electrode) separated by cloth (separator) impregnated with sulphuric acid (electrolyte). This kind of cell delivers energy irreversibly (it cannot be recharged) and is called a primary battery. Secondary batteries, such as lead-acid and nickel-cadmium accumulators, which operate reversibly (they can be recharged) were discovered later. The lead-acid batteries were the first to be applied for electrical cars, and they are still very widely used for heavy duty systems (forklifts etc.). Since then, the technological leap of accumulator development was enormous, especially with portable electronics booming, yet the construction principles of all electrochemical cells remain the same.

Currently, on the market, there are two main electrochemical energy storage devices differing essentially by their storage mechanisms and nature of electrode materials: the well-spread lithium-ion battery (LIB) technology which dominates the market and electrochemical capacitors (ECs) or supercapacitors often referred to as electrical double-layer capacitors (EDLCs). In both cases, the cells are constituted of positive and negative electrodes electrically separated by a porous membrane (separator), and these elements are immersed in an electrolyte permitting the ion current flow. In case of supercapacitors, the energy is stored electrostatically in an electrical double-layer (EDL) which is formed at the electrode/electrolyte interface. Owing to this physical type of storage, the time constant of electrical double-layer capacitors (EDLCs) is of the order of few seconds and the systems can be charged/discharge many times (up to million cycles) without deterioration of the electrodes. In order to enhance the amount of charges stored and the power of EDLCs, electrode materials with highly developed specific surface area and high electrical conductivity are desirable. Therefore, nanoporous carbons, essentially low cost activated

carbons (ACs), are the most used electrode materials in EDLCs. Contrary to traditional capacitors, the maximum voltage of EDLCs must be limited to relatively small values in order to avoid the electrochemical decomposition of the electrolyte. Since the specific energy and power of EDLCs are proportional to the square of voltage, the trick is obviously to implement electrolytes with the highest electrochemical window. This is the reason why organic electrolytes, e.g., tetraethylammonium tetrafluoroborate (Et_4NBF_4) in acetonitrile, are the most currently implemented in symmetric carbon/carbon EDLCs, enabling 2.7 – 2.8 V to be reached. The power density of these capacitors is very high (up to 10 – 20 kW/kg) in comparison to LIBs (1 – 2 kW/kg). However, the energy density of EDLCs is low (only 10 Wh/kg), whereas for lithium ion batteries it can reach 250 Wh/kg.

In the search of high energy electrochemical capacitors, hybrid systems have been suggested during the last decade. The most novel and performing one is the lithium-ion capacitor (LIC), which combines a positive EDL electrode made of activated carbon and a redox negative one made of graphite. Owing to the low intercalation potential of lithium into graphite (ca. 100 mV vs. Li/Li^+), the LIC operational voltage can reach 4 V, enabling energy density values up to 40 Wh/kg to be reached while still keeping power in the range of 5-10 kW/kg. Notwithstanding, a key disadvantage in the generally used LIC construction is related to the fact that a third auxiliary electrode made of metallic lithium is generally introduced in the cell to realize graphite pre-lithiation before being able to operate the AC/lithiated graphite cell. This additional electrode complicates the cell construction, and lithium remaining in the cell after the pre-lithiation step can cause safety issues, e.g., thermal runaway, during operation of the systems.

In recent years, alternative strategies have been attempted to simplify the LIC cell construction and to circumvent these problems. Highly concentrated electrolyte in slight excess was used as source of lithium ions for the graphite negative electrode. However, during ions consumption, the electrolyte conductivity decreases, which is relatively unsuitable for high power systems. Another strategy was to use lithium metal oxide (Li_yMeO_x) acting as irreversible reservoir of lithium ions in the positive activated carbon electrode. Lithium is extracted from this oxide during the pre-lithiation step, and then the residual oxide remains electrochemically inactive during cycling of the LIC cell. However, most of the lithium metal oxides suggested until now required to applying potentials higher

than 4.5 V vs. Li/Li^+ to fully extract (extractable) lithium ions, which may cause parasitic oxidation reactions on activated carbon.

The objective of the present doctoral thesis was to improve the concept of LIC with sacrificial lithiated load in the positive AC electrode, by designing materials with high lithium content and low lithium extraction potential (targeted value <4.0 V vs. Li/Li^+), and defining conditions enabling to reduce their amount. The manuscript is divided in five chapters:

Since the LIC is a hybrid system involving an EDL positive electrode and a negative battery one, chapter I is first dedicated to a literature review presenting EDLCs and LIBs. The charging/discharging mechanisms and performance of these systems, together with the types of electrode materials, are presented. The last part of the chapter details the state-of-the-art on the types of LIC systems investigated in the literature. A special attention is paid to the various pre-lithiation methods, particularly to a critical presentation of the data concerning the use of sacrificial lithiated material in the positive electrode.

The second chapter introduces the procedure established to optimize the pre-lithiation conditions of graphite using an AC/$Li_{0.65}Ni_{1.35}O_2$ positive electrode. Although containing a relatively small amount of lithium, the initial choice of $Li_{0.65}Ni_{1.35}O_2$ has been guided by literature data revealing a complete irreversibility of lithium extraction. The low amount of extractable lithium in this material (120 mAh/g) has been an excellent stimulus to define experimental conditions enabling to reduce the proportion of $Li_{0.65}Ni_{1.35}O_2$ in the positive electrode (indeed, the higher the remaining dead mass in the positive electrode, the lower the specific energy of the resulting LIC). Hence, the chapter details the conditions used to form the thinnest solid electrolyte interphase (S.E.I.) and the pulse method enabling then to optimize $Li_{0.65}Ni_{1.35}O_2$ utilization for graphite lithiation. Obviously, with so little available lithium amount, the LIC cell performance is not enough satisfactory, requiring to implement richer materials in the next chapters.

Based on the previously defined conditions, rich lithiated oxides of high theoretical capacity ca. 900 mAh/g, e.g., Li_5AlO_4, Li_6ZnO_4 and Li_8ZrO_6, were investigated in Chapter III. In particular, we detail the profitable effect of mixing the oxides with multiwalled

carbon nanotubes (MWCNTs) by ball-milling in order to enhance the conductivity of electrodes and thereof to reduce the lithium extraction potential and enhance the amount of lithium extracted. Although high irreversible capacity could be reached with these materials, we demonstrate that, due to bit too high lithium extraction potential, the cycle life of the LIC is not totally satisfactory, requiring the implementation of better performing lithium rich oxides.

Chapter IV introduces lithium rhenium oxide (Li_5ReO_6) as lithium rich oxide with low band gap fulfilling the main required conditions for such sacrificial material. Contrary to the case of the materials described in Chapter III, additional processing of the material by ball-milling with conducting agent is not necessary to almost totally extract all available lithium ions at potential lower than 4.3 vs. Li/Li^+. With this material, we then define electrochemical parameters allowing the LIC cells to demonstrate a fantastic cycle life at high charge/discharge current. The specific energy and power (Ragone plot) is also determined in order to validate the targeted concept of the thesis.

The objective of chapter V was to design a sacrificial material performing at least as well as Li_5ReO_6 while being renewable. In this context, we present 3,4–dihydroxybenzonitrile dilithium salt, further named Li_2DHBCN, as internal source of lithium ions introduced in addition to activated carbon in the positive electrode. We demonstrate that Li_2DHBCN performed beyond our expectations by displaying a very low lithium extraction potential c.a. 3.2 V vs. Li/Li^+. Good efficiency of this material for the dedicated purpose in LIC is then highlighted by cycle life tests and Ragone plot realization. The last part of chapter V is finally devoted to the realization of real two-electrode LIC (without any lithium reference electrode) using the pouch cell technology. We detail in particular the new parameters which had to be selected to get an optimized operation of the cells; the electrochemical performance of the LIC pouch cell with sacrificial Li_2DHBCN is presented and discussed.

Finally, the general conclusion underlines the main breakthroughs accomplished during this research and the perspectives for future developments in the field of lithium-ion capacitors and also parent systems based on the use of more abundant sodium.

CHAPTER I

Literature review

The main objective of the review part of this dissertation is to introduce the two mechanisms of energy storage occurring simultaneously in lithium-ion capacitors (LIC), i.e. electrical double-layer (EDL) charging at the positive electrode and redox reaction with staging at the negative graphite electrode. In addition, we will also consider the potential materials which could be used in the positive electrode as sacrificial source of lithium for graphite pre-lithiation, This will lead us to detail the optimal properties of materials and electrolytes which are used in EDL capacitors and lithium ion batteries (LIBs). The last part of the review will be dedicated to present the state-of-the-art on LICs.

I. 1. Electrical double-layer capacitors (EDLCs)

The first patent which describes the principle of EDLCs is dated back to 1957 based on Becker work [3]; then EDLCs were introduced on the market in 1969 by the company SOHIO [4]. However, the real interest for those devices started after the launching of a research and development program by the US Department of Energy (DOE) in 1989 [5]. The main goal was to create systems which would provide the necessary power boost in hybrid electric vehicles (HEV) during acceleration and enable to recuperate the braking energy. Nowadays, there are several supercapacitor producers, like Maxwell, Nesscap, Yunasko, Nichicon, NEC/Tokin or BlueSolutions, which offer a range of products with capacitance from few up to thousands of farads.

I. 1.1. The electrical double-layer

The first historical model of EDL was proposed by Herman von Helmholtz who suggested the formation of two layers at the border of the electrode-electrolyte interface when an electrode is polarized. In the example of a negatively polarized electrode, one layer is constituted of electrons on the surface of the electrical conductor and the second one of a monolayer of ions accumulated close to the electrode surface in the electrolytic solution [6]. This simplified EDL can be regarded as an electrical capacitor of capacitance C_{EDL} expressed by equation (1) [7]:

$$C_{EDL} = \frac{\varepsilon_0 \cdot \varepsilon_r \cdot S}{d} \quad (1)$$

where ε_0 is the vacuum permittivity ($\varepsilon_0 = 8.854 \cdot 10^{-12}$ F/m), ε_r the relative permittivity of the electrolyte, *S* the surface area of the electrode/electrolyte interface, *d* the effective thickness of the EDL determined by the radius of ions. Since the thickness of the EDL is less than 1 nm, the EDL capacitance is very high.

Later, Louis Georges Gouy and David Chapman proposed separately a model taking into account the motion of ions and stating that the capacitance depends on the ions concentration [8], as given by equation (2):

$$C_{GC} = \frac{\varepsilon \cdot \kappa}{4 \cdot \pi} cosh \frac{z}{2} \tag{2}$$

κ being the Debye-Hückel length presented in equation (3):

$$\kappa = \sqrt{\frac{8 \cdot \pi \cdot n \cdot e^2 \cdot z^2}{\varepsilon \cdot k \cdot T}} \tag{3}$$

where *k* is the Boltzmann constant ($1.38 \cdot 10^{-23}$ J/K), *n* the concentration of ions per cm^3, *T* the absolute temperature in K and *z* the charge number of ions.

More than twenty years later, Otto Stern proposed a model which merged a compact and a diffusive layer [9], whereas David C. Graham divided it into two regions: a layer of ions adsorbed on the electrode surface, named inner Helmholtz plane (IHP), and a layer formed by the diffuse ions in the vicinity of the electrode surface, named outer Helmholtz plane (OHP) [10]. In the Graham's model, the double-layer capacitance is described by equation (4):

$$\frac{1}{C_G} = \frac{1}{C_H} + \frac{1}{C_{GC}} \tag{4}$$

where C_H is the capacitance related to the Helmholtz compact double-layer, C_{GC} the capacitance related with the Gouy-Chapman diffuse layer.

The model used nowadays takes into account solvated ions and it was described by John Bockris, Karl A. Müller and Michael A. Devanathan, referred to as BMD model (Figure 2). The inner Helmholtz plane (IHP) passes through the center of specifically adsorbed ions

and adsorbed solvent molecules, the OHP through the center of solvated ions, and beyond the OHP there is a diffuse layer region [11].

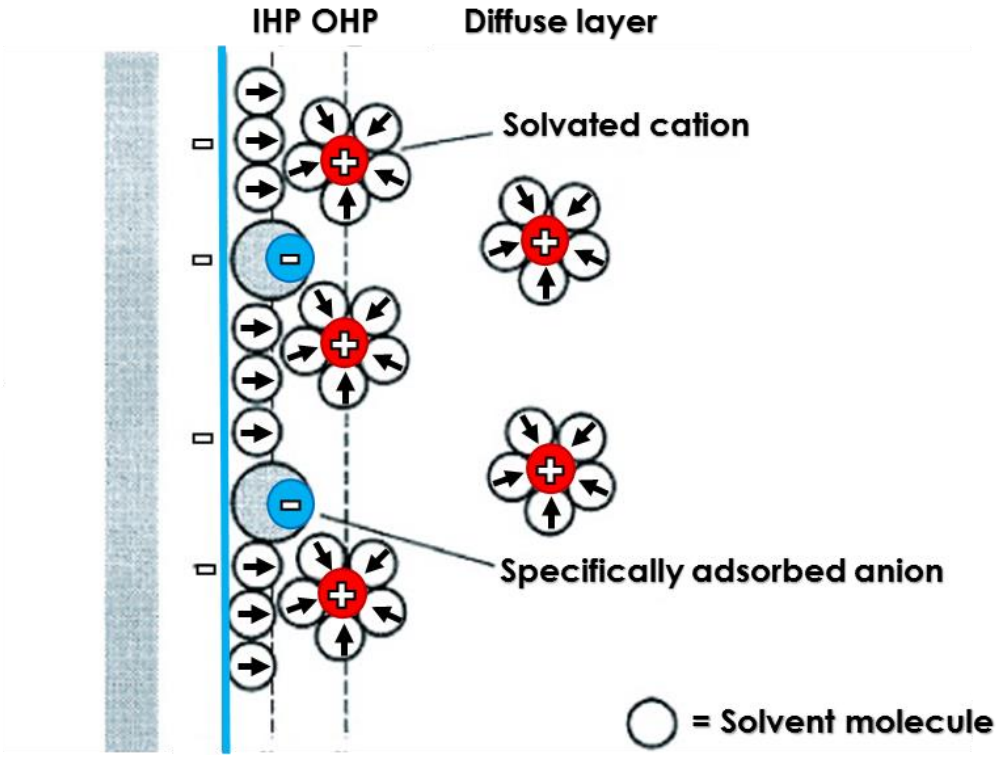

Figure 2 BMD electrical double-layer model in the example of a negatively charged electrode (adapted from [11]).

I. 1.2. Energy storage in EDLCs

Figure 3 shows a schematic representation of a symmetric EDL capacitor with two identical electrodes made of an active material coated on the surface of current collectors. Taking into account equation (1), the most often used electrode material is activated carbon, with high specific surface area, reaching values of 2000-2500 m^2/g. A porous membrane is placed between the electrodes to physically separate them and also to serve as electrolyte reservoir. When a polarization is applied to the system, ions from the bulk of the electrolyte are attracted to the electrode of opposite polarity (Figure 3).

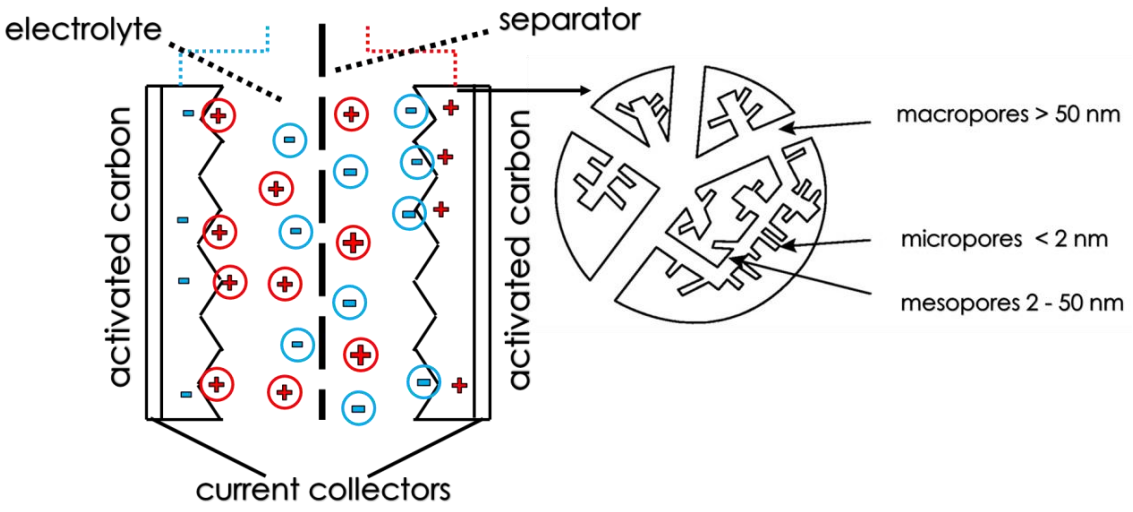

Figure 3 Scheme of a symmetric EDLC during charging. A magnification of the texture of activated carbon is presented on the right [7].

As seen in Figure 3, the whole device of capacitance C can be considered as equivalent to two capacitors connected in series (5):

$$\frac{1}{C} = \frac{1}{C_+} + \frac{1}{C_-} \tag{5}$$

where C_+, C_- are the capacitance of the positive and negative electrode. It is worth noting that, although the two carbon electrodes are identical, they generally display different capacitance values due to different size and mobility of cations and anions. According to equation (5), the capacitance of the system is essentially controlled by the electrode with the lowest value of capacitance.

When the capacitor is charged at constant current (galvanostatic mode), the potential of the electrodes diverges linearly as shown in Figure 4, while the cell voltage increases also linearly.

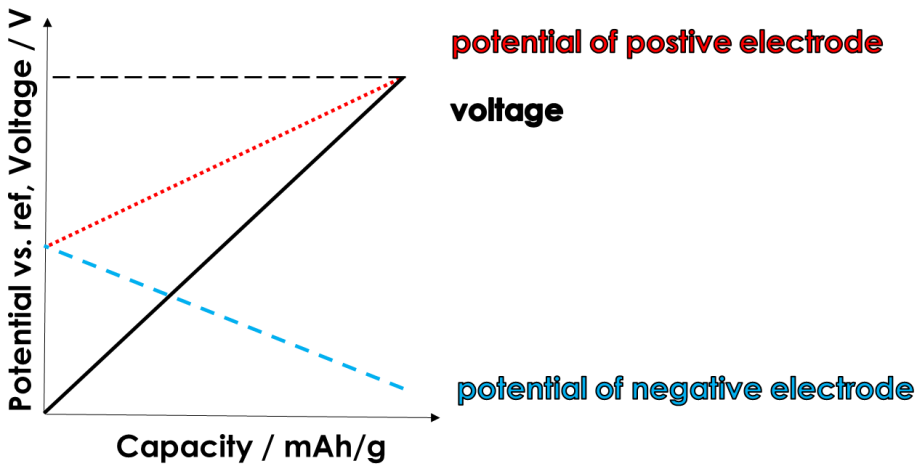

Figure 4 Electrodes potential and cell voltage changes during galvanostatic charging of an EDLC, where the red dotted curve is the potential of the positive electrode, the blue dashed curve the potential of the negative electrode and the solid black curve the voltage.

The energy of the EDLC cell is directly related to both capacitance *C* and voltage *U*, according to equation (6):

$$E = \frac{1}{2} \cdot C \cdot U^2 \tag{6}$$

Similarly, the power depends also on voltage and can be expressed by equation (7):

$$P = \frac{U^2}{4 \cdot R_s} \tag{7}$$

where R_s is the equivalent series resistance of the device which comes from [12]:

- The interfacial resistance between the electrode material and the current collector;
- The resistance of the electrode material;
- The resistance of the electrolyte;
- The ionic (diffusion) resistance related with ion mobility in the separator and accessibility to small pores.

I. 1.3. Carbon electrode materials for EDLCs

The electrodes are the crucial part of an electrochemical capacitor which determines the performance of the system. Since nanoporous carbon is the common electroactive material of EDLCs electrodes and of the positive electrode of lithium-ion capacitors (LICs), a special attention to this material will be paid in this section.

I. 1.3.1 Activated carbon

The carbonaceous electrode materials for EDLCs must be selected/designed so as to enable high specific energy and power and long cycle life. Therefore, the desirable criteria are:

- Well-developed specific surface-area (SSA);
- Good electrical conductivity;
- High stability, especially resistance to oxidation;
- Low production cost;
- Controlled porous texture;
- Easy handling and manufacturing of electrodes.

- ***Preparation of activated carbons***

The most often, activated carbons are prepared in two steps including the carbonization of a carbon rich precursor and activation of the resulting char. Carbonization is performed by heat treatment of the precursor under flow of inert gas; the properties such as texture and structure of the char depend on the type of precursor and processing conditions [13]. There is a vast number of natural organic precursors which were investigated in the literature for manufacturing activated carbons: wood, fruit stones, coffee grounds, nut shells, leaves, starch, sucrose, corn grain, pitch, lignite, peat etc. [14,15,16,17,18,19,20,21]. The chars obtained after carbonization display a poorly developed specific surface area, and most of the pores are clogged at the entrance. In order to improve the SSA and to open the closed pores, the chars must be activated either chemically or physically.

Chemical activation is performed at 400 – 700 °C in the presence of chemical reagents such as KOH [22], H_3PO_4 [23] or $ZnCl_2$ [24]). By this process, it is possible to obtain materials

with specific surface area higher than 2000 m^2/g [12,25]. Physical activation does not involve any chemical substance, but it requires higher temperature in the range from 700 °C to 1000 °C. A flow of oxidizing gas such as air, CO_2, steam or mixture of these gases enables to develop the porosity and specific surface area by opening the clogged pores during controlled burn-off according to the reactions (8 to 11) [26]:

$$C + H_2O \rightarrow CO + H_2 \quad (8)$$

$$C + CO_2 \rightarrow 2CO \quad (9)$$

$$C + O_2 \rightarrow CO_2 \quad (10)$$

$$2C + O_2 \rightarrow 2CO \quad (11)$$

Recent works about biomass materials containing group I and II elements in their structure, such as tobacco [27] or seaweeds [28], have shown that the materials can be self-activated during the carbonization.

- ***Porous texture of activated carbons***

Activated carbons are characterized by a high level of disorder and complexity of nano-scale units. Based on X-ray diffraction measurements, the first structural/nanotextural model of non-graphitizable carbon was proposed by Franklin (Figure 5a) [29]. In this 2D model, units made of stacks of few graphene layers are differently oriented and interconnected, creating the porosity [30]. Later, Stoeckli proposed a model in which the AC porosity is created by a single crumpled graphene ribbon (Figure 5b) [31]. More recently, Harris suggested curved graphene layers, including some fullerene related structures (Figure 5c) [32]. Due to this particular textural arrangement of graphene units, activated carbons display a moderate conductivity in comparison to other carbonaceous materials such as carbon nanotubes (CNTs). Therefore, during the fabrication of ECs electrodes, it is necessary to add small amounts of carbon black or CNTs as percolator [33,34].

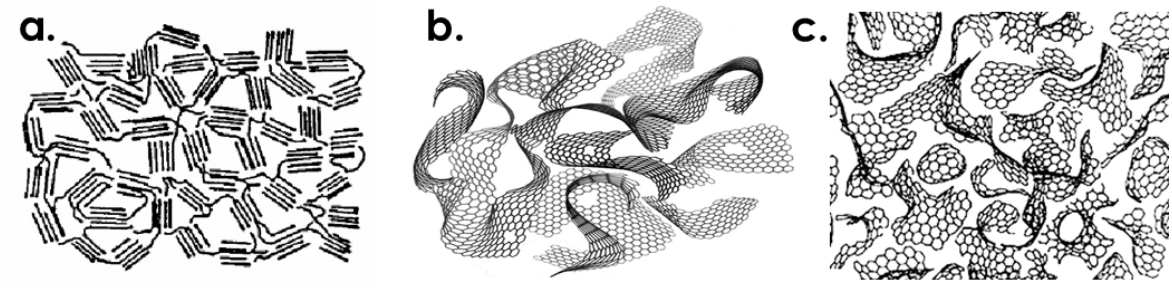

Figure 5 Models of non-graphitizable carbons according to a) Franklin [29], b) Stoeckli [31] and c) Harris [32].

The porous texture of activated carbon depends on the kind of precursor as well as the carbonization and activation parameters, and is related to the pore size/shape and tortuosity which determine charge propagation and the capacitance properties. The IUPAC has classified pores into three main categories: macropores (pore size > 50 nm), mesopores (pore size from 2 to 50 nm) and micropores (pore size < 2 nm) which can be further divided in supermicropores (pore size 0.7 – 2 nm) and ultramicropores (pore size < 0.7 nm) [35]. In general, only meso- and micropores are considered to take part in the charge storage mechanisms of ECs, whereas the contribution of macropores is rather negligible. Micropores are responsible for the high specific surface area of ACs and consequently high values of capacitance, especially at low current, whereas the mesopores enable better ions transportation throughout the material and are especially effective at high currents [36]. For this reason, it is important to design ACs with appropriate ratio of meso- and micropores in order to lower the equivalent series resistance R_S and increase the capacitance [37]. Some studies indicate that the optimal ratio between micro and mesopores volumes should be between 20 and 50% [38].

The porosity of materials is currently investigated by gas (carbon dioxide/CO_2 and nitrogen/N_2) adsorption at a fixed temperature and measuring the amount of gas adsorbed versus relative pressure. CO_2 adsorption is generally performed at 273 K, whereas nitrogen adsorption is realized at the boiling temperature of liquid nitrogen which is 77 K. The obtained data are presented in the form of adsorption/desorption isotherms [39,40]. Generally, the estimation of specific surface area is based on the Brunauer-Emmett-Teller theory (BET), yet for materials with highly developed specific surface area this approach

may lead to overestimation or underestimation of S_{BET} depending on the value of pore size [41]. Currently, the density functional theory (DFT) starts to gain more attention as it takes into account the capillary effects and adsorption in pores of different size and geometry on the material surface [42].

- ***Surface functionality of activated carbons***

Activated carbons are built-up of graphene fragments where edges and defects are at the origin of surface functionality seen in Figure 6 [26]. The types of groups present on the surface of carbon materials are either acidic or basic. Acidic groups include carboxyl, phenol and lactone groups, whereas amine, carbonyl, ether and pyrone are basic groups. The surface groups have an influence on the wettability of activated carbons, and they can also affect the electrochemical properties especially through faradaic contributions [43].

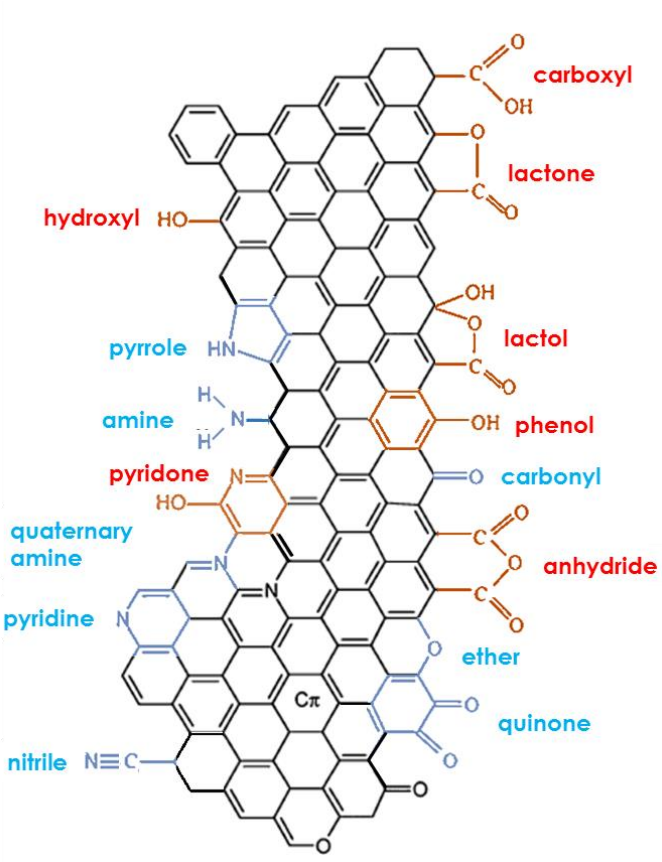

Figure 6 Possible functionalities on the surface of carbon; their acidity is represented by a color, red for acidic groups and blue for basic ones (adapted from [44]).

I. 1.3.2 Graphene

Graphene is a two dimensional (2D) carbon material, which specific surface area can reach in theory 2670 m^2/g, as it is considered to be consisting of a single layer of carbon atoms with hypothetical thickness of 0.335 nm. Owing to the delocalization of π electrons, graphene is an excellent conductor of heat and electricity. In practice, due to relatively strong π-π interactions, graphene sheets have the tendency to stack on each other (Figure 7), leading to decrease of specific surface area. In some reports on graphene-based electrodes, the capacitance is claimed to reach high values up to 120 F/g in organic electrolytes [45]. However, there is a great controversy in the claimed values, especially in aqueous electrolyte, because most of the materials are highly oxidized and can no longer be considered as graphene.

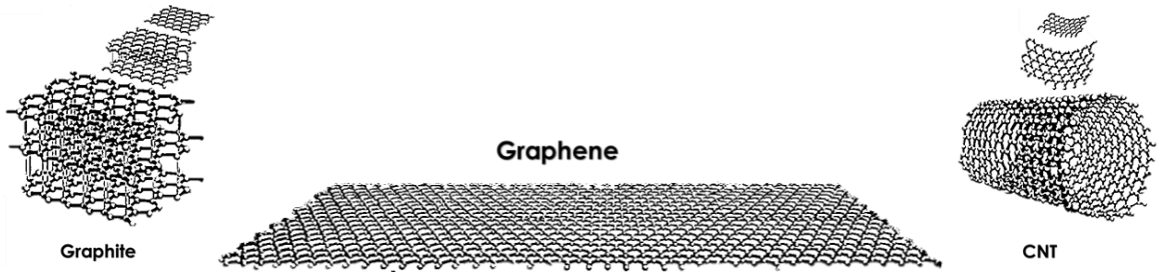

Figure 7 Theoretical graphene model as well as stacking of several graphene layers into graphite, and rolling-up of graphene layer into carbon nanotube [46].

I. 1.3.3 Carbon nanotubes (CNT)

Carbon nanotubes (CNTs) are constituted of one or several graphene layers which are rolled-up; accordingly, they are called single-wall carbon nanotubes (SWCNTs) and multiwalled carbon nanotubes (MWCNTs), respectively. These one dimensional (1D) structures are presented in Figure 8.

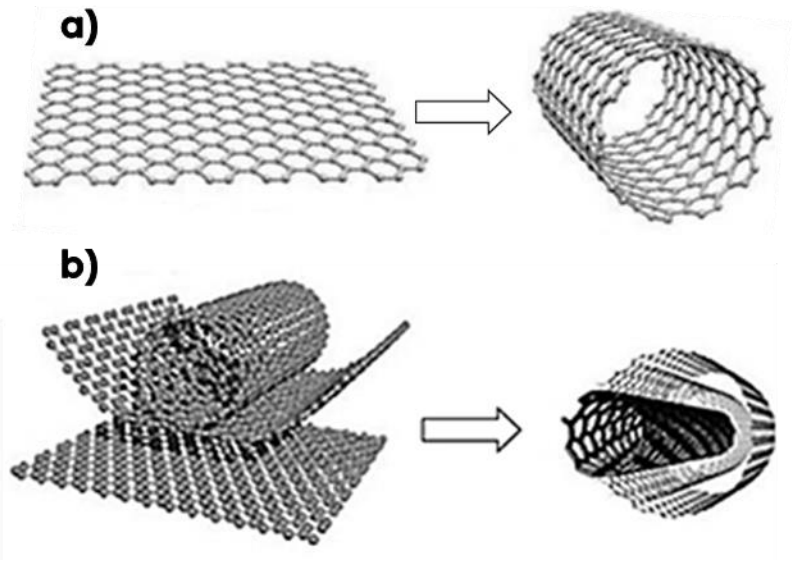

Figure 8 Formation and structure of a) SWCNT and b) MWCNT [47].

The most often, CNTs are produced on a catalyst by chemical vapor deposition (CVD) in an atmosphere of carbon feed gases such as methane or acetylene [48]. In comparison to activated carbon, carbon nanotubes have rather a low specific surface area (100 to 1000 m^2/g) and a low density, which greatly limits their use as electrode material in EDLCs due to the resulting low volumetric capacitance and energy. Owing to their structure, CNTs display a high electrical conductivity, which makes them very interesting as conductivity additives in electrodes or as support for non-conducting materials, for example MnO_2 [43].

Other types of carbons, such as templated carbons [43], were also investigated in ECs, but they do not display any improved performance as compared to AC, and are consequently not of great interest for this application. A special mention must be for some grades of carbon black which are used as universal conductivity additive in electrochemical storage devices (EDLCs, batteries, lithium-ion capacitors) [49].

I. 1.4. Electrolytes used in electrochemical capacitors

Considering the equations (6) and (7) for energy and power, the most important properties of electrolytes to be taken into consideration for application to EDLC systems are the voltage window in which the electrolyte can operate without decomposition and the

electrical conductivity. The charge which can be stored and the resistance of the electrode material depend on the electrolyte properties as the ionic radius of solvated or desolvated ions, mobility of ions in the pores of electrodes and the molar conductivity of ions [50]. Electrolytes for EC applications can be divided into aqueous, organic and ionic liquids [51,52,53]. As the value of electric permittivity is higher for aqueous solutions than for organic ones, in general the capacitance for the same electrode material is higher in the former medium [54,55]. Moreover, the conductivity of aqueous electrolytes can be one or two orders of magnitude higher than in the case of organic electrolytes, which is of interest for enhancing the power. However, the operational voltage window of organic electrolytes is much higher than for the aqueous ones, justifying their widely extended application for high energy storage devices. In addition to the previously considered criteria, ideally an electrolyte should be:

- Stable in a wide temperature range;
- Environmentally benign;
- Economically approachable.

None of the currently available electrolytes meets all of these demands.

I. 1.4.1 Organic electrolytes

Organic electrolytes are composed of an organic salt dissolved in an organic solvent. They can operate in a wide voltage range up to 2.7 V and even 2.8 V [56], and are the main type of electrolyte used in commercial devices. They are generally constituted of quaternary ammonium salts dissolved in solvents of high relative permittivity, either propylene carbonate (PC) or acetonitrile (ACN). PC as solvent proposed by Ue *et al.* [57] displays a wide electrochemical window and it resists to hydrolysis in presence of water. The stability window of PC reaches 5 V on a glassy carbon electrode [57], whereas it is less than 3.0 V with activated carbon [58]; when the voltage reaches 3.0 V in a cell with AC electrodes, the electrolyte is oxidized and gases evolve. Notwithstanding, due to higher viscosity than ACN, PC is not worth to be used below -30 °C [59]. Tetraethylammonium tetrafluoroborate (TEA-BF_4) is the widely employed salt in commercially available supercapacitors [60].

For various salts with tetrafluoroborate anions, Figure 9 shows that the conductivity increases with salt concentration up to a certain value after which it slightly decreases [61]. In case of TEA-BF_4, the conductivity reaches its maximum for a concentration of 1 mol/L; the other salts enable slightly higher conductivity at higher concentration. However, the high cost of salts like EMIM-BF_4 (1-ethyl-3-methylimidazolium tetrafluoroborate) or MEPY-BF_4 (1-ethyl-1-methylpyrrolidinium tetrafluoroborate) precludes their industrial application. Since the maximal conductivity of TEMA-BF_4 is reached at a concentration of 2 mol/L, this salt can be used at such concentration in large scale devices in order to avoid ion depletion during charging at high power [62]. Among the salts considered in Figure 9, EMIM-BF_4 and TMPY-BF_4 (tetramethylene-pyrrolidinium tetrafluoroborate) have the highest solubility in PC, allowing higher ionic conductivity to be reached.

Notwithstanding, the cycle life and voltage window of AC/AC capacitors operating in organic electrolytes are extremely sensitive to traces of moisture. Consequently, it is recommended to use electrolytes containing less than 20 ppm of water, and activated carbon electrodes must be carefully dried under vacuum before being soaked with the electrolyte. The respect of these constrains causes a dramatic increase of the costs of capacitors based on organic electrolytes.

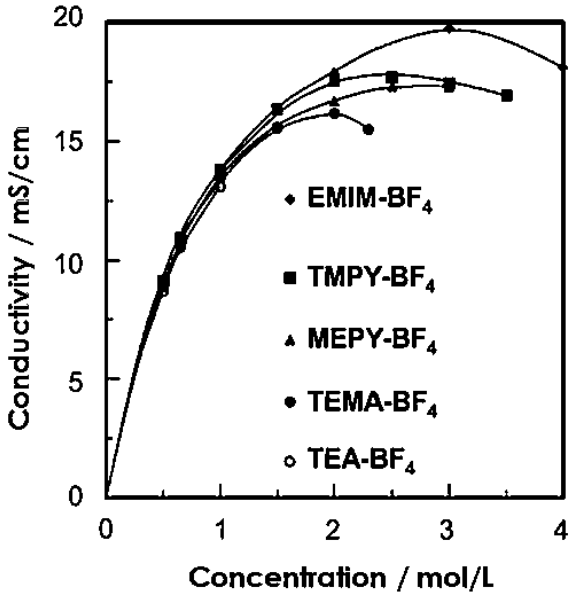

Figure 9 Conductivity vs. concentration of various quaternary ammonium salts dissolved in PC at 25 °C [61].

I. 1.4.2 Ionic liquids

Ionic Liquids (ILs) are defined as compounds consisting entirely of ions (an organic cation and an organic or inorganic anion) with melting point arbitrary limited to 100°C [63]. As they do not contain any solvent, they display interesting properties such as [63]:

- Negligible vapor pressure;
- Low flammability;
- Environmentally benign;
- Stability in a wide temperature range; broad electrochemical stability even higher than 2.8 V [64,65,66].

Such properties should potentially make them interesting electrolytes for energy storage applications. However, they display a very low ionic conductivity in comparison to most organic electrolytes; for example, the conductivity of TEA-BF_4 in PC can reach 0.02 S/cm [67], whilst it is generally less than 0.01 S/cm for ILs. Consequently, the power of systems based on this type of electrolytes is dramatically reduced [68]. In addition, when floating tests are performed on these systems in order to get realistic values of capacitance, it turns out that the maximum voltage is 3.1–3.5 V [69]. Hence, the practical use of ionic liquids in electrochemical capacitors is still highly questionable.

I. 1.4.3 Aqueous electrolytes

As compared to organic electrolytes, aqueous electrolytes are very cheap, and their implementation in electrochemical capacitors does not require the use of a neutral atmosphere and drastic drying of carbon electrodes. For these reasons, the AC/AC capacitors in aqueous electrolyte are much cheaper than their organic electrolyte counterpart. Additionally, the conductivity of aqueous solutions is generally one order of magnitude higher than for organic electrolytes, which is in favor of high power devices [70]. Potassium hydroxide (KOH) and sulphuric acid (H_2SO_4) were the first electrolytes used for supercapacitors; the concentration of these solutions can be increased to decrease the R_s value and maximize the power. However, with these aqueous solutions, the operating voltage is restricted to less than 1.0 V [71], which limits the specific energy of the devices. Khomenko *et al.* have however shown that it is possible to extend the operating voltage of

the system in sulphuric acid up to 1.6 V, either by proper balancing the mass ratio of positive and negative electrodes and/or by implementing carbons of different structure (surface functionality and porosity) for each electrode [72]. Notwithstanding, all non-noble metal current collectors are corroded by sulphuric acid, which limits the interest of such medium for electrochemical capacitors.

Recently, AC/AC capacitors implementing eco-friendly aqueous solutions of salts (for example alkali sulfates) with pH close to neutrality were claimed to display outstanding voltage values up to ca. 2V [73,74]. Under potentiostatic floating, cells with stainless steel current collectors demonstrated an excellent cycle life up to ca. 1.6 V, which is actually around twice higher than in sulphuric acid [75]. Such high operational voltage can be related to the strong solvation of ions, yet it is more likely that it is due to a high over-potential of di-hydrogen evolution owing to local pH increase in the porosity of the AC negative electrode. Lately, by using a mixed electrolyte constituted of lithium sulphate and potassium iodide, Abbas *et al.* have shown that the energy density of an AC/AC cell approaches the value obtained in organic electrolyte [76].

Conclusion

From the foregoing, the specific energy density of electrochemical capacitors is dictated essentially by the stability window of the electrolyte, which is still below 3.0 V in the symmetric AC/AC configuration with use of organic electrolyte. Consequently, the specific energy is ca. 10 Wh/kg as compared to 250 Wh/kg for lithium-ion batteries. Hence, it seems that a clue towards high energy supercapacitors could be the lithium-ion capacitor (LIC), i.e. through hybridization of a negative battery electrode (graphite) and a positive activated carbon one, while using a lithium salt dissolved in organic solvent. The further paragraphs will first introduce the lithium-ion battery from which the LIC uses the negative electrode and the electrolyte, to finish with presenting the state-of-the-art on LICs.

I. 2. Lithium-ion batteries (LIBs)

As previously mentioned, the lithium-ion capacitor (LIC) is constituted of an EDL-type positive electrode and a negative redox one (the most often made from graphite), and it uses a lithium salt as electrolyte, for example $LiPF_6$. By this way, the negative electrode operates at around 100 mV vs. Li/Li^+ which allows the cell voltage to reach ca. 4.0 V, against only 2.7 V in a traditional EDL capacitor. The specific purpose of our work is to use a sacrificial material (added to the positive activated carbon electrode) from which lithium is extracted irreversibly during the first galvanostatic charge. For these reasons, it is extremely interesting to devote a part of the literature review to the materials and energy storage mechanisms involved in lithium-ion batteries. In this part of the manuscript, we will review the information on solid electrolyte interphase (S.E.I.) formation on the negative electrode and on staging phenomena during lithium intercalation into graphite. We will also present the cathodic materials used in LIB cells, which operate similarly to the sacrificial material during the first charge in our concept, apart that they further demonstrate reversible lithium insertion.

I. 2.1. Principle of LIB operation

Metallic lithium is not directly applied as anode material, as dendrites would be formed during cycling, leading to short-circuit of the cell and even thermal runaway. To circumvent this problem, graphite has been suggested as anode material, acting as host for lithium at potential ca. 100 mV vs. Li/Li^+ [77].A scheme of LIB cell is represented in Figure 10, together with the redox reactions taking place during charge and discharge for the particular case of a $LiCoO_2$ cathode. During charging, Li^+ is removed from the cathode material network, transported through the electrolyte and intercalated into the structure of the anode material. By analogy, lithium ions are deintercalated from the anode and re-inserted into the cathode material during discharging of the system.

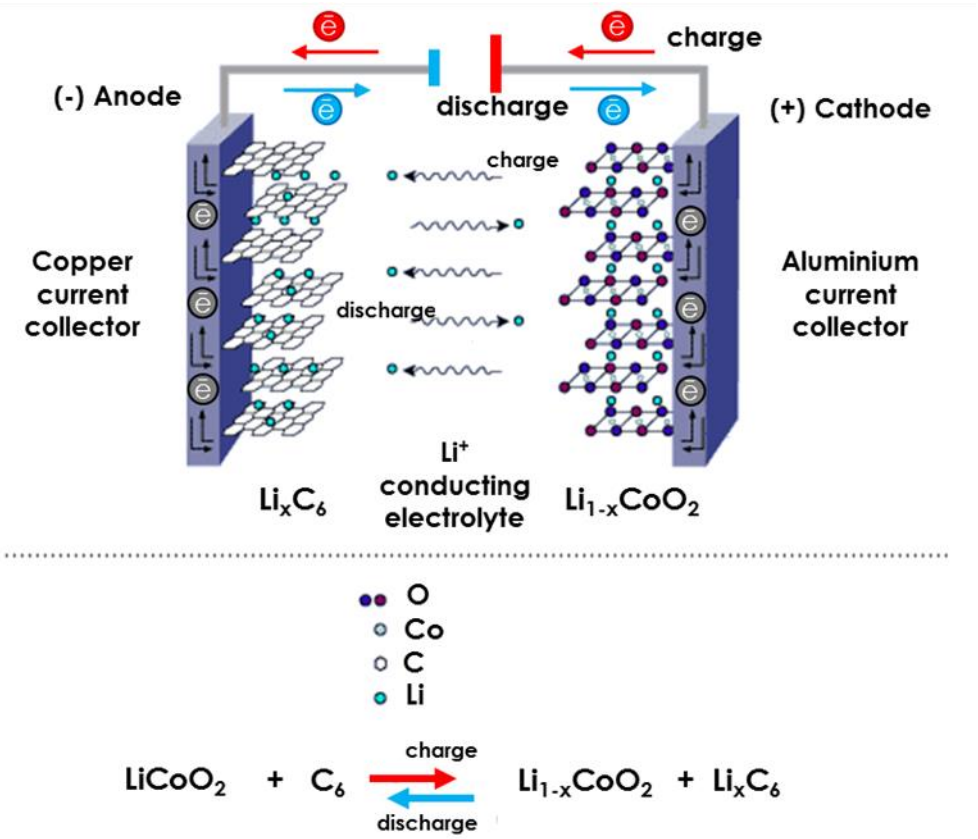

Figure 10 Schematic representation of a lithium-ion battery based on a $LiCoO_2$ cathode and of the redox processes taking place during charge and discharge [77].

The intercalation and extraction process for the negative and positive electrodes takes place in five fundamental steps [77]:

1) Diffusion or migration of solvated lithium ions;
2) Desolvation and introduction of lithium ions inside the vacant spots of the material;
3) Diffusion and/or migration of the ions through the solid electrolyte interphase (S.E.I.);
4) Transition reaction of electrode materials;
5) Diffusion of lithium ions throughout bulk of the material.

Most of the commercially available LIBs utilize a liquid electrolyte constituted of a lithium salt ($LiPF_6$, $LiClO_4$ $LiBF_4$ etc.) dissolved in organic solvents, such as carbonates (e.g., ethylene carbonate (EC), dimethyl carbonate (DMC), diethyl carbonate (DEC), ethyl methyl carbonate (EMC)). Sometimes, additives like vinyl carbonate (VC) are used to

stabilize the electrolyte/electrode interphase [78]. The electrodes are separated by a well-wettable porous membrane, which enables the migration of solvated lithium ions, while avoiding any short-circuit. To enhance the safety of LIBs, the electrolyte can be as well in gel or solid state, especially when high safety is required.

For most cathodic materials, the extraction of lithium ions takes place ca. 3.0 – 4.0 V vs. Li/Li^+, while lithium intercalates into graphite close to 0 V vs. Li/Li^+; hence, the energy of a LIB system reaches from 100 to 250 Wh/kg [77].

I. 2.2. Cathode materials

A positive electrode (cathode) of LIB must contain lithium ions which can be extracted and re-inserted into the host structure during cycling of the cell. For optimized performance of the system, a cathodic material of LIB should meet several requirements [77]:

- To enhance the capacity of the system, the material should have the ability to reversibly exchange high amount of lithium;
- To maximize cell voltage, lithium extraction/insertion should occur at high potential;
- To extend the cycle life of the cell
    - both forms of the cathodic material which appear during charging/discharging should be chemically stable;
    - the redox reaction should be reversible and not alter the structure of the material;
- To minimize the electrode polarization; the material should display a high conductivity.

Moreover, from the application point of view, the material should be cheap, environmentally benign and light in order to reduce the final weight of the cell [79].

The first example of materials containing lithium ions in their structure was presented in 1980 by Mizushima and Goodenough. These researches have revealed that it is possible to remove lithium ions electrochemically from the network of $Li_{1-x}CoO_2$ [80] and $Li_{1-x}NiO_2$ [81] and to obtain a system which can operate at around 4 V when a graphite anode is used. Since then a wide variety of possible cathode materials for lithium-ion batteries has been

investigated, including metal oxides, metal sulphides, poly(sulphides), nitrides, azides, and recently organic derivatives [82,83,84,85]. Nevertheless, the most often used cathode materials for commercial lithium ion-batteries are $LiCoO_2$ and $LiNiO_2$ with two dimensional structure and $LiMn_2O_4$ with three dimensional structure. The layer ($LiCoO_2$ and $LiNiO_2$) and tunnel ($LiMn_2O_4$) network organization of these compounds enable a fairly reversible Li^+ extraction at potentials higher than 4 V *vs.* Li/Li^+ [86].

I. 2.2.1. Layered materials

In 1991, the Japanese Company - Sony introduced the first LIB on the market, using lithium cobalt oxide ($LiCoO_2$) and graphite as positive and negative electrodes, respectively. $LiCoO_2$ is the most commonly used material for the large scale production [77]. The layered structure of $LiCoO_2$ comes from an alternate sequence of CoO_6 octahedra and Li layers [87]. The potential profile during lithium extraction/insertion from/into the structure of lithium cobalt oxide is presented in Figure 11. The potential of $LiCoO_2$ is initially close to 3.0 V vs. Li/Li^+, and it increases progressively to reach 4.2 V vs. Li/Li^+ for a practical capacity of 150 mAh/g, which corresponds to extracting approximately half of the total number of lithium ions; correspondingly, the oxidation degree of cobalt changes from Co^{3+} to Co^{4+} [100]. Extracting more lithium from the electrode by reaching higher potential leads to an irreversible change of the lithium cobalt oxide crystal lattice [88] and partial exothermic decomposition of the electrolyte. Additionally, the partial dissolution of Co^{3+} in the electrolyte can also lead to short cycle life of the cell [89]. In order to improve the stability of $LiCoO_2$, Park *et al.* proposed to cover the surface with neutral oxides as Al_2O_3, MgO or SnO_2 [90,91,92]; by creating such layer on $LiCoO_2$, the cycle life is improved and the electrode potential can be increased up to 4.5 V vs. Li/Li^+ without any detrimental changes in the electrode structure. Such oxide layer formed on the cathode can favorably influence three important aspects:

1) Better physical separation of oxidized active material from the electrolyte [93,94,95,96];
2) Improved stability of the cathode material during storage so-called shelf life (when the charged cell is not connected to a device) as well as during electrochemical insertion and extraction processes;

3) Stabilization of $LiCoO_2$ stabilization by a layer of Al_2O_3 or MgO created on its surface with which hydrofluoric acid (HF) formed in the electrolyte can react (indeed, HF can be formed when water in the electrolytic solution reacts with $LiPF_6$ [97,98,99]).

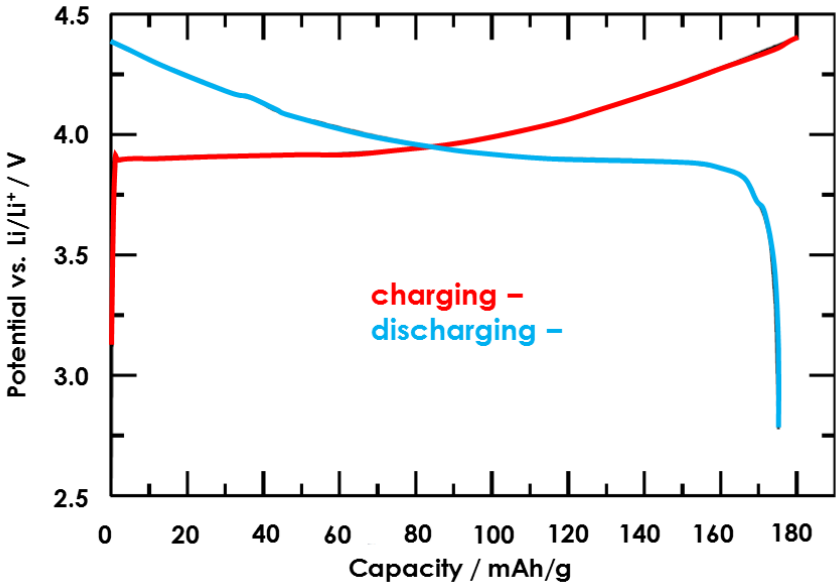

Figure 11 Potential profiles during electrochemical oxidation and reduction of $LiCoO_2$ [100].

Transition metal compounds like titanium sulphide (TiS_2), owing to their layered structure, allow the intercalation of lithium ions while switching from IV to III oxidation state of titanium during the oxidation/reduction process in the cell [101]. Despite its high capacity of ~200 mAh/g and low price, $LiNiO_2$ is not widely used as a cathode material in commercial systems. The divalent nickel ions tend to occupy the space between the layers which should be reserved for Li^+ [102]. Furthermore, during operation at high potentials, oxygen is released and the layered structure of $LiNiO_2$ is destroyed [100]. In order to avoid the irreversible phase transition related to the destroying of the layer structure caused by oxygen evolution during cycling, $LiNiO_2$ might be coated with a layer of TiO_2 [103], ZrO_2 [104], or Ni^{3+} can be substituted with Co^{3+} [105], Mg^{2+} or Ti^{4+} [106,107].

I. 2.2.2. Spinel-type materials

The structure of spinel-type materials can be generally described as AB_2O_4, where A and B are metal atoms. The most important example is $Li_XMn_2O_4$, which was firstly investigated by Thackeray *et al.* [108,109]. Despite, its lower capacity in comparison to $LiCoO_2$, $Li_XMn_2O_4$ has better kinetics of lithium extraction and better stability at higher values of potential, as there is no irreversible phase transition due to oxygen evolution. The stoichiometric composition of $LiMn_2O_4$ can be easily obtained and it is often used as a cathode material in lithium-ion batteries [100]. Moreover, it is cheap and environmentally benign, which makes it even more attractive for commercial application. However, at lower potentials, Mn^{2+} can dissolve in the electrolyte due to the disproportion reaction (12):

$$Mn^{3+} + Mn^{3+} \leftrightarrow Mn^{4+} + Mn^{2+} \quad (12)$$

Afterwards, a layer of metallic manganese can be created on the negative carbon electrode and block the transport of lithium ions. Furthermore, the creation of Jahn-Teller local distortions causes mechanical damage to the crystal structure of this compound. Nevertheless, the destroying of crystal structure which may lead to electrolyte oxidation can be overcome by doping the cathode with; Al^{3+}, Co^{3+}, Fe^{3+}, Li^{+}, Mg^{2+}, Ni^{2+} or Zn^{2+} [110,111,112,113,114,115]; cells implementing such doped material exhibit better cycle life, and higher operating potential when 1 mol/L $LiPF_6$ in EC:DMC (vol. rat. 1:1) is used as electrolyte [116,117].

I. 2.2.3. Olivine type materials

In 1997, Padhi proposed lithium iron phosphate ($LiFePO_4$) as a material which can be used in LIBs, as it is easy to synthesize and environmentally friendly [118]. Owing to strong bonding between iron and oxygen atoms, oxygen evolution is prevented during oxidation of the electrode material. Additionally, $LiFePO_4$ is chemically and thermally resilient and allows multiple extraction and insertion of lithium ions at potential of 3.4 V vs. Li/Li^+ [119], and its theoretical capacity is equal to 170 mAh/g [100]. In order to increase the very low conductivity of $LiFePO_4$ (near 10^{-9} S/cm), various cations have been introduced in the structure [120,121,122] to minimize the diffusion path for electrons and ions. Generally the

conductivity can be increased by reduction of the grain size [123,124,125] or also by coating the particles with a conductive carbon layer [126,127].

I. 2.2.4. Lithiated organic salts

The most recently used cathode materials in lithium-ion batteries include organic molecules. Unlike the formerly used inorganic materials, lithiated organic salts are considered as a step toward the "green" lithium-ion batteries [128,129,130]. Lithiated organic cathode materials with alkoxy functional groups in their aromatic structure are characterized by extraction potential of only 3 V vs. Li/Li^+ [131,132,133,134,135,136], whereas most of the lithium metal oxides have an extraction potential ca. 4 V vs. Li/Li^+. This rather low value of potential leads to relatively low energy density of the LIBs. Additionally the dissolution of the cathode material in the electrolyte is one of the biggest issues.

Compounds such as poly(dimercaptothiadiazole) or poly(2,5-dihydroxy-1,4-benzoquinone-3,6-methylene) [84,137] were the first organic materials able to react reversibly with lithium ions during the electrochemical oxidation/reduction process, with a high theoretical capacity of 375 mAh/g and 340 mAh/g, respectively. However, their oxidized form is partially soluble in the most often used organic electrolytes, such as 1 mol/L $LiPF_6$ in EC:DMC, which reduces the cycle life. Nonetheless, in order to improve the electronic conductivity, high amount of conductive additives were necessary [138].

Notably, there are lithiated organic materials with better stability and conductivity, for example dilithium rhodizonate ($Li_2C_6O_6$), which can be easily synthesized from rhodizonic acid dihydrate via the reaction with lithium carbonate (Li_2CO_3) (13) [128]:

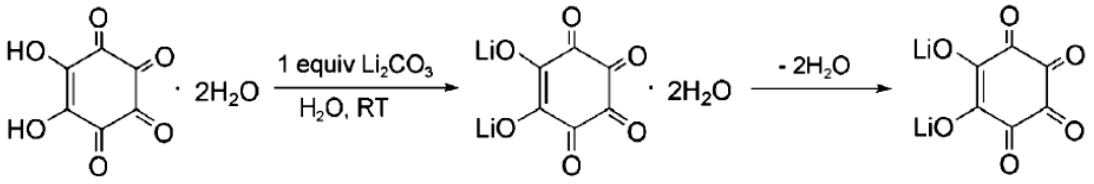

(13)

and then directly used as electrode material. It has a total capacity of 580 mAh/g and can be cycled from 1.5 V to 3.5 V vs. Li/Li^+. The process of oxidation/reduction is shown in the

equations (14) for the example 3,6-dihydroxy-2,5-dimethoxy-p-benzoquinone dilithium salt [139]:

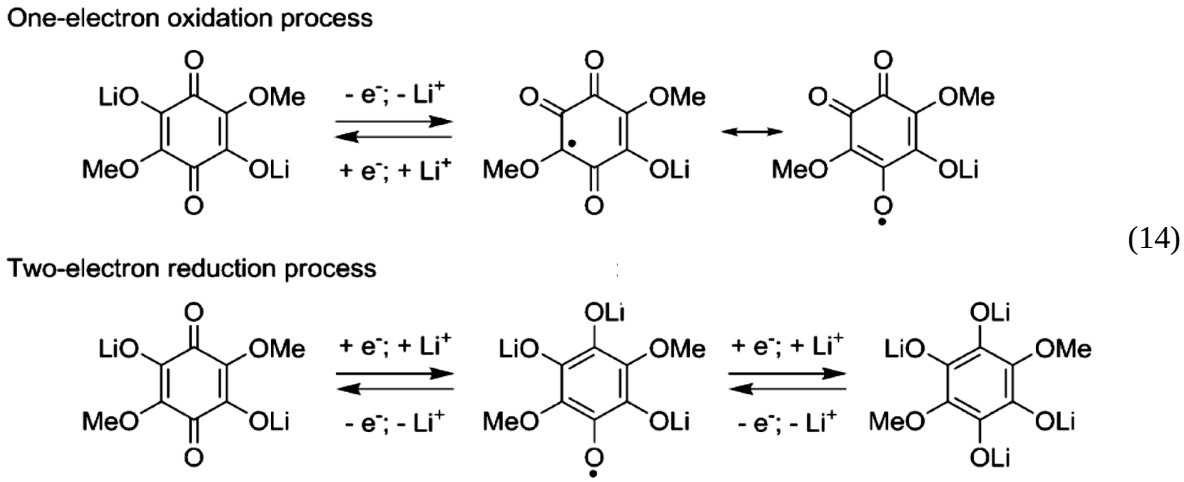

(14)

Despite the higher conductivity, lower price and low environmental impact of lithiated organic compounds, their biggest flaws are the low value of their redox potential and their poor reversibility (up to 25% of loss during the first 5 redox cycles [139]); hence, their application in LIBs is still limited [128,139]. However, when considering our purpose of using a sacrificial lithium source in the positive electrode of LICs, lithiated organic compounds may be very promising, as the low potential of lithium extraction may enable to avoid side reactions related with electrolyte oxidation at high potentials.

I. 2.3. Anode materials

One of the biggest breakthroughs in the field of anode materials was the introduction of carbon based materials [140]. In the first Sony lithium-ion batteries, petroleum coke with a capacity of 180 mAh/g was used as anode. From the middle of the 1990s' most of the available LIBs utilized graphite anodes with a specific capacity of around 300 mAh/g, yet there are also some other interesting alternatives such as lithium titanium oxides which can operate at very high current rates, around 20C and higher.

I. 2.3.1. Carbon materials

The most frequently used form of carbon in LIBs is graphite [83], yet other forms as hard carbons (HC) [141,142,143] and soft carbons (SC) [141,142,144] may be also used as

anode. As shown in Figure 12a, graphite is made of a regular sequence of large graphene layers bonded to each other by van der Waals forces, whereas hard and soft carbons are constituted of small units of very few graphene layers [140] (Figure 12b–c); these units are more or less parallel to each other in case of soft carbons, leading them to be transformed into graphite during high temperature treatment (>2000°C); by contrast, the units are totally misoriented in hard carbons and these materials are not graphitizable. Usually graphite exists in the hexagonal form where adjacent layers are shifted by one C-C bond distance, giving the ABA stacking (Figure 13a–b).

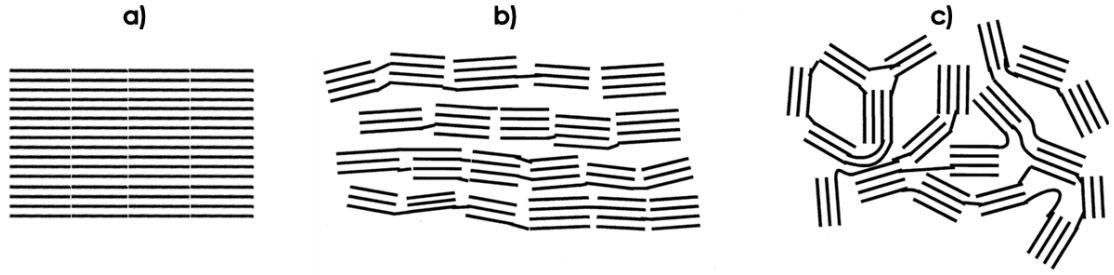

Figure 12 Comparison of structure/texture of a) graphite, b) soft carbon and c) hard carbon [143].

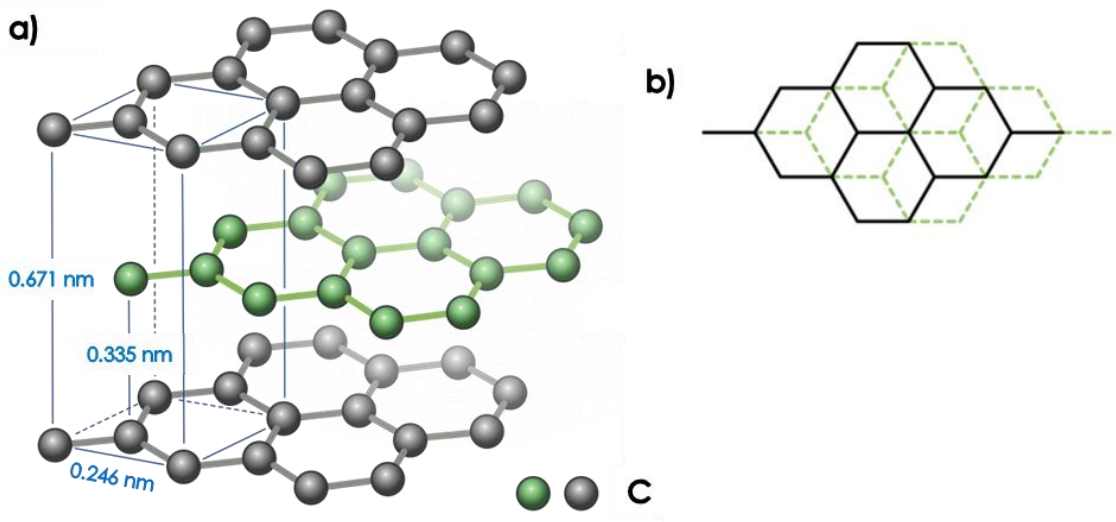

Figure 13 Crystal structure of graphite with ABABA stacking of graphene layers [100].

Figure 14 shows the galvanostatic charge/discharge (reduction/oxidation) of graphite in a cell where metallic lithium is used as counter and reference electrode. During the first charge, the potential of the graphite electrode decreases rapidly till reaching a value around 0.20 V vs. Li/Li^+, from which several plateaus (better shown in the inset) reveal a staging effect, i.e., the transition from one intercalation stage to another. The 4^{th} stage intercalation compound, where one interval over four is occupied by lithium ions (see Figure 15) is first formed at higher potential, and is then followed by 3^{rd}, 2^{nd} and 1^{st} stage (see Figure 15), with occupancy of 1 interval over 3, 2, 1, respectively, when the potential decreases. When the 1^{st} stage intercalation compound is totally formed, all interlayer spaces are occupied by lithium, which gives a composition of LiC_6, corresponding to a capacity of 372 mAh/g. In addition, when lithium is intercalated into graphite, the stacking of graphene layers adjacent to lithium changes from the AB sequence in graphite to the AA one in the graphite intercalation compound; Figure 16 shows the change of ABABA stacking to the AAAAA one in case of the 1^{st} stage intercalation compound [100].

The important information from Figure 14 is that when the sign of current is reversed to oxidize the graphite intercalation compound, a part of the total discharge capacity is not recovered. This part is called the irreversible capacity (Q_{irr}) and is due to the formation of the solid electrolyte interphase (S.E.I.) which occurred at around 0.80 V vs. Li/Li^+ during the first discharge [100]. The charge which is reversibly exchanged during the subsequent charges/discharges is called the reversible capacity (Q_{rev}).

The S.E.I formation will be further described in paragraph I. 2.5 and I. 2.6. However, it has to be mentioned that the S.E.I. is extremely profitable for LIB operation as it covers graphite and allows for lithium ions desolvation before their intercalation. In other words, since lithium penetrates desolvated, its de-intercalation from graphite occurs without any exfoliation, and consequently the cycle life of LIB cells based on graphite anode is excellent [83].

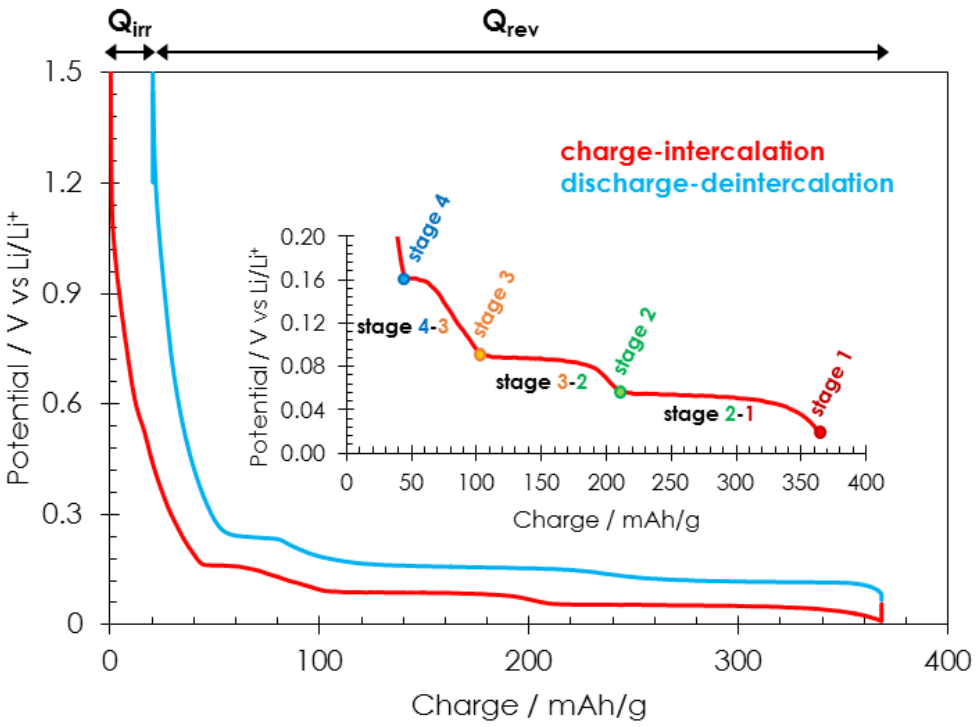

Figure 14 Charge/discharge profiles showing the intercalation (red) /deintercalation (blue) processes of lithium into/from graphite; the inset displays better the staging effect [83]. The electrolyte was 1 mol/L $LiPF_6$ in EC:DMC. Li/Li^+ was used as counter and reference electrode.

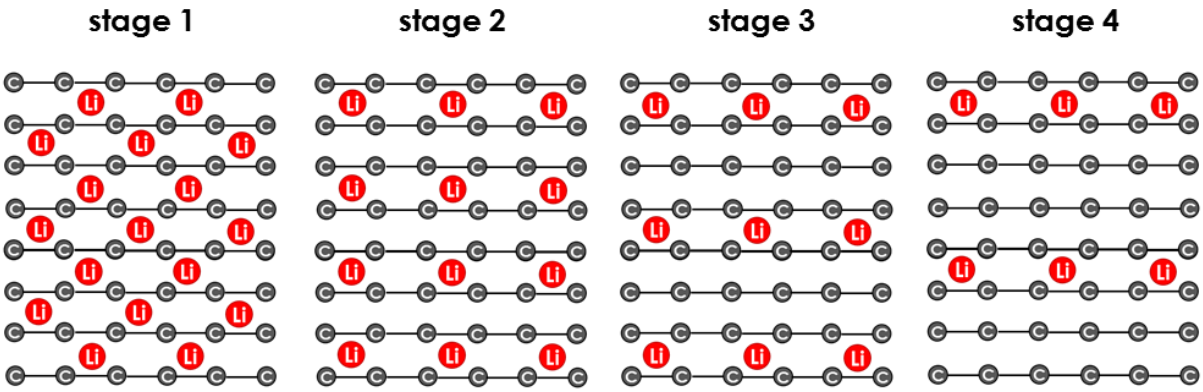

Figure 15 Schematic representation of the different stages of intercalation into graphite [100].

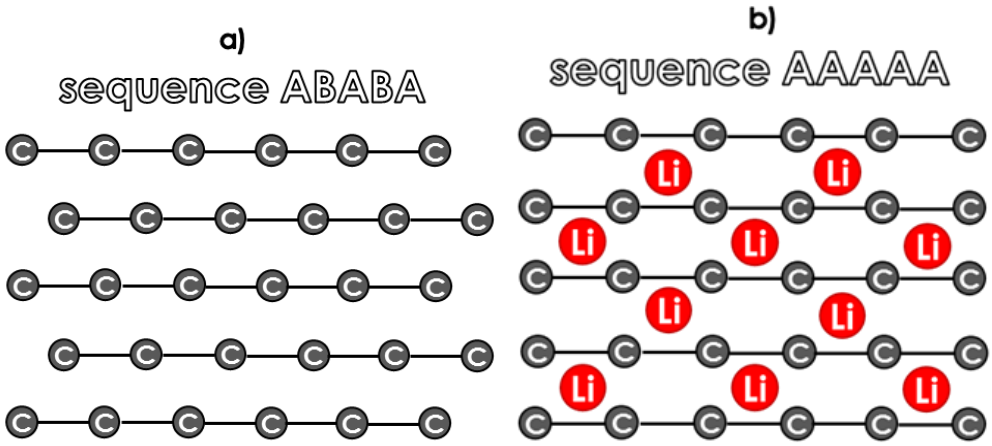

Figure 16 Shift from the ABABA sequence of graphene layers in graphite to the AAAAA one in the 1st stage intercalation compound [100].

Although graphite displays excellent properties, its reversible capacity is relatively moderate, requiring to looking for other materials in order to enhance the specific energy of batteries. In this context, it has been claimed that reversible capacities up to 600 mAh/g may be reached when hard carbons are applied as anode materials [145], whereas with graphite the maximum capacity is only 372 mAh/g. An example of charge/discharge curve in hard carbon is shown in Figure 17. By comparison with Figure 14 for graphite, the reversible capacity is much higher in case of the hard carbon and no staging effect is observed at low potential, due to the totally disordered structure of this material [146]. However, it is worth noting that the irreversible capacity is much higher than with graphite. Generally, it is suggested that the value of Q_{irr} is proportional to the BET specific surface area of the material; hence, the most promising carbons are the ones with a low specific surface area. Notwithstanding, this trend is far to be verified in all cases, and the correlation with the active surface area (ASA) seems to be more relevant [147].

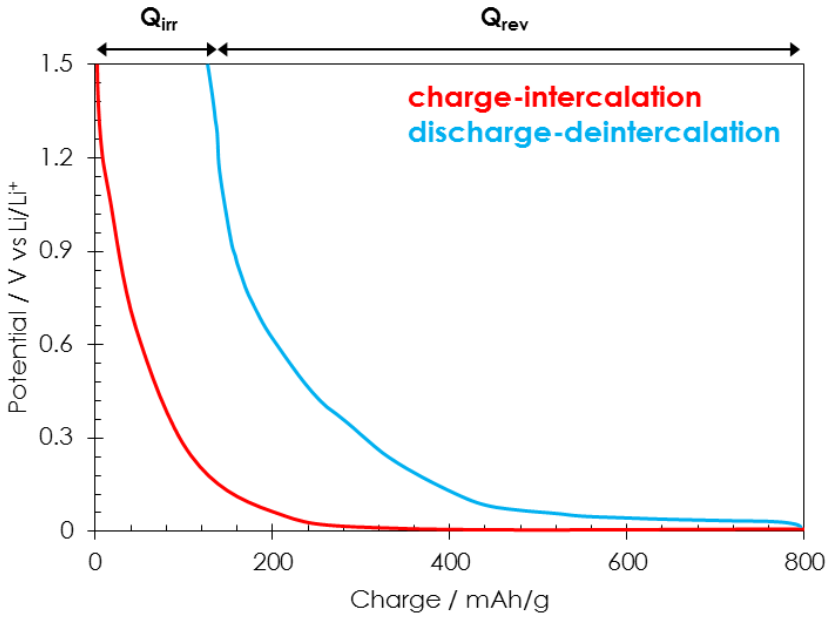

Figure 17 Galvanostatic reduction (red)/oxidation (blue) of hard carbon in 1 mol/L $LiPF_6$ in EC:DMC electrolyte [145].

To explain the high capacity observed with hard carbons,

Figure 18b suggests that lithium ions might be situated on both sides of a graphene layer, whereas in graphite each lithium layer is associated to one graphene layer (Figure 18a) [142].

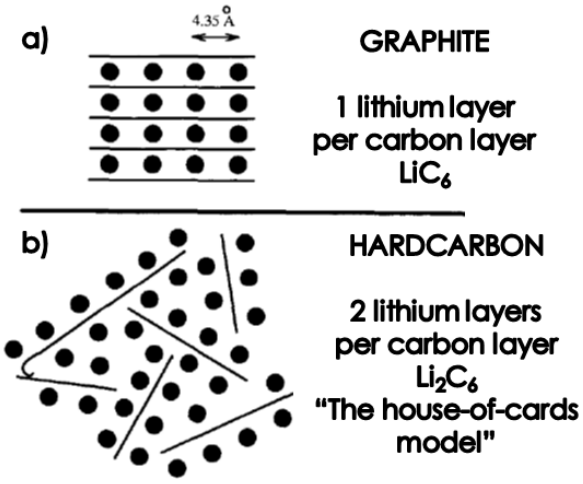

Figure 18 Schematic representations of fully intercalated a) graphite and b) hard carbon [142].

I. 2.3.2 Titanium oxides

Anode materials based on titanium oxides, owing to their chemical stability and low price, are considered as a possible alternative to graphite; the most promising and frequently investigated example in this family is $Li_4Ti_5O_{12}$ (LTO). The spinel structure of LTO allows the reversible insertion of Li^+, since the lattice parameters of the oxidized and reduced structures are almost identical (the lattice parameter a_c for the oxidized form is 0.8357 nm and for the reduced one 0.8353 nm); this is called a "zero-strain" transition [148].

Unfortunately, LTO displays much lower capacity than graphite (175 mAh/g compared to 372 mAh/g) and the insertion/deinsertion occurs at around 1.55 vs. Li/Li^+, which reduces the voltage of LIBs based on this anodic material, and consequently their specific energy. Nevertheless, the superior cyclability of LTO owing to negligible strain and absence of lithium plating (which may occur with some carbons at potential close to 0 V vs. Li/Li^+) are advantages. Similarly to e.g., $LiFePO_4$, LTO displays a very low conductivity. In order to surpass this issue, the grain size might be reduced [149,150] (to increase the diffusion rate of lithium ions through the crystal network of the anode) or the material can be coated with a conducting layer of carbon, copper or silver [151,152,153]. Another strategy is to prepare a nanocomposite including nanocrystalline LTO and carbon nanofibers (CNF) by ultracentrifugation (Figure 19).

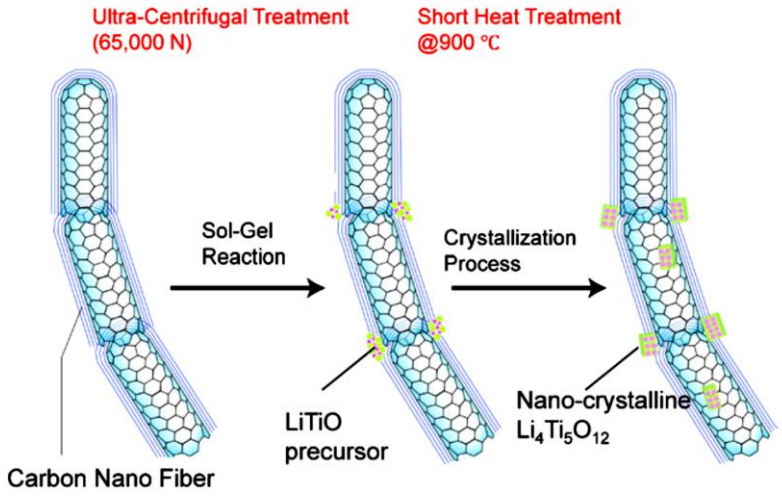

Figure 19 Preparation of the CNF/nano-crystalline LTO composite by ultracentrifugation [155].

Tetrabutyl titanate [$Ti(OC_4H_9)_4$], lithium acetate and CNF are mixed by ultracentrifugation, while a sol-gel reaction creates the LTO precursor attached to CNF surface, and a short heat-treatment at 900 °C leads to nanocrystalline LTO. As the LTO particles size is in the range of nm and they are well dispersed in the CNF material, the conductivity of the material is high enabling it to operate at high current up to 50 C [154,155].

Titanium dioxide, under the anatase, rutile and TiO_2-B polymorphic forms, might be also attractive for its high theoretical capacity of 335 mAh/g. It is also possible to obtain anatase and TiO_2-B in the form of nanotubes, nanorods or nanowires. For instance, TiO_2-B in the form of nanowires displays a high capacity (around 300 mAh/g), good cyclic stability and non-toxicity [156]. However, the operational voltage of system with TiO_2-B is ca. 3.0 V, which limits the energy density of the device.

I. 2.4. Electrolytes for LIBs

An appropriate electrolytic solution for LIB should fulfill the following criteria [77]:

- Electrochemical stability in a wide potential range (up to 5 V);
- High lithium ion transport number (in order to reduce the concentration polarization of the cell);
- High conductivity in a wide temperature range (~10^{-3} S/cm at temperatures between -40 to 90 °C);
- Thermal stability;
- Chemical inertness to other components of the cell.

Generally, there are four basic groups of electrolytes applied in LIBs: liquid, gel, polymeric and ceramic electrolytes. The first group includes lithium salts dissolved in organic solvents (usually carbonates). Both polymeric and gel electrolytes are based on an ion conducting phase obtained by dissolution of lithium salts in polymers with high molecular mass; obviously, gel electrolytes include a solvent. In comparison to liquid electrolytes, polymer electrolytes have lower conductivity and lower ion transportation; however, they can play simultaneously the role of separator. Ceramic electrolytes, which are solid inorganic materials, are not used in commercial cells, as they are brittle materials. Currently, most of the commercially available lithium-ion batteries use liquid electrolytes. Polar aprotic

solvents with high dielectric constant can dissolve the lithiated salts at concentrations higher than 1 mol/L. Propylene carbonate (PC) as solvent was found not to be a good solvent because solvated lithium ions intercalate in the structure of graphite and provoke its exfoliation during deinsertion [84]. Therefore, different solvents, such as ethylene carbonate (EC), dimethyl carbonate (DMC), diethyl carbonate (DEC) and ethyl methyl carbonate (EMC) are widely used nowadays (Figure 20). Interestingly, electrolyte can be also mixtures of few solvents to have low viscosity and high conductivity. Especially, by using different mixtures of solvents, it is possible to modify the morphology of the S.E.I layer in order to get a continuous layer on the surface of the anode material [84].

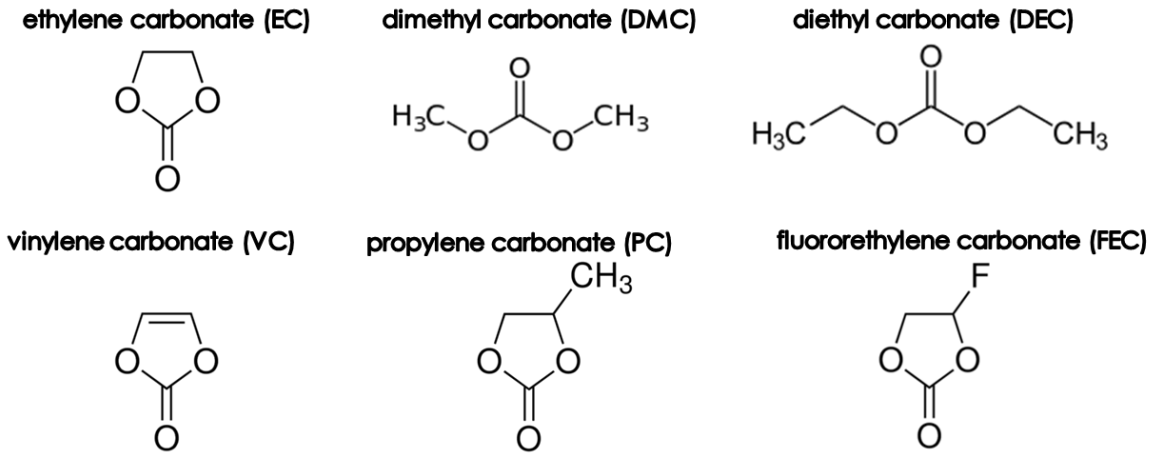

Figure 20 The most common solvents used for lithium-ion batteries with liquid electrolytes [83].

Lithium hexafluorophosphate ($LiPF_6$) is the most often used lithium salt for liquid electrolytes, owing to the high conductivity (>10^{-3} S/cm). However, it is expensive and highly hygroscopic. What is more, electrolytes based on $LiPF_6$ must be free of moisture in order to avoid the reaction of $LiPF_6$ with water which gives hydrofluoric acid (HF) [169].

I. 2.5. Chemistry of S.E.I. formation on the lithium surface

The contact of metallic lithium with air atmosphere during its production process creates a thin film consisting of hydroxides, carbonates and oxides on its surface (Figure 21a) [157]. If metallic lithium is introduced into a polar aprotic solution, a part of the initially formed layer dissolves and, during polarization, it reacts with the other components of the

electrolyte to form a solid layer called solid electrolyte interphase (S.E.I) (Figure 21b). Since the thickness of this film increases with the next cycles of charge/discharge, it becomes an electronic insulator, and though, limits the migration of mobile ions through its bulk. If there are cracks in the formed layer, in a next step, the electrolyte penetrates in it (Figure 21c) and reacts with the metal creating a complex and heterogeneous multilayer. Dissolution of metal can lead to damaging of the S.E.I. followed by uneven distribution of charge through the cell. If the S.E.I. layer is damaged, the active metal surface is in direct contact with the electrolyte, which leads to the creation of dendrites (Figure 21d) [140]. During further operation of the cell, the dendrites can perforate the separator, and cause short-circuits between the electrodes and thermal runaway. Therefore, metallic lithium is not used as electrode in lithium batteries [157].

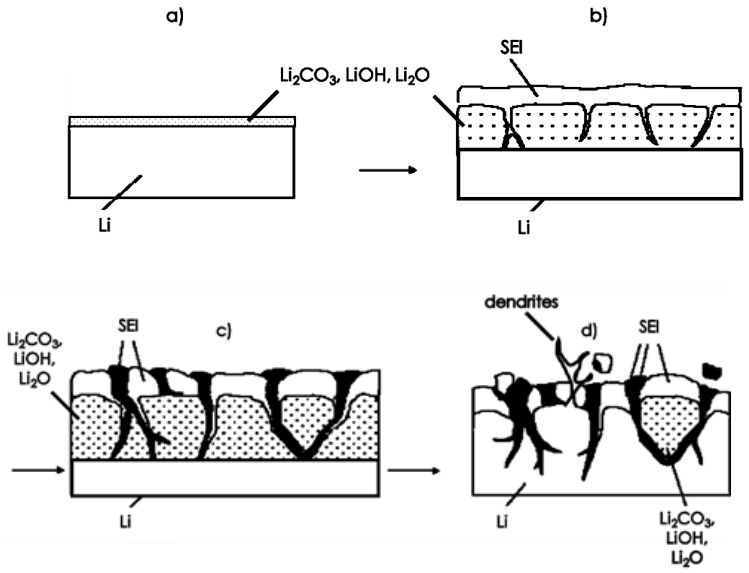

Figure 21 Schematic representation of a S.E.I formation on the surface of metallic lithium: a) Outer layer on as-received metallic lithium; b) S.E.I. formation after contact of a lithium electrode with the electrolyte and its polarization; and c) dissolution of the outer layer; d) further dissolution of the outer layer and final damaging of S.E.I. [157].

I. 2.6. Chemistry of S.E.I. formation on the carbon surface

The presence of a S.E.I. is beneficial for the cyclability and safety of LIBs. The S.E.I. layer created on the surface of graphite prevents from further reduction of the electrolyte during the next charge cycles of the cell [158]. The stability and reversibility of the intercalation

process in graphite is highly depending on the formed S.E.I. which is related to the electrolyte composition [140]. In case of EC, DMC, DEC based electrolytes, the formed S.E.I. enables for the desolvation of the Li^+ ions so graphite does not exfoliate during cycling. By contrast, when using a lithium salt dissolved in propylene carbonate (PC) with a graphite anode, electrolyte decomposition and co-intercalation of PC take place simultaneously at potentials lower than 0.9 vs. Li/Li^+ [159]. PC co-intercalation during charge leads to graphite exfoliation during discharge, thus commercially available lithium-ion batteries with graphite anode are usually based on EC [206] and mixtures of EC together with other solvents [160]. Nevertheless, still many researchers seek for the suitable composition of the organic solvents responsible for the S.E.I. formation with the lowest irreversible capacity. For example, the addition of vinylene carbonate (VC) seems to reduce the amount of evolving gases during the S.E.I. formation and limits Q_{irr} [161].

Through the years, various analytical techniques have been used to know the exact composition of the S.E.I., as scanning tunneling microscopy (STM), atomic force microscopy (AFM), dilatometry, infra-red spectroscopy (IR) or Raman spectroscopy. These data could provide information about the S.E.I.'s stability, morphology, mechanisms responsible for its formation, and its influence on the systems performance [162,163,164,165]. The layers created on the surface of metallic lithium are mainly composed of Li_2CO_3 [166]. However, the composition of the S.E.I. depends on the applied electrolyte; in case of electrolyte based on EC, the S.E.I. consists of lithium alkyl carbonates (e.g. $(CH_2OCO_2Li)_2$), whereas PC decomposes to $CH_3CH(OCO_2Li)CH_2OCO_2Li$ and DMC to CH_3OCO_2Li [167], and LiF (due to the presence of water) [168]. The most comprehensible studies allow predicting the reaction mechanisms occurring at the carbon electrode/electrolyte interphase. Under polarization in presence of $LiPF_6$ in EC:DMC, the reaction can be described by the equations 15 to 17) [169]:

$$2EC + 2e^- + 2Li^+ \rightarrow (CH_2OCO_2Li)_2 \downarrow + CH_2 = CH_2 \uparrow \quad (15)$$

$$EC + 2e^- + 2Li^+ \rightarrow LiCH_2CH_2OCO_2Li \downarrow \quad (16)$$

$$DMC + e^- + Li^+ \rightarrow CH_3 \bullet + CH_2OCO_2Li \downarrow \frac{and}{or} CH_3OLi \downarrow + CH_3OCO \bullet \quad (17)$$

As it can be seen, the free radicals which are formed as result of reaction (17) can further either react with the electrode surface to create Li-C bonds, or recombine/undergo disproportionation reaction to form gases as C_2H_4, CH_4 or H_2 [169].

The thickness of the S.E.I. layer can vary from few to dozen of nanometers [170,171]; however, due to its partial solubility in the electrolyte, it is hard to estimate its precise thickness [172]. Therefore, to describe the composition and morphology of a S.E.I. multilayer, some models were presented in the literature [169,171,173,174,175]. All the proposed representations include a dense layer of inorganic compounds as Li_2O, Li_3N, LiX (X = F, Cl, etc.) and a porous layer of organic species as ROLi, $ROCO_2Li$, $RCOO_2Li$ (where R is an alkyl group). Due to partial dissolution of the S.E.I. in the electrolyte, the composition and morphology of this solid layer can change during cycling [176] or storage in absence of applied current [177]. Moreover, the S.E.I. is likely to become thicker at lower potential values (at the intercalated state) and thinner at higher potentials (at the deintercalated state) but it may vary depending on the material [178]. Despite the high complexity of the S.E.I. formation, this process can be optimized and controlled when the nature and composition of the electrolyte, as well as all the applied additives, are well known [165]. Furthermore, the creation of the solid electrolyte interface is supervised by the value of current applied during the first charge of the cell [179,180]. It was observed that the use of higher currents during the S.E.I. formation reduces the value of irreversible capacity. This is related to the formation of a thinner and continuous passive layer on the surface of the graphite electrode [180]. Although the S.E.I is formed during the first charge, it continues to grow under continuous cycling, referred to as maturing of the S.E.I. [181].

The appropriate potential of S.E.I. formation is generally considered to be around 0.8 V vs. Li/Li^+ [171,178], yet some literature reports indicate that the S.E.I. starts to be formed from 1.0 V or even 2.0 V vs. Li/Li^+ [182,183,184]. In order to prepare a cell to function in a proper way, it is eligible to assist the S.E.I. layer to be formed before lithium intercalation into graphite starts, e.g., before ca. 0.25 V vs. Li/Li^+ [182]). As shown in Figure 22, if the reduction of the electrolyte components takes place before the intercalation process, the surface of the graphite electrode (Figure 22a) is stabilized by a passive layer (Figure 22b). The passive layer which tightly covers the whole surface of the graphite electrode leads to

high reversibility of the processes occurring during cycling [185]. There are few mechanisms describing the causes for capacity fade under cycling of a system with graphite electrode. Firstly, if the passivation layer is not continuous, the solvent compounds can intercalate together with lithium ions, entailing exfoliation and amorphization of graphite [186]. Secondly, some products of the solvent reduction lead to deactivation of the graphite particles [185]. For instance, the application of PC as solvent can result in evolution of propene and exfoliation of graphite [157]. Finally, small volumetric changes of the electrode during cycling create small cracks in the S.E.I. (Figure 22c). In such situation, the electrolyte components are in direct contact with the active surface of the electrode. Unfortunately, maturing of the S.E.I. upon cycling (even if the process takes place on a small scale) leads to the creation of a thicker interfacial layer than before cycling, which increases the electrode resistivity (Figure 22d) [169].

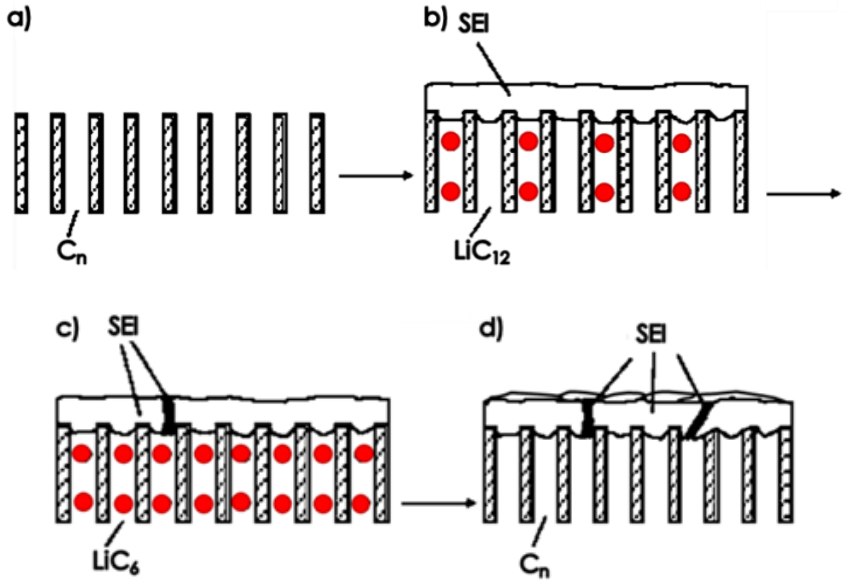

Figure 22 Schematic representations of a) graphite electrode; b) graphite electrode covered by a S.E.I. layer; c) S.E.I. cracking; d) maturing of the passive layer upon cycling [157].

Preferably, the S.E.I. should be highly conductive for lithium ions, and at the same time, have a low electronic conductivity. Furthermore, it should be continuous and homogenous in terms of morphology and composition. In order to be able to adapt to uneven electrochemical treatment and gases evolution close the electrode, a desired S.E.I. should

be an elastic compact layer which covers the whole surface of the electrode active material [187,188]. Besides, when a graphite electrode is used, cycling of the cell leads to creating a multilayered S.E.I on the surface of the anode. To precisely reduce the reactive species at higher potential values, intercalation usually is performed by the galvanostatic method. By forming the passive layer on the surface of graphite at different potentials in ethylene carbonate-diethyl carbonate solutions containing $LiClO_4$, $LiPF_6$, and $LiN(SO_2CF_3)_2$, Yokoto *et. al* [189] could confirm a change of S.E.I. morphology.

Conclusion

Owing to the chemical reactions occurring in lithium-ion batteries and the high potential difference between the electrodes (almost 4.0 V), the energy stored is much higher than in traditional electrochemical capacitors operating in organic electrolytes, where the charges are stored electrostatically on the active surface of the electrodes. Even though the energy density of LIBs is around 200 Wh/kg, their low cycle life and limited power remains a limiting factor for a number of applications. Therefore, lithium-ion capacitors (LICs) which implement a battery-like negative electrode, for example graphite, and activated carbon as positive one seem to be a good alternative combining some of the advantages of LIBs and EDLCs. However, as it will be demonstrated in the next section of this literature review, the pre-lithiation of graphite still remains a complicated issue. Our proposition in this thesis to use a sacrificial material added to the positive AC electrode could enable the elimination of the auxiliary lithium electrode used in the presently available LIC systems. Later, we will see that the properties described above for the ideal cathodic materials are very useful to determine good candidates for our concept of LIC. Also, the information about S.E.I. formation will be also very useful to determine conditions allowing to optimize the S.E.I. morphology and probably to improve the electrochemical performance of the system, in particular its power.

I. 3. Lithium-ion capacitors (LICs)

Regardless the advantages of EDLCs and LIBs presented in the previous paragraphs, the energy and power outputs are still a problem for supercapacitors and batteries, respectively. In this context, the lithium-ion capacitor (LIC) is a recently developed device, which exhibits higher energy density than an EDLC and is characterized by comparable power [154,190]. The first LIC presented by Amatucci *et al.* [191,192] used $Li_4Ti_5O_{12}$ (LTO) as negative electrode and activated carbon as positive one, and 1.0 mol/L $LiPF_6$ in EC:DMC as electrolyte [191]. Since then, systems implementing various anode materials (graphite, hard carbon, etc.) have been investigated to enhance the energy and retain the power output at similar level as in EDLCs.

Since lithium-ion capacitors are very novel energy storage devices, the number of literature reports about these systems is not as vast as in case of LIBs or EDLCs, but starts to increase very rapidly from year to year. Since this thesis is essentially focused on the use of pre-lithiation materials, this paragraph will pay a particular attention to the various pre-lithation methods used until now.

I. 3.1. Principle of energy storage in LICs

In LICs, the energy is stored via two simultaneous mechanisms. On the positive side, the charges are accumulated electrostatically on the active surface of a porous material, e.g., activated carbon, whilst on the negative one; lithium ions are intercalated/deintercalated into/from the structure of a battery-like anode. Therefore, the materials which are the most commonly used for the negative electrode are graphite, hard carbon, soft carbon or lithium titanium oxide. The general construction of the cell is the same as for a lithium-ion battery, where the active materials for negative and positive electrode are deposited on copper and aluminum current collectors, respectively, and both electrodes are separated by a porous membrane and immersed in the lithium ions conducting electrolyte (Figure 23) [193].

According to the formula (18) for cell capacitance:

$$\frac{1}{C} = \frac{1}{C_+} + \frac{1}{C_-} \qquad (18)$$

in the case of a LIC, $C_+ << C_-$, and consequently $C \approx C_+$. By contrast, applying equation (18) for a symmetric EDLC gives $C \approx \frac{1}{2} C_{\pm}$, e.g., the capacitance of LIC is roughly doubled as compared to EDLC, while using similar total mass of electrode materials. Besides, when a graphite negative electrode is used it also allows to extend the voltage range (as it operates near 0 V vs. Li/Li^+) and boost the energy of the cell.

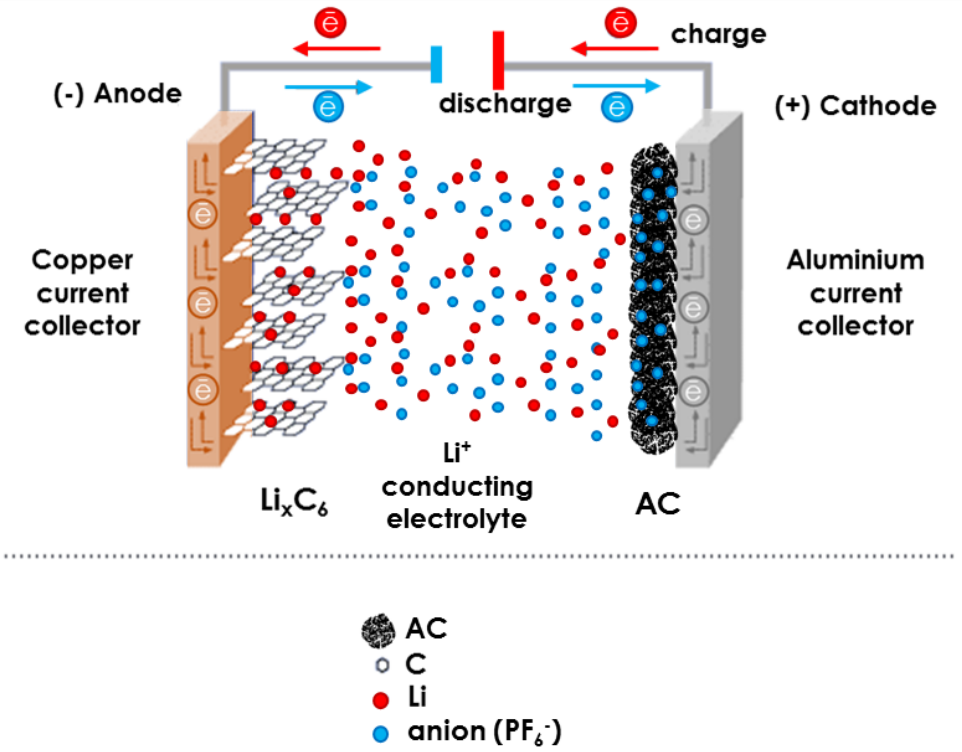

Figure 23 Schematic representation of LIC with graphite intercalation compound (GIC) as negative electrode and activated carbon as positive electrode [193].

The later issue can be easily understood by comparing the galvanostatic charge/discharge profiles of EDLC and LIC cells (Figure 24). As it is shown in Figure 24a, the change of potentials for both positive and negative electrode is linear when EDLC is considered; the voltage of the system is limited to 2.7 V in case of organic electrolytes such as 1mol/L tetraethylammonium tetrafluoroborate in acetonitrile ($TEA^+BF_4^-$/ACN). In case of LIC (Figure 24b), only the potential of the positive electrode varies linearly, while the potential of the negative one is almost constant. Notwithstanding, the voltage profile of full LIC cell

is linear during charge and discharge, exhibiting the characteristics of a capacitor. The maximum voltage of the LIC depends essentially on the type of anode material, and reaches its highest value with graphite, ca. 4.0 V, owing to the low value of intercalation/deintercalation potential, ca. 100 mV vs. Li/Li^+[193]. To describe the difference between the two discussed systems, their equivalent circuits are also presented in Figure 24. It can be easily seen that the model is more complicated for LIC than for EDLC. The complexity comes from the existence of the S.E.I. layer (with capacitance C_{SEI} and resistance R_{SEI}), likewise the negative electrode material (C_G and R_G for the graphite electrode). The impedance terms Z_wLi^+ and Z_wA^- correspond to the diffusion rate of lithium ions and anions into/from the electrode material, respectively.

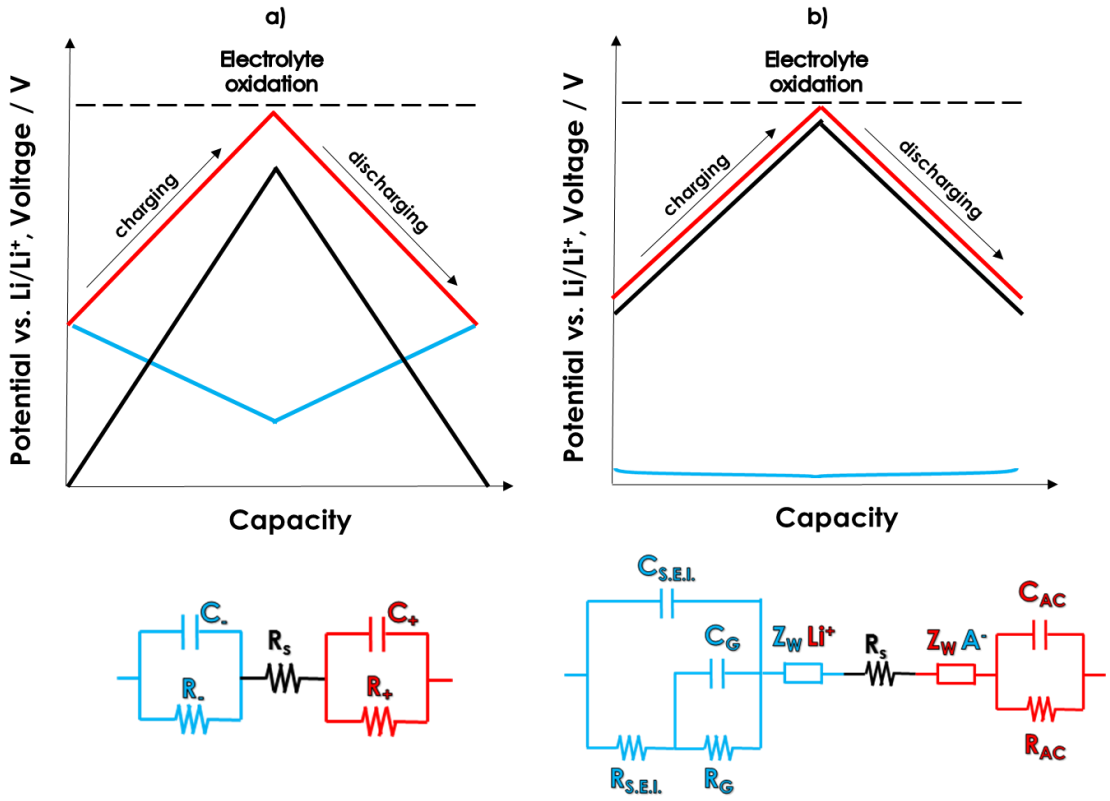

Figure 24 Charge/discharge profiles of a) EDLC and b) LIC where: red – potential of positive electrode, blue – potential of negative electrode and black –voltage of the cell. Respective equivalent circuits are given below each system [193,194].

I. 3.2. Lithium sources for pre-lithiation of carbon anodes

Before being able to operate a LIC, it is preliminary necessary to transform the carbon electrode into a battery-like anode. The process during which lithium ions are introduced into the negative electrode structure is often referred to as pre-lithiation [193]. Currently, three main sources of lithium ions are proposed in the literature to ensure the anode pre-lithiation: an auxiliary metallic lithium electrode, the lithiated electrolyte or a composite lithiated cathode material.

I. 3.2.1. Pre-lithiation with an auxiliary metallic lithium electrode

In 2006, Fuji Heavy Industry [195] and Aida *et al.* [196,197] introduced a concept of cell where an auxiliary metallic lithium electrode was used to pre-lithiate carbon. Beside the additional sacrificial lithium plate and the graphite negative electrode, activated carbon was used to work as positive one. According to the producer of the commercially available ULTIMO cells - JM Energy Corporation [198], the entire metallic lithium should be utilized to form the graphite intercalation compound (GIC) during the pre-lithiation process. The LIC with such prepared GIC can be reversibly charged and discharged in a voltage window between ca. 1.9 V - 3.8 V. The energy and power output of the ULTIMO device is 7.6 Wh/kg and 1.4 kW/kg, respectively, in comparison to 4.2 Wh/kg and 2.1 kW/kg for an EDLC operating up to 2.7 V (values are expressed per mass of whole device) [199]. However, the whole process with metallic lithium manipulation must be done under inert atmosphere; otherwise, short circuit of the cell and/or thermal runaway can occur. However, the construction of such system, as presented in Figure 25, is rather complicated. It is made of a succession of two stacks of positive and negative electrodes separated by a porous membrane, followed by one auxiliary lithium electrode [198]. Lithium must be first intercalated into graphite (negative electrode) using the metallic lithium (auxiliary electrode); then the hybrid cell formed by the graphite intercalation compound (negative electrode) and activated carbon (positive electrode) can be cycled.

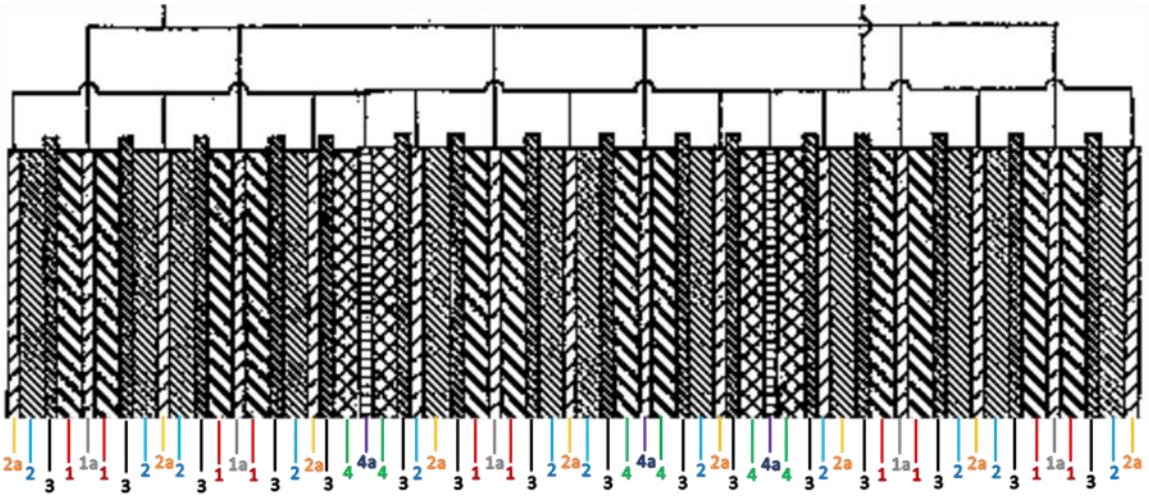

Figure 25 Concept of the LIC module with the auxiliary metallic lithium electrode for the pre-lithiation of graphite anode. 1-positive electrode 1a-positive electrode current collector, 2-negative electrode, 2a- negative electrode current collector, 3-separator, 4-metallic lithium auxiliary electrode, 4a-current collector of metallic lithium auxiliary electrode [200].

I. 3.2.2. Pre-lithiation with lithium ions from the electrolyte

Recently, Béguin *et al.* [201,202] presented a concept of LIC in which lithium ions come from a highly concentrated electrolytic solution. Since the electrolyte is an integral part of all the system, it was possible to avoid the application of metallic lithium and all the safety issues related to its use. The electrochemical cell was constructed of AC positive electrode and graphite as negative one. Unlike to commonly used 1 mol/L $LiPF_6$ in EC:DMC, the electrolyte was a 2 mol/L solution of bis(trifluoromethane)sulfonimide lithium salt/LiTFSI in EC:DMC; the choice of LiTFSI was guided by its much higher solubility than conventional lithium salts.

Figure 26 presents the pre-lithation step of the LIC system with AC as positive electrode and graphite as negative one. When current is passed in the cell, the potential of the AC electrode (red curve) increases, while the potential of the negative graphite one (blue curve) decreases, owing to intercalation of lithium ions coming from the electrolytic solution. However, since the maximum potential of the positive electrode must be limited ca. 4.2 V vs. Li/Li^+ to avoid electrolyte oxidation, it is not possible to introduce all the necessary

lithium ions with one charge pulse at C/10 (where C indicates the theoretical capacity of the graphite). Therefore, after such pulse, the cell was let at open circuit for 1 h, before applying a next C/10 pulse until the potential of the positive electrode reached again 4.2 V vs. Li/Li^+, and so on. This kind of sequence was repeated until the potential of negative electrode reached 0.105 V vs. Li/Li^+, corresponding to the second stage intercalation compound, LiC_{12}. It must be pointed out that this procedure was very effective owing to the higher self-discharge of the EDL activated carbon electrode as compared to the redox graphite one.

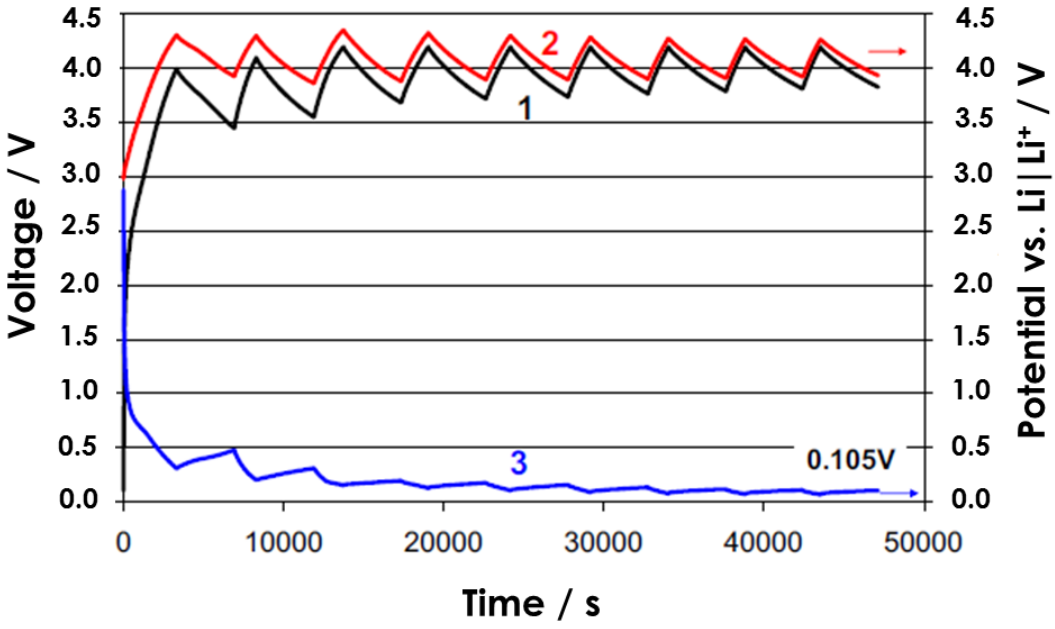

Figure 26 Pre-lithiation of graphite from the electrolyte at C/10 in a cell using graphite as negative electrode and AC as positive one; a lithium reference electrode is added to monitor the potentials of both electrodes: (1-black) voltage, (2-red) and (3-blue) potential profiles of the positive and negative electrodes. Each charge pulse is followed by a 60 min OCV period. The electrolyte was 2 mol/L LiTFSI in EC/DMC 1:1.

Notwithstanding, even though there is an excess of lithium ions in the electrolyte, the pre-lithiation process leads to a noticeable depletion of electrolyte concentration. Consequently, it causes a decrease of conductivity which unfortunately leads to a reduction of power of the system.

I. 3.2.3. Pre-lithiation with lithium ions from a composite positive electrode

Recently, a new concept based on adding a selected cathode material (e.g. lithium metal oxide - LMO, from which lithium can be irreversibly extracted during the 1st charge of the cell) to the AC - based positive electrode has been presented. As in the previous case where lithium was taken from the electrolyte, this concept avoids the use of metallic lithium, but in this case it also avoids the depletion of electrolyte concentration. However, after the pre-lithiation step, dead mass remains in the positive electrode, which requires selecting cathodic materials of high irreversible capacity to reduce this negative impact. The first material used in this concept was lithium molybdate (Li_2MoO_3) of high total capacity of 270 mAh/g [203]. Figure 27 represents the scheme of a LIC cell where Li_2MoO_3 is used as lithium source material in the composition of the positive electrode [203]. However, the lithium extraction from Li_2MoO_3 is completed at a potential (4.7 V vs. Li/Li^+) which is higher than the oxidation limit of the electrolyte (~4.5 V vs. Li/Li^+ for 1.3 mol/L $LiPF_6$ in EC:DMC). Additionally, around 30% of lithium ions may be re-inserted into the cathode material, and thus cause perturbations in the operation of the LIC.

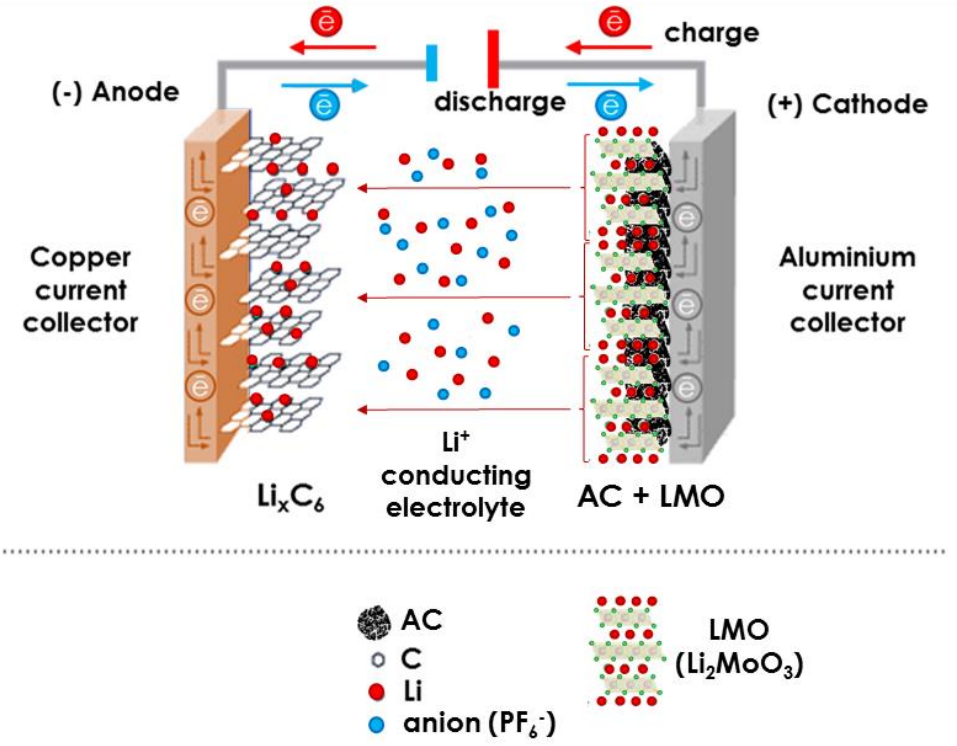

Figure 27 Schematic representation of a LIC with a composite positive electrode including a material from which lithium maybe irreversibly extracted during the 1st charge [203].

In the following years, Park *et al*. proposed some improvements to the described concept. The most important one was the addition of Li_2RuO_3 (LRuO) to the already existing positive electrode [204]. The composite positive electrode contained 64.4 wt.% of activated carbon, 25.6 wt.% of LMoO and LRuO was added in amount of 5 wt.% or 10 wt.% (at the expense of the amount of activated carbon). Since the value of irreversible capacity for lithium ruthenium oxide is close to 5%, this additive was expected to boost the energy of the previous system also at low current. Nevertheless, lithium extraction from the presented composite appears still at around 4.7 V vs. Li/Li^+. Another attempt was based on utilizing lithium iron oxide (Li_5FeO_4) with a high irreversible capacity of 680 mAh/g [205]. However, the extraction process is again completed at 4.7 V vs. Li/Li^+; in addition, Li_5FeO_4 is easily oxidized and cannot be handled in air.

Nonetheless, the recently introduced lithium cobalt oxide (Li_6CoO_4, LCoO) finally appears as an alternative to all the previously mentioned materials where lithium extraction takes place at high potential [206]. Beside the high value of irreversible capacity which accompanies extraction of lithium from Li_6CoO_4 (600 mAh/g), the process is completed at much lower potential (4.3 V vs. Li/Li^+) than with the other oxides. Thereby, the absence of side reactions (such as electrolyte oxidation) during the pre-lithiation step leads to an improved cycle life of the LIC. Figure 28 shows the potential profiles of the positive electrode (a) and negative electrode (b) during the charge of a beaker-type of cell constituted of AC/ Li_6CoO_4 positive electrode and hard carbon as negative one in 1.3 mol/L $LiPF_6$ dissolved in EC/DMC. As it can be seen, if Li_6CoO_4 is present in the composition of the positive electrode (Figure 28a, PE with Li_6CoO_4) more lithium is available in comparison to the AC positive electrode without Li_6CoO_4. Figure 28b demonstrates a much higher doping capacity of the negative carbon electrode, ca. 1.1 mAh, which is also evidenced by the lower value of the reached potential ca. 0.2 V vs. Li/Li^+. The authors have observed an improved cycle life of this cell in comparison to a conventional LIC where the carbon electrode was pre-lithiated with metallic lithium [206]. Two cells were compared in the voltage range from 1.5 to 3.9 V at a constant current rate 10C; the electrolyte was 1.3 mol/L $LiPF_6$ dissolved in EC/DMC. In case of the cell doped with Li_6CoO_4, the capacitance retention after 1000 cycles was 98.8 %, whereas using metallic lithium for doping it was 70.5 %.

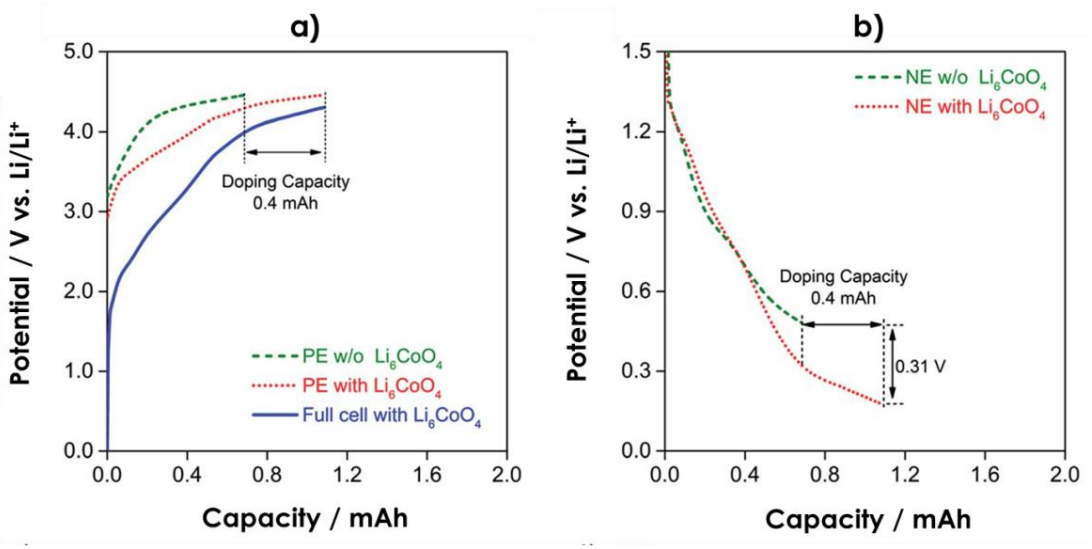

Figure 28 Galvanostatic profiles during charging of a cell constituted of hard carbon negative electrode and Li_6CoO_4 /AC or AC positive one in 1.3 mol/L $LiPF_6$ dissolved in EC/DMC electrolyte: a) potential profile of the positive electrode with Li_6CoO_4 as sacrificial lithium source (PE with Li_6CoO_4 – red dotted line) and without Li_6CoO_4 (PE w/o Li_6CoO_4 – green dashed line); the voltage profile of the full cell with Li_6CoO_4 as lithium source for the pre-lithiation is represented as blue solid line; b) potential profile during pre-lithiation of the negative electrode with the Li_6CoO_4 /AC composite positive electrode (NE with Li_6CoO_4 – red dotted line) and without Li_6CoO_4 in the positive electrode (green dashed line).

This part of the manuscript aimed to reveal that each method to pre-lithiate the anode material has its pros and cons. It particularly demonstrated that the use of an internal source of lithium incorporated in the positive composite electrode is one of the most interesting approaches in the LICs field, provided that materials with high irreversible capacity are applied (to reduce the dead mass in the positive electrode) and that lithium can be extracted at relatively low potential. The perspective to eliminate metallic lithium without perturbing the electrolyte conductivity is attractive.

Conclusion

The concept of LIC with sacrificial lithium source incorporated together with activated carbon in the positive electrode seems the most interesting at the time. It simplifies the construction of the electrochemical cell and avoids depletion of lithium ions concentration

in the electrolytic solution. The materials used so far are lithiated metal oxides with either small amount of available lithium or high potential of lithium extraction. In addition, all the studies involving sacrificial metal oxides were done in a beaker type of cell, without attempting to build any prototype.

It would be interesting for the purpose of this thesis to develop LIC systems with a composite positive electrode including compounds of high irreversible capacity from which lithium ions can be extracted at potential lower than 4.2 V vs. Li/Li^+. The objective would be to reduce the proportion of this compound in the positive electrode, while being able to reach at the least the LiC_{12} graphite intercalation compound (GIC) and more preferably LiC_6. Of course, to do that it requires to establishing an optimized protocol for the pre-lithiation of graphite, using an already known cathode material with low extraction potential; this material will be a part of the positive electrode composition together with activated carbon. Basic system parameters such as safe operational voltage of the electrochemical cell and current density will be established.

The next step will be to synthesize novel materials with high amount of lithium ions, to reduce their amount in the composite positive electrode. Finally, renewable materials, such as lithiated organic compounds (mentioned in paragraph I. 2.2.4.), will be considered as "green" and cheap source of lithium ions at relatively low extraction potential. Such organic materials will be also used to develop the first pouch lithium-ion capacitor implementing a sacrificial material for graphite pre-lithiation.

CHAPTER II

Establishing the pre-lithiation conditions

Introduction

To establish conditions for the pre-lithiation of the negative electrode in LICs, it is necessary to find a material from which lithium ions are irreversibly extracted. What is more, the process should take place at potential below 4.5 V vs. Li/Li^+ in order to prevent undesirable side reactions, such as oxidation of the positive electrode during cycling. The first material investigated as a possible source of lithium ions to pre-lithiate the graphite electrode in lithium-ion capacitor was layered lithium nickel oxide ($Li_{1-X}Ni_{1+X}O_2$; LNiO). According to Rougier *et al.* [102], lithium is reversibly extracted at potential ca. 4.0 V vs. Li/Li^+ from the lithium-deficient lithium nickel oxides; however, the reaction becomes irreversible if the lithium ions deficiency x is greater than 0.2 (Figure 29) [102].

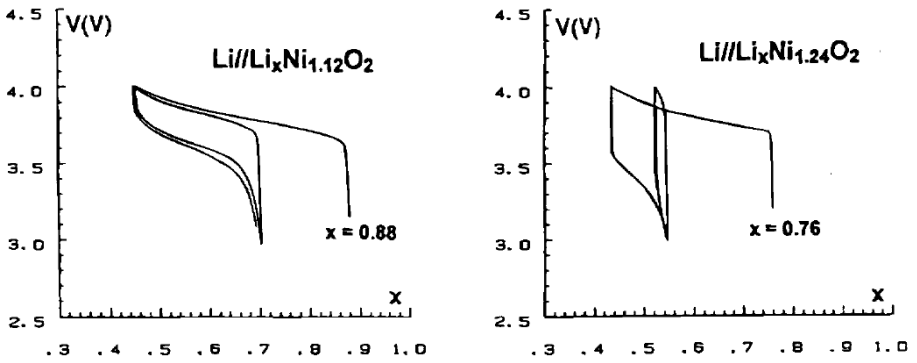

Figure 29 Variation of the cell voltage vs. composition for the first two charge/discharge cycles of $Li/LiNi_{x+1}O_2$ cells (x = 0.12, 0.24) under a current density of 280 pA/cm^2 [102].

Therefore, lithium nickel oxide with the composition $Li_{0.65}Ni_{1.35}O_2$ was used as a reservoir of lithium ions in the positive composite electrode for graphite pre-lithiation in a LIC. The study performed on $Li_{0.65}Ni_{1.35}O_2$ was intended to allow establishing and optimizing the pre-lithiation conditions for the future chapters III, IV and V dedicated to the use of sacrificial materials with higher lithium content and/or lower extraction potential. All the experiments were performed in an El-Cell type of cell which does not contain any excess of electrolyte as it is for the beaker type of cell, as used by Park *et al.* [203,204,205,206]

II. 1. Synthesis and structural characterization of $Li_{0.65}Ni_{1.35}O_2$

In our study, the $Li_{0.65}Ni_{1.35}O_2$ composition was chosen to maintain the conditions for irreversible lithium ions extraction [102]. To synthesize this non-stoichiometric lithium nickel oxide, lithium carbonate (Li_2CO_3) and nickel (II) oxide (NiO) were mixed in molar ratio NiO/Li_2CO_3 = 4.15 in a mortar for 30 min, mixture was sintered at 600 °C hold time 10 h under air, cooled down to room temperature, grinded and then sintered at 700 °C for 15 h (Figure 30). The elemental composition of the material has been confirmed to be $Li_{0.65}Ni_{1.35}O_2$ by atomic absorption spectroscopy.

The XRD pattern of the synthesized $Li_{0.65}Ni_{1.35}O_2$ material is presented in Figure 30. According to the full pattern matching based on Rietveld refinement, the material is a pure lithium nickel oxide phase crystallizing in the trigonal symmetry (R3m) of lattice parameters: a = 0.29055(3) nm, b = 0.29055(3) nm and c = 1.42541(6) nm (c/a ratio = 4.905) with R_{WP} parameter equal to 3.31. These data are in good agreement with the work of Rougier *et al.* [102] as reported in Table 1. The higher value of *a* for the synthesized material is related to the higher amount of divalent nickel ions between the planes. The *c/a* ratio (*c/a* = represents established Li/Ni order) illustrates the change in the cubic symmetry of lithium nickel oxide. Furthermore, the increase of the Ni-O (S_{NiO}) distance and decrease of *z* reveals the presence of additional divalent nickel ions within the NiO_2 slab. The higher deviation of the oxygen position from the 0.25 value along the c-axis when *a* decreases can be attributed to the increase of the structural anisotropy.

This structural modification enlarges the Li-O_2 interslab space and narrows the Ni-O_2 slab. As it can be seen, the materials presented in Table 1 are characterized by a different thickness of the slab, S_{Ni-O2}, and of the interslab space. This shrinkage of the interslab space thickness I_{Li-O2}, is related to the presence of divalent nickel ions, partially replacing lithium ions, causing a steric effect and electrostatic interactions among the divalent nickel and oxygen. The observed evolution of the interslab thickness vs. the amount of extra nickel ions has a great impact on the electrochemical behavior. Therefore, the electrochemical performance of the $Li_{0.65}Ni_{1.35}O_2$ electrode will be presented in the following part of this chapter (section 2).

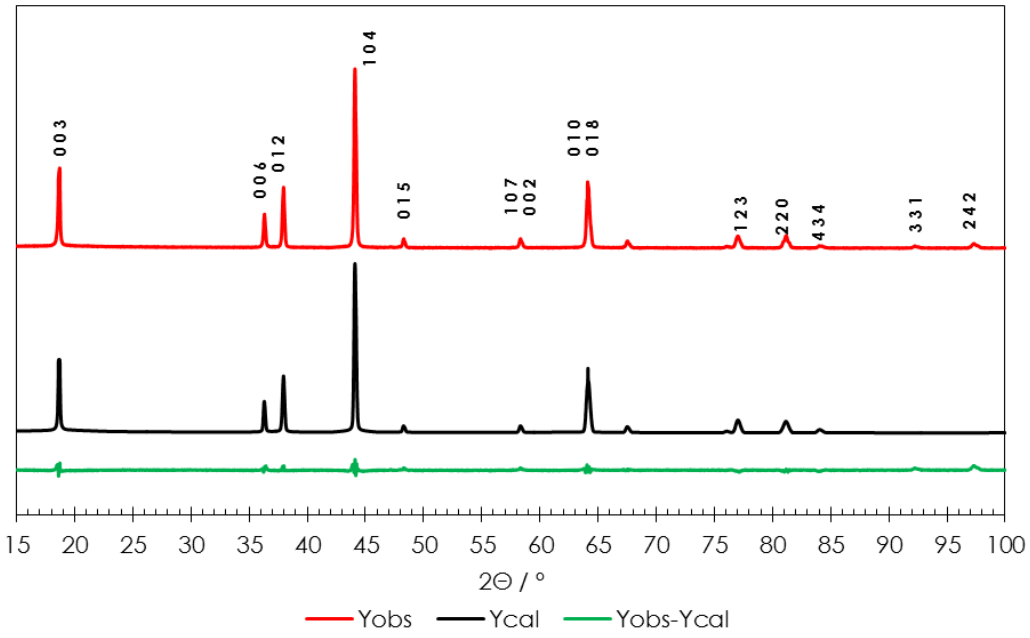

Figure 30 XRD characterization of the synthesized $Li_{0.65}Ni_{1.35}O_2$. Red: experimental diagram;black: calculated diagram; green: difference between observed and calculated data.

Table 1 Cell parameters of the synthesized $Li_{0.65}Ni_{1.35}O_2$ material obtained from full pattern matching based on Rietveld refinement. $I_{Li\text{-}O2}$ interslab space, $S_{Ni\text{-}O2}$ thickness of the Ni-O slab, z_{ox} position of the oxygen atoms, R_{WP} – correlation between observed and calculated diffractograms. For comparison the data published by Rougier et al. [102] are included.

Composition	*a* [nm]	*c* [nm]	*c/a*	z_{ox}	$S_{Ni\text{-}O2}$ [nm]	$I_{Li\text{-}O2}$ [nm]	R_{wp}
$Li_{0.95}Ni_{1.05}O_2$ [102]	0.28807	1.42092	4.931	0.2588	0.2118	0.2618	9.6
$Li_{0.90}Ni_{1.10}O_2$ [102]	0.28879	1.42330	4.928	0.2579	0.2147	0.2597	8.4
$Li_{0.80}Ni_{1.20}O_2$ [102]	0.28965	1.42460	4.919	0.2577	0.2154	0.2594	8.2
$Li_{0.65}Ni_{1.35}O_2$	**0.29055**	**1.42541**	**4.905**	**0.2561**	**0.2226**	**0.2530**	**3.3**
$R_{WP}^2 = \left[\frac{\sum w(y_{obs.} - y_{calc.})^2}{\sum w(y_{obs.})^2}\right]$		All data points were taken under consideration; $y_{obs.}$ and $y_{calc.}$ correspond to the observed and calculated count numbers for a data point, respectively.					

II. 2. Electrochemical extraction of lithium ions from sacrificial metal oxide $Li_{0.65}Ni_{1.35}O_2$

Lithium nickel oxide was electrochemically investigated in half-cells with metallic lithium as both reference and counter electrode, and the electrolyte was 1 mol/L $LiPF_6$. Due to the resistive character of $LiNiO_2$ [102], a relatively high amount of carbon black is required to enhance the electrode conductivity. Therefore, the positive electrode was composed of 65 wt.% lithium nickel oxide ($Li_{0.65}Ni_{1.35}O_2$), 10 wt.% polyvinylidene fluoride (PVdF) binder dispersed in 1-methyl-2-pyrrolidinone (NMP) and 25 wt.% conductive additive Super C65 (Imerys). The detailed procedure for coated electrode preparation, cell assembly and electrochemical conditions are given in the experimental annex (A.3).

The 3-electrode cyclic voltammogram of $Li_{0.65}Ni_{1.35}O_2$ in Figure 31a clearly shows that the extraction of lithium ions takes place during the first anodic scan in the potential range of 4.1–4.3 V vs. Li/Li^+ (red curve). Interestingly, no current peak is observed during the subsequent cathodic scan, thus confirming the irreversible lithium extraction. During the 2^{nd} cycle (green curve), the anodic current is negligible at 4.2–4.3 V, revealing that the major part of lithium is extracted from $Li_{0.65}Ni_{1.35}O_2$. The specific capacity of $Li_{0.65}Ni_{1.35}O_2$ was determined by galvanostatic charge/discharge (Figure 31b). At C/20 (charge within 20 h), the measured gravimetric capacity is close to 120 mAh/g, in good agreement with previous studies [102]. Figure 31b also reveals the irreversible character of the extraction reaction since, after the first oxidation, less than 20 mAh/g can be recovered upon subsequent reduction of the electrode. Upon further cycling, no other electrochemical activity was measured for this material.

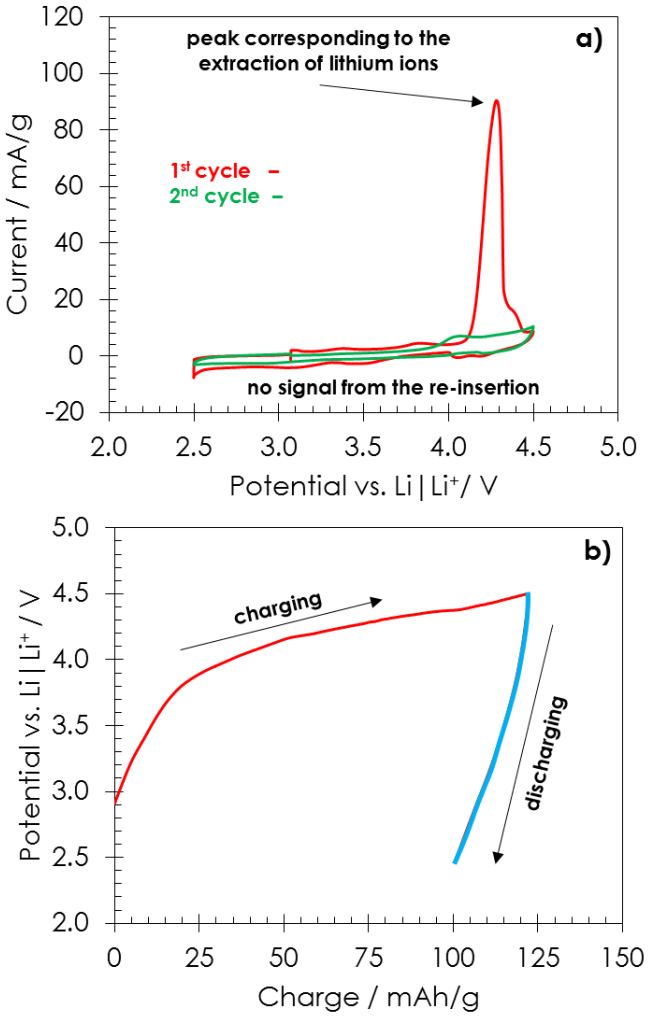

Figure 31 a) Cyclic voltammogram of the $Li_{0.65}Ni_{1.35}O_2$ electrode (scan rate 0.06 mV/s) in 1mol/L $LiPF_6$ electrolyte. The red curve shows the first cycle with extraction of lithium ions at ca. 4.2 V vs. Li/Li^+. The second cycle is represented by the green line. b) Galvanostatic charge/discharge profile of $Li_{0.65}Ni_{1.35}O_2$ at C/20. Both types of curves were recorded vs. Li/Li^+ reference electrode.

II. 3. Pre-lithiation of graphite with $Li_{0.65}Ni_{1.35}O_2$ in a full cell configuration

The irreversible specific capacity determined for $Li_{0.65}Ni_{1.35}O_2$ makes it possible to tune the electrodes compositions in a LIC and to balance the graphite and activated carbon electrode masses together with the $Li_{0.65}Ni_{1.35}O_2$ one. The amount of lithium nickel oxide was set as low as possible and adjusted to obtain at least the second stage intercalation compound LiC_{12}. A separated experiment realized in a graphite/lithium cell at C/20 showed that

approximately 220 mAh/g are required to successively form the S.E.I. and the LiC_{12} compound because of the relatively low lithium content in the LiNiO composition.

Taking into account the practical irreversible capacity of LNiO ($Q_{LNiO} = 120$ mAh/g) and the capacity to form the second stage intercalation of graphite ($Q_G = 220$ mAh/g), in order to reach the composition LIC_{12} with lithium ions coming from LNiO, it is necessary to fulfill the requirement (19):

$$m_{LNiO} \cdot Q_{LNiO} = m_G \cdot Q_G \qquad (19).$$

Hence, 1.83 mass units of LNiO are necessary to intercalate 1 mass unit of graphite. Since m_G should be equal to m_{AC} to optimize the energy and power density [201], and taking into account that the positive electrode contains 80% of electrochemically active materials (AC + LiNO, the remaining is 5 wt.% PVdF binder and 15 wt.% of Super C65), it comes that 55 wt. % of LNiO is necessary in the LNiO/AC composite to reach the second stage graphite intercalation compound LiC_{12}, and consequently that the amount of activated carbon is 25 wt.%.

Figure 32 shows the galvanostatic pre-lithiation of graphite used as negative electrode in a cell with $LiPF_6$ electrolyte, where the positive electrode is composed of a mixture of activated carbon and $Li_{0.65}Ni_{1.35}O_2$; $Li_{0.65}Ni_{1.35}O_2$ is the active material during this step, and the potentials of both electrodes are recorded vs. a metallic lithium electrode used as reference. The S.E.I. formation and intercalation in the graphite electrode was performed at C/20 until reaching one of the potential limits: 4.5 V vs. Li/Li^+ for the positive electrode to avoid electrolyte oxidation or 0.01 V vs. Li/Li^+ for the negative electrode to avoid lithium plating. As it can be seen in Figure 32a, the capacity at the end of charge is only 160 mAh/g, and it is relatively far from the required value of ca. 220 mAh/g to form the second stage graphite intercalation compound.

Notwithstanding, we decided to cycle the LIC thus obtained at 0.25 A/g in the voltage range 2.2 – 4.3 V, and the result is shown in Figure 32b. After 200 cycles, the capacitance of the LIC starts already to drop and this drop is even accelerated when increasing the current to 0.5 A/g. Hence, this property seems to support the generally accepted statement

that at least the second stage intercalation compound should be formed for a good cyclic performance of the LIC [207].

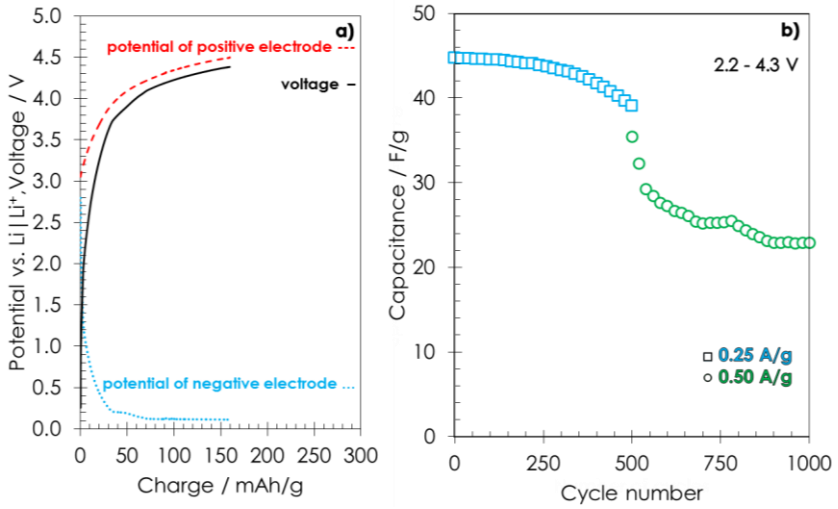

Figure 32 a) Galvanostatic pre-lithiation of graphite in a cell using a composite AC/$Li_{0.65}Ni_{1.35}O_2$ electrode as lithium source. The S.E.I. and lithium intercalation into graphite is done at C/20. The potential limits for positive and negative electrodes are 4.50 V and 0.01 V vs. Li/Li^+. Colors of the curves: red for the potential of positive electrode; blue for the potential of negative electrode; black for the voltage profile. The electrolyte is 1 mol/L $LiPF_6$ in 1:1 EC/DMC. Li/Li^+ is the reference electrode; b) Cycling performance of the LIC cell at 0.25 A/g (blue squares), 0.50 A/g (green circles) (current expressed per mass of activated carbon) in the voltage range from 2.2 V to 4.3 V. The capacitance values are expressed per total mass of both electrodes.

II. 4. Modification of the procedure for graphite pre-lithiation with AC/$Li_{0.65}Ni_{1.35}O_2$ as lithium source

To reach the second stage graphite intercalation compound, while having the same amount of LNiO in the positive electrode, we decided to change the electrochemical conditions for graphite pre-lithiation. First, the S.E.I. was formed at C/5 instead of C/20 (C is the capacity to reach the composition LiC_6) until reaching a potential of 0.2 V vs Li/Li^+, which is assumed to be the end of S.E.I. formation. This relatively higher value of current was selected according to reference [180] in order to form a thin passive layer (S.E.I.) and consequently to reduce as much as possible the resistance of the negative electrode and to enhance the cycle life of the system. Thereafter, lithium was intercalated in the graphite electrode at C/20 until reaching one of the potential limits: 4.5 V vs. Li/Li^+ for the positive

electrode to avoid electrolyte oxidation, or 0.01 V vs. Li/Li^+ for the negative electrode to avoid lithium plating. Nonetheless, as shown in Figure 33, this procedure did not allow to reach the potential corresponding to the formation of LiC_{12} (100 mV vs. Li/Li^+) [186]. Once more, as in the previous conditions, it seems that the amount of lithium contained in the positive composite electrode is not sufficient to enable the formation of the S.E.I. and second stage LiC_{12}.Therefore, as suggested in reference [180], we have decided to apply sequences of 2 h rest period followed by current pulse at C/20 in order to involve a part of lithium ions contained in the electrolyte in the intercalation process; as shown in Figure 33, the pulses were applied until reaching the potential of 100 mV vs. Li/Li^+ for the negative electrode (Figure 33).

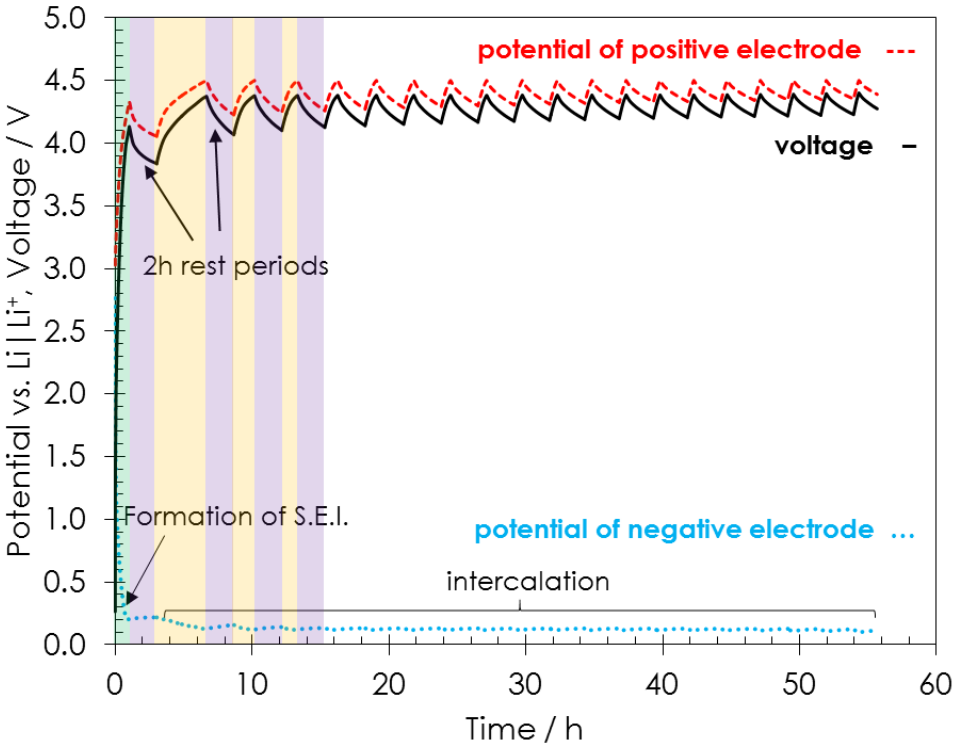

Figure 33 Galvanostatic pre-lithiation of graphite in a cell using a composite AC/ $Li_{0.65}Ni_{1.35}O_2$ positive electrode as lithium source. The S.E.I. (area highlighted in green) is created at C/5 and lithium is intercalated into graphite at C/20 (dotted lines). The potential limits for positive and negative electrodes are 4.50 V and 0.01 V vs. Li/Li^+, respectively; rest periods of 2 h were applied when one of these limiting criteria was reached. Colors of the curves: red for the potential of positive electrode; blue for the potential of negative electrode; black for the cell voltage profile. The electrolyte is 1 mol/L $LiPF_6$ in 1:1 EC:DMC. Li/Li^+ is the reference electrode.

Figure 34 shows a transformation of Figure 33, where the time involved in the relaxation periods was not taken into account, enabling thereof to determine the total charge capacity to form the S.E.I. and to lithiate graphite at the negative electrode; it gives a nonrealistic value of 380 mAh/g (Figure 34a). In fact, one must take into account that, after each relaxation period, some charge is consumed to reach the potential of the graphite electrode just before the relaxation. This charge has been subtracted for all sequences, giving the green curve presented in Figure 34b; the total charge used for S.E.I. formation and lithium intercalation into graphite is then 220 mAh/g. Interestingly, we have superimposed on the same Figure 34b in black dashed–dotted line the profile obtained for graphite intercalation/deintercalation in a cell using a metallic lithium disk as counter and reference electrode. The two profiles are identical, confirming that the procedure which we used to process the data of the cell with sacrificial LNiO is correct. It is also interesting to observe that the green curve just finishes when the formation of the second stage graphite intercalation compound is completed.

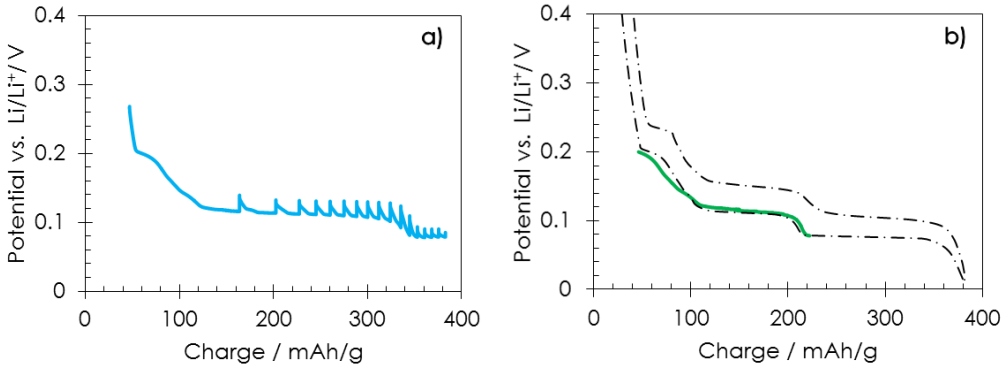

Figure 34 Part of Figure 33 after S.E.I. formation presenting galvanostatic (current pulses of C/20) pre-lithiation of graphite in a cell using a composite AC/$Li_{0.65}Ni_{1.35}O_2$ positive electrode as lithium source: a) cumulated capacity (blue solid line); b) cumulated capacity after subtracting the capacity involved after each relaxation period to reach the same electrode potential as before relaxation (green solid line) and profile of lithium intercalation into graphite using a cell where metallic lithium is the counter and reference electrode (black dashed–dotted line).

After the pre-lithiation step, the residual Li-Ni-O oxide is inactive and only AC is electrochemically active in the positive electrode. Hence, the LIC cells have been cycled at various values of current density expressed per gram of activated carbon 0.25 A/g, 0.50 A/g and 0.65 A/g) in the voltage range from 2.0 V to 4.3 V. Figure 35 shows the potential

profiles of the positive (dashed red) and negative (dotted blue) electrodes and the voltage profile of the cells (solid black) for the first galvanostatic cycles. In all cases, the voltage profile of the cell exhibits the triangular shape typical of a capacitive behavior (Figure 35).

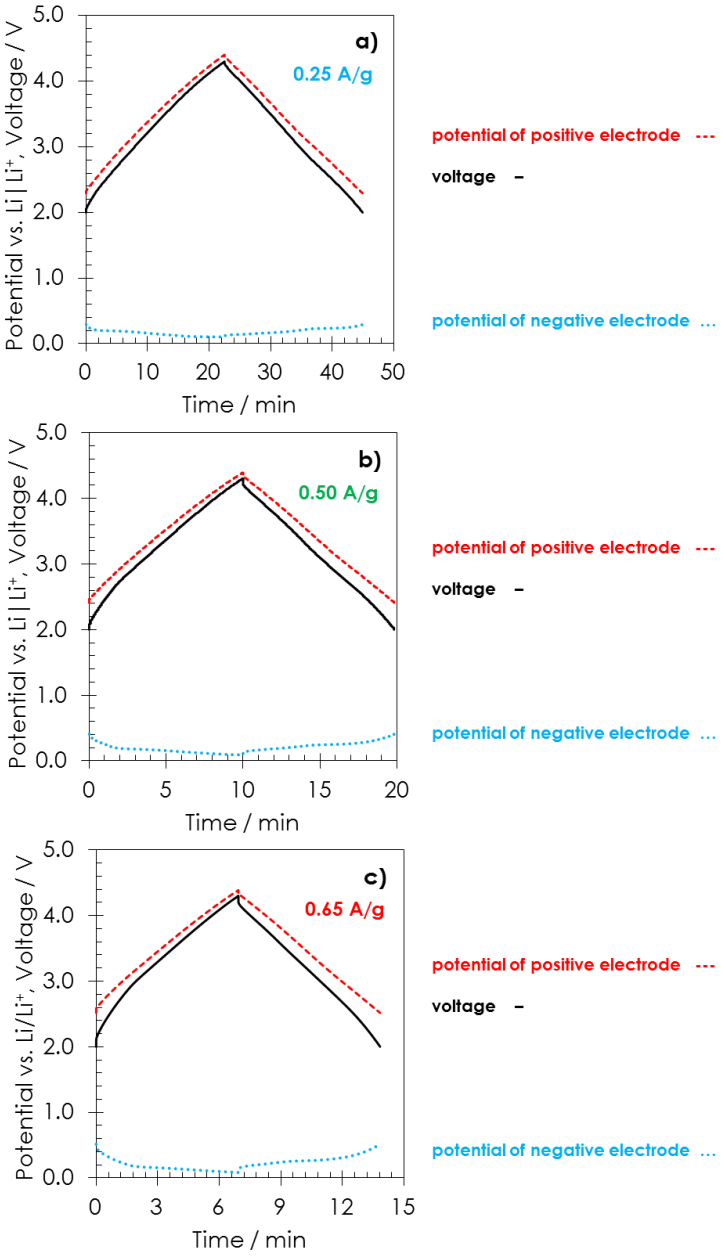

Figure 35 Typical galvanostatic charge/discharge profiles recorded for a LIC where prelithiation of graphite was realized with an AC/$Li_{0.65}Ni_{1.35}O_2$ positive electrode: a) 800th cycle at 0.25 A/g; b) 1300th cycle at 0.50 A/g; c) 1800th cycle at 0.65 A/g. Voltage profile of LIC (solid black); potential profiles of positive electrode (dashed red) and negative electrode (dotted blue). The values of current density are expressed per gram of activated carbon.

These plots clearly show that, independently on the current density used, the potential of the positive electrode is below 4.2 V and the potential of the graphite electrode above 80 mV.

Figure 36 showing the plot of capacitance vs. cycle number, demonstrates that the cell voltage range from 2.0 V to 4.3 V is not optimal for long cyclic life. The capacitance fade of 48 % after 1800 cycles suggests that the operating voltage of the LIC constructed with sacrificial lithium nickel oxide should probably be adjusted.

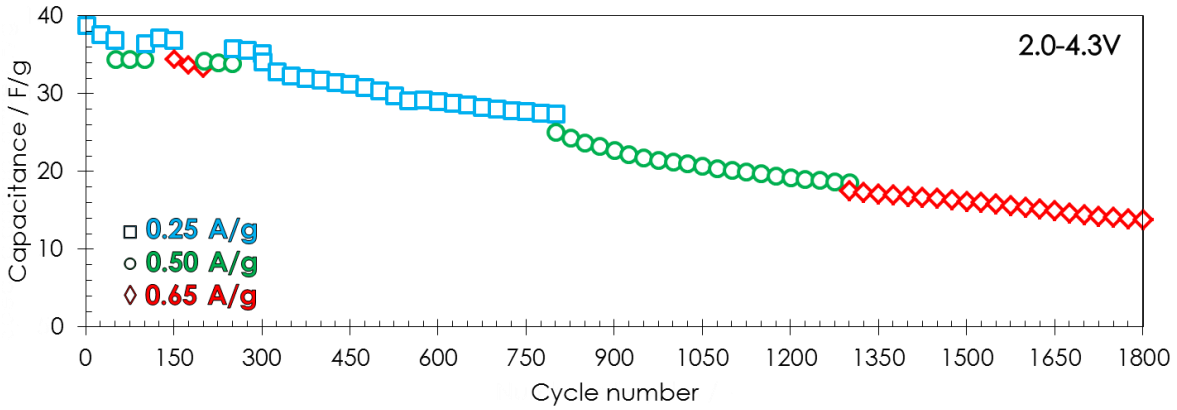

Figure 36 Cycling stability of the LIC where pre-lithiation of graphite was realized with an AC/$Li_{0.65}Ni_{1.35}O_2$ positive electrode. The current values expressed per gram of activated carbon are 0.25 A/g (blue squares), 0.50 A/g (green circles) and 0.65 A/g (red diamonds). The cell voltage range was from 2.0 V to 4.3 V. The first 300 galvanostatic charge/discharge cycles were performed in order to condition the system. The capacitance values are expressed per gram of electrode materials.

To disclose the reason for the poor cyclic performance of the LIC when operating in a potential range from 2.0 V to 4.3 V, it is necessary to look at the electrochemical performance of the residual composite electrode after Li extraction. Figure 37 shows the current response of this electrode for a cyclic voltammetry potential sweep from 1.5 V to 4.5 V vs. Li/Li^+. When the potential of this electrode is lower than 2.2 V vs. Li/Li^+, a negative current leap appears which is attributed to the formation of a S.E.I. layer on the surface of activated carbon. On the other side, the anodic peak seen at around 4.2 V vs. Li/Li^+ (which diminishes for the next cycle) is the most probably related to the extraction of lithium ions remaining in the lithium nickel oxide structure. Therefore, to obtain a stable

performance of the LIC system with sacrificial AC/LNiO electrode, it is necessary to adjust the operating voltage for avoiding that the potential of the positive electrode would not exceed its safe limits.

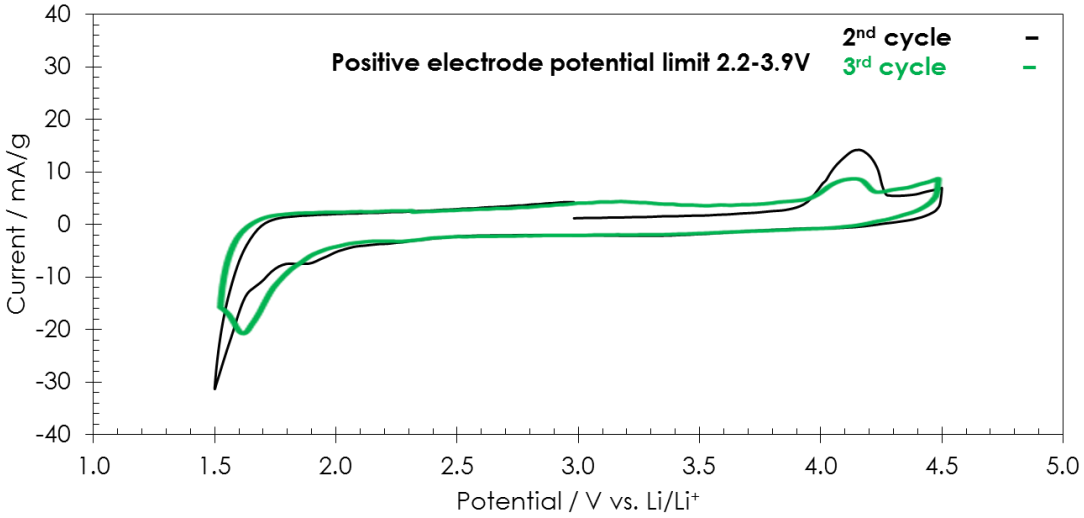

Figure 37 Cyclic voltammogram of the AC/$Li_{0.65}Ni_{1.35}O_2$ electrode in 1 mol/L $LiPF_6$ electrolyte (scan rate 0.06 mV/s) after galvanostatic extraction of lithium ions: from its structure up to ca. 4.5 V vs. Li/Li^+ 2nd cycle (black curve) and 3rd cycle (green curve).

II. 5. Adjustment of the operating voltage of the LIC with AC/LNiO positive electrode

Taking into account the above mentioned information, the LIC where graphite was lithiated with help of the AC/$Li_{0.65}Ni_{1.35}O_2$ composite electrode has been cycled at various values of current density expressed per gram of activated carbon (0.25 A/g, 0.50 A/g and 0.65 A/g) in the voltage range from 2.2 V to 3.8 V. Figure 38 shows the voltage profiles of the cell (solid black), and the potential profile of the positive (dashed red) and negative (dotted blue) electrodes, after 500 cycles at each current density. In all cases, the voltage profile of the cell exhibits the triangular shape typical of a capacitive behavior (Figure 38). These plots clearly show that, independently on the current density used, the potential of the positive electrode is below 3.9 V and the potential of the graphite electrode above 80 mV. It suggests that the cell voltage range from 2.2 V to 3.8 V should prevent from any electrolyte oxidation and S.E.I. formation at the positive electrode, and metallic lithium plating at the negative electrode.

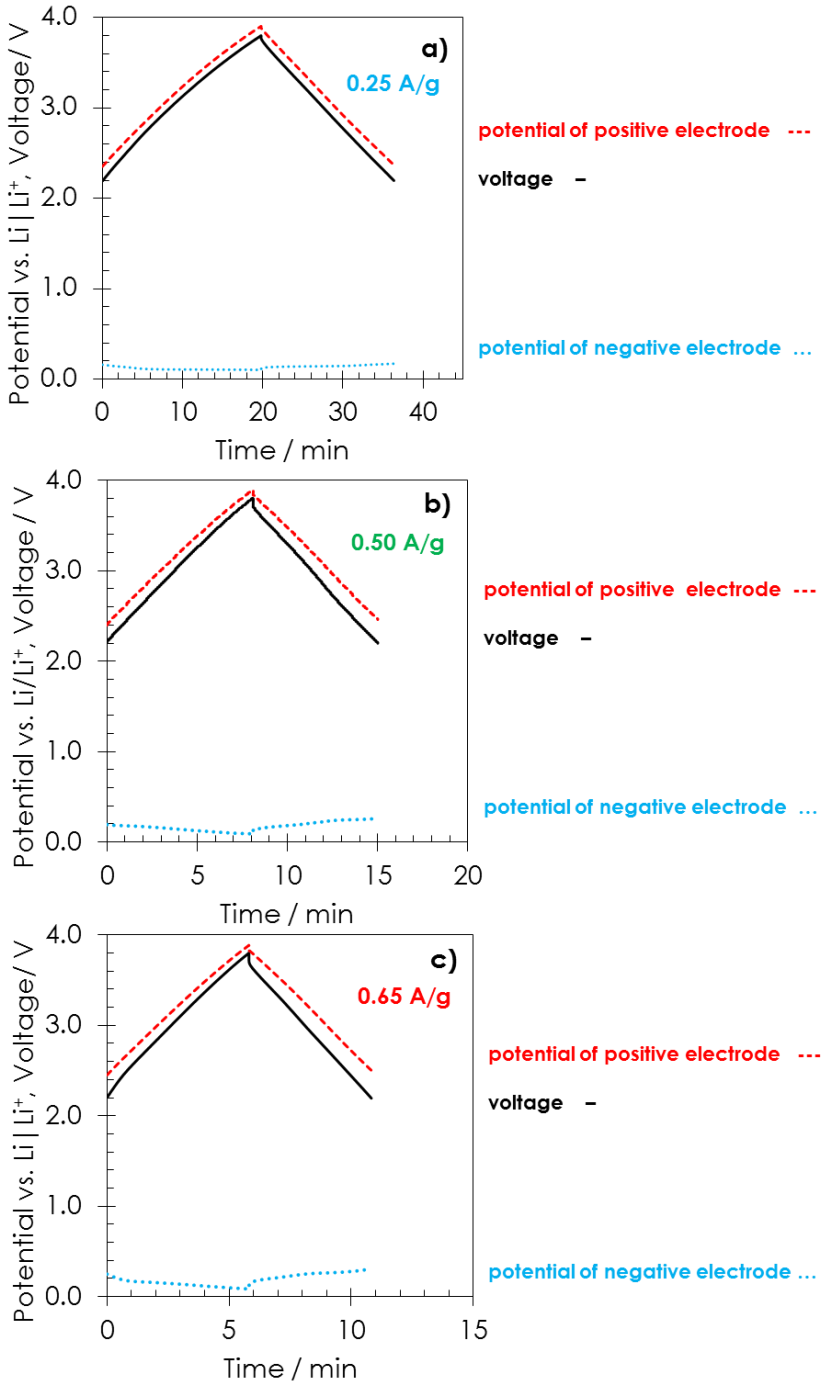

Figure 38 Galvanostatic charge/discharge profiles recorded for a LIC where pre-lithiation of graphite was realized with an AC/$Li_{0.65}Ni_{1.35}O_2$ positive electrode: a) 800th cycle at 0.25 A/g; b) 1300th cycle at 0.50 A/g; c) 1800th cycle at 0.65 A/g. Voltage profile of LIC (solid black); potential profile of positive electrode (dashed red) and negative electrode (dotted blue). The values of current density are expressed per gram of activated carbon.

Figure 39 showing the plot of capacitance vs. cycle number in the voltage range 2.2 – 3.8 V confirms that this new voltage limit allows to gain a more stable cycle performance of the LIC. As in previous experiments, during the first 300 cycles, the cell was cycled at 0.25, 0.50 and 0.65 A/g (currents expressed per mass of activated carbon, corresponding to C/2, C and 1.5C rates for the graphite electrode). At 0.25 A/g, a specific capacitance of 32 F/g was observed (capacitance expressed per total mass of electrodes); the capacitance values at 0.50 A/g and 0.65 A/g are 30 F/g and 25 F/g, respectively. In Figure 39, it also seen that, when returning to 0.25 A/g after the first 300 cycles, the initial capacitance is recovered without any noticeable fade. After 1800 cycles, the capacitance is 22 F/g at 0.65 A/g as compared to the initial value of 28 F/g after 150 cycles at this current density. Hence, the fade is of the order of 22% showing that the LIC constructed with sacrificial lithium nickel oxide is a system which requires improvements.

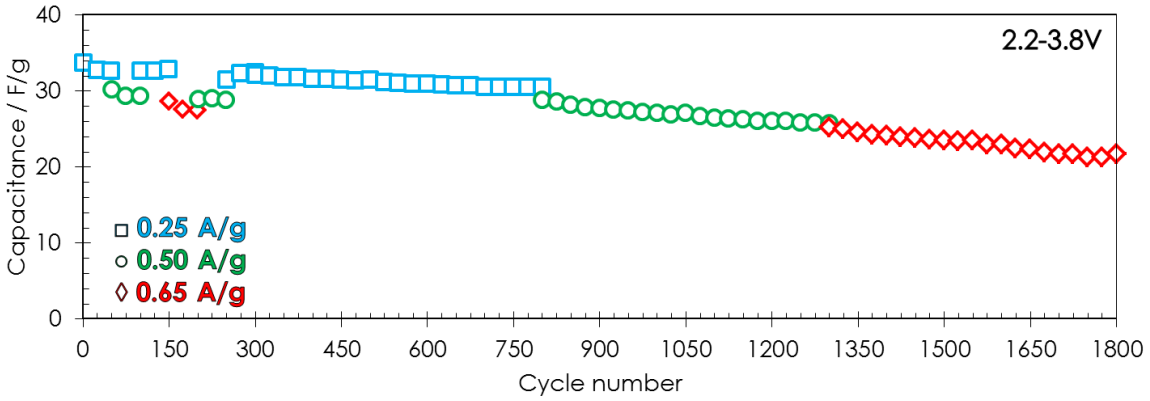

Figure 39 Cycling stability of the LIC where prelithiation of graphite was realized with an AC/$Li_{0.65}Ni_{1.35}O_2$ positive electrode. The current values expressed per gram of activated carbon are 0.25 A/g (blue squares), 0.50 A/g (green circles) and 0.65 A/g (red diamonds). The cell voltage was from 2.2 V to 3.8 V. The first 300 galvanostatic charge/discharge cycles were performed in order to condition the system. The current values are expressed per gram of activated carbon and the capacitance values per total mass of electrodes.

The Ragone plot of the previous LIC operating in the voltage range from 2.2 to 3.8 V is compared in Figure 40 with the plots of EDLCs implementing the same AC either 1 mol/L $TEABF_4$ in ACN or 1mol/L $LiPF_6$ in EC:DMC at a voltage up to 2.7 V. As expected, the specific energy is higher for the LIC than for the EDLCs. However, due to the relatively high amount of $Li_{0.65}Ni_{1.35}O_2$ in the positive electrode and also to the relatively low

capacity of this oxide, the energy of the LIC is not as high as expected. Besides, at high power, the extracted energy drops quite noticeably; this is obviously due to the low conductivity of the residual oxide in the positive electrode. At 0.1 kW/kg, the specific energy is around 15 – 20 Wh/kg which is very close to the values for the traditional symmetric EC systems in 1 mol/L $TEABF_4$ in ACN or 1mol/L $LiPF_6$ in EC:DMC.

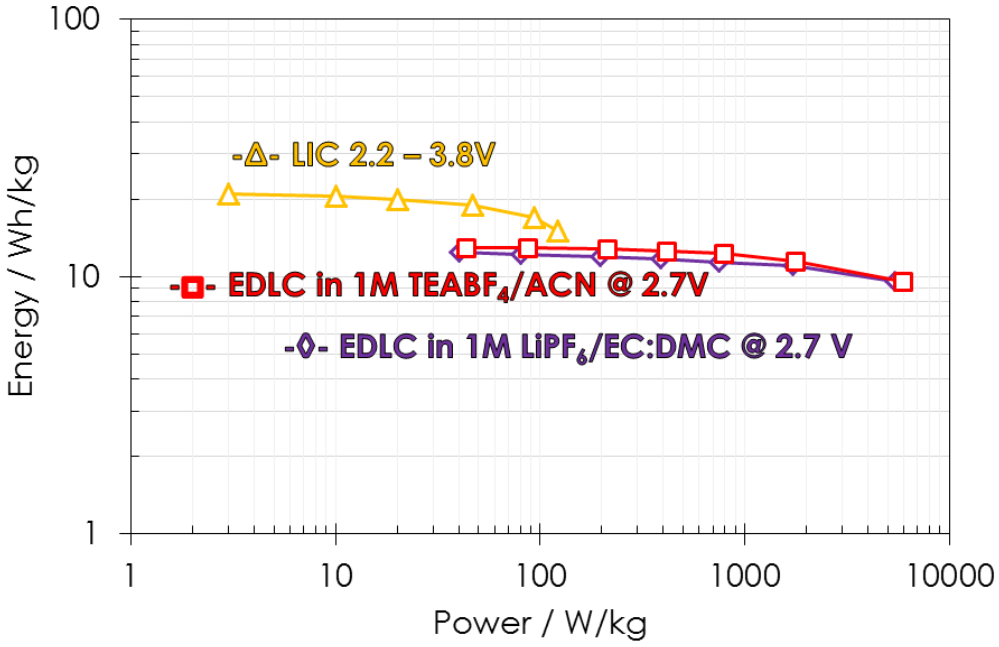

Figure 40 Comparative Ragone plots of EDLCs and of the LIC where prelithiation of graphite was realized with an AC/$Li_{0.65}Ni_{1.35}O_2$ composite electrode. The voltage range was 2.2 – 3.8 V for the LIC and 0 – 2.7 V for the EDLCs using the same activated carbon either in 1 mol/L $LiPF_6$ in EC:DMC or 1 mol/L $TEABF_4$ in acetonitrile.

II. 6. Improvement of the positive electrode conductivity by introducing MWCNTs to the AC/$Li_{0.65}Ni_{1.35}O_2$ composite

As shown in Figure 40, the LIC where graphite has been lithiated with help of an AC/$Li_{0.65}Ni_{1.35}O_2$ composite electrode displays a relatively fair power output. It means that the nanoparticles of lithium nickel oxide hinder the effective electron transport between the AC cores. Besides, the high temperature of annealing required to obtain the $Li_{0.65}Ni_{1.35}O_2$/AC electrode can also result in semiconductive properties of the positive electrode. Therefore, to boost the power of the LIC and enhance the conductivity of the

AC/LiNiO electrode, multiwalled carbon nanotubes (as-received MWCNTs, 5 wt.%) have been added together with of carbon black in the positive electrode. Assuming that MWCNTs allow better charge propagation and diffusion of ions in the electrode, owing to their mesoporous character, the amount of $Li_{0.65}Ni_{1.35}O_2$ in the AC/$Li_{0.65}Ni_{1.35}O_2$ composite electrode has been slightly reduced to 45 wt.% (10% wt. lower than in the previous composite), and the AC content increased to 35 wt.%.

The impedance spectroscopy data reveal the difference in resistivity of the LICs where Super C65 (Figure 41a) or Super C65 + MWCNTs (Figure 41b) were used as conductive additive for the positive electrode, where the composition was as follows AC 35 wt.%, LNiO 45 wt.%, Super C65 10 wt.%, MWCNT 5 wt.% and PVdF 5 wt.%. Before pre-lithiation of graphite, both systems display comparable Nyquist plots with similar value of equivalent distributed resistance (EDR) of 11 Ohms, estimated by Z fitting. However, after the extraction of lithium from LNiO, the EDR value for the cell with only carbon black added is 59 Ohms, and almost two times lower (28 Ohms) when MWCNTs are also added in the positive composite electrode. The higher value of EDR after the extraction process is related to the resistive character of the oxide. A small increase of equivalent series resistance (ESR) from 2 Ohm to 6 Ohm can be also observed for both cells after the pre-lithiation step.

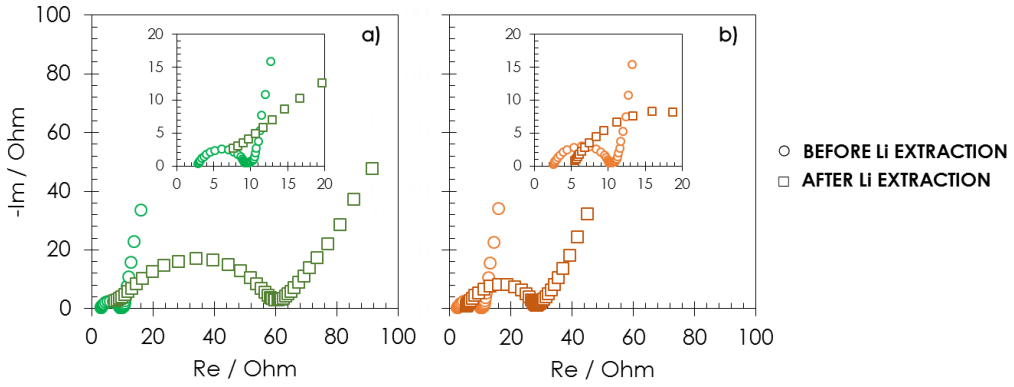

Figure 41 Nyquist plots of cells using a composite AC/$Li_{0.65}Ni_{1.35}O_2$ positive electrode containing a) only C65; b) a mixture of C65 and MWCNT as conductive agent. The data were collected before (circles) and after (squares) extraction of lithium ions from lithium nickel oxide. The composition of the electrode with only Super C65 was: AC 25 wt.%, LNiO 55 wt.%, Super C65 15 wt.% and PVdF 5 wt.%. For the electrode containing MWCNTs, it was: AC 35 wt.%, LNiO 45 wt.%, Super C65 10 wt.%, MWCNT 5 wt.% and PVdF 5 wt.%.

The cyclic performance of the LiC where the lithiation was realized with the AC/$Li_{0.65}Ni_{1.35}O_2$ electrode containing 5 wt.% of MWNTs is shown in Figure 42 in the voltage range from 2.2 V to 3.8 V. After the first 300 cycles during which the cell was formatted at 0.25, 0.50 and 0.65 A/g (currents expressed per mass of activated carbon), the capacitance measured at 0.25 A/g rapidly decays, and the trend is the same for higher values of current. As compared to Figure 39, where only Super C65 was used as conductive additive, the presence of MWCNTs in the positive electrode has a detrimental effect on the performance; the capacitance fades by more than 50% after 1800 cycles.

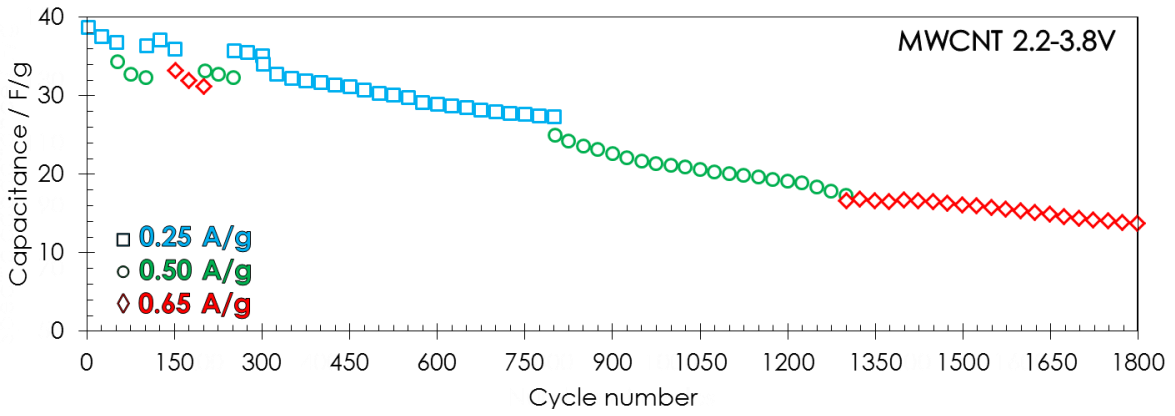

Figure 42 Cycling stability of the LIC where prelithiation of graphite was realized with an AC/$Li_{0.65}Ni_{1.35}O_2$ positive electrode containing 5 wt.% of MWCNTs + 5 wt.% Super C65. The current values expressed per gram of activated carbon are 0.25 A/g (blue squares), 0.50 A/g (green circles) and 0.65 A/g (red diamonds). The cell voltage range was from 2.2 V to 3.8 V. The capacitance values are expressed per total mass of electrodes.

Figure 43 presents the cyclic voltammogram of the AC/$Li_{0.65}Ni_{1.35}O_2$ composite electrode with addition of MWCNT (red line) after lithium extraction in the potential range of 1.5 – 4.5. V. For comparison, the CV of the same kind of electrode without MWCNTs additive (only Super C65) is also shown (black line). In case of the electrode containing MWCNTs, one can see a more intense negative current leap at potential below 2.5 V vs. Li/Li^+ , indicating a more developed S.E.I. formation on the surface of the electrode. This kind of phenomenon is not surprising, as previous work by Frackowiak *et al.* has demonstrated a huge irreversible capacity when as-received multiwalled carbon nanotubes are used as

negative electrode in a lithium cells [208]. Obviously, the residual metal catalyst remaining in the nanotubes after their fabrication could also contribute to this irreversible behavior.

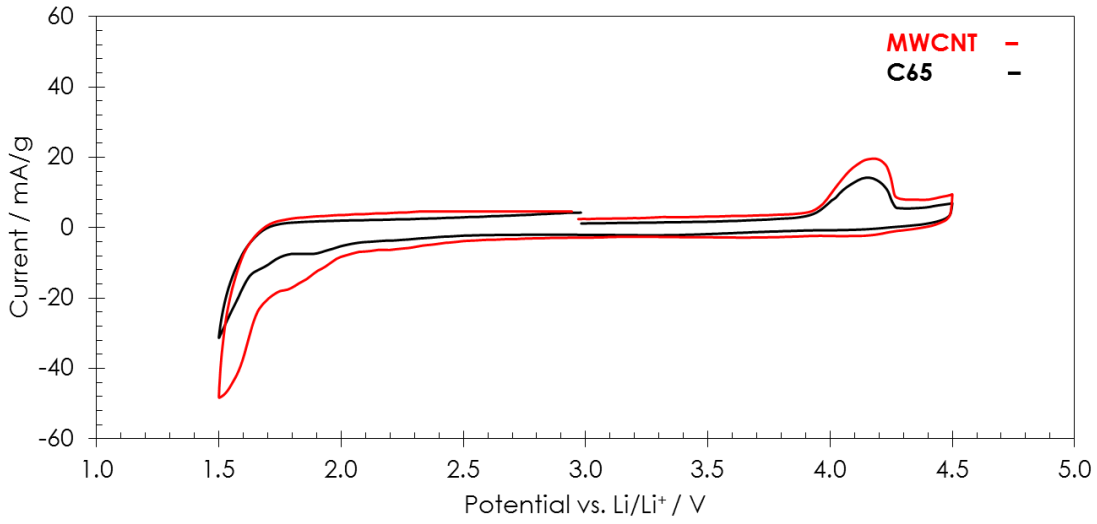

Figure 43 Cyclic voltammogram (scan rate 0.06 mV/s) of the AC/$Li_{0.65}Ni_{1.35}O_2$ electrode with only Super C65 (black) or a mixture of Super C65 and MWCNTs (red line) after galvanostatic extraction of lithium ions from its structure up to ca. 4.5 V vs. Li/Li^+. The electrolyte was in 1 mol/L $LiPF_6$ in EC:DMC.

Conclusion

Lithium nickel oxide, $Li_{0.65}Ni_{1.35}O_2$, can be used as a part of the positive electrode material in lithium-ion capacitors in order to serve as sacrificial lithium ions reservoir for pre-lithiating the negative electrode. The extraction of lithium occurs irreversibly at a low potential ca. 4.2 V vs. Li/Li^+ during the first charge, allowing electrolyte oxidation to be avoided during this process. The full LIC cell assembled with a composite AC/$Li_{0.65}Ni_{1.35}O_2$ positive electrode and graphite negative one can operate up to 3.8 V with good cyclablity and efficiency, without any parasitic reaction (e.g. electrolyte decomposition or/and lithium plating).

Such an approach simplifies the assembly process of LICs, while being safer in usage conditions owing to avoiding the use of metallic lithium. However, due to the low irreversible capacity of $Li_{0.65}Ni_{1.35}O_2$, the amount of Li-Ni-O oxide remaining as a dead-mass in the positive electrode after the pre-lithiation process causes a reduction of specific

energy in comparison to traditional LICs using a metallic lithium auxiliary electrode. Therefore, to reduce this slightly detrimental aspect, our future efforts in applying the present concept will be dedicated to the development of sacrificial materials exhibiting higher irreversible extraction capacity and lower extraction potential.

CHAPTER III

Lithium rich transition metal oxides for improving the electrochemical performance

Introduction

In the previous chapter, we have defined the conditions for an optimal extraction of lithium from $Li_{0.65}Ni_{1.35}O_2$. However, it turned out that the amount of lithium contained in this material is too low for reducing its proportion in the positive electrode. As a result, the conductivity of the composite electrode was relatively fair; the introduction of MWCNTs in the electrode enabled to reduce the EDR of the LIC, unfortunately at the expense of the electrochemical stability window, partly probably related to the presence of residual catalyst in MWCNTs.

Hence, the main objective of this chapter is to look for lithiated oxides with higher lithium content in order to enhance the proportion of AC in the composite positive electrode of LIC. On the basis of literature search [209,210], we suggest three lithium rich oxides: lithium aluminum oxide (Li_5AlO_4, LAlO), lithium zinc oxide (Li_6ZnO_4, LZnO) and lithium zirconium oxide (Li_8ZrO_6, LZrO), with high theoretical capacities of 1067 mAh/g, 941 mAh/g and 884 mA/hg, respectively. Additionally, these three oxides are composed of abundant elements and are easy to prepare by annealing of starting materials at high temperature. However, none of these lithiated oxides was investigated electrochemically, and it is presently impossible to predict their electrochemical activity, especially the irreversibility of lithium extraction. As the electrochemical behavior of the three materials is very similar, the attention will be essentially focused on lithium zinc oxide.

III. 1. Synthesis and structural characterization of lithium metal oxides with high amount of lithium

According to literature, Li_6ZnO_4, Li_5AlO_4 and Li_8ZrO_6 were obtained by annealing Li_2O_2/ZnO [209], Li_2O_2/Al_2O_3 [209], Li_2O_2/ ZrO_2 [210] mixtures in molar ratios 3.5, 5.5, 4.5, respectively, under air. In each case, the oxides were grinded in a mortar for 30 min; then, the mixture was placed in an alumina crucible and heated at 2°C/min up to 650 °C, held at this temperature for 24 h and then cooled down to room temperature after which material was grinded in a mortar.

The X-ray diffractogram of the prepared lithium zinc oxide (LZnO) is shown in Figure 44 (red curve). This diagram could be easily indexed in the tetragonal lattice ($P4_2$/nmc space

group), with cell parameters α, β, γ = 90.000°, a = 4.660 Å, b and c = 6.533 Å, calculated by Rietveld refinement with a R_{WP} value of 5.8. These values fit well with the parameters α, β, γ = 90.000°, a = 4.651 Å, b and c = 6.528 Å given in [211]. The green curve in Figure 44 showing the difference between the observed (red curve) and calculated (black curve) data demonstrates a good purity of the material.

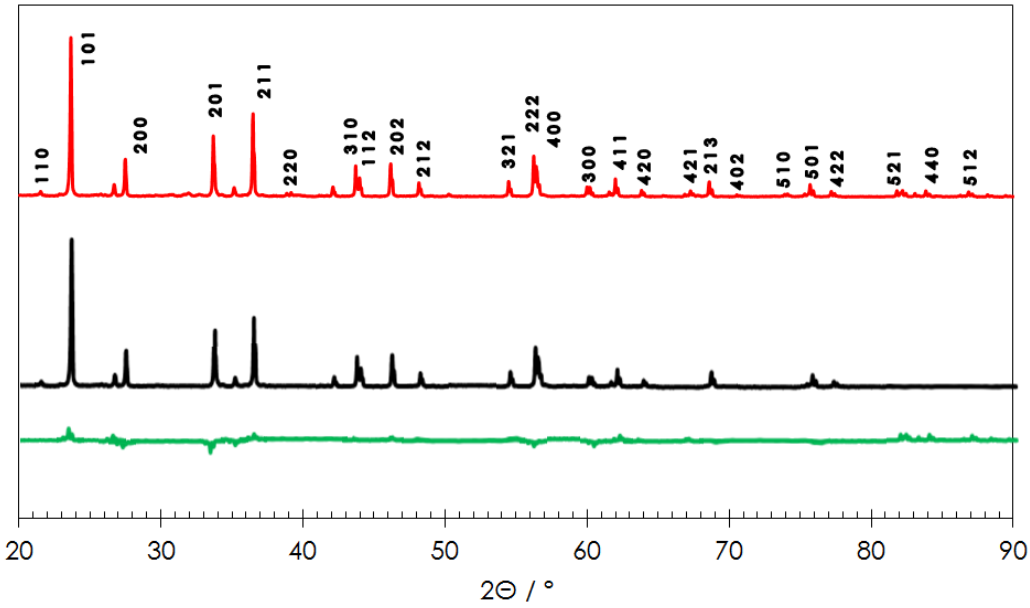

Figure 44 XRD (CuKα = 1.5405 Å) characterization of the synthesized Li_6ZnO_4. Black line: calculated diagram; red line: observed diagram; green line: difference between observed and calculated data.

The X-ray diffractogram of the prepared lithium aluminum oxide (LAlO) is shown in Figure 45 (red curve) and is compared to the reference from [211] (black curve). The parameters for the orthorhombic symmetry (Pbca space group) calculated by Rietveld refinement are α, β = 90.000°, γ = 120.000°, a = 9.051 Å, b = 9.179 Å and c = 9.220 Å, with a R_{WP} value of 7.4. These values fit well with the parameters α, β = 90.000°, γ = 120.000°, a = 9.044 Å, b = 9.175 Å and c = 9.213 Å given in ref [211].

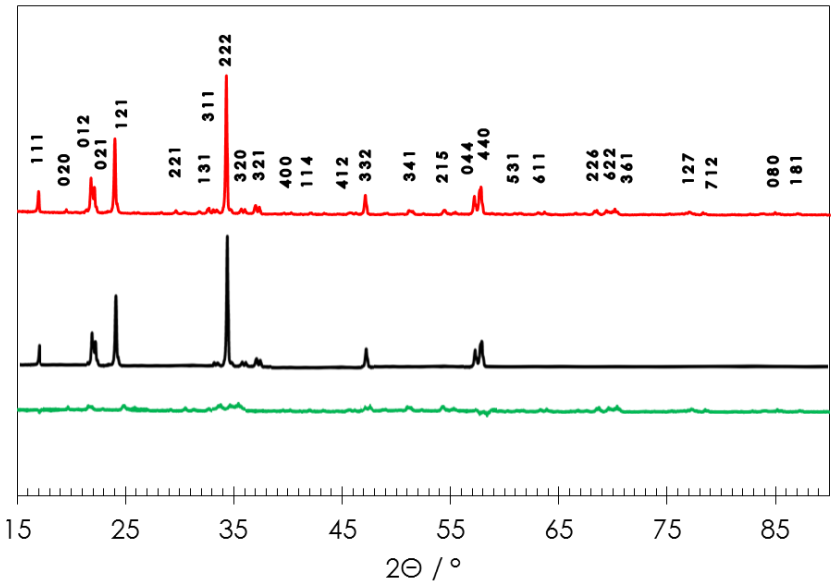

Figure 45 XRD (CuKα = 1.5405 Å) characterization of the synthesized Li_5AlO_4. Black line: calculated diagram; red line: observed diagram; green line: difference between observed and calculated data.

The X-ray diffractogram of Li_8ZrO_6 is shown in Figure 46. The crystal lattice parameters in trigonal symmetry (R3 space group) calculated by Rietveld refinement are α, β, γ = 53.813°, a, b and c = 6.120 Å with R_{WP} = 4.4, respectively. These values fit well with the lattice parameters α, β, γ = 53.813°, a, b and c = 6.118 Å given in ref [211].

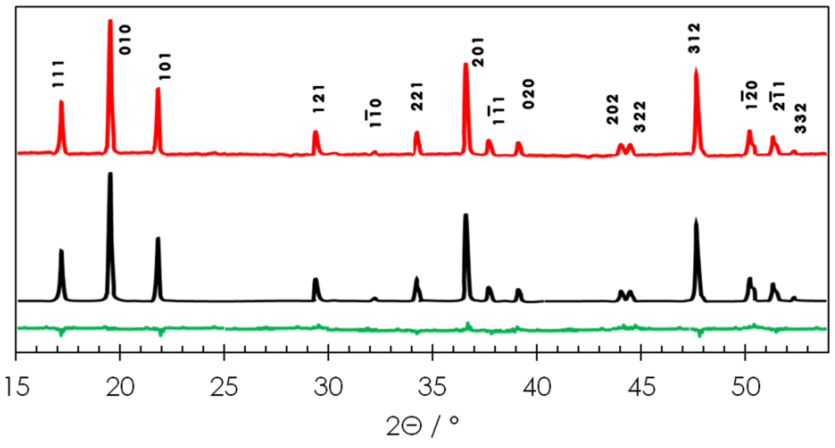

Figure 46 XRD (CuKα = 1.5405 Å) characterization of the synthesized Li_8ZrO_6. Black line: calculated diagram; red line: observed diagram; green line: difference between observed and calculated data.

III. 2. Electrochemical performance of lithium zinc oxide

The reversibility of lithium extraction was studied on composite positive electrodes made of 40 wt.% of LZnO, 40 wt.% of AC 15 wt.% of Super C65 and 5 wt.% of polytetrafluoroethylene (PTFE) binder. During galvanostatic charging/discharging of the electrode at C/20 (where C corresponds to the theoretical capacity of Li_6ZnO_4) from OCP up to 4.5 V vs. Li/Li^+, the charge capacity reaches 150 mAh/g and, upon reversing the current, a part of lithium can be reinserted in the material with a relatively high polarization; overall, the irreversible capacity was extremely low with only 40 mAh/g (Figure 47a). The irreversible capacity could be increased by increasing the upper potential to 4.7 V vs. Li/Li^+ (Figure 47b) and 4.9 V vs. Li/Li^+ (Figure 47). When reaching 4.9 V vs. Li/Li^+, the irreversible capacity is almost 400 mAh/g; however, it cannot be excluded that, at such high potential, a part of the charge may be consumed for electrolyte oxidation as there is an increase of slope at potential higher than 4.5 V vs. Li/Li^+ (Figure 47c).

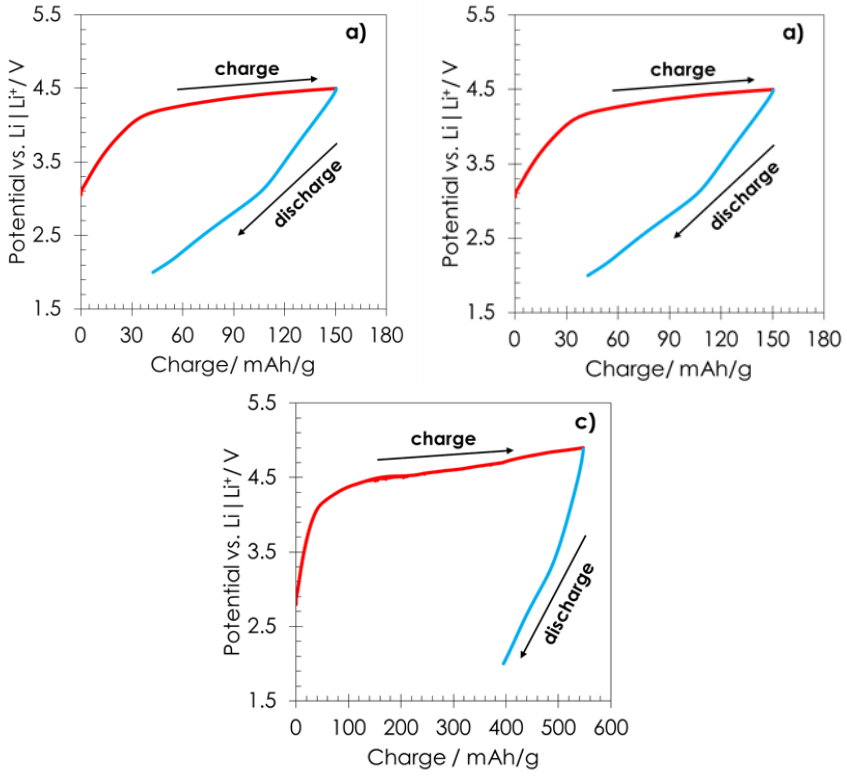

Figure 47 Galvanostatic (C/20) charge of Li_6ZnO_4 from OCP up to a) 4.5 V, b) 4.7 V and c) 4.9 V vs. Li/Li^+ and discharge to 2.0 V vs. Li/Li^+. The composition of the electrode was 40 wt.% of LZnO, 40 wt.% of AC, 15 wt.% of Super C65 and 5 wt.% of PTFE.

III. 3. Ball milling of LZnO, LAlO and LZrO with various conductive agents to increase the amount of lithium extracted

As already mentioned previously, the extraction potential should be limited to 4.5 V vs. Li/Li^+ to avoid electrolyte oxidation. Therefore, LZnO was ball milled (mixer mill Retsch MM200) for 1 h at a frequency of 20 Hz to reduce the grain size and enhance the diffusion of lithium ions during the extraction. The vessel and balls used for milling were made from tungsten carbide (WC) in order to avoid any contamination which could arise if stainless steel would be used. The mass ratio between the balls and the material was always 16 as 1g of the substrates occupied around 1/3 of the total volume of the vessel. Figure 48 presents the X-ray diffractogram of the Li_6ZnO_4 powder after milling. As compared to the diffractogram of Figure 44, the lines are at similar positions, with some changes of relative intensity, whereas few additional lines of negligible intensity appear in the background.

After milling, the line-width increases (see for example the inset in Figure 48 for the 101 line), which reveals a diminishing of crystallites size. The crystallite size calculated by applying the Scherrer equation decreases from 70 nm to 57 nm after ball-milling. Additionally, the upward shift of the 101 line of $2\Theta° = 23.25$ to 23.55 after milling reveals a small decrease of the interlayer distance.

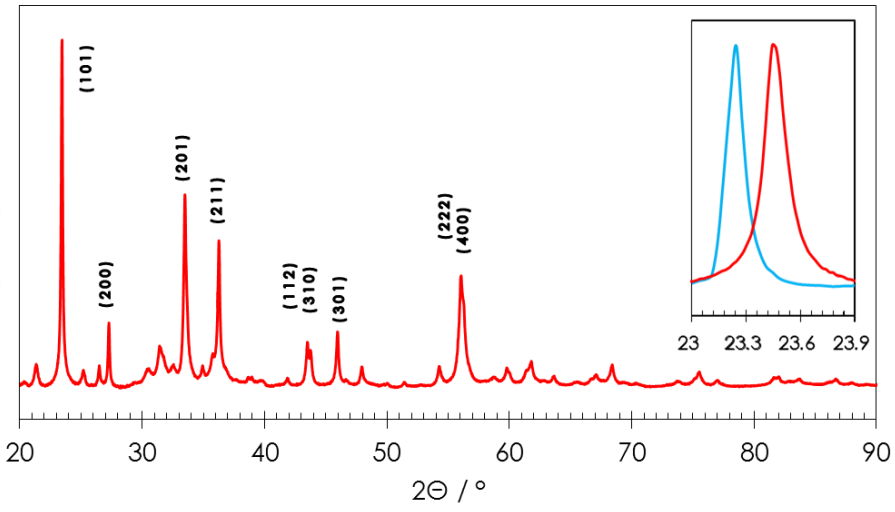

Figure 48 XRD (CuKα = 1.5405 Å) characterization of Li_6ZnO_4 after ball milling for 1h at 20 Hz. The inset shows a magnification of the 101 line in as-received (blue) and ball-milled (red) Li_6ZnO_4.

Self-standing composite electrodes were made from a mixture of 40 wt.% of ball-milled LZnO, 40 wt.% of AC, 15 wt.% of Super C65 and 5 wt.% of PTFE, and were investigated galvanostatically vs. Li/Li^+. As compared to Figure 47a, where identical electrochemical conditions were used, the amount of irreversibly extracted lithium is very slightly enhanced (Figure 49), which reveals that ball-milling of LZnO is not effective.

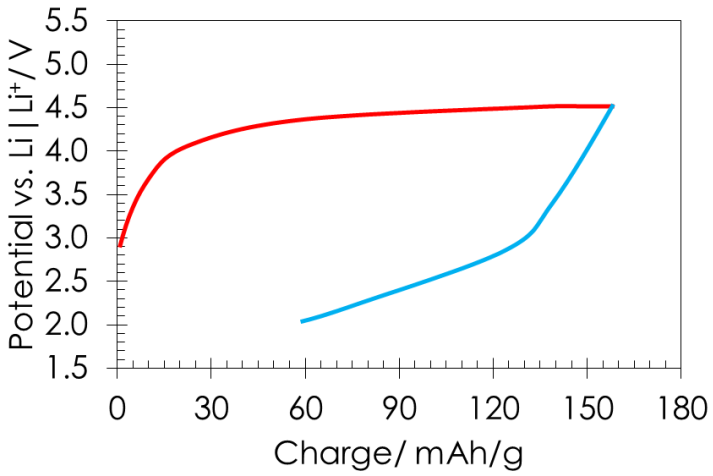

Figure 49 Galvanostatic (C/20) charge of ball-milled Li_6ZnO_4 from OCP up to 4.5 V vs. Li/Li^+ and discharge to 2.0 V vs. Li/Li^+. The composition of the electrode was 40 wt.% of ball-milled LZnO, 40 wt.% of AC, 15 wt.% of Super C65 and 5 wt.% of PTFE. The electrolyte was 1 mol/L $LiPF_6$ in EC:DMC. Li/Li^+ was used as a counter and reference electrode.

The next attempt to reduce the lithium extraction potential was to improve the electrode conductivity by ball-milling Li_6ZnO_4 together with the conductivity additive, i.e. only Super C65, only MWCNTs or a mixture of MWCNTs with Super C65. Since the MWCNTs (Sigma Aldrich) contained remains of nickel catalyst (which could be source of electrolyte decomposition) as shown by transmission electron microscopy (TEM) in Figure 50a, and energy dispersive X-rays (EDX) in Figure 50c, they were treated at 2400 °C under argon. Figure 50b and d confirm that nickel has been evaporated after this treatment; the as-received and purified samples will be further called MWCNT and MWCNT–p, respectively.

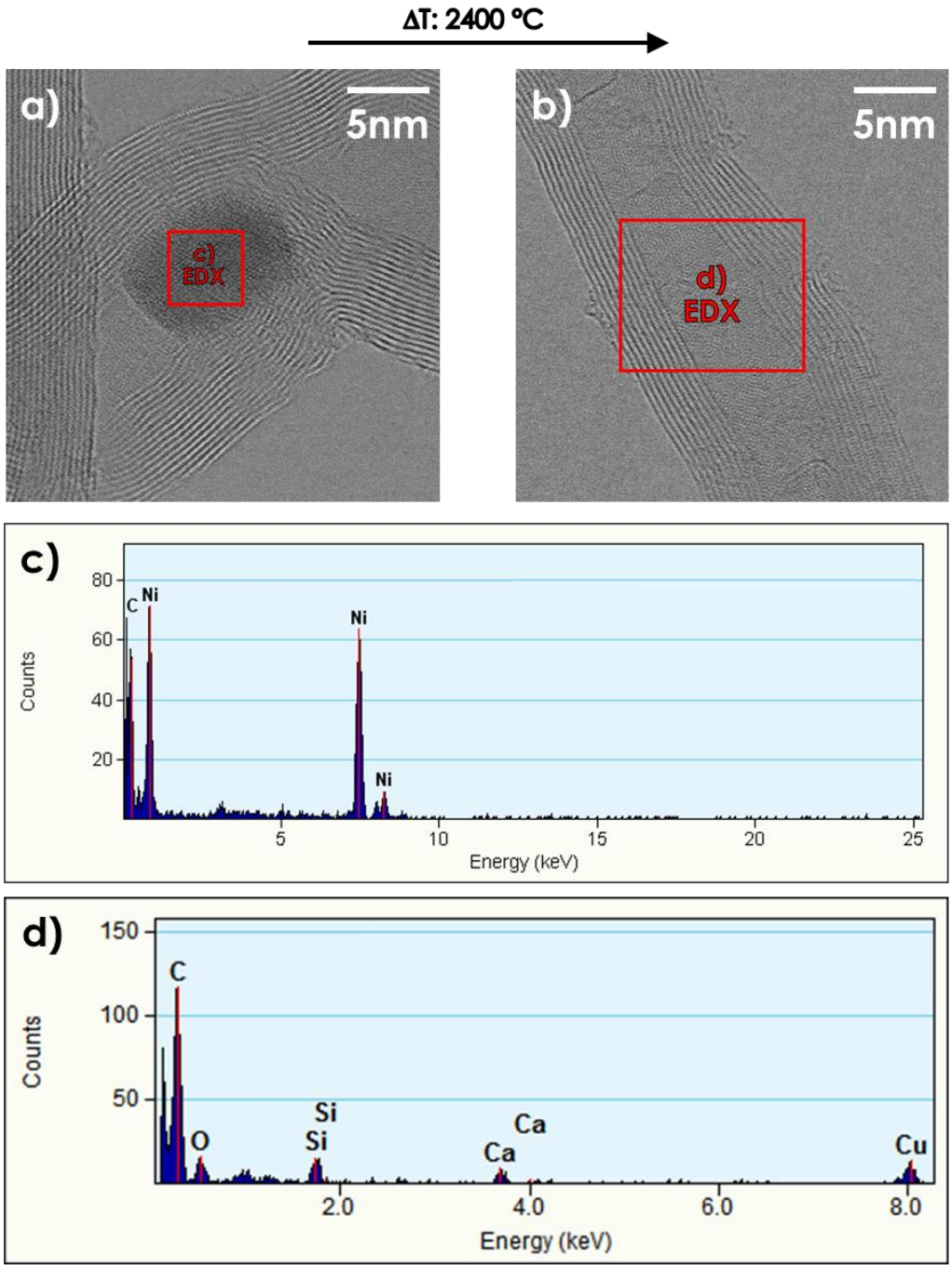

Figure 50 TEM characterization of a) as-received MWCNTs and b) MWCNTs–p obtained after heat treatment at 2400 °C under argon; c) EDX analysis of as-received MWCNTs and d) MWCNT–p in the area selected by the red square in the TEM images.

73 wt.% of LZnO together with (a) 27 wt.% of Super C65, (b) 27 wt.% of MWCNT–p and (c) mixture of 18 wt.% of Super C65 and 9 wt.% of MWCNT–p was ball-milled for 1h at a

frequency of 20 Hz under argon atmosphere (the vial was filled inside a glove-box with argon atmosphere). Then, self-standing electrodes were prepared according to the usual procedure by mixing the ball-milled material together with AC and PTFE in order to reach final compositions of (a) 40 wt.% LZnO, 40 wt.% AC, 15 wt.% Super C65, 5 wt.% PTFE, (b) 40 wt.% LZnO, 40 wt.% AC, 15 wt.% MWCNT–p, 5 wt.% PTFE, (c) 40 wt.% LZnO, 40 wt.% AC, 10 wt.% Super C65 + 5 wt.% MWCNT–p, 5 wt.% PTFE.

The galvanostatic charge/discharge of these materials at C/20 (where C corresponds to the theoretical capacity of LZnO, e.g., 941 mAh/g) is shown in Figure 51a – c. When using either Super C65 or MWCNT–p alone, (Figure 51a and b), the galvanostatic characteristics are relatively comparable to those shown in Figure 47. By contrast, when the electrode contains 10 wt.% Super C65 + 5 wt.% MWCNT–p, the charge capacity and irreversible capacity are remarkably enhanced, reaching 620 mAh/g and 450 mAh/g, respectively (Figure 51c). However, the slight increase of slope at potential higher than 4.5 V vs. Li/Li^+ may indicate that the observed values are overestimated due to the minor oxidation of the electrolyte. Consequently, the realistic value of irreversible lithium extraction capacity is closer to 400 mAh/g. Complementary information on the electrochemical performance of the materials was obtained from cyclic voltammograms (Figure 51d – f) recorded at a scan rate of 0.06 mV/s in the potential range from 2.0 to 4.8 V vs. Li/Li^+. In Figure 51d – f, it can be seen that the highest lithium amount is extracted during the first cycle at around 4.4 – 4.5 V vs. Li/Li^+. Peaks appear at around 2.5 V vs. Li/Li^+ at the end of the first scan, revealing cathodic phenomena. They could be partly attributed to a small amount of lithium reinserted in the electrode. However, they are more pronounced for the electrodes containing MWCNTs (Figure 51e and f) and can be attributed to the fact that a solid electrolyte interphase (S.E.I.) can be already formed on carbon nanotubes at such potential, as it was reported by Frackowiak *et al*. [212] for MWCNTs annealed at 2500°C and is presented in Figure 52. This interpretation is confirmed (Figure 51e and f) by the second cycle, which shows that the intensity of the anodic peak is much smaller and the cathodic one is dramatically reduced, supporting the idea of a S.E.I. contribution during the first cycle. Although lithium extraction seems to be completed after the second cycle, a small irreversible anodic leap still exists above 4.5 V vs. Li/Li^+ during the third and next cycles, probably due to electrolyte oxidation as previously suggested from galvanostatic data.

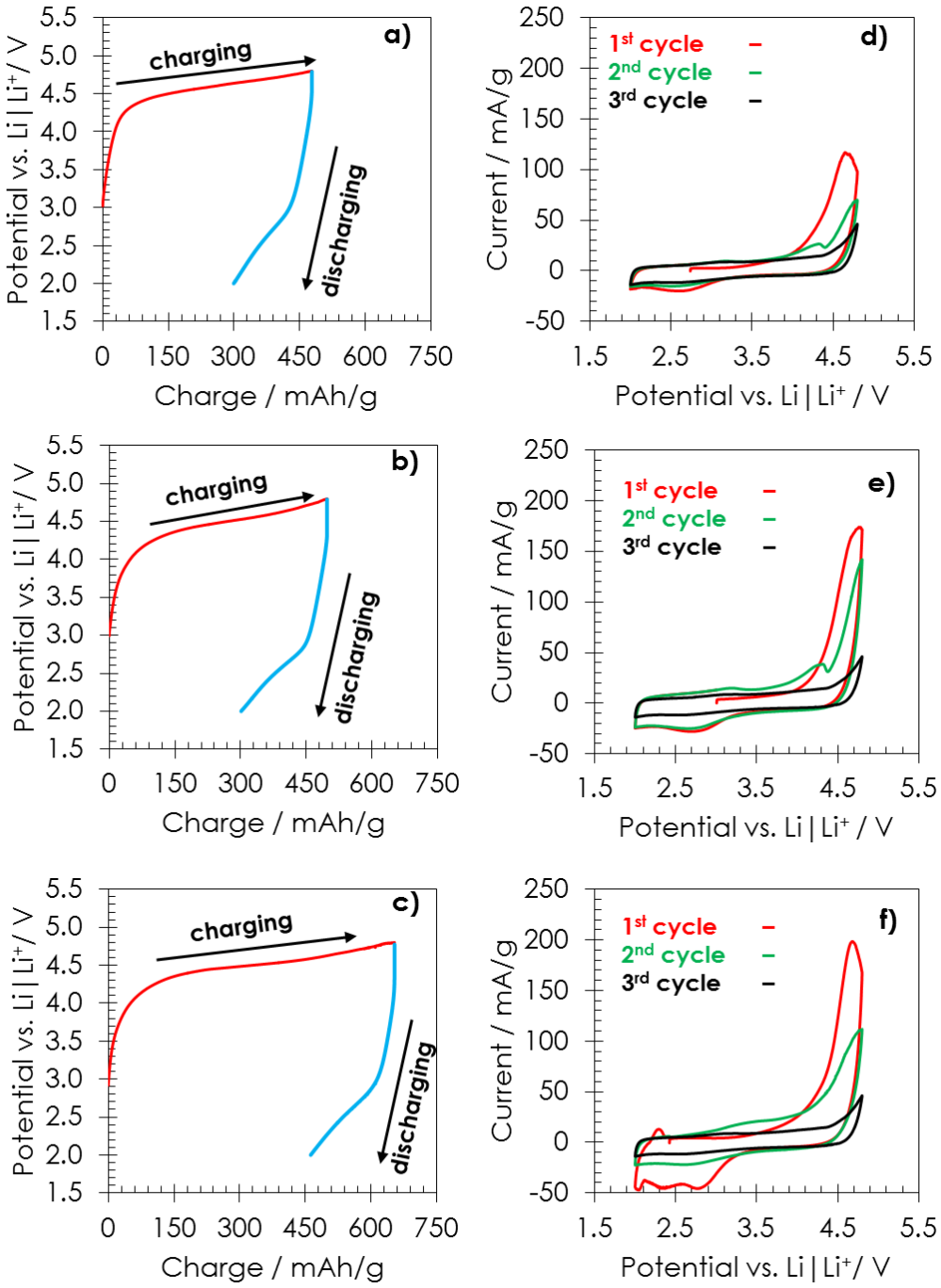

Figure 51 Galvanostatic charge at C/20 up to 4.8 V vs Li/Li^+ and discharge to 2.0 V vs Li/Li^+ (a to c), and cyclic voltammograms at 0.06 mV/s (d to f) of Li_6ZnO_4 ball milled together with various conductivity additives. Electrodes with a and d) 15 wt.% of Super C65, b and e) 15 wt.% of MWCNT–p, c and f) 10 wt.% of Super C65 + 5 wt.% of MWCNT–p. In addition to the conductivity additives, all electrodes contained 40 wt. % of LZnO, 40 wt.% of AC and 5 wt.% PTFE. The electrolyte was 1 mol/L $LiPF_6$ in EC:DMC. Li/Li^+ was used as a counter and reference electrode.

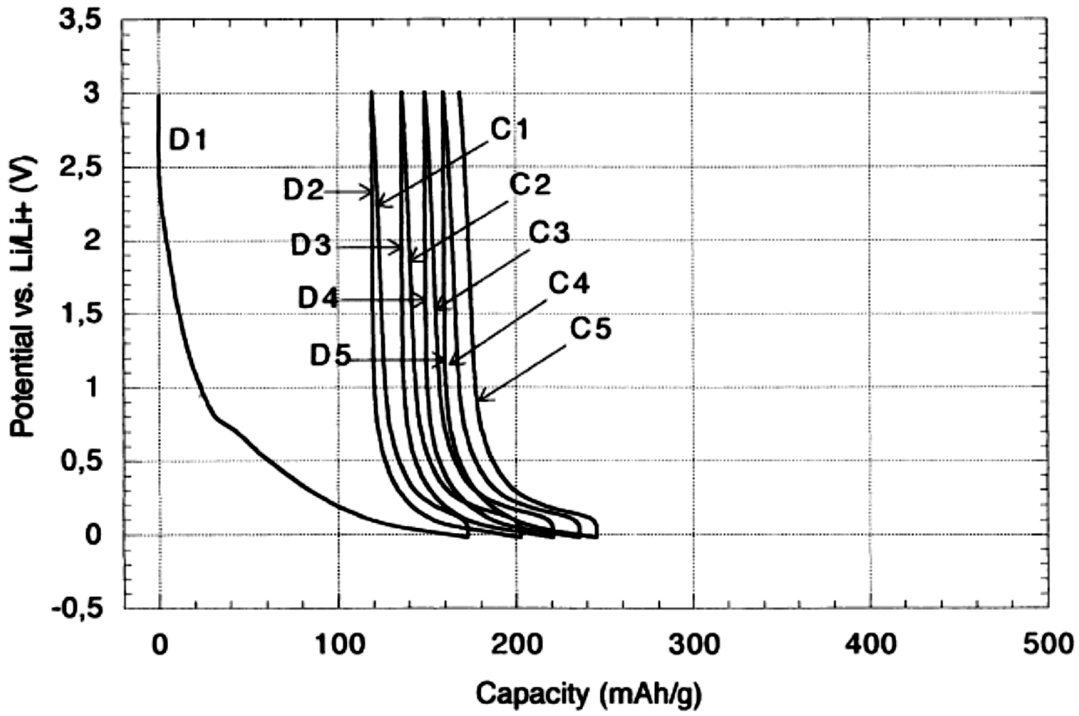

Figure 52 Galvanostatic charge/discharge of MWCNT heat-treated at 2500°C. The electrolyte was 1 mol/L $LiPF_6$ in EC:DMC. Li/Li^+ was used as counter and reference electrode [212]. During the first discharge (D1), the galvanostatic curve deviates from verticality at around 2.5 V vs. Li/Li+, revealing starting of S.E.I. formation; it was suggested that the mesoporous character of MWCNTs is responsible of such behaviour.

Li_5AlO_4 (Figure 53b and e) and Li_8ZrO_6 (Figure 53 c and f) were also ball-milled for 1 hour with the mixture of 10 wt.% Super C65 + 5 wt.% MWCNT–p, and tested in the same electrochemical conditions as Li_6ZnO_4 (Figure 53 a and d). The cyclic voltammograms recorded during the first cycle are quite comparable for the three materials, yet the highest irreversible capacity of 460 mAh/g is displayed by Li_6ZnO_4. Hence, for further investigation as sacrificial material in LIC, only Li_6ZnO_4 will be implemented.

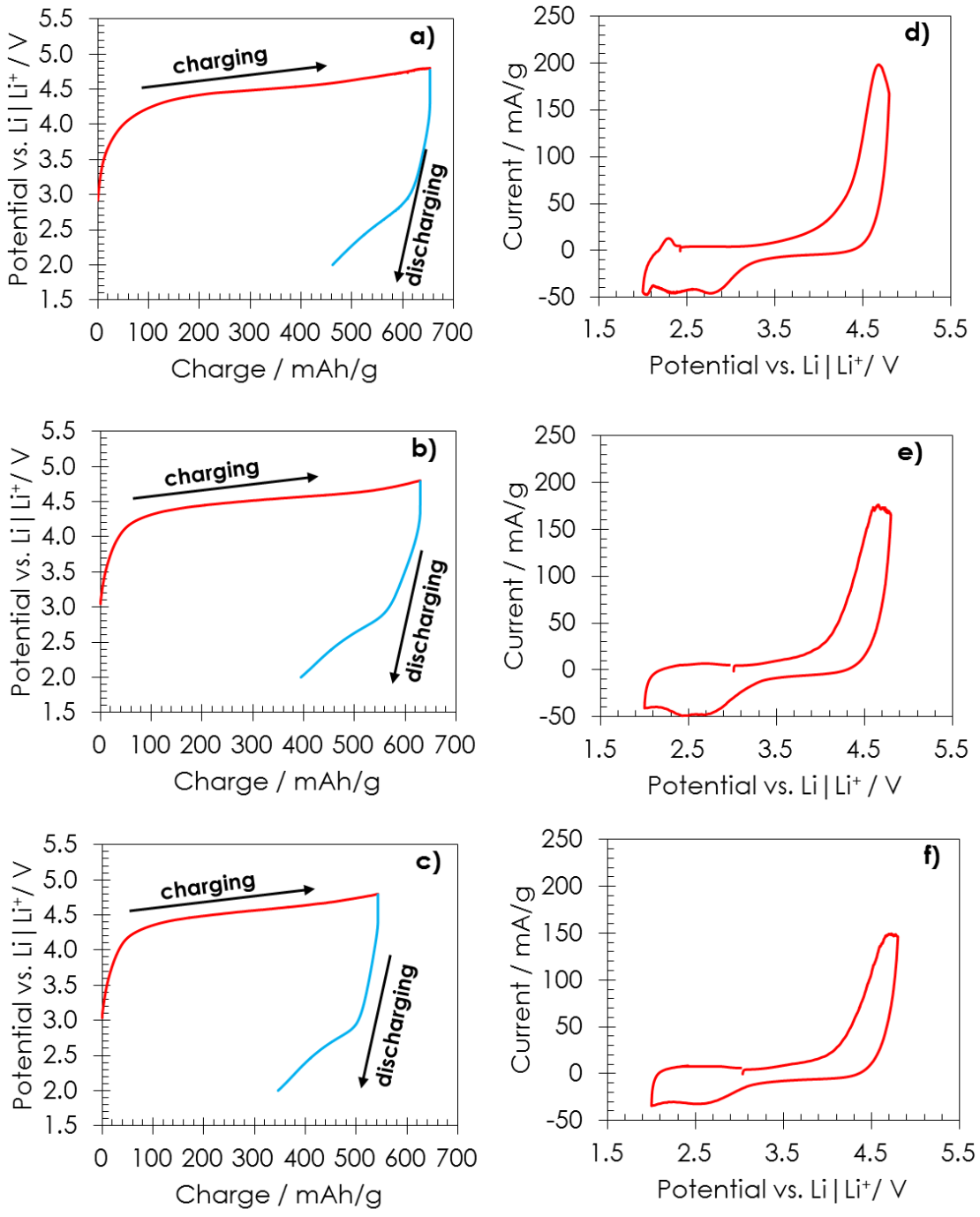

Figure 53 Galvanostatic charge of lithiathed oxides, at C/20 up to 4.8 V vs Li/Li^+ followed by discharge to 2.0 V vs Li/Li^+ (a to c), and cyclic voltammograms (d to f) at 0.06 mV/s. a and d) Li_6ZnO_4; b and e) Li_5AlO_4, c and f) Li_8ZrO_6. The electrodes contained 10 wt.% of Super C65 + 5 wt.% of MWCNT–p, 40 wt.% of lithiated metal oxide, 40 wt.% of AC and 5 wt.% PTFE. The electrolyte was 1 mol/L $LiPF_6$ in EC:DMC. Li/Li^+ was used as a counter and reference electrode.

III. 4. LIC system with lithium zinc oxide as sacrificial lithium source

LZnO ball-milled with Super C65 and MWCNT–p was used as sacrificial material in the positive electrode of LIC cells. The final composition of this electrode was: 40 wt. % of LZnO, 40 wt.% of AC, 10 wt.% of MWCNT–p, 5 wt.% of Super C65, 5 wt.% of PTFE. The negative electrode was composed of 91 wt.% of graphite, 8 wt.% of PVdF and 1 wt.% of C65. In order to optimize the power and energy density of the cell, the mass ratio between AC and graphite was selected around 1 [201]; this was done by adjusting the thickness of the positive and negative electrodes.

In a first trial, the S.E.I. formation and subsequent intercalation of lithium into graphite was realized at C/20 (where C corresponds to the theoretical capacity of graphite, e.g., 372 mAh/g). It was decided to stop the experiment either when the potential of the positive electrode reaches 4.5 V vs. Li/Li^+ (to avoid electrolyte oxidation) or when the potential of the negative electrode reaches 0.01 V vs. Li/Li^+ (to avoid lithium plating). Figure 54a shows that the limit of 4.5 V vs. Li/Li^+ is reached by the positive electrode, while the potential of the graphite electrode is close to 0.08 V vs. Li/Li^+, and the total capacity 380 mAh/g. If one assumes that the capacity at 0.25 V correspond to the S.E.I. formation, with a value of ca. 70 mAh/g, the capacity corresponding to lithium intercalation is 310 mAh/g, meaning that the composition of the graphite intercalation compound is close to LiC_7. Hence, using LZnO ball-milled with conductivity additive, a high level of graphite intercalation can be obtained without detrimental oxidation of the positive electrode. In addition, owing to the high irreversible capacity of LZnO, it was possible to reduce its amount to 40 wt.% while increasing the AC amount to 40 wt.% as compared to the case presented in Chapter II, where the amount of LNiO in the electrode was 55 wt.% and the amount of AC 25 wt.%.

Unfortunately, when LIC was cycled galvanostatically at 0.25 A/g in the voltage range 2.2 – 4.1 V, a relatively high ohmic drop was observed (when the current is reversed) from the 1^{st} cycle for the positive electrode, and consequently for the cell (Figure 54b); after 35 cycles, the drop of capacitance is extremely demonstrating failure of the cell (Figure 54c). This fair performance of the LIC cell could be related to the relatively high irreversible capacity, leading to a high resistance of the negative electrode.

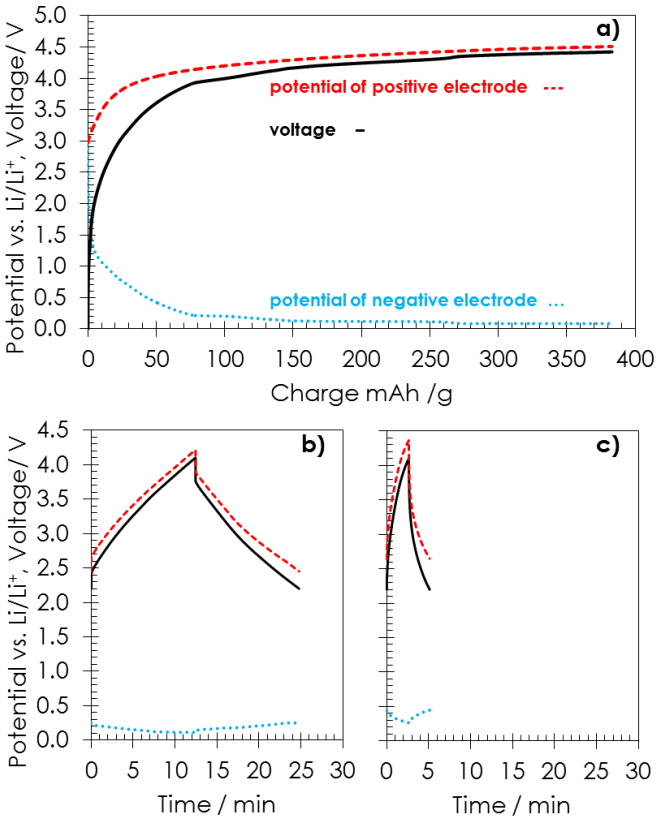

Figure 54 a) Galvanostatic pre-lithiation of graphite at C/20 in a cell using a composite positive electrode with a mixture of ball-milled LZnO + MWCNTs + Super C65 (the final composition of this electrode is 40 wt. % of LZnO, 40 wt.% of AC, 10 wt.% of C65, 5 wt.% of MWCNT and 5 wt.% of PTFE. The negative electrode contains 91 wt.% of graphite, 8 wt.% of PVDF and 1 wt.% of C65. The mass ratio between AC and graphite was 1. The potential limits for positive and negative electrodes are 4.50 V and 0.01 V vs. Li/Li^+, respectively. Color of the curves: red dashed for the potential of positive electrode; blue dotted for the potential of negative electrode; black solid for the cell voltage profile. The electrolyte is 1mol/L $LiPF_6$ in 1:1 EC/DMC. Li/Li^+ is the reference electrode. After lithiation, the LIC was cycled at 0.25 A/g (expressed per mass of activated carbon) between 2.2 V and 4.1 V: b) 1^{st} cycle and c) 35^{th} cycle.

Therefore, in another experiment to reduce the extent of S.E.I. formation, a higher current of C has been applied till reaching a potential of 0.2 V vs Li/Li^+ [157]; then, after a rest period of 2h, graphite has been pre-lithiated at C/20. As it can be seen in Figure 55a, the irreversible capacity is moderately reduced to ca. 40-50 mAh/g. After completing the pre-lithiation of graphite, the LIC system has been cycled at 0.25 A/g in the voltage range of 2.2 – 4.1 V (Figure 55b-c). Even though there is a noticeable improvement as compared to

the previous case where the S.E.I. was formed at C/20 (Figure 54b-c), the capacitance decay after only 35 cycles is remarkable, while the ohmic drop of the positive electrode is still very high. Hence, it seems that the resistive character of the used oxide has a detrimental effect upon the cyclic life and it is necessary to look for other materials with better conductivity and lower extraction potential of lithium ions.

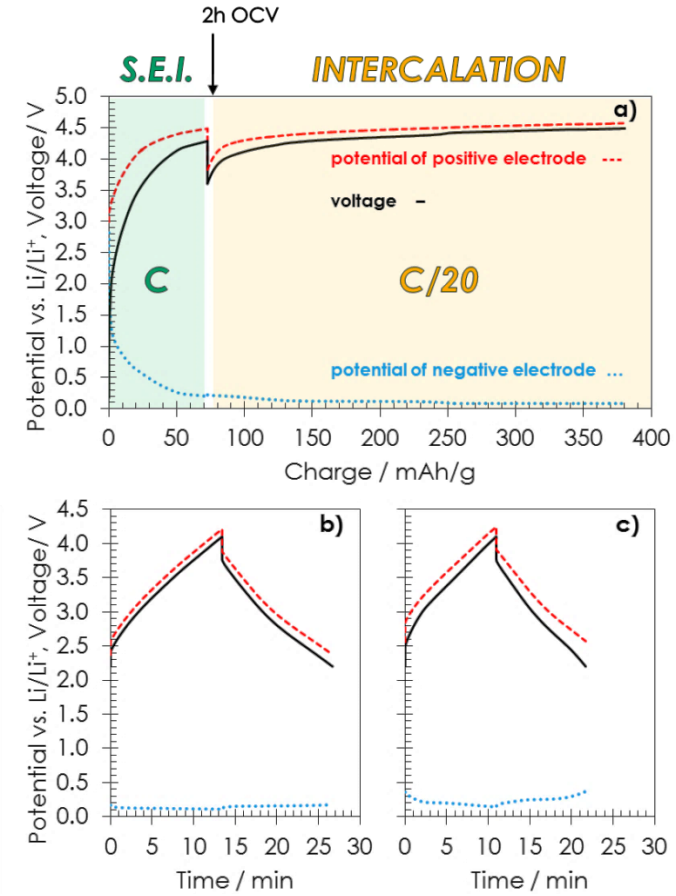

Figure 55 a) Galvanostatic formation of S.E.I. at C till reaching a potential of 0.2 V vs. Li/Li^+ (area highlighted in green) followed by a rest period of two hours and lithium intercalation into graphite at C/20 (area highlighted in orange). The cell uses a composite positive electrode with a mixture of ball-milled LZnO + MWCNTs + Super C65 (the final composition of this electrode is 40 wt. % of LZnO, 40 wt.% of AC, 10 wt.% of C65, 5 wt.% of MWCNT and 5 wt.% of PTFE. The negative electrode contains 91 wt.% of graphite, 8 wt.% of PVDF and 1 wt.% of C65. The mass ratio between AC and graphite was 1. The potential limits for positive and negative electrodes are 4.50 V and 0.01 V vs. Li/Li^+, respectively. Color of the curves: red dashed for the potential of positive electrode; blue dotted for the potential of negative electrode; black solid for the cell voltage profile. The electrolyte is 1mol/L $LiPF_6$ in 1:1 EC/DMC. Li/Li^+ is the reference electrode. After lithiation, the LIC was cycled at 0.25 A/g (expressed per mass of activated carbon) between 2.2 V and 4.1 V: b) 1st cycle and c) 35th cycle.

Conclusion

Lithium aluminum oxide (Li_5AlO_4), lithium zinc oxide (Li_6ZnO_4) and lithium zirconium oxide (Li_8ZrO_6) were electrochemically investigated for the first time. The three oxides demonstrated a high irreversibility of lithium extraction. However, despite their high theoretical capacity, only a part of lithium could be irreversibly extracted. Assuming that such poor performance could be related to their low conductivity, we have ball-milled the oxides together with the conductivity additive. When using simultaneously MWCNTs and carbon black, it was then possible to enhance the irreversible capacity up to 400 mAh/g, 450 mAh/g and 350 mAh/g for Li_5AlO_4, Li_6ZnO_4 and Li_8ZrO_6, respectively. However, the LIC cells based on S.E.I. formation and graphite pre-lithiation from these lithiated oxides demonstrated a high ohmic drop of the positive electrode. For future improvement, we believe that it could be worth to coat the oxide particles by deposition of a thin layer of pyrolytic carbon, as it is done for example in lithium-ion batteries for cathodic materials like $LiFePO_4$.

However, considering the worse electrochemical performance of the three oxides in LIC as compared to the reported one for Li_6CoO_4 [213], the difficulty of lithium extraction and high resistivity with Li_5AlO_4, Li_6ZnO_4 and Li_8ZrO_6 can find its explanation in their high band gap, ranging from 4.0 to 5.0 eV [213], whereas it is only 2.5 eV with Li_6CoO_4 [213]. The partial substitution of Al, Zn or Zr by other metals could be an appropriate solution in future works to optimize the conductivity. For the course of the present work, we have decided to investigate Li_5ReO_6 which has a band gap of 2.2 eV [211]; this will be the object of chapter IV.

CHAPTER IV

Lithium rhenium oxide as a promising material for graphite pre-lithiation

Introduction

As it has already been mentioned, the auxiliary lithium electrode complicates the LIC cell construction, due to the remaining metallic lithium which may cause thermal runaway. What is more, when a relatively concentrated lithium salt is applied instead of such electrode, the decrease of electrolyte conductivity leads to unstable performance of the cell. Therefore, lithium metal oxides were introduced to pre-lithiate the negative electrode (see chapters II and III) in order to deal with the issues related to the presence of an auxiliary metallic lithium electrode or depletion of concentration when lithium feeding is from the electrolyte. However, due to an unsatisfactory cycle life of the systems utilizing $Li_{1-X}Ni_{1+X}O_2$ as well as Li_6ZnO4, Li_5AlO_4 and Li_8ZrO_6, other lithium metal oxides should be proposed for the composite positive electrode. According to the conclusion of Chapter III, it seems that lithium metal oxides with low band gap and high lithium content could be good candidates as sacrificial materials. One possibility would be to use lithium rhenium (VII) oxide, Li_5ReO_6 (further symbolized as LReO in this chapter). The synthesis and X-ray diffraction characterization of LReO was firstly reported by Morss *et al.* [214]. The band gap of this material is 2.159 eV which is smaller value than for the lithiated oxides presented in chapter III (around 5 eV) [211]. In this chapter, we are the first to report about the electrochemical behaviour of Li_5ReO_6.

IV. 1. Synthesis and characterisation of lithium rhenium oxide and of a composite Li_5ReO_6/AC electrode

Owing to its high theoretical capacity of 423 mAh/g, LReO is an interesting material for the positive composite electrode, provided that the major part of lithium can be irreversibly extracted at low potential. Similarly to the other lithiated oxides presented in Chapters II and III, LReO was synthesized by sintering at high temperature. In this case, a Li_2O_2/Re mixture in molar ratio 3 was grinded for 30 min in a mortar. The mixture placed in an alumina crucible was heated in air at 2°C/min up to 375 °C and held at this temperature for 1 h, and then the material was cooled down to room temperature and grinded again for 30 min. Then, it was heated up to 600°C, held at this temperature for 1 h, cooled down to room temperature and grinded, and the same procedure was repeated for the next heating at 725 °C for 1 h. Figure 56 presents the XRD pattern of the synthesized lithium rhenium

oxide. The cell parameters estimated by full pattern matching: a = 5.0653 Å, b = 8.7315 Å, c = 5.0288 Å, α = 90.000°, β = 110.216°, γ = 90.000° are in agreement with the data published by Morss *et al.* for a monoclinic crystal with space group C2/m and parameters a = 5.0649 Å, b = 8.7314 Å, c = 5.0277 Å, α = 90.000°, β = 110.187°, γ = 90.000° [214]. The R_{WP} value of 8.73 proves an accurate fitting and confirms high purity of the obtained material.

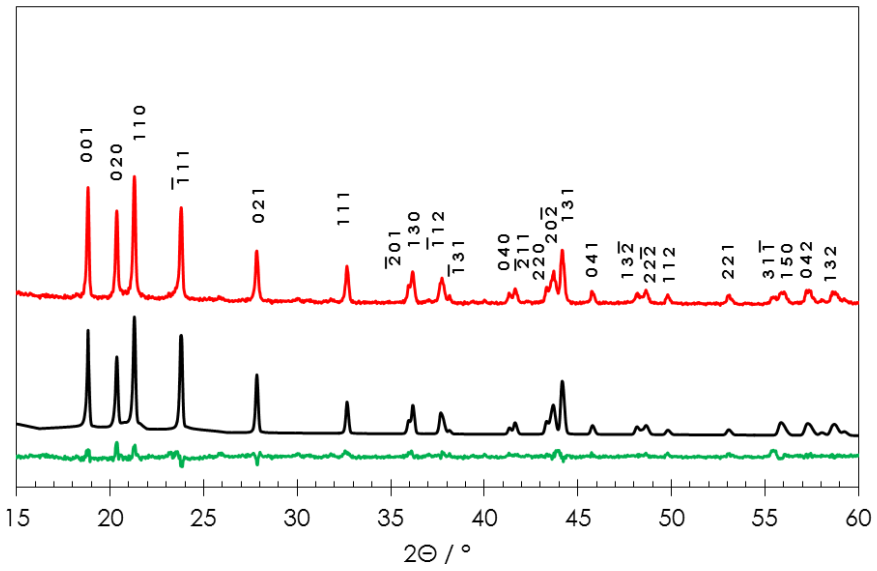

Figure 56 XRD (CuKα= 1.5405 Å) pattern of the synthesized lithium rhenium oxide (red curve). The black curve is the pattern calculated on the basis of full pattern matching for cell parameters determination. The green line represents the difference between the experimental and calculated patterns.

The prepared lithium rhenium oxide (LReO) was used to prepare a composite electrode composed of 40 wt.% of LReO, 40 wt.% of AC, 15 wt.% of Super C65 and 5 wt.% of polytetrafluoroetylene (PTFE) binder. Figure 56a presents the SEM picture of this electrode showing that the carbon matrix is a dim part surrounding the LReO particles which are brighter due to their lower electronic conductivity. The EDS mapping demonstrates that the oxygen (Figure 57b) and rhenium (Figure 57c) elements are spread evenly across the whole electrode material. The overlay of the spots of these two elements on the SEM picture (Figure 57d) shows that they are perfectly superimposed with all the bright dots observed in Figure 57a, confirming that the latter are due to lithium rhenium oxide.

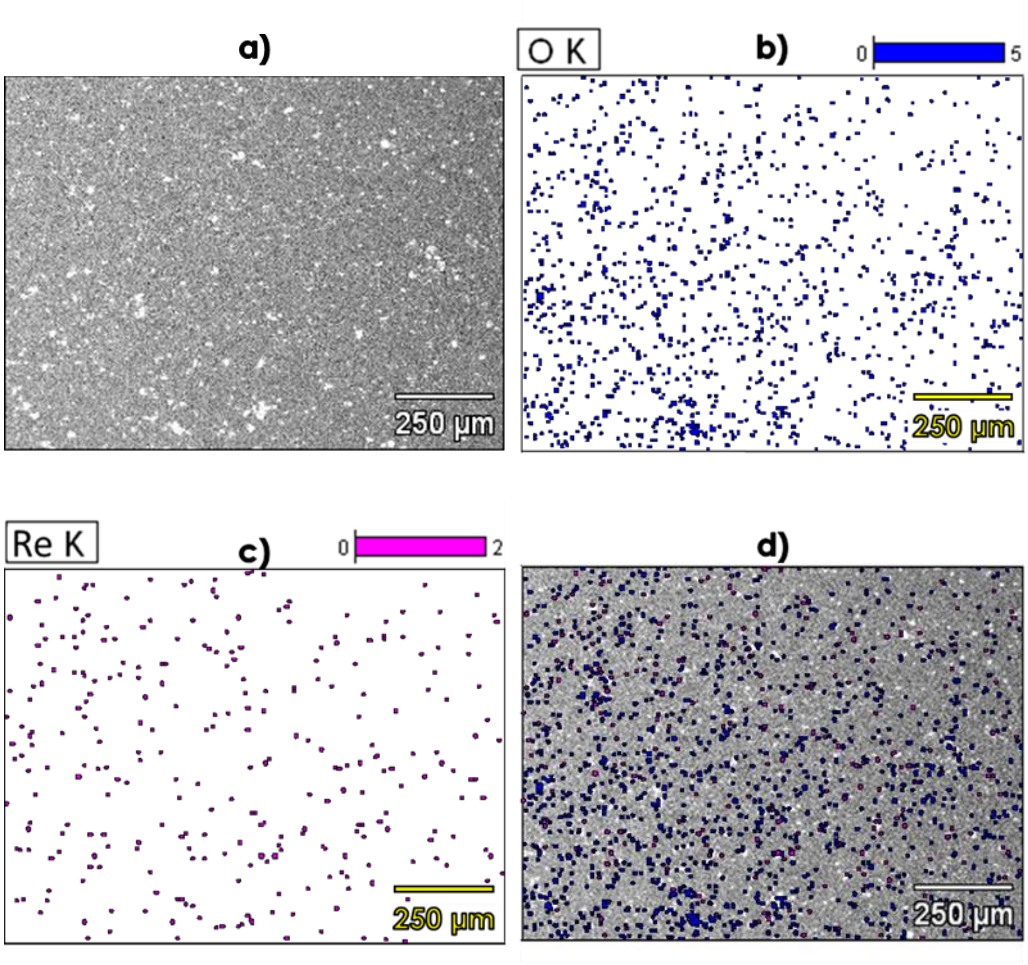

Figure 57 SEM and EDS analysis of the composite LReO/AC electrode: a) SEM image; b) mapping of oxygen; c) mapping of rhenium; d) overlay of oxygen and rhenium dots on the SEM image showing an ideal superimposition with the bright dots.

IV. 2. Electrochemical irreversibility of lithium rhenium oxide Li_5ReO_6

The first cycle irreversible capacity of LReO in the composite LReO/AC (40 wt.% of LReO, 40 wt.% of AC, 15 wt.% of Super C65 and 5 wt.% of PTFE) electrode was determined vs. metallic lithium counter/reference electrode by cyclic voltamperometry and galvanostatic charge/discharge. The first voltamperometry cycle (Figure 58a) reveals that the anodic current related to the lithium extraction process starts to increase ca. 3.8 V vs. Li/Li^+ and reaches its maximum ca. 4.5 V vs. Li/Li^+. The cathodic scan exhibits weak broad humps which indicate almost irreversible lithium extraction. During the second

cycle (green line), the voltammogram displays a nearly rectangular current response associated with the capacitive behavior of AC present in the composite electrode (Figure 58a). However, a slight increase of the current can be observed at potentials higher than 4.2 V vs. Li/Li^+, which does not disappear when performing additional scans as shown in Figure 58b. Such behavior could be attributed to electrolyte decomposition, which might be even catalyzed by rhenium oxide [215]. Therefore, in the next parts of this paper, special care has been paid to control the maximum potential reached by the positive electrode of the LIC upon cycling.

The galvanostatic charge/discharge at C/20 (where C corresponds to the theoretical capacity of LReO of 423 mAh/g) in the potential range from 2.0 – 4.5 V vs. Li/Li^+ (Figure 58c) shows an oxidation plateau at around 4.2 V, and the absence of plateau during negative polarization demonstrates the irreversibility of the process. In order to estimate the oxidation limit of the LReO/AC composite electrode, the anodic polarisation has been prolonged to higher potentials. As it can be seen from Figure 58d, after the first irreversible lithium extraction plateau, there is another irreversible plateau which can be related to electrolyte oxidation. This second plateau is directly correlated with the irreversible deviation which has been observed on the CVs of Figure 58a-b at potentials higher than 4.2 V vs. Li/Li^+. The irreversible capacity of lithium extraction determined by the position of the inflexion point in Figure 58d is close to 410 mAh/g, reaching almost the theoretical value of 423 mAh/g.

IV. 3. *In-situ* XRD study of lithium extraction from lithium rhenium oxide Li_5ReO_6

Figure 59 presents i*n-situ* XRD patterns of the LReO/AC (40 wt.% of AC, 40 wt.% of LReO, 15 wt.% of Super C65 and 5 wt.% of PTFE) electrode recorded during 1 h open circuit periods after 0.5 h galvanostatic pulses at C/20 until reaching a potential of 4.5 V vs. Li/Li^+. Figure 60 displays the galvanostatic plot (Left) during lithium extraction and XRD patterns (Right) at specific potential values.

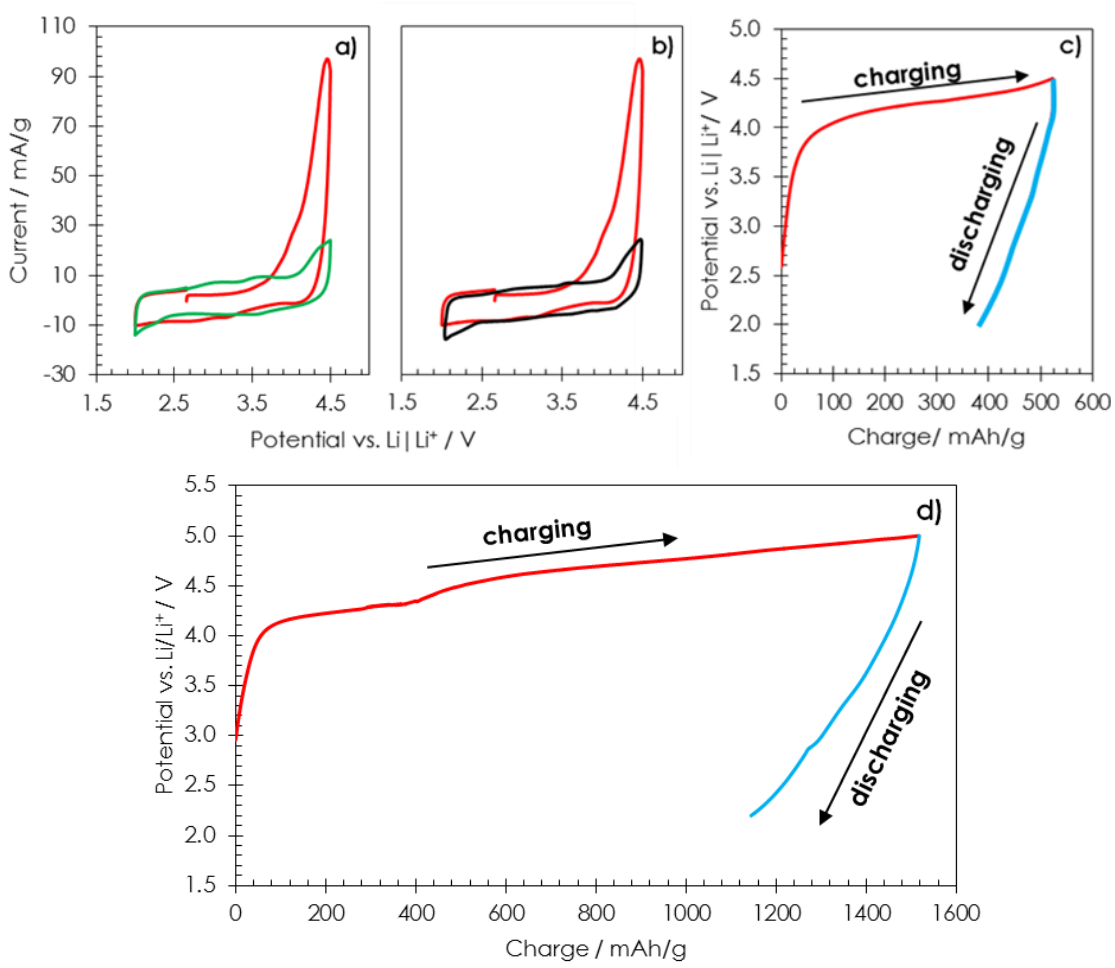

Figure 58 Electrochemical performance of the LReO/AC composite electrode vs. metallic lithium counter/reference electrode in 1 mol/L $LiPF_6$ in EC:DMC; a) and b) cyclic voltamperometry at 0.06 mV/s (1^{st} cycle: red line; 2^{nd} cycle: green line; 4^{th} cycle: black line); c) galvanostatic charge/discharge at C/20 up to 4.5 V vs. Li/Li^+; d) galvanostatic charge/discharge at C/20 up to 5.0 vs. Li/Li^+ showing a second plateau attributed to electrolyte oxidation at potential higher than 4.5 V vs. Li/Li^+.

The XRD pattern recorded during the initial open circuit period at 2.9 V vs. Li/Li^+ (Figure 60 (Right a)) displays the characteristic lines of LReO with additional peaks at 38.47º and 18.05º which are attributed to components of the cell used for the measurements. Up to 3.8 V vs. Li/Li^+, the diffractograms do not reveal any structural change of LReO (Figure 59 and Figure 60 (Right b)), which is in agreement with the galvanostatic plot, since the oxidation plateau of LReO is not started at 3.8 V vs. Li/Li^+ (position b in Figure 60 (Left)). The structural changes occur in the potential range between 3.8 V and 4.3 V vs. Li/Li^+.

Once 4.3 V vs. Li/Li^+ is reached, the LReO material is amorphous (Figure 60 (Right d)) and there are no further changes observed in the diffractograms neither during charging up to 4.5 V, nor during the subsequent discharge to 2.2 V vs. Li/Li^+ or the second charge.

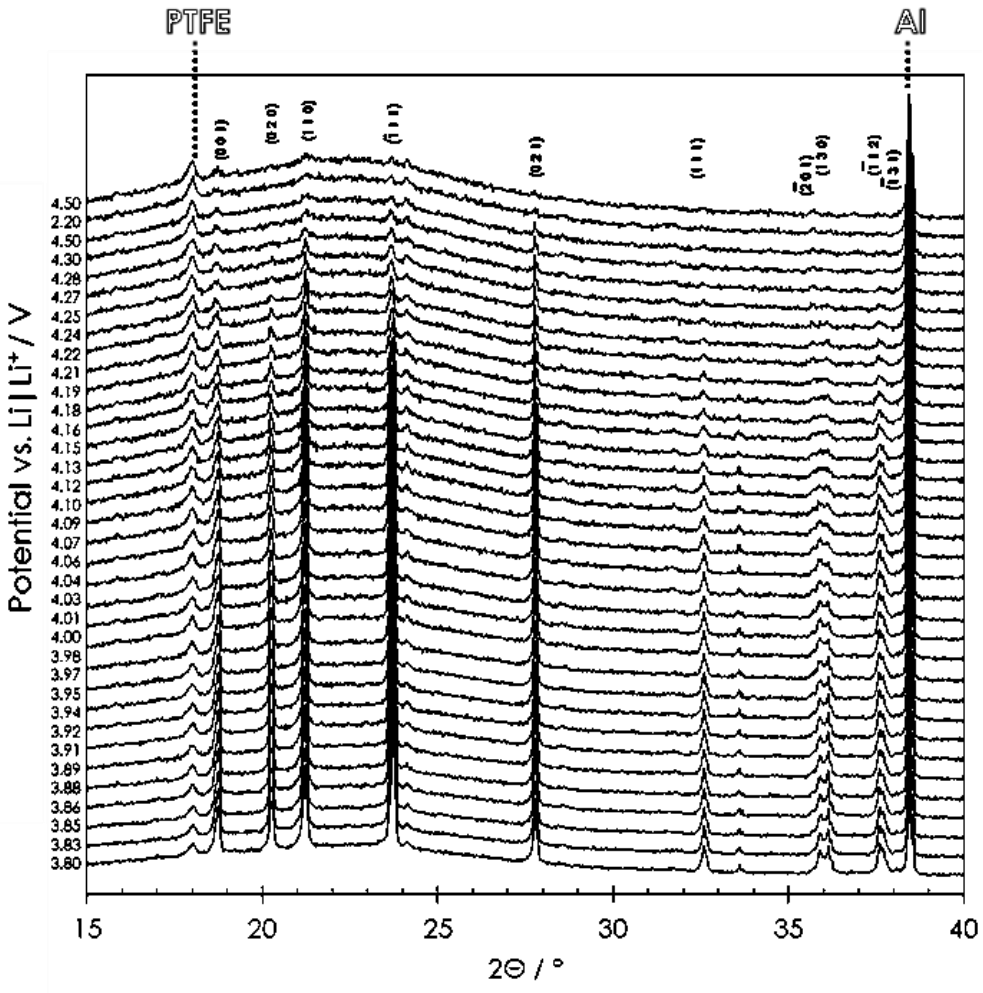

Figure 59 *In-situ* X ray diffractograms recorded during galvanostatic lithium extraction from LReO (being a part of composite electrode composed of 40 wt.% of AC, 40 wt.% of LReO, 15 wt.% of Super C65 and 5 wt.% of PTFE) and showing amorphization at high potential. Each pattern was obtained at a different potential indicated on the Y axis. The peaks marked with Miller indices relate to the LReO phase. The other peaks coming from the cell components (aluminum foil, PTFE) are also marked.

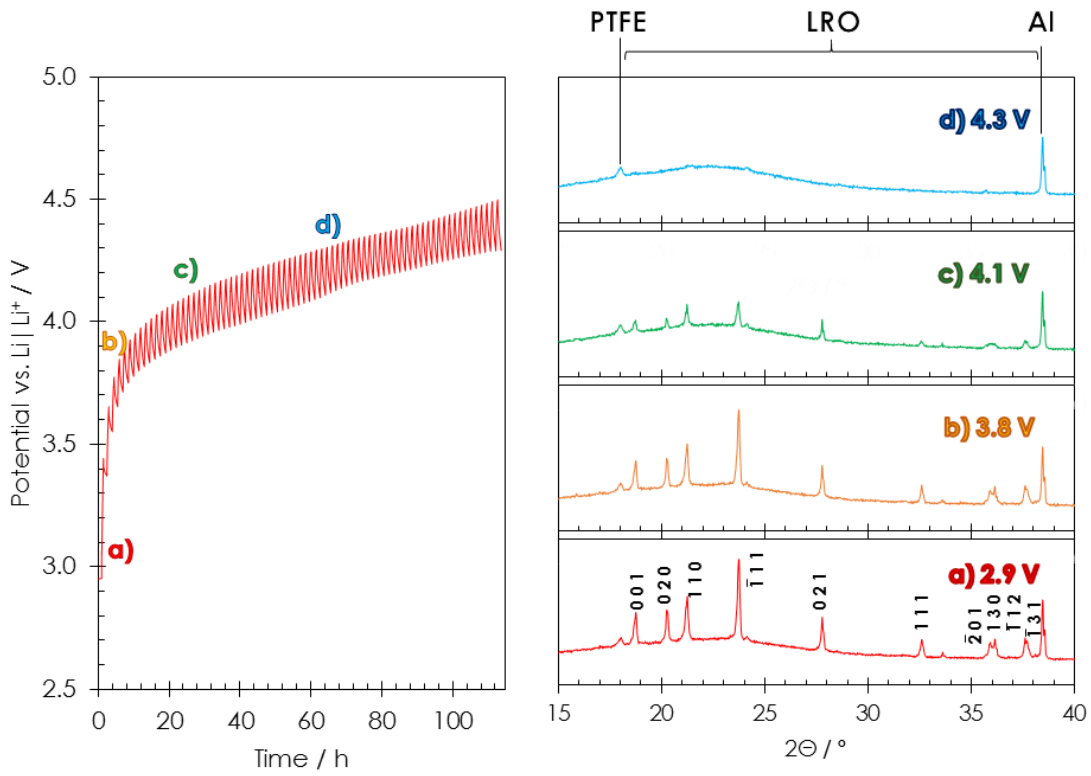

Figure 60 *In-situ* XRD investigation coupled with electrochemical oxidation of LReO/AC: (Left) Galvanostatic plot with 0.5 h pulses at C/20 followed by 1 h open circuit periods (vertical segments) in the potential range from 2.0 V to 4.5 V vs. Li/Li^+. (Right) X ray diffractograms recorded at a) OCP (2.9 V) and after polarization up to b) 3.8 V, c) 4.1 V and d) 4.3 V vs. Li/Li^+. The electrolyte was in 1 mol/L $LiPF_6$ in EC:DMC. Electrode composition: 40 wt.% of AC, 40 wt.% of LReO, 15 wt.% of Super C65 and 5 wt.% of PTFE.

IV. 4. Realization of a LIC cell with composite Li_5ReO_6/AC electrode

Taking into account the theoretical capacities of LReO (423 mAh/g) and graphite (372 mAh/g), it comes that the LReO/graphite mass ratio should be at least 0.88 to provide enough lithium to reach the composition LiC_6 during pre-intercalation of graphite. In addition, to realize a LIC with optimized power, it is recommended to introduce equal masses of activated carbon (AC) and graphite in the positive and negative electrode, respectively [201], meaning that the LReO/AC mass ratio in the positive electrode should be 0.88.

Since this electrode should also contain 15 wt.% of Super C65 and 5 wt.% of PTFE, these conditions are strictly met when using 37 wt.% of LReO and 43 wt. of AC. Further in this manuscript, the LReO-based electrodes will be realized with 40 wt.% of AC, 40 wt.% of LReO, 15 wt.% of Super C65 and 5 wt.% of PTFE.

The galvanostatic pre-lithiation of graphite was performed in a two-electrode cell using in addition a lithium pin as reference/counter electrode and applying different current conditions. To avoid any side reaction, the established potential limits are the same as in the case of LNiO [216], i.e. 4.5 V and 10 mV vs. Li/Li^+. Figure 61 displays i) the extraction of lithium ions from the LReO-based positive electrode observed as a potential plateau c.a. 4.3 V vs. Li/Li^+ (red curve); ii) the solid electrolyte interphase (S.E.I.) formation followed by graphite intercalation (blue line) represented by successive plateaus corresponding to stage transitions (inset blue line); iii) the voltage profile of the full cell (black line).

In Figure 61a, a constant current of C/20 (where C correspond to the theoretical capacity of graphite, i.e. 372 mAh/g) was applied during the entire experiment until the graphite intercalation compound LiC_6 was almost reached, seen as the final plateau below 100 mV vs. Li/Li^+ in the inset. In a second experiment, taking into account literature data revealing a reduction of S.E.I. development by increasing current [180,216], the S.E.I. was formed at C rate down to a potential of 0.2 V vs. Li/Li^+, after which a 2h rest period at OCV period was applied, and followed by lithium intercalation into graphite at C/20 (Figure 61b).

The negative electrode has been examined by SEM after the S.E.I. formation (once the potential reached 0.2 V vs. Li/Li^+) either at C/20 (Figure 62a) or C (Figure 62b). At C/20, a thick and cracked layer can be observed, and the graphite particles are non-differentiable (Figure 62a). In contrast, if the S.E.I. is formed at C rate, the graphite particles covered by a thin and continuous layer can be still distinguished (Figure 62b).

The different thicknesses of the S.E.I. layer can be related to the values of capacity required to reach 0.2 V vs. Li/Li^+, e.g., 64 mAh/g and 39 mAh/g at C/20 and C, respectively. These experiments suggest that, forming a thin S.E.I. layer by applying a high current should enable to reduce the resistance of the LIC and thereof to boost its power performance.

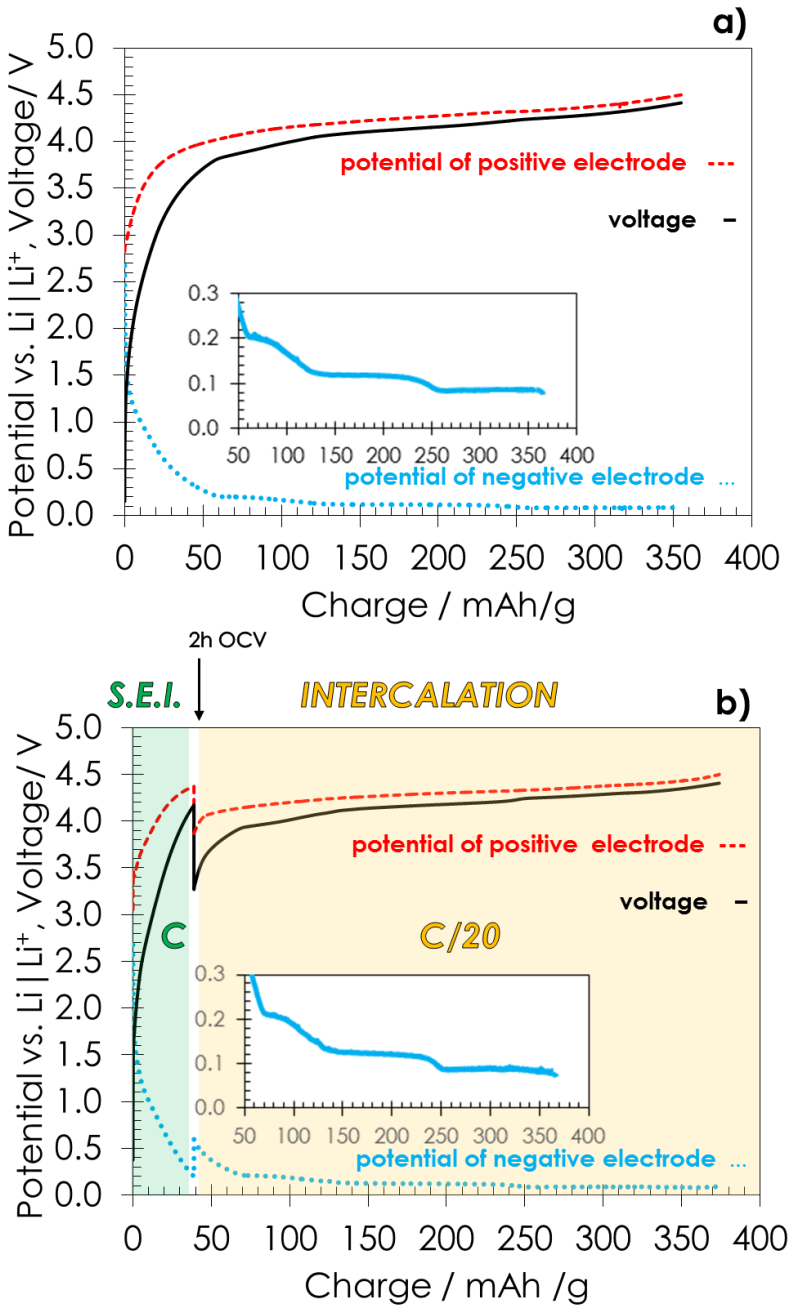

Figure 61 Pre-lithiation of graphite in a 2-electrode cell with LReO/AC positive electrode and metallic lithium as reference electrode. Galvanostatic profiles of the composite positive electrode (red dashed line), negative graphite electrode (blue dotted line with the visible staging effect as inset) and voltage of the cell (black solid line): a) S.E.I. formation and intercalation at C/20; b) S.E.I. formation at C followed by 2h OCV and intercalation at C/20. The electrolyte was in 1 mol/L $LiPF_6$ in EC:DMC. The positive electrode was composed of 40 wt.% of AC, 40 wt.% of LReO, 15 wt.% of Super C65 and 5 wt.% of PTFE.

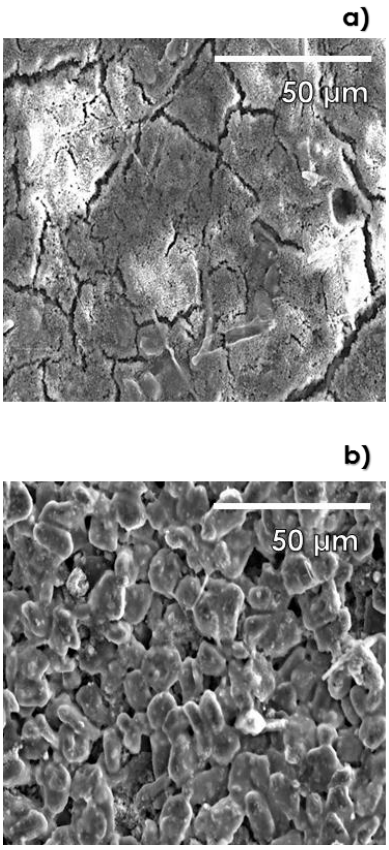

Figure 62 SEM images of the graphite negative electrode with the S.E.I. formed at a) C/20 and b) C.

Once the S.E.I. was formed in the conditions given in Figure 61b, the LIC was cycled galvanostatically with monitoring the potential profiles of the positive and negative electrodes. Figure 63a–c shows the galvanostatic charge/discharge curves at different current densities of 0.25 A/g, 0.50 A/g and 0.65 A/g (presented per mass of activated carbon or graphite) in the cell voltage range from 2.2 V to 4.1 V, where both electrodes operate in a safe potential window. The potential of the positive electrode (red dashed line) does not reach values lower than 2.0 V or higher than 4.2 V vs. Li/Li^+, which enables to avoid a S.E.I. formation on the surface of activated carbon or electrolyte oxidation, respectively. The lowest potential values for the graphite electrode (blue dotted line) are 49 mV, 23 mV and 13 mV vs. Li/Li^+ for currents of 0.25 A/g, 0.50 A/g and 0.65 mA/g, respectively, and are in all cases higher than 0 V vs. Li/Li^+ from which metallic lithium deposition can start with further risk of short circuit and thermal runaway.

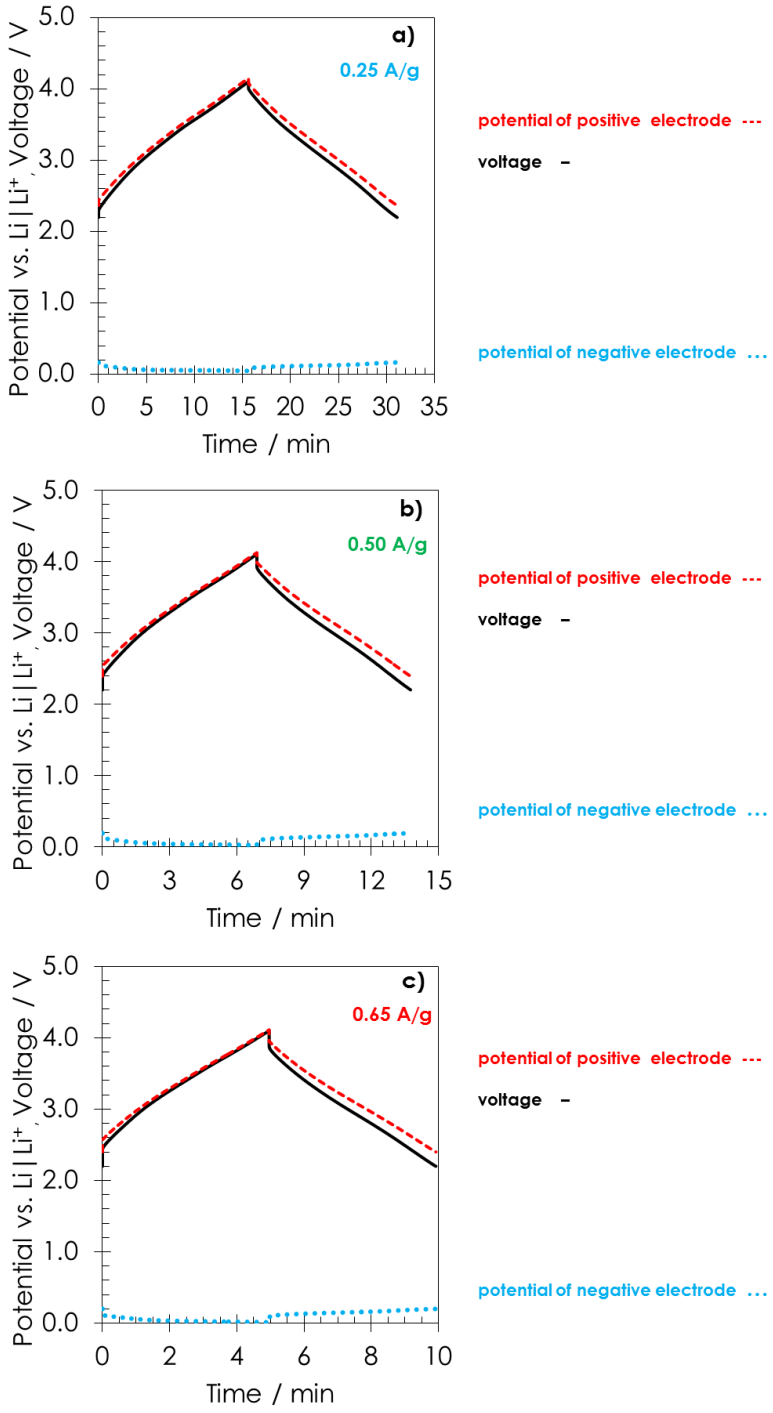

Figure 63 LIC with lithium reference electrode) where the S.E.I. was formed at C and graphite lithiated at C/20 at different current densities of: a) 0.25 A/g; b) 0.50 A/g and c) 0.65 A/g (values given per gram of activated carbon). Galvanostatic charge/discharge profiles of the composite positive electrode (red dashed line), negative graphite electrode (blue dotted line) and of the cell (black solid line). The electrolyte was 1 mol/L $LiPF_6$ in EC:DMC. The positive electrode was composed of 40 wt.% of AC, 40 wt.% of LReO, 15 wt.% of Super C65 and 5 wt.% of PTFE.

IV. 5. Cycle life of the LIC systems based on the positive Li_5ReO/AC composite electrode

The dependence of specific capacitance (expressed per total mass of electrodes) vs. cycle number is shown in Figure 64a-b and Figure 64b for S.E.I. formed at C/20 and C, respectively. Both cells were cycled in the voltage range from 2.2 V to 4.1 V at current densities from 0.25 A/g to 0.65 A/g. The initial 300 cycles presented in the insets of Figure 64 (referred to as conditioning cycles) were performed to stabilize the capacitance values. As it can be seen the capacitance slightly decreases during the first cycles at 0.25 A/g, and then stabilizes during the last 50 cycles (from the 250th to the 300th cycle). For both LICs, the capacitance strongly depends on the value of applied current and, as expected, is lower for the higher current values.

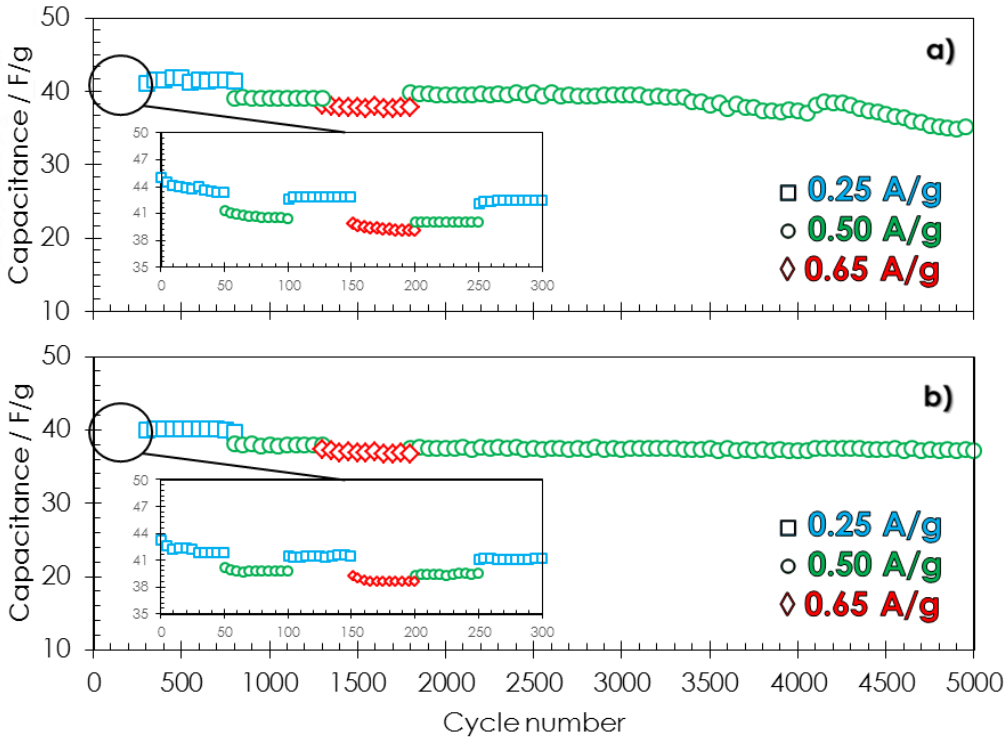

Figure 64 Specific capacitance of LICs vs. cycle number at different current values of 0.25 A/g (blue squares), 0.50 A/g (green circles) and 0.65 A/g (red diamonds) in the voltage range 2.2 V – 4.1 V: a) S.E.I. formed at C/20; b) S.E.I. formed at C. The current is expressed per mass of activated carbon and capacitance is expressed per total mass of electrodes. The electrolyte was in 1 mol/L $LiPF_6$ in EC:DMC. The positive electrode was composed of 40 wt.% of AC, 40 wt.% of LReO, 15 wt.% of C65 and 5 wt.% of PTFE.

The comparison of the cycle life of the two cells after ca. 2000 cycles reveals that the cell with the S.E.I. formed at C exhibits a stable capacitance up to 5000 cycles (Figure 64b), whereas the cell in which the S.E.I. was formed at C/20 displays a continuous capacitance fade after ca. 3500 cycles (Figure 64a). Similarly to the case of negative electrodes for LIBs, it proves that forming a thin and unbroken S.E.I. layer by applying a higher current [180] is mandatory for providing good electrochemical performance to the LIC.

Figure 65 compares the Ragone plots of the LIC (where the S.E.I. was formed at C and lithium intercalated into graphite at C/20) in its optimal voltage range of 2.2 – 4.1 V and of EDLCs with the same AC, either in 1 mol/L $LiPF_6$ in EC:DMC or 1 mol/L $TEABF_4$ in acetonitrile, and cycled up to their maximum voltage of 2.7 V. The specific energy and specific power values are expressed per total mass of the electrodes. The plot demonstrates that, for the currents set in these experiments, the energy density of the LIC is around 40 – 60 Wh/kg, which is almost four times higher than in the case of the ECs with organic electrolytes, where the values of energy are around 12 Wh/kg.

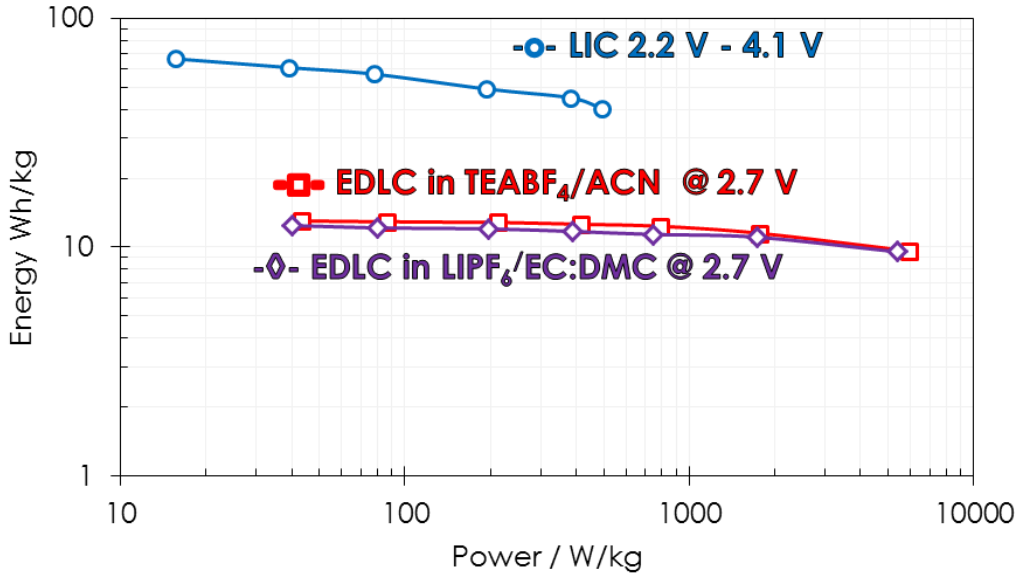

Figure 65 Ragone plots of the LIC (prepared from the LReO/AC composite electrode) in the voltage range of 2.2 - 4.1 V and of EDLCs using the same AC as electrode material either in 1 mol/L $LiPF_6$ in EC:DMC or 1 mol/L $TEABF_4$ in acetonitrile and charged up to 2.7 V.

Figure 66 and Figure 67 show the dependence of cell cycle life when the voltage range is extended below 2.2 V and above 4.1 V, which were previously indicated as safety limits to avoid possible side reactions occurring at the positive electrode (Figure 58a-b). When the LIC system operates in the voltage range from 1.8 V to 4.1 V (Figure 66), the capacitance values continuously decline at each cycle, very likely due to the formation of a S.E.I on the surface of the positive electrode. Similarly, an unstable cycle life is observed when the system operates in the voltage range from 2.5 to 4.3 V (Figure 67). In this case, although the maximum potential of the positive electrode is only 4.2 V, the poor performance could be due to the catalytic effect of rhenium oxide on electrolyte decomposition. Hence, we can confirm that the previously suggested window of 2.2 – 4.1 V is perfectly adapted for the LIC where graphite has been lithiated with help of an AC/LReO composite electrode. This voltage range is even higher than the one recommended for the ULTIMO commercial system where pre-lithiation is done with help of a lithium auxiliary electrode [198].

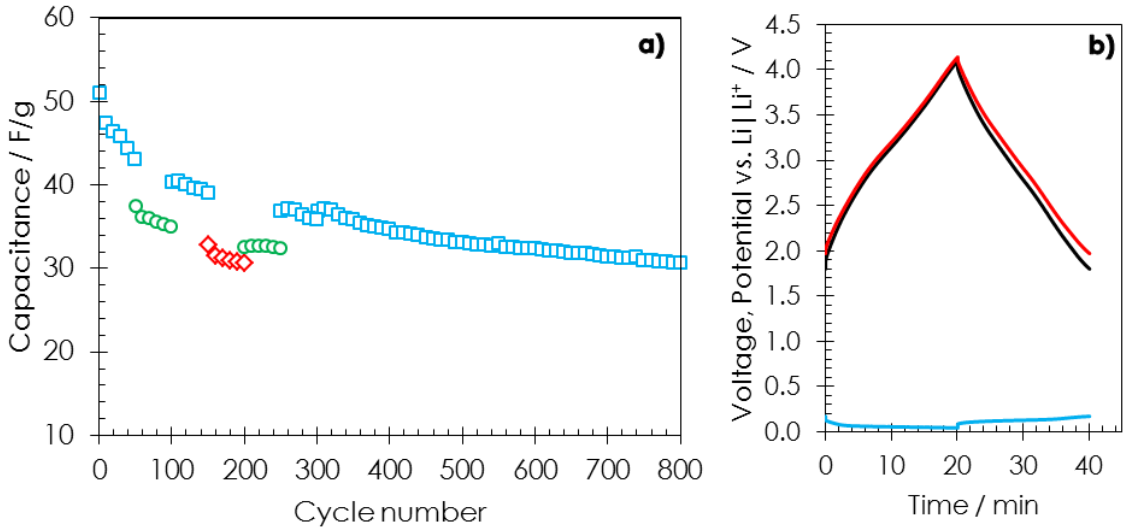

Figure 66 LIC where the S.E.I. was formed at C and graphite lithiated at C/20 with help of a LReO/AC composite electrode using 1 mol/L $LiPF_6$ in EC:DMC as electrolyte: a) specific capacitance of the LIC vs. cycle number at different current values of 0.25 A/g (blue squares), 0.50 A/g (green circles) and 0.65 A/g (red diamonds) in the voltage range 1.8 V – 4.1 V; b) galvanostatic charge/discharge profiles in the voltage range 1.8 V – 4.1 V for the positive electrode (red line), negative graphite electrode (blue line) and cell voltage (black line); when the voltage is as low as 1.80 V, the potential of the positive electrode is 1.97 V vs. Li/Li^+. The current is expressed per mass of activated carbon and capacitance is expressed per total mass of electrodes.

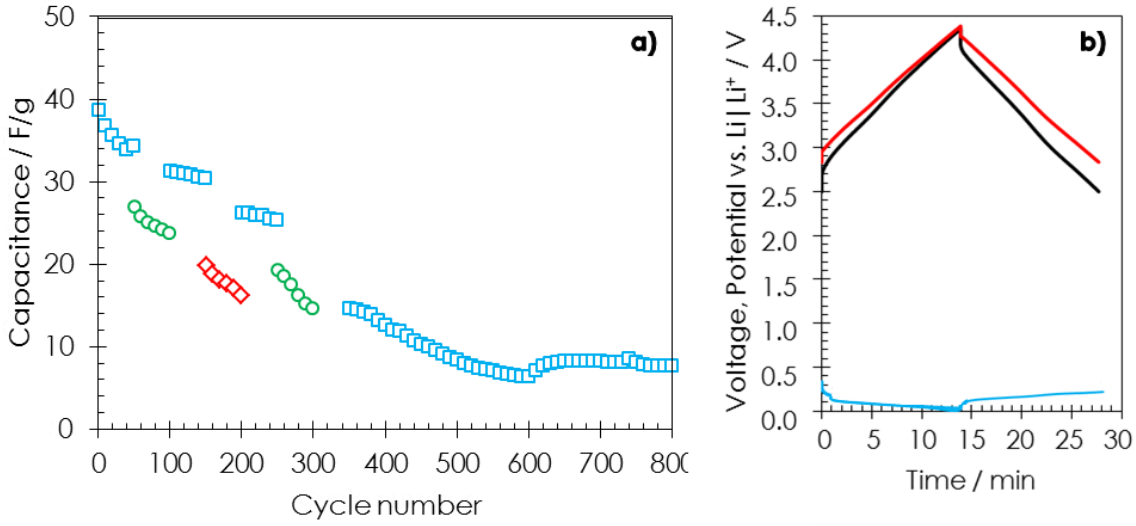

Figure 67 LIC where the S.E.I. was formed at C and graphite lithiated at C/20 with help of a LReO/AC composite electrode using 1 mol/L $LiPF_6$ in EC:DMC as electrolyte: a) specific capacitance of the LIC vs. cycle number at different current values of 0.25 A/g (blue squares), 0.50 A/g (green circles) and 0.65 A/g (red diamonds) in the voltage range 2.5 V – 4.3 V; b) galvanostatic charge/discharge profiles in the voltage range 2.5 V – 4.3 V for the positive electrode (red line), negative graphite electrode (blue line) and cell voltage (black line); when the voltage is as high as 4.30 V, the potential of the positive electrode is 4.2 V vs. Li/Li^+. The current is expressed per mass of activated carbon and capacitance is expressed per total mass of electrodes.

Conclusion

Whereas other lithium rich materials failed in chapter III, lithium rhenium (VII) oxide (Li_5ReO_6, LReO) appears as a good candidate meeting the essential requirements for S.EI. formation and graphite pre-lithiation. The relatively high specific capacity of LReO (423 mAh/g), allowed to reduce its quantity in the positive composite electrode to 40 wt.%.

We demonstrated that lithium ions are irreversibly and completely extracted from LReO at potential c.a. 4.3 V vs. Li/Li^+, at which oxidation reactions of the electrolyte can be still excluded. Furthermore, when using high current during S.E.I. formation, e.g., C rate, an homogenous and thin S.E.I. is formed on the graphite electrode, thereby reducing the cell resistance. In these conditions, when restricting the operating voltage range to 2.2 - 4.1 V to

avoid electrolyte oxidation and formation of a S.E.I. on the surface of the positive electrode, the LIC exhibits excellent cycle life.

Hence, our prediction related to necessary low value of band gap for successful application of pre-lithiation with sacrificial material is verified when using Li_5ReO_6. However the limited abundance and relatively high price of rhenium are a disadvantage for using a rhenium-based material in LICs. Therefore, it is still necessary to look either for more abundant lithiated metal oxides of low band gap which could be economically justified or for another family of materials. The second case will be considered in chapter V where a renewable organic material will be implemented.

CHAPTER V

Lithiated organic material as a “green” source of lithium

Introduction

Despite the high irreversible capacity of LReO and the excellent cycle life of the LIC system based on its use as sacrificial material in the composition of the positive electrode, it is necessary to find a more ecologically friendly and economic approach, while ensuring the lowest lithium extraction potential. Lithiated organic compounds described in the literature [128,130,134] as possible cathode materials for LIB possess several interesting properties for LIC application. First of all, the value of extraction potential is relatively low, ca. 3.0 V vs. Li/Li^+. Next, the specific capacity is relatively high, in the range from 200 mAh/g to 400 mAh/g. Last and foremost, lithiated organic materials present an irreversible character of lithium extraction which can be associated to the dissolution of their oxidized form [128,130,134]. For the application in LIB, this irreversibility is a disadvantage, whereas for the application as sacrificial lithium source in LIC it might be much desired.

Lithium can be irreversibly extracted from some compounds, such as dilithium squarate ($Li_2C_4O_4$), oxalate ($Li_2C_2O_4$), ketomalonate ($Li_2C_3O_5$) and di-ketosuccinate ($Li_2C_4O_6$), which were presented as possible additives in the composition of cathode to compensate the irreversible capacity related to the S.E.I. formation [217]. However, implementing these materials requires a high amount of highly conductive agent (around 30 wt.% of high surface graphitized carbon) in order to extract lithium. In this chapter, we will consider 3,4–dihydroxybenzonitrile dilithium salt which has never been synthesized and mentioned in the literature as electrode material. It possess a high value of theoretical capacity, ca. 365 mAh/g, and as it will be shown, lithium ions can be irreversibly extracted at ca. 3.2 vs. Li/Li^+.

V. 1. Synthesis and characterization of 3,4–dihydroxybenzonitrile dilithium salt (Li_2DHBCN)

3.7 mmol of 3,4–dihydroxybenzonitrile (Sigma Aldrich) were introduced at room temperature in 15 ml of anhydrous tetrahydrofuran (THF anhydrous, Sigma Aldrich) under argon atmosphere inside glove-box and stirred for 15 min until complete dissolution, after which 7.4 mmol of lithium hydride (LiH, Sigma Aldrich) were added to the transparent solution, and the mixture was stirred for 15 h. According to equation (20), hydrogen

evolved during the reaction and a white precipitate of Li_2DHBCN was formed. After filtration, the solid Li_2DHBCN was dried at 150 °C under vacuum for 5h in a glass oven (Büchi).

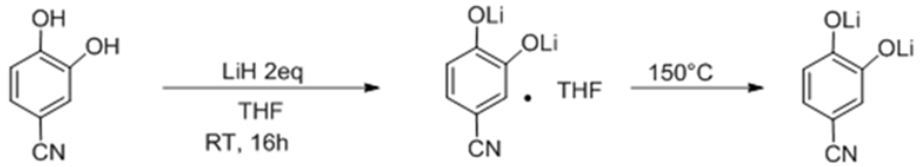

(20)

Figure 68a – b shows the IR spectra in KBr pellet of as-received Li_2DHBCN after filtration (the dried Li_2DHBCN is extremely sensitive to moisture and reacted with the atmosphere during recording its IR spectrum) and of 3,4–dihydroxybenzonitrile for comparison purpose. Characteristic lines of THF are easily identified in the spectrum of as-received Li_2DHBCN (Figure 68b) in the range from 2882 to 2979 cm^{-1} (C–H stretching) and at 1041 cm^{-1} (C–O stretching). The proof of lithiation in Figure 68b is given by the disappearance of the characteristics O-H lines in the range from ca. 3000 to 3500 cm^{-1} (Figure 68a). Interestingly the spectrum of Li_2DHBCN shows a characteristic band at around 488 cm^{-1}, which according to Zhu *et al*. [218] could be attributed to the Li–O vibration.

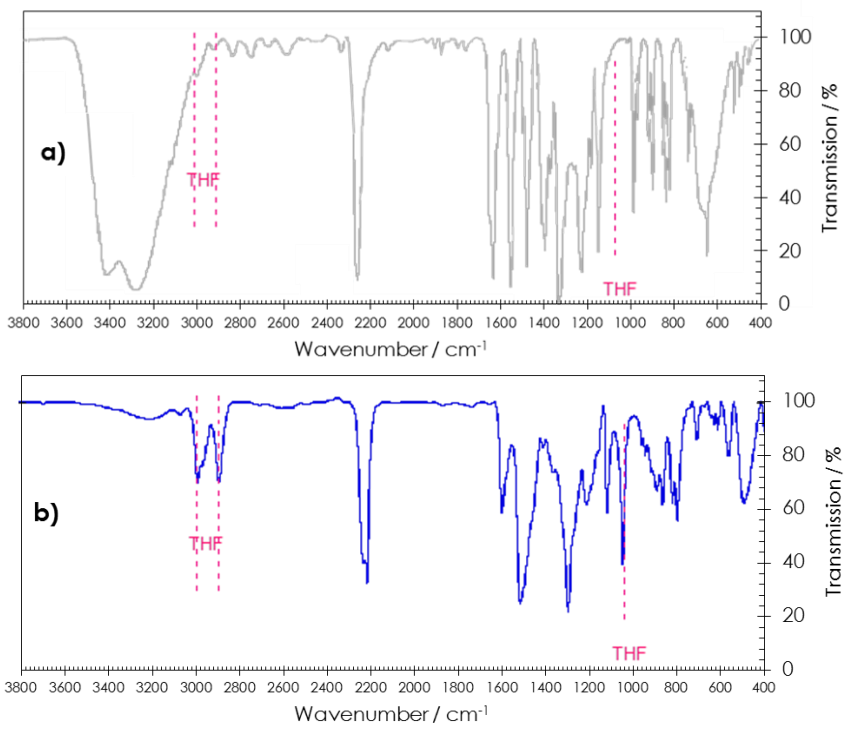

Figure 68 IR spectra of a) 3,4–dihydroxybenzonitrile; b) as-received Li_2DHBCN

Dried Li_2DHBCN was introduced in air tight aluminum crucible in glove–box under argon atmosphere and analyzed by differential scanning calorimetry (DSC) (Figure 69). The absence of any signal at temperatures lower than 100°C proves that THF (and water) were well-eliminated during drying. In the range of temperatures from 150 to 230 °C, there is slight deviation of base line which is attributed to fast amorphization, characteristic for lithiated organic compounds [219].Between 285 and 305 °C, Li_2DHBCN is exothermally decomposed with formation of Li_2CO_3, as already proved by Poizot *et al.* for tetrahydroxy-p-benzoquinone dilithium salt (Li_2DHDMQ) [219].

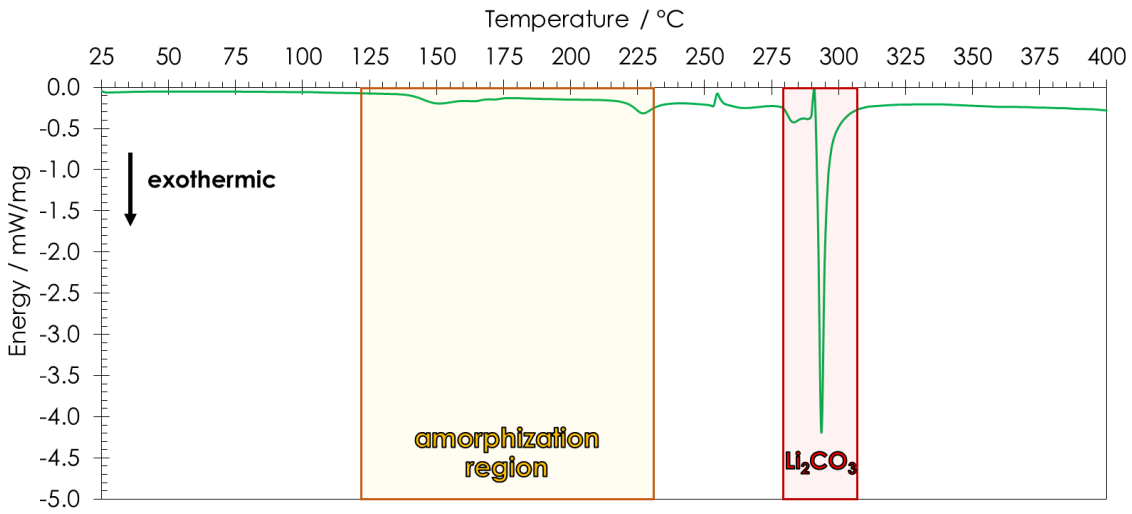

Figure 69 DSC thermogram of dried Li_2DHBCN at a heating rate of 10 °C/min.

In the ^{13}C NMR spectrum of dried Li_2DHBCN (Figure 70), the peaks at 165 ppm and 156 ppm are attributed to the –C–OLi carbons in 3 and 4 position of CN, respectively. The signals at 125 ppm and 117ppm are related to the C–H carbons of the aromatic ring. The shift at 124 ppm comes from the carbon atom of the CN group. The carbon atom of the aromatic ring close to the C≡N group gives the signal at 95 ppm. The huge peak at 50 ppm is due to deutered methanol (CD_3OD) used as solvent.

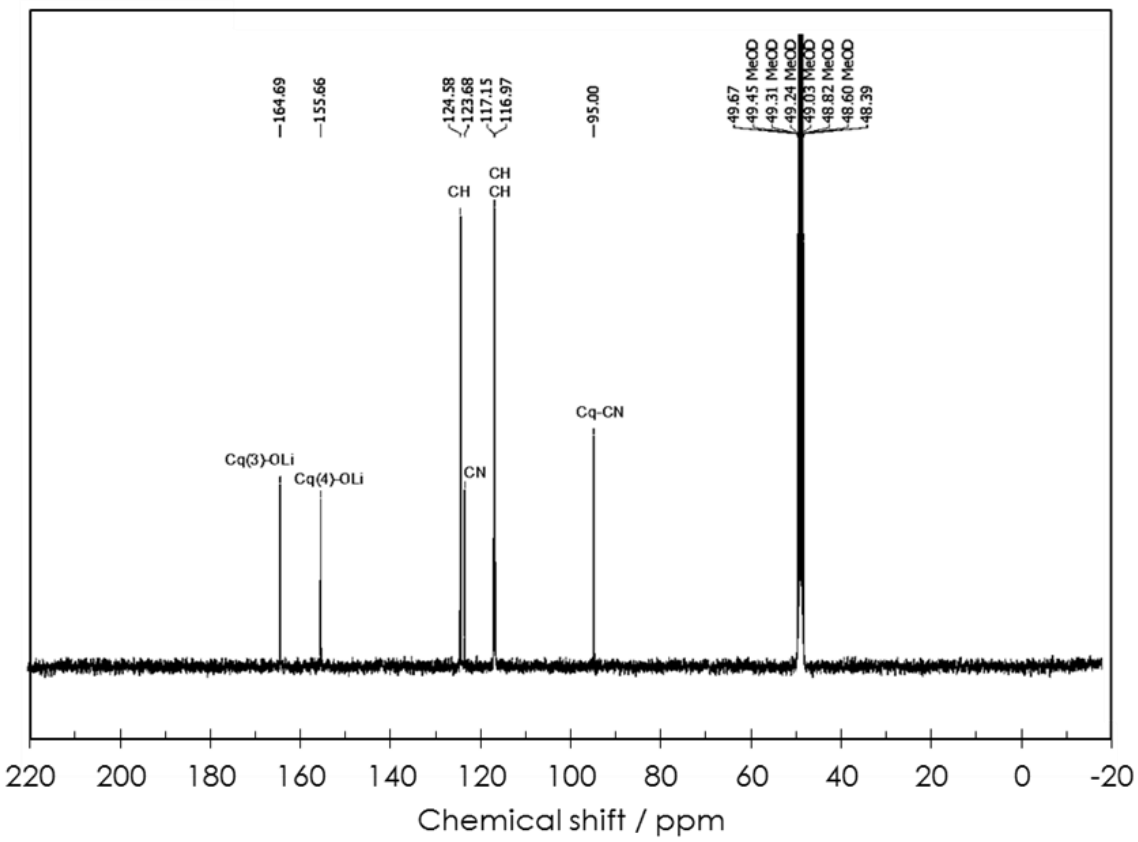

Figure 70 ^{13}C NMR spectrum of dried Li_2DHBCN at 500 MHz. Deuterated methanol - CD_3OD - was used as solvent and as internal standard for chemical shifts.

The ^{1}H nuclear magnetic resonance (NMR) spectrum of dried Li_2DHBCN is presented in Figure 71. The peak at 6.4 ppm with integration ratio of 1 characterizes the single aromatic proton in ortho position of –CN. The multiplet at around 6.7 ppm with intensity ratio of 2 is attributed to the two other aromatic protons. The peak at 3.2 ppm is due to protons of incompletely deuterated methanol. The peak at 4.8 ppm is characteristic of HDO and is attributed to partial decomposition of Li_2DHBCN into 3,4–dihydroxybenzonitrile due to moisture present in the atmosphere of in deuterated methanol.

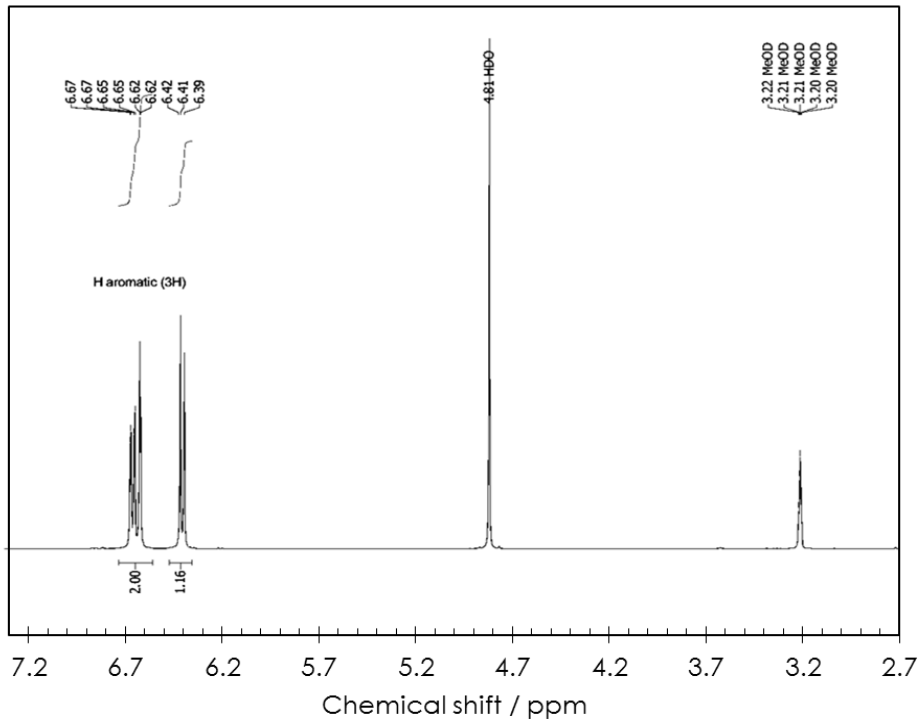

Figure 71 ^{1}H NMR spectrum of dried Li_2DHBCN at 500 MHz. Deuterated methanol - CD_3OD - was used as solvent and as internal standard for chemical shifts.

V. 2. Preparation of composites electrodes including Li_2DHBCN

Two different compositions of electrodes were realized either for determining the electrochemical performance of Li_2DHBCN (65 wt.% Li_2DHBCN, 30 wt.% Super C65 and 5wt.% of PTFE) or for pre-lithiation of graphite in LIC (40 wt.% AC, 40 wt.% Li_2DHBCN, 15 wt.% Super C65 and 5wt.% of PTFE). Since dried Li_2DHBCN is sensitive to moisture, it was necessary to fabricate the electrodes inside an argon filled glove–box. However, before to do such, either Super C65 alone or AC and Super C65 were mixed in air atmosphere together with PTFE (60 wt.% dispersion in water, Aldrich) in 1/1 volume ratio water/isopropanol solution in order to reach the following composition of the solid mixture after evaporation of the liquid phase: i) 85.7 wt.% of Super C65 and 14.3 wt.% of PTFE for the electrode which will contain only Super C65; ii) 66.7 wt.% of AC, 25 wt.% of Super C65 and 8.3 wt.% of PTFE for the electrode which will contain Super C65 and AC. The

liquids were evaporated at 100°C under fume-hood, and the solid was further dried in a vacuum stove at 120 °C for 12 h.

Then, the dried solid was transferred in a glove–box, where it was mixed with an appropriate amount of Li_2DHBCN (in 10-20 mL of n-heptane) so as to reach the final composition of the solid mixture either i) 65 wt.% Li_2DHBCN, 30 wt.% Super C65 and 5wt.% of PTFE or ii) 40 wt.% AC, 40 wt.% Li_2DHBCN, 15 wt.% Super C65 and 5wt.% of PTFE. After natural evaporation of excess n-heptane, the wet mass was placed in a mortar to get dough which was rolled to form a 250 µm thick sheet. Electrodes of diameter 16 mm were cut from the sheet and dried under vacuum in Büchi glass oven at 120 °C for 12 h.

SEM images of an electrode are presented in Figure 72. The observable cracks are probably related to solvent evaporation; indeed, as the preparation was realized in a glove-box, the sheet could not be homogenized by calendaring. The brighter parts on the images are due to charges accumulation on the 3,4–dihydroxybenzonitrile dilithium salt particles much less conductive than carbon.

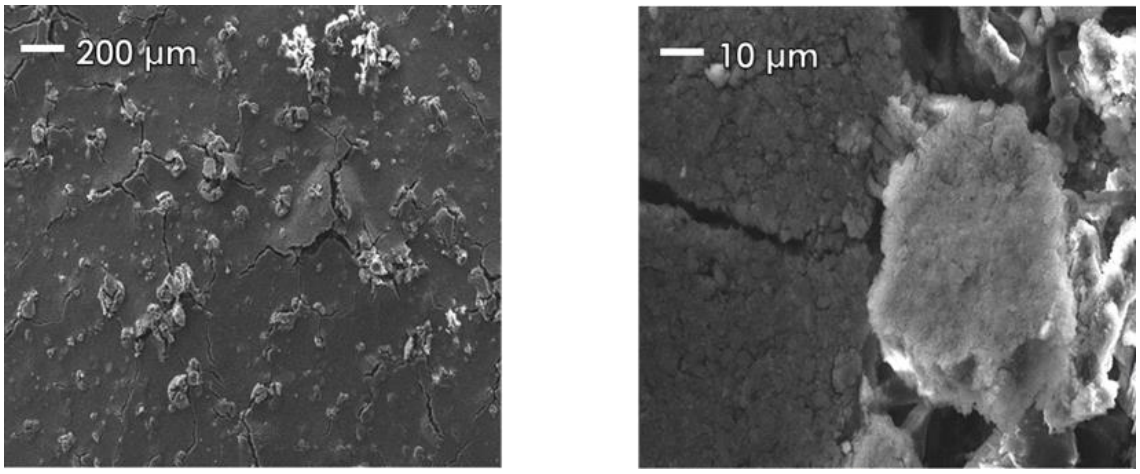

Figure 72 SEM images of a composite electrode with 40 wt.% of AC, 40 wt.% of Li_2DHBCN, 15 wt.% of Super C65 and 5wt.% of PTFE: the left image displays a general view, whereas the right one shows a magnification close to a crack.

V. 3. Electrochemical lithium extraction from Li_2DHBCN

The electrochemical performance of Li_2DHBCN (composite electrode containing 65 wt.% Li_2DHBCN, 30 wt.% Super C65 and 5wt.% of PTFE) was determined in a two-electrode cell where metallic lithium played the role of counter and reference electrode. During the first cycle, the cyclic voltammogram (Figure 73a) shows an anodic peak (red line) connected to lithium extraction starting from ca. 3.0 V vs. Li/Li^+ with a maximum ca. 3.7 V vs. Li/Li^+. The cathodic scan does not display any peak, which proves that lithium extraction from this material is fully irreversible. During the second cycle (green line), still a small anodic peak is observed, which totally disappears in the next scans. The galvanostatic charge/discharge profiles at C/10 in the potential range from 2.0 – 4.5 V vs. Li/Li^+ (where C corresponds to the theoretical capacity of the 3,4-dihydroxybenzonitrile dilithium salt, e.g., 364 mAh/g) (Figure 73b) display an extraction plateau at around 3.2 V vs. Li/Li^+, and a complete irreversibility of the process.

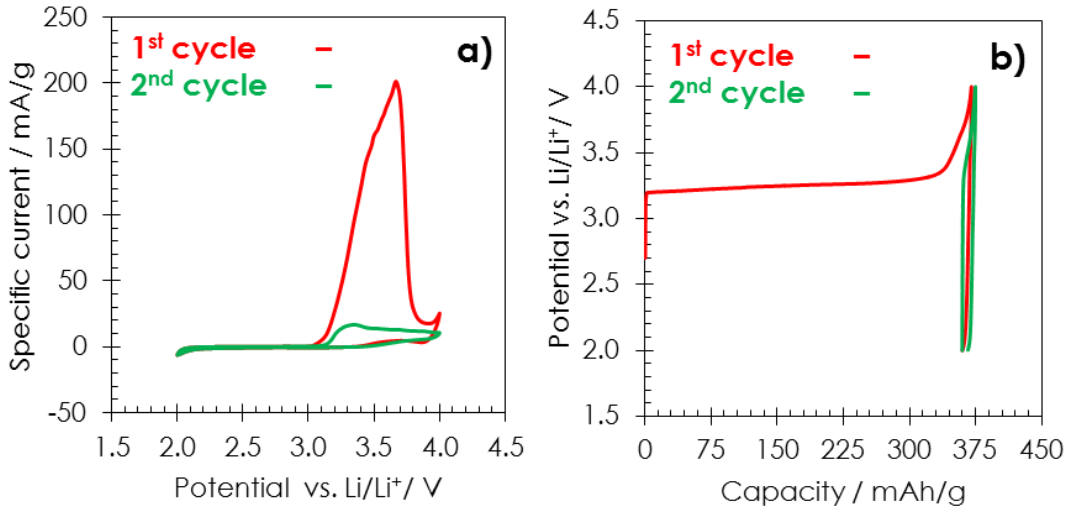

Figure 73 Electrochemical performance of 3,4-dihydroxybenzonitrile dilithium salt: a) cyclic voltammetry at 0.06 mV/s; b) galvanostatic charge/discharge at C/10. The red lines represent the first cycle and the green lines the second cycle. The electrodes were composed of 65 wt% Li_2DHBCN, 30 wt% Super C65 and 5 wt% PTFE binder. The experiments were performed in 1 mol/L $LiPF_6$ dissolved in EC: DMC (vol. ratio 1:1) electrolyte with metallic lithium counter/reference electrode.

In order to estimate the oxidation limit of the electrode material, the anodic polarization of the composite electrode has been prolonged to higher potentials. As it can be seen from Figure 74, after the first irreversible lithium extraction plateau, there is a potential rise followed by another endless irreversible plateau at potential higher than 4.5 V vs. Li/Li^+, which might be associated to electrolyte oxidation (Figure 74b). Hence, the exact value of irreversible lithium extraction capacity was determined by the position of the inflexion point, at ca. 360 mAh/g in Figure 74a, demonstrating that all lithium present in Li_2DHBCN (theoretical value of 365 mAh/g) will be available for graphite lithiation.

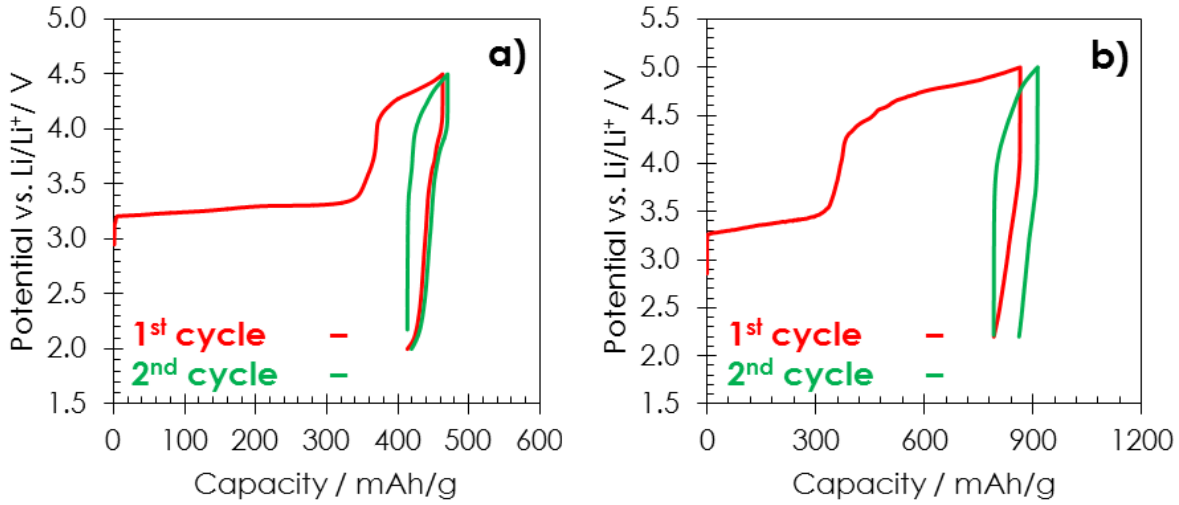

Figure 74 Galvanostatic charge/discharge profiles of 3,4-dihydroxybenzonitrile dilithium salt at C/10. The lithium extraction takes place till ca. 4.0 V vs Li/Li^+. The second plateau ca. 4.5 V vs. Li/Li^+ is attributed to side reactions such as electrolyte oxidation. The electrodes were composed of 65 wt% Li_2DHBCN, 30 wt% Super C65 and 5 wt% PTFE binder. The experiments were performed in 1 mol/L $LiPF_6$ dissolved in EC: DMC (vol. ratio 1:1) electrolyte with metallic lithium counter/reference electrode.

V. 4. Realization and performance of LIC cell where graphite is pre-lithiated with AC/Li_2DHBCN composite positive electrode

The composition of the composite positive electrode was determined by taking into account the irreversible capacity of Li_2DHBCN ($Q_{Li2DHBCN} = 365$ mAh/g) and the reversible of graphite (Q_G = 372 mAh/g for LiC_6 formation). Hence, for full intercalation of graphite, the mass ratio of Li_2DHBCN ($m_{Li2DHBCN}$) and graphite (m_G) should be (21):

$$\frac{m_{Li2DHBCN}}{m_G} = \frac{Q_G}{Q_{Li2DHBCN}} = \frac{0.372}{0.365}\frac{[Ah/g]}{[Ah/g]} = 1.02 \qquad (21)$$

Since the mass of graphite m_G should be equal to the mass of activated carbon m_{AC} to optimize the energy and power of the system [201]), and the total mass of AC and Li_2DHBCN should represent 80 wt.% of the total electrode mass, it comes that $m_{AC} \sim m_{Li2DHBCN} \sim 40\%$. Consequently, for all further experiments, we have adopted the following composition of the positive electrode: 40 wt.% AC YP80F, 40 wt.% Li_2DHBCN, 15 wt.% Super C65 and 5wt.% of PTFE (for electrode preparation, see V.2).

The electrochemical pre-lithiation of graphite was realized in two-electrode cell (from El-Cell) with AC/Li_2DHBCN and graphite as positive and negative electrode, respectively, and a lithium pin as reference. Figure 75 shows the galvanostatic characteristics, where the S.E.I. was formed at C and intercalation at C/10 (where C is the theoretical capacity of graphite, i.e. 372 mAh/g). The potential limits were fixed at 4.00 vs. Li/Li^+ for the positive electrode and 0.01 V vs. Li/Li^+ for the negative one, to prevent from electrolyte oxidation and lithium plating, respectively. When the potential of the negative electrode reached 0.20 V vs. Li/Li^+ (for which it can be considered that the S.E.I. is totally formed), the potential of the positive electrode was ca. 3.95 V vs. Li/Li^+, which is very close to the positive electrode limit. Therefore, at this point, the cell was let at OCV for two hours, after which lithium was intercalated at C/10. In Figure 75 it can be seen that the total capacity is around 250 mAh/g, which is much lower than the expected 360-370 mAh/g. Hence, it seems that a part of Li_2DHBCN could be dissolved, probably because of the use of too high current (C) during the S.E.I. formation. To verify this hypothesis, the next experiment will be performed with a current of C/10 during all the process.

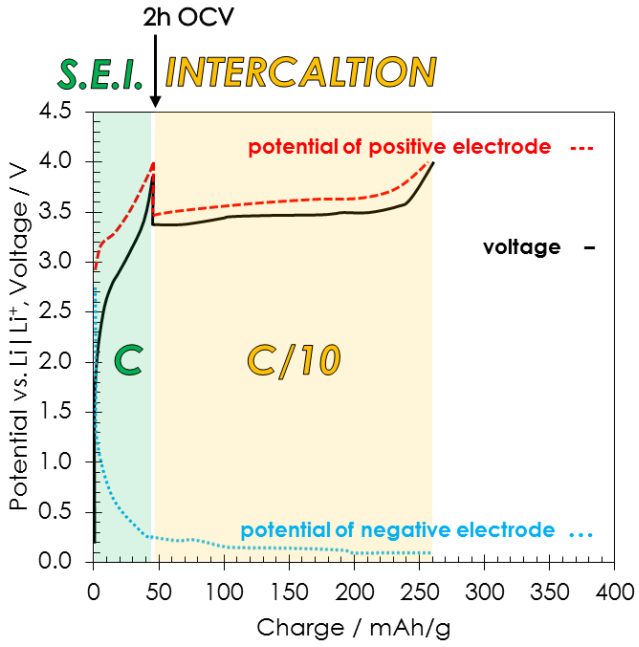

Figure 75 Profiles of electrodes potential and cell voltage during galvanostatic S.E.I. formation and graphite lithiation with help of a composite positive electrode composed of 40 wt.% AC YP80F, 40 wt.% Li_2DHBCN, 15 wt.% Super C65 and 5wt.% of PTFE. The S.E.I. was formed at C till reaching a potential of 0.2 V vs. Li/Li^+ (area highlighted in green); then, after a rest period of two hours, lithium was intercalated into graphite at C/10 (area highlighted in yellow). The potential limits for positive and negative electrodes are 4.0 V and 0.01 V vs. Li/Li^+, respectively. Color of the curves: red for the potential of positive electrode; blue for the potential of negative electrode; black for the cell voltage profile. The electrolyte is 1 mol/L $LiPF_6$ in EC: DMC.

Figure 76 shows the galvanostatic characteristics of electrodes potential and cell voltage when a constant current of C/10 (where C is the theoretical capacity of graphite, i.e. 372 mAh/g) was applied throughout the whole experiment, with potential limits fixed at 4.0 V and 10 mV vs. Li/Li^+, in order to avoid possible side reactions. From the profile of the positive electrode, it is seen that lithium is extracted from Li_2DHBCN ca. 3.2 V vs. Li/Li^+. The total capacity reaches 360 mAh/g, which is close to the value predicted according to the respective masses of electrodes components. However, taking into account the irreversible capacity corresponding to the S.E.I. formation (approximately 40 mAh/g), it comes that the amount of lithium reversibly intercalated into graphite corresponds to 320 mAh/g, meaning that graphite is not totally saturated with lithium. Since the amount of

lithium reversibly intercalated/deintercalated during LIC operation is very small, this is obviously not an issue at all.

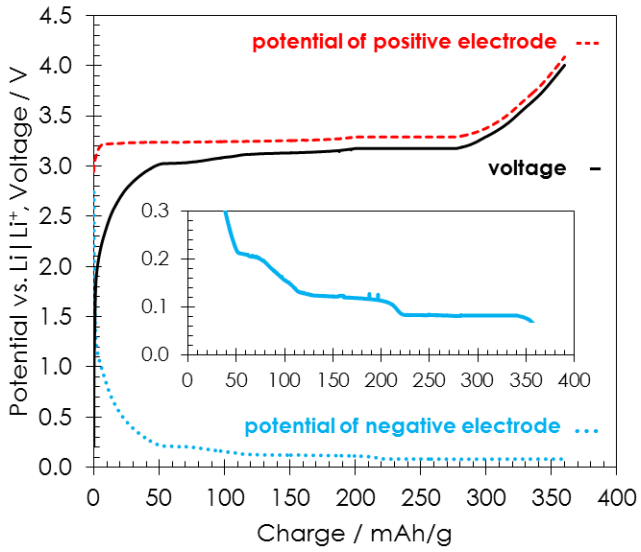

Figure 76 Profiles of electrodes potential and cell voltage during galvanostatic (C/10) S.E.I. formation and graphite lithiation with help of a composite positive electrode composed of 40 wt.% AC, 40 wt.% Li_2DHBCN, 15 wt.% Super C65 and 5wt.% of PTFE. The solid black line represents the cell voltage, whereas the dashed red line and dotted blue line are the profiles of positive and negative electrodes, respectively. The continuous blue line in the inset shows an expansion of the negative electrode profile to better evidence the stage transitions. The electrolyte is 1 mol/L $LiPF_6$ in EC: DMC.

Once lithiation of the graphite electrode was completed, the LIC was cycled galvanostatically, while monitoring the cell voltage and the potentials of positive and negative electrode. Figure 77a – c shows the galvanostatic charge/discharge profiles for different current densities of 0.25 A/g, 0.50 A/g and 0.65 A/g (expressed per mass of activated carbon/graphite) in the voltage range from 2.2 V to 4.0 V. In this voltage range, the potential of the positive electrode (red dashed line) is always higher than 2.2 V, which avoids the possibility of S.E.I. formation on the surface of AC, and lower than 4.0 V vs. Li/Li^+, which avoids electrolyte oxidation. Considering the graphite electrode, the lowest potential values (blue dotted line) are 37 mV, 20 mV and 15 mV vs. Li/Li^+ for currents of 0.25 A/g, 0.50 A/g and 0.65 mA/g, respectively. Hence, whatever the current, the graphite

electrode potential is always higher than 0 V vs. Li/Li^+; in other words, lithium plating cannot occur, and risks of short circuit and thermal runaway do not exist in such conditions.

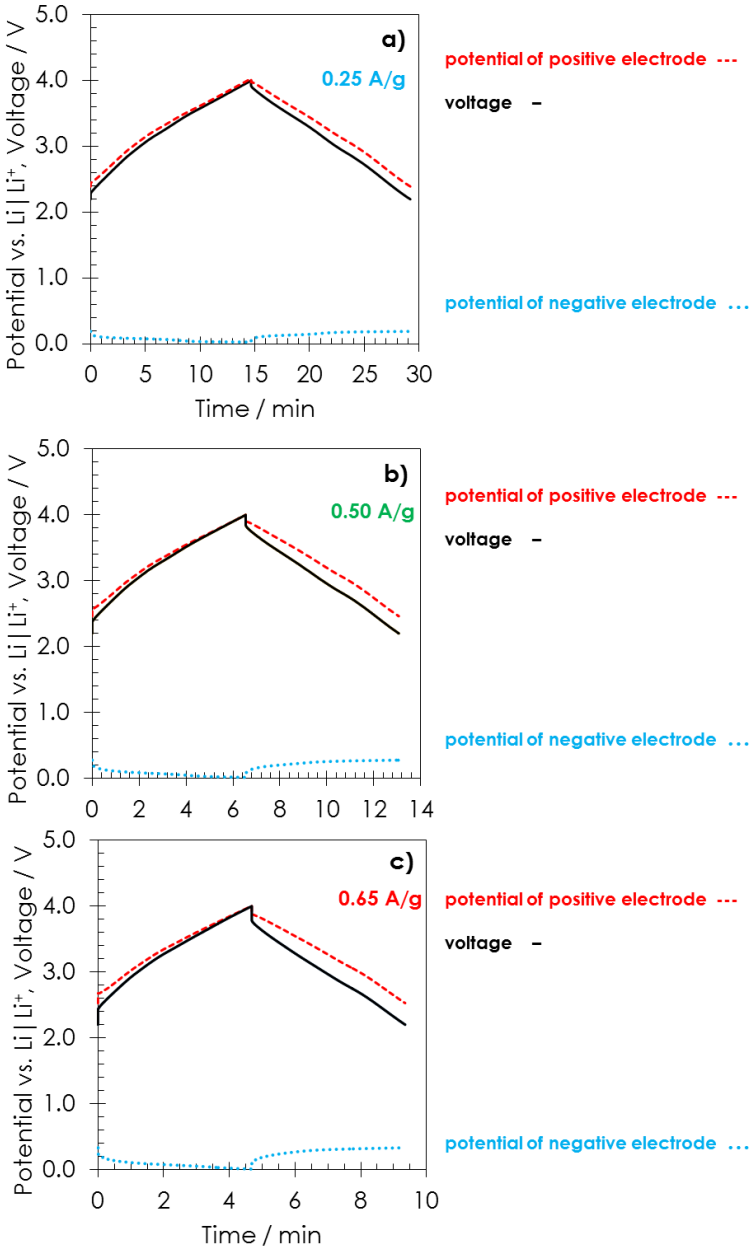

Figure 77 Galvanostatic charge/discharge of LIC with sacrificial composite positive electrode based on Li_2DHBCN at a) 0.25 A/g, b) 0.50 A/g and c) 0.65 mA/g (current per gram of activated carbon) in the voltage range from 2.2 to 4.0 V. The composition of the positive electrode is 40 wt.% AC, 40 wt.% Li_2DHBCN, 15 wt.% Super C65 and 5wt.% of PTFE. The electrolyte is 1 mol/L $LiPF_6$ in EC: DMC. The black solid line represents the cell voltage; the dashed red line and the blue dotted lines are the potential profiles of the positive and negative electrodes, respectively.

The cycle life of the previous kind of cell has been investigated by repeated galvanostatic cycling in the voltage range 2.2 V – 4.0 V with current densities from 0.25 A/g to 0.65 A/g. Figure 78 shows the dependence of capacitance (expressed per total mass of electrode materials) vs. cycle number. The first 300 cycles shown in the inset of Figure 78 were used for formatting the cell; the capacitance values slightly decrease during the first 100 cycles, but then they are quite stable for a given value of current. Obviously, the capacitance depends strongly on current and, as expected, is lower for higher currents. From 1800 to 5000 cycles at 0.50 A/g, the capacitance fade of the cell is extremely low, demonstrating that pre-lithiation at C/10 enabled the realization of well-performing LIC.

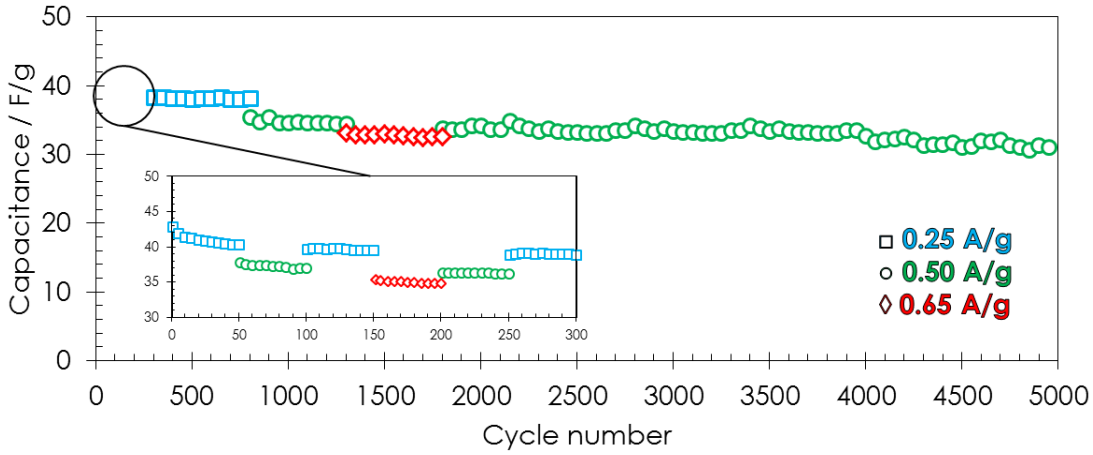

Figure 78 Cycle life of a LIC with sacrificial composite positive electrode based on Li_2DHBCN where S.E.I. formation and pre-lithiation has been performed at C/10. The LIC has been cycled at 0.25 A/g (blue squares), 0.50 A/g (green circles) and 0.65 A/g (red diamonds) in the voltage range from 2.2 to 4.0 V. The electrolyte was 1 mol/L $LiPF_6$ in EC:DMC.

Figure 79 presents comparative Ragone plots of the LIC (with S.E.I. formation and pre-lithiation at C/10) in its optimal operating voltage range of 2.2 – 4.0 V and of EDLCs realized with the same activated carbon, either in 1 mol/L $LiPF_6$ or 1 mol/L $TEABF_4$, and cycled up to their maximum voltage of 2.7 V. The energy and power densities values are given for the total mass of electrodes materials. The graph proves that, for the currents used in these experiments, the specific energy of the LIC is around 40 – 60 Wh/kg, which is four times higher than for the EDLCs in organic electrolytes with a specific energy around 12 Wh/kg.

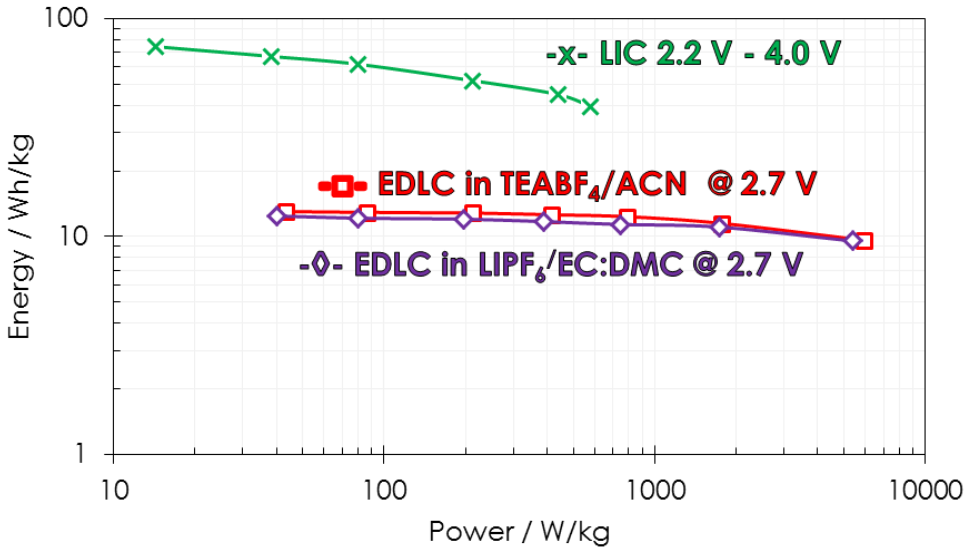

Figure 79 Ragone plots of the LIC in 1 mol/L $LiPF_6$ in EC:DMC and of EDLCs based on the same activated carbon either in 1 mol/L $TEABF_4$ in ACN or in 1M $LiPF_6$ in EC:DMC. For the LIC, the S.E.I. has been formed and graphite pre-lithiated with help of sacrificial Li_2DHBCN at C/10. The LIC is cycled in the voltage range 2.2 - 4.0 V; the EDLCs using the same AC as electrode material are charged up to 2.7 V.

In order to enhance the energy of the LIC based on the renewable lithium source, we have tried to slightly increase the maximum voltage value up to 4.1 V. Unfortunately, as shown in Figure 80, there is a very slight but visible continuous capacitance decay, which might be connected to electrolyte oxidative decomposition from the early cycles, and this decay accelerates when current is set to 0.65 A/g after 1350 cycles. Hence, for stable operation of the LIC based on positive electrode containing delithiated Li_2DHBCN, it is necessary to limit the upper voltage limit to 4 V. This value seems to be even slightly higher than the one of 3.8 V claimed by JM Energy for the ULTIMO system [200].

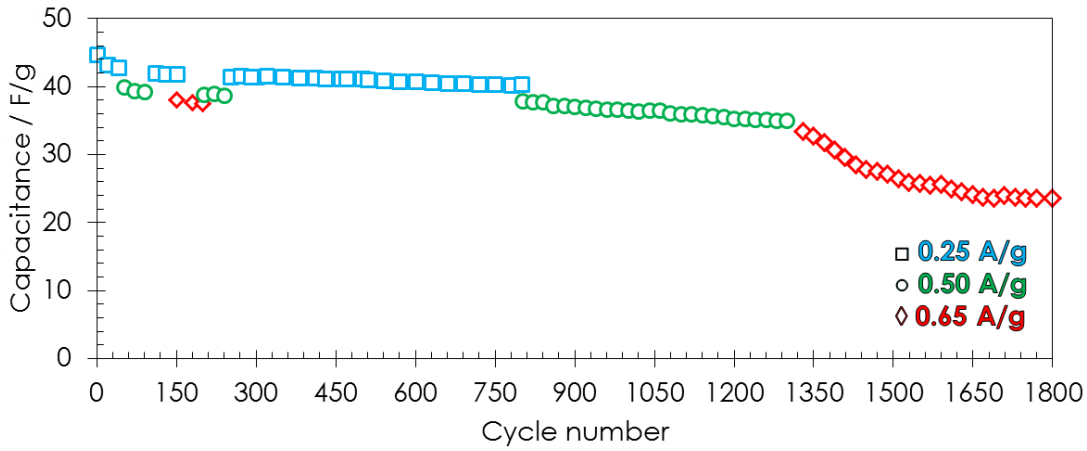

Figure 80 Cycle life of a LIC with sacrificial composite positive electrode based on Li_2DHBCN where S.E.I. formation and pre-lithiation has been performed at C/10. The LIC has been cycled at 0.25 A/g (blue squares), 0.50 A/g (green circles) and 0.65 A/g (red diamonds) in the voltage range from 2.2 to 4.1 V. The electrolyte was 1 mol/L $LiPF_6$ in EC:DMC.

V. 5. Realization of a LIC pouch-cell prototype with Li_2DHBCN /AC composite positive electrode

One of the objectives of our work was to build a LIC cell prototype based on graphite negative electrode lithiated from a sacrificial material included in the positive AC electrode. Rectangular positive and negative electrodes were placed parallel to each other in an envelope (called triplex: polymer layers surrounding a central Al foil) which was sealed under vacuum in an argon filled glove-box. A schematic representation of the pouch cell is given in Figure 81; its realization will be described below.

A self-standing positive electrode material with PTFE as binder was prepared inside argon filled glove–box in the same conditions as described in paragraph V. 2. of this chapter. A square piece of self-standing electrode material (3 cm x 3 cm) is then stuck on the surface of an aluminum current collector (thickness 35 µm, 3 cm x 5.5 cm) precoated with a thin layer of conducting glue DAG PF407A (Henkel). Then, the electrode is dried under vacuum at 120°C for 12 h in a Büchi glass oven.

For the negative electrode, a rectangular copper foil (3 cm x 5.5 cm) was coated with a graphite based layer (3 cm x 3 cm) as described in paragraph A. 4. of the experimental

annex; the graphite-based electrodes were dried under vacuum at 120 °C for 12 h. Cellulose separators (thickness 25 µm) were cut in square shape pieces (5 cm x 5 cm) and dried under vacuum at 120 °C for 12 h. Triplex foils (thickness of 150 µm) were cut in rectangles (12 cm x 7 cm) and folded by half to create the triplex body of the cell; the triplex foils were dried under vacuum at 80 °C for 12 h. All the pouch-cell construction was realized in argon-filled glove-box. A separator was placed at the middle of the two halves of the triplex foil and was sealed between those two halves with the use of a vacuum sealer (Henkelman) installed inside the glove-box. The two terminals (graphite-based electrode and Li_2DHBCN/AC electrode) were positioned on each side of the separator and held in place by use of office clips. Afterwards the sides of the triplex body were sealed together with the positive or negative terminal. With the use of an automatic pipet, 500 µL of 1 mol/L $LiPF_6$ were introduced in the cell from the remaining opened upper part of the triplex body, and then this part was sealed under vacuum. The ready cells were removed from the glove-box and electrochemically tested.

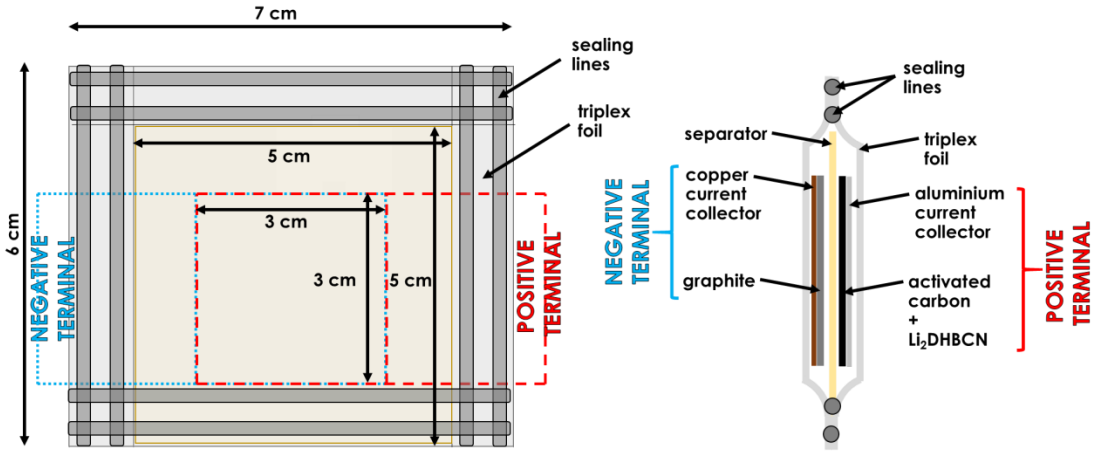

Figure 81 Frontal view (left image) and side view (right image) of a pouch-cell prototype.

The voltage profile of the cell (with positive electrode based on AC/Li_2DHBCN and graphite as negative one in $LiPF_6$ electrolyte) during S.E.I. formation and pre-lithiation at C/10 is presented in Figure 81. The initial voltage profile is the same as for the cell with reference lithium pin shown in Figure 76, but as the S.E.I. formation was completed a sudden drop of voltage occurred which may be related to short- circuit of the cell (Figure

82). At the same time, we could observe a swelling of the pouch (Figure 83) indicating that gases evolved during the S.E.I. formation which is the common process well described in the literature; for example from EC the solid $(CH_2OCO_2Li)_2$ and ethylene $CH_2=CH_2$ is formed [167,168,169] as presented in equation (15) of the literature review.

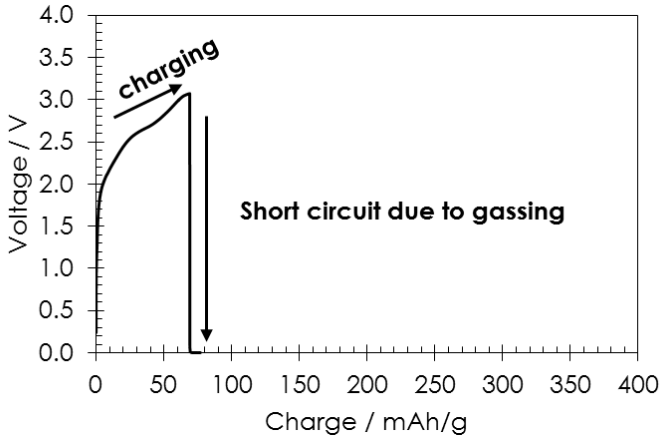

Figure 82 Voltage profile of a two-electrode pouch-cell constituted of AC/Li_2DHBCN positive electrode and graphite negative one during S.E.I. formation at C/10.

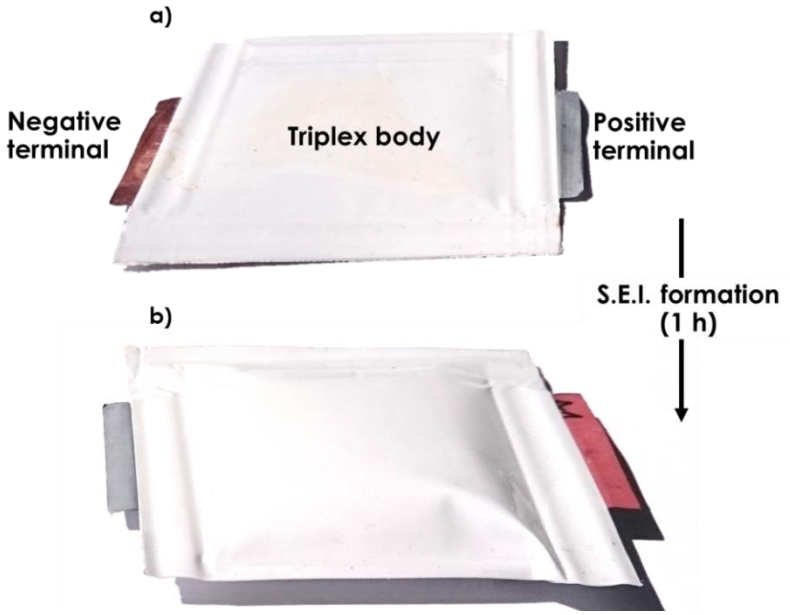

Figure 83 Two-electrode pouch-cell constituted of AC/Li_2DHBCN positive electrode and graphite negative one: a) initial cell and b) swelling after S.E.I. formation at C/10.

To solve the problem related with gassing, the size of the pouch made from triplex envelop was increased to 7 cm x 24 cm, in order to create a volume (referred to as "dead space") for storing the gases evolved during S.E.I. formation, as shown in Figure 84. Additionally, the part of the cell including the positive and negative electrodes was placed between two rigid plastic plates hold by three office clippers creating a constant pressure on the cell. The pouch-cell was placed vertically in the glove-box, so all of the gases formed during galvanostatic (C/10) S.E.I. formation and pre-lithiation are gathered in the dead space. As expected, during S.E.I. formation, the part of the cell called dead-space, has swollen. Therefore, once pre-lithiation has been completed, the cell was sealed as close as possible of the edge of electrodes in order to eliminate the upper part containing gases.

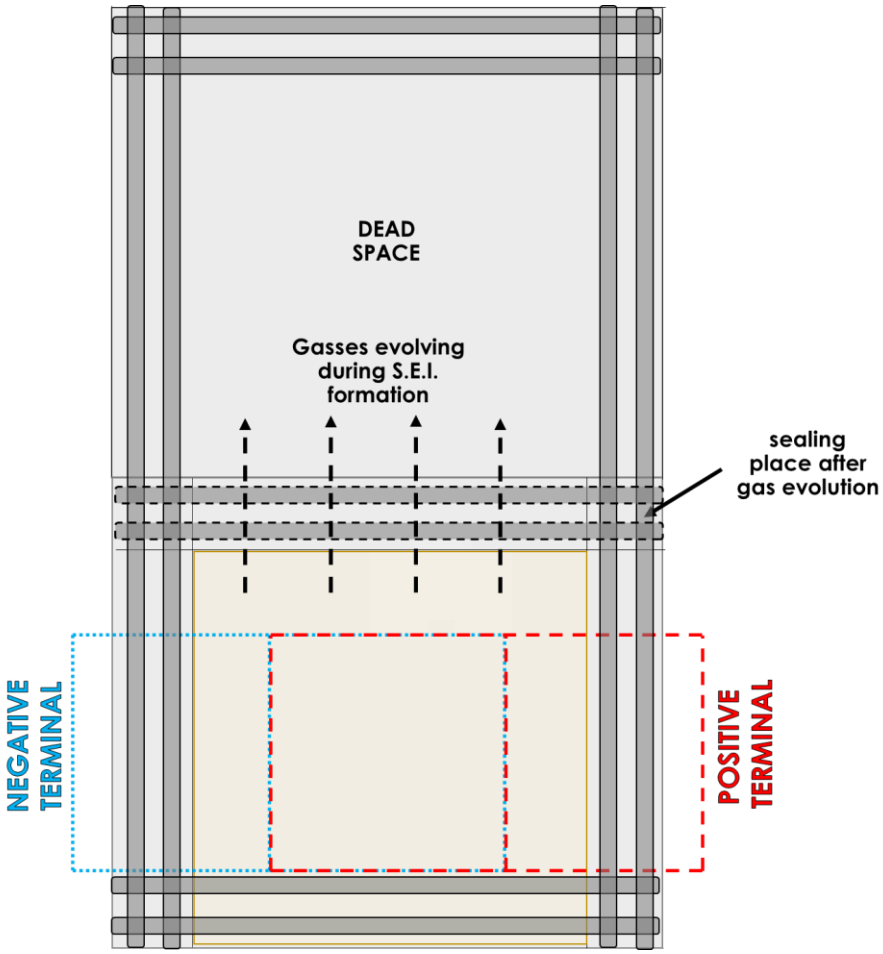

Figure 84 Schematic representation of the pouch LIC cell for gathering the gases evolved during S.E.I. formation in the dead space.

As shown in Figure 85, this modification enabled to successfully obtain a pre-lithiation voltage profile similar to the one demonstrated by the laboratory type of cells (see Figure 76). In particular, at voltage higher than 3.3 V, one can observe the successive plateaus corresponding to staging during lithium intercalation into graphite. However, the values of voltage are slightly higher in the LIC pouch cell than in the laboratory one, which could reveal a higher resistance of the former cell.

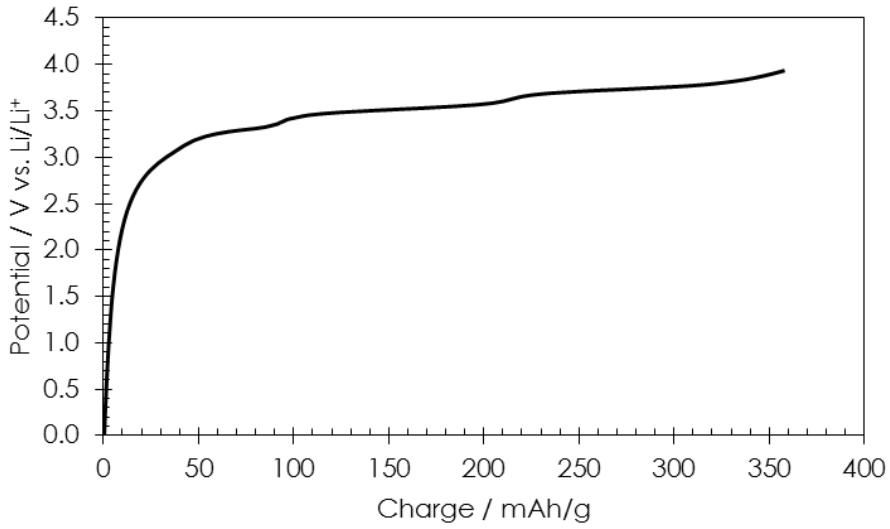

Figure 85 Voltage profile during S.E.I. formation and pre-lithiation of graphite at C/10 in a pouch two-electrode cell constituted of AC/Li_2DHBCN positive electrode and graphite negative one. A dead volume was used for gas accumulation. 1 mol/L $LiPF_6$ in EC:DMC was used as electrolyte.

After graphite lithiation, the two-electrode LIC was cycled at 0.25 A/g (Figure 86). It can be seen that, despite the accurate voltage profile during graphite pre-lithiation, the ohmic drop during current reversal in the first cycle is relatively high, and it even increases after 50 cycles, while it should rather decrease owing to better wetting of the electrodes by the electrolyte. Hence, although the feasibility of a pouch two-electrode LIC with sacrificial Li_2DHBCN in the positive electrode AC has been demonstrated, the performance during cycling is still not totally satisfactory. In the future, to improve the performance, it will be necessary to pay more attention on better coating sticking on the aluminum collector by attempting calendaring. Adding a small amount of MWCNT–p in the positive electrode material could also enhance its conductivity.

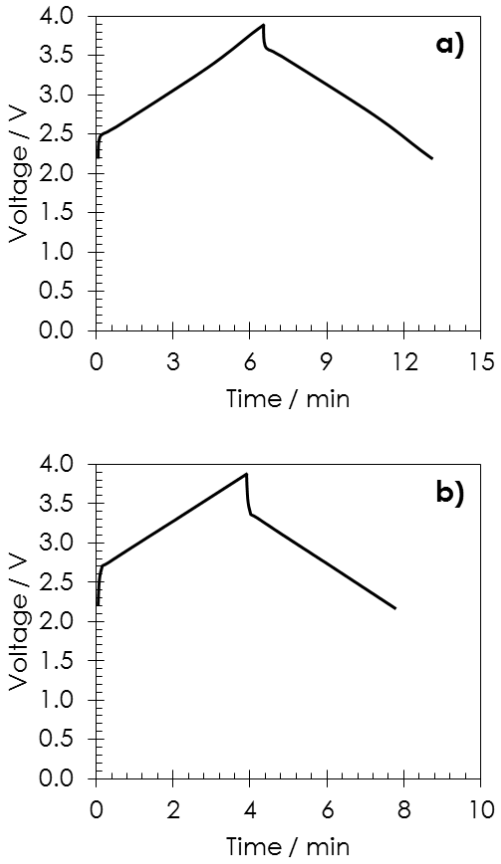

Figure 86 Galvanostatic charge/discharge at 0.25 A/g (expressed per mass of activated carbon) of the LIC pouch cell made of AC/Li_2DHBCN positive electrode and graphite negative one in the voltage range 2.2 – 3.9 V: a) 1st cycle and b) 50th cycle. The electrolyte was 1 mol/L $LiPF_6$ in EC:DMC. A larger pouch was used in order to eliminate the gases evolved during S.E.I. formation by sealing. The composition of the positive electrode was 40 wt.% AC, 40 wt.% Li_2DHBCN, 15 wt.% Super C65 and 5wt.% of PTFE.

Conclusion

3,4-dihydroxybenzonitrile dilithium salt (Li_2DHBCN) is an interesting renewable material which can be used in combination with activated carbon for intercalation of lithium into graphite. Once lithium is irreversibly extracted from Li_2DHBCN, the later remains as a dead mass in the positive electrode of the cell which can further operate as a LIC. As compared to the traditional LIC, the advantage of this construction resides in the elimination of the auxiliary lithium electrode, enabling increased safety and cost reduction of the electrochemical system. The peculiar advantages of Li_2DHBCN are i) low lithium

extraction potential which limits the risks of electrolyte electrochemical oxidation; ii) high value of irreversible capacity, enabling to reduce its mass in combination with activated carbon in the positive electrode.

The LIC cell in which the pre-lithiation was performed at C/10 exhibits an outstanding cyclic life, with an operating voltage range of 2.2 to 4.0 V. This range allows the formation of a S.E.I. to be avoided on the surface of activated carbon, and prevents from electrolyte oxidation at the positive electrode. An increase of maximum voltage even by 0.1 V had a detrimental effect on the cyclic performance which may be related to the decomposition of the organic electrolyte.

Finally, for the first time, the conditions for realizing pouch two-electrode LICs based on sacrificial lithiated material have been determined. These data are extremely encouraging to pursue in this research direction both by looking for more performing renewable materials and by optimizing the positive electrode construction

GENERAL CONCLUSION

Incorporating the lithium source in the positive activated carbon electrode of LICs is an elegant alternative to get rid of the auxiliary lithium electrode and thereof increase safety and reduce the cost of the final system. Before using the cell as a LIC, the solid electrolyte interface (S.E.I.) must be formed and lithium ions intercalated into graphite. To be viable, the concept must involve a sacrificial material with high irreversible capacity, to reduce as much as possible the inactive mass after the pre-lithiation step, and with low extraction potential of lithium ions in order to limit the risks of electrolyte oxidation. In this context, the present work has identified two materials, lithium rhenium (VII) oxide (Li_5ReO_6) or 3,4-dihydroxybenzonitrile dilithium salt (Li_2DHBCN), which were revealed to be interesting candidates fulfilling the previous requirements. Other materials, such as non-stoichiometric lithium nickel oxide ($Li_{0.65}Ni_{1.35}O_2$), lithium aluminum oxide (Li_5AlO_4), lithium zinc oxide (Li_6ZnO_4), lithium zirconium oxide (Li_8ZrO_6) were interesting to better understand the characteristic of this concept of cell. In comparison to Li_5ReO_6, Li_2DHBCN offers the huge advantage of irreversible lithium extraction at potential of 3.2 V vs. Li/Li^+, and in addition to be renewable.

In all cases, we have shown that the amount of lithium consumed to form the S.E.I. on the graphite electrode can be reduced by application of a higher current; it turned out that, in these conditions the passivating layer on carbon is thinner and more homogenous. Notwithstanding, once lithium is intercalated, the performance of the resulting LIC dramatically depends on the voltage range; the safe range in the LIC with sacrificial lithium source is c.a. 2.2 – 4.0 V, which fits quite well with the range from 2.2 to 3.8 V claimed for the commercially available ULTIMO system where graphite is pre-lithiated with help of an auxiliary metallic lithium electrode. By using these conditions in our system, it is totally possible to avoid the formation of a S.E.I. on the positive activated carbon electrode, and also electrolyte oxidation on this electrode. In the optimized conditions defined in this thesis, the LIC with sacrificial Li_2DHBCN displayed an excellent cycle life, demonstrating for the first time the promises of renewable materials in this concept.

Whereas other works presented in literature with sacrificial oxides used beaker cells with a great excess of electrolytes, we demonstrated in our experiments the feasibility of the concept in cells where electrolyte only soaked the separator, without any excess. More

importantly, we could even design a pouch-type of LiC with Li_2DHBCN/AC composite electrode and graphite negative one, where it was possible to successfully lithiate graphite and to further perform galvanostatic cycling. The first realization of such "GREEN" LICs is very encouraging to pursue further research, both by looking for more performing renewable materials and by optimizing the positive electrode construction. The identification of the reasons for relatively high ohmic drop during the change of polarization will undoubtedly provide clues for finding optimizations.

Even if graphite is still the most popular material for lithium-ion batteries, it presents the disadvantage of possible lithium plating when high currents are applied. Obviously, this issue should be considered in the case of LICs, where it is expected to use higher currents than in lithium-ion batteries. Hence, the implementation of higher potential anodes based on e.g., antimony, tin, etc, and their composites with hard carbon should be very carefully considered in LICs with sacrificial lithiated material.

The next point to be considered for large scale development of these hybrid capacitors is the low abundance of lithium. In other words, all the work accomplished until now should be reproduced with sodium, knowing in particular that some novel directions will be needed to develop such concept. As example, as far as sodium intercalation is concerned, carbons are not much performing: the sodium intercalation capacity of graphite is almost negligible and intercalation in hard carbons occurs at very low potential which surely would lead to plating at high current. Consequently, there are huge prospects for developing novel anode materials and sacrificial cathodic materials source of sodium ions for S.E.I. formation and insertion in the host negative electrode.

EXPERIMENTAL ANNEX

A. 1. Electrochemical techniques

A. 1.1. Cyclic voltammetry (CV)

Cyclic voltammetry (CV) is one of the basic electrochemical techniques for testing electrochemical cells. During CV, the potential or voltage is varied at a given scan rate expressed in V/s in the selected potential ΔE or voltage range ΔU. For electrochemical capacitors (ECs), the cyclic voltammogram, represented as $I = f(U)$, has almost a rectangular shape corresponding to electrostatic charge accumulation (Figure 87a). In contrast, for batteries, there is a rise of anodic or cathodic current at the potential where a chemical reaction occurs, either oxidation or reduction (Figure 87b). If the reaction is reversible, the surface area of the two peaks should be similar.

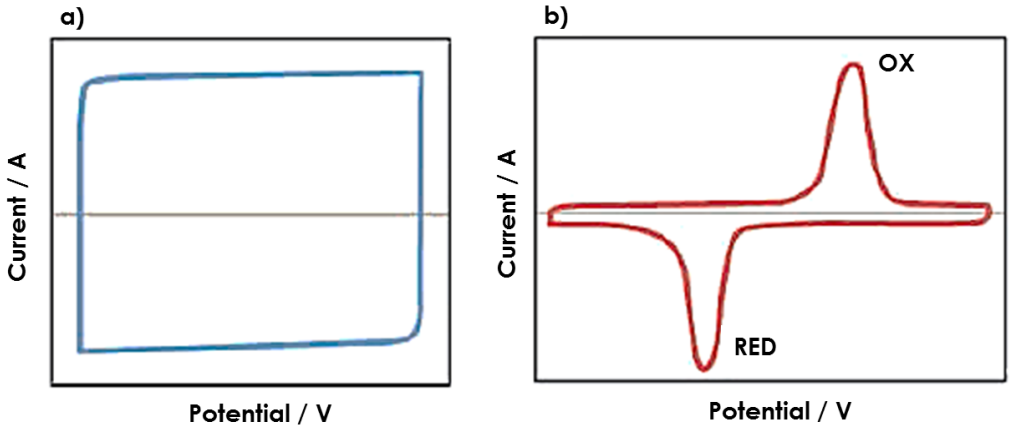

Figure 87 Typical cyclic voltammograms for a) ECs b) batteries [220].

Cyclic voltammetry was used in this work for estimating the irreversible character of lithium extraction from different lithium sources. The scan rate was the most often 0.06 mV/s in the range from 2.0 V to 4.5 V vs. Li/Li^+ (if not indicated differently in the text). Relatively low scanning rate was necessary to observe the redox reactions.

A. 1.2. Galvanostatic charge with potential limitation (GCPL)

Beside cyclic voltammetry, galvanostatic charge with potential limitation (GCPL) is the second most utilized electrochemical technique for testing cells; it allows to precisely determine the capacitance (or capacity) of an electrochemical cell. In this case, a constant

current (I = const.) is applied to the cell until reaching the set potential or voltage, and the curve E or $U = f(t)$ is plotted. For a typical EC, the charge/discharge profile has a triangular shape as shown in Figure 88. Since the energy is stored electrostatically in ECs, the typical charge/charge discharge time of ECs is of the order of tens of seconds/few minutes. The capacitance C is calculated from the amount of charge Q accumulated in the operating voltage range ΔU :

$$C = \frac{Q}{\Delta U} = \left[\frac{A \cdot s}{V}\right] \equiv [F]$$

Then the capacitance is expressed in Farads / F and can be later expressed per mass, surface or volume.

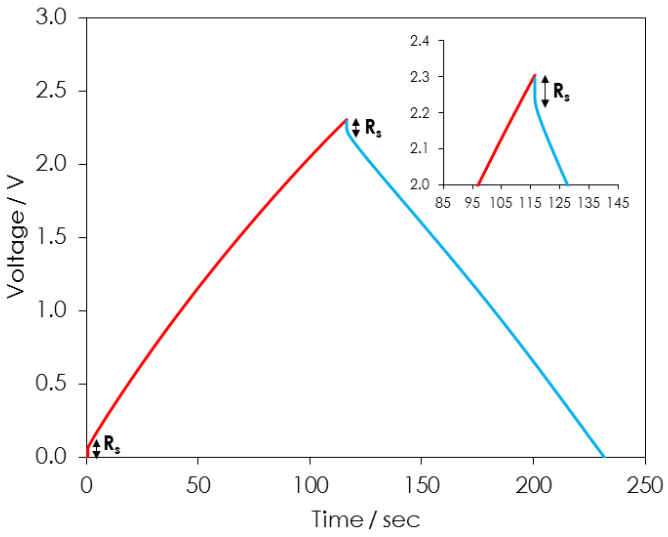

Figure 88 Typical charge (red line)/discharge (blue line) profile of an electrochemical capacitor with the inset presenting the enlargement showing the voltage drop due to the resistance of the cell.

In the case of a redox electrode or an accumulator, there is a well-defined plateau at the potential (or voltage) at which the redox reaction(s) occurs (Figure 89). The charging/discharging time of batteries is rather counted in hours, as it involves the bulk of the electrode materials. The current applied to cycle batteries is the most often defined as C-rate which expresses the time (in hours) needed to reach the practical capacity of the system. For example, C-rates as C/20 or C/5 for a graphite electrode mean that the

intercalation process takes 20 or 5 hours, respectively, to reach a capacity of 372 mAh/g, i.e. the composition LiC_6. The capacity can be calculated according to formula:

$$Q = \frac{I \cdot t}{m} = \left[\frac{mA \cdot h}{g}\right]$$

where I – current used, t – time of charge or discharge and m – mass of material, yet it can be also expressed per volume or surface.

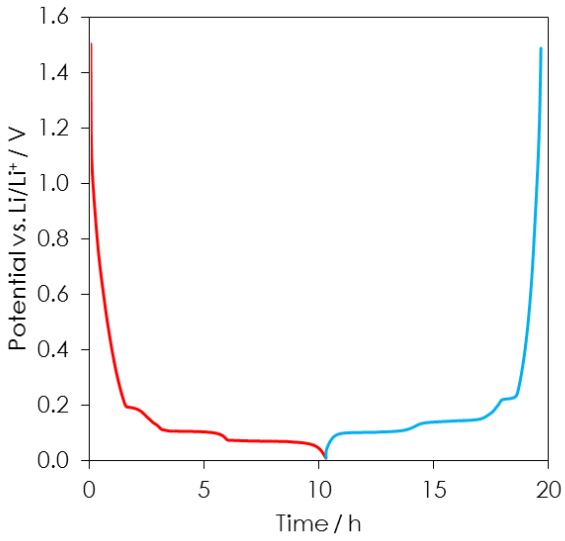

Figure 89 Typical charge/discharge profile of a redox graphite electrode at C/10. Color red is for charging, blue for discharging of the electrode.

The ratio of discharge/charge time gives a rough estimation of the process reversibility: if $\Delta t_{dis}/\Delta t_{ch} = 1$, then the process is fully reversible; if $\Delta t_{dis}/\Delta t_{ch} < 1$, it means that the process is irreversible or some parasitic reactions occur in the system as oxidation of electrolyte, graphite exfoliation etc.

A. 1.3. Electrochemical impedance spectroscopy (EIS)

Electrochemical impedance spectroscopy (EIS) allows determining the real and imaginary components of the impedance response of an electrochemical cell as a function of

frequency. It requires a special equipment to apply a small alternating current (AC). The most widely used method is to set a sinusoidal signal of required potential with small amplitude at several frequencies (f). The impedance data can be represented as a Nyquist plot which shows the imaginary part of impedance versus the real part. Figure 90 displays the Nyquist plot of the Randles circuit of ideal capacitor (1) and real capacitor (2) which consists of the equivalent series resistance (R_S) in series with the parallel combination of the double-layer capacitance (C_{dl}) and the charge transfer resistance (R_f) in series with the Warburg element (W; impedance of semi-infinite diffusion). Four important parameters can be identified from the Nyquist plot: the Equivalent Series of Resistance (R_S) is mainly related to the resistivity/conductivity of the electrolyte, the Equivalent Distributed Resistance (R_f) related to the electron transfer through the electrode material, the Warburg region is the part of the plot tilted at 45 ° which is related to the diffusion of ions, the capacitive behavior of the material which is represented by the vertical line. EIS was performed in the range of frequencies from 10 mHz to 100 kHz and amplitude 5mV when the cell was in the equilibrium state which means there was no current fluctuation.

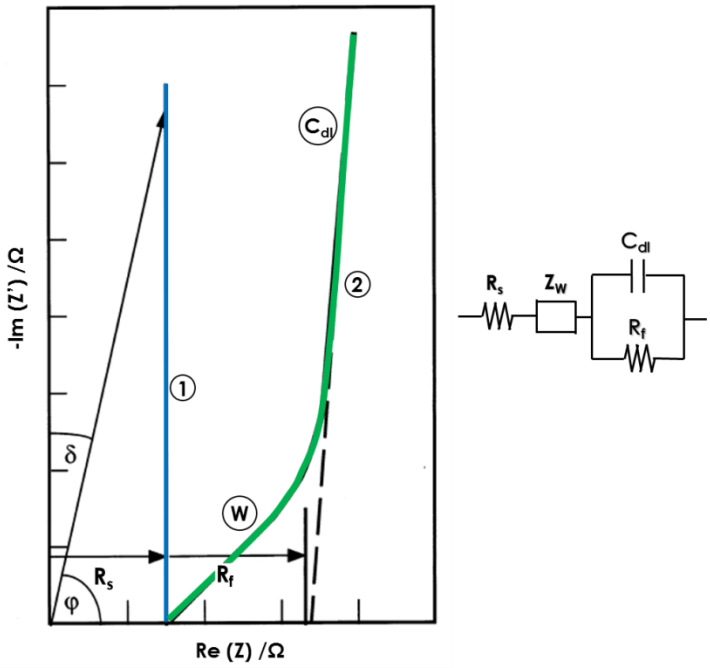

Figure 90 Nyquist plot for the Randles circuit of (1) an ideal capacitor; (2) a real capacitor consists of the equivalent series resistance (R_S) in series with the parallel combination of the double-layer capacitance (C_{dl}) and the charge transfer resistance (R_f) in series with the Warburg element (W) [221].

All electrochemical investigations were performed using a multichannel potentiostat/galvanostat with impedance channels (VMP3, Biologic); the data were collected by the EC-Lab V10.41 software.

A. 2. Characterization of the activated carbons used for positive electrode of LIC

Two kinds of activated carbons, YP50F and YP80F (named similarly in the main text), were purchased from Kuraray (Japan). In order to evaluate which one will be used for the fabrication of the composite positive electrode, their characteristics were examined by gas adsorption and electrochemical methods.

The nitrogen adsorption isotherms were recorded at 77 K using an ASAP 2020 (Micromeritics). The amount of material for each experiment was around 60 mg; prior to the measurements, the samples were degassed for 12 h at 350 °C. The 2D non-local density functional theory (2D-NLDFT) was used to determine the pore size distribution (PSD).The nitrogen adsorption isotherms at 77K of the two carbons, together with their pore size distribution (PSD), are represented in Figure 91. The BET specific surface area (S_{BET}) is 1658 and 2293 m^2/g for YP50F and YP80F, respectively. For YP80F, V_{MICRO} = 0.80 cm^3/g, V_{MESO} = 0.23 cm^3/g, L_0< 2 nm = 1.02 nm and for YP50F, V_{MICRO} = 0.63 cm^3/g, V_{MESO} = 0.06 cm^3/g, L_0< 2 nm = 0.86 nm. Hence, YP50F is essentially a microporous carbon, whereas YP80F has a more developed porosity with a remarkable amount of mesopores.

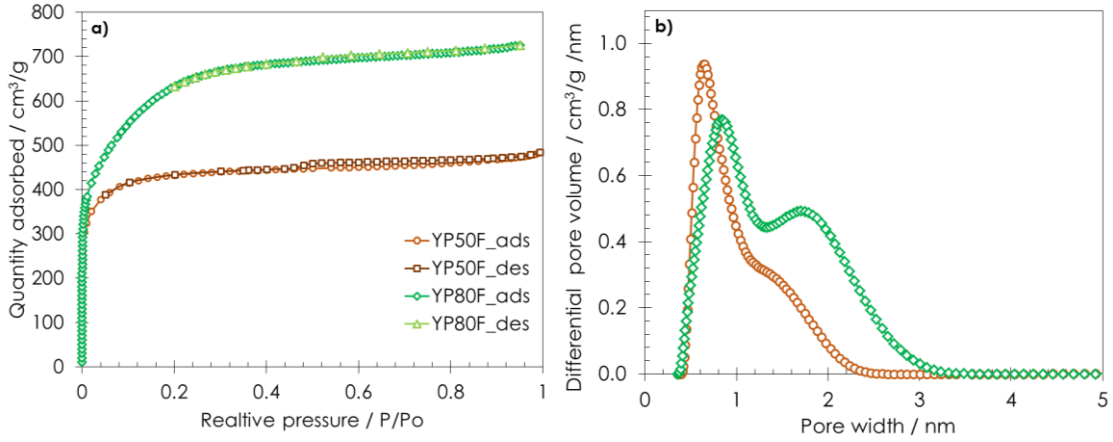

Figure 91 a) Nitrogen adsorption/desorption isotherms at 77K and b) pore size distribution of the activated carbons YP50F (orange circles) and YP80F (green diamonds).

The EDLC performance of the two materials was determined in AC/AC symmetric El-Cell cells using 1 mol/L lithium hexafluorophosphate ($LiPF_6$, Solvionic) in ethylene carbonate and dimethylcarbonate (EC:DMC vol. ratio 1:1). In these cells, the electrodes were in the form of self-standing pellets with diameter 16 mm containing 80 wt.% of YP80F or YP50F, 15 wt.% of Super C65 (Imerys) and 5 wt.% of polytetrafluoroethylene PTFE (Sigma Aldrich, 60 wt.% of PTFE in water suspension). A Whatman GF/A glassy fiber separator of thickness 230 µm and diameter 18 mm was placed between electrodes. The CVs of the two carbons (Figure 92) demonstrate noticeably higher capacitance for YP80F than for YP50F. This has been confirmed by galvanostatic charge/discharge at 1 A/g, giving capacitance values of 25 F/g and 38 F/g (expressed per total mass of electrodes) for YP50F and YP80F, respectively.

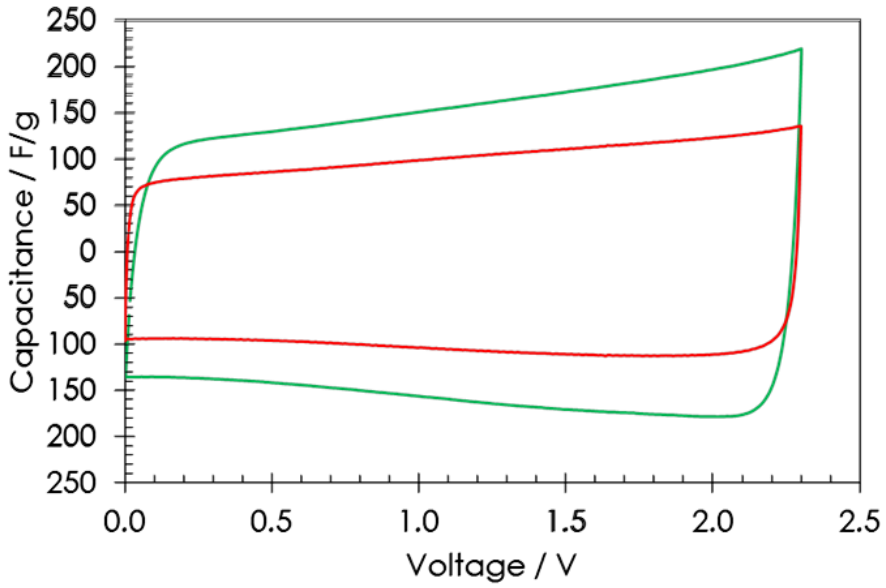

Figure 92 Cyclic voltammograms at 5 mV/s for AC/AC symmetric cells using 1 mol/L $LiPF_6$ in EC:DMC as electrolyte with YP50F (orange curve) and YP80F (green curve) electrodes.

Owing to its high capacitance, but also to its reasonable amount of mesopores favoring the diffusion of electrolyte species, the activated carbon Kuraray YP 80F has been further used as part of the composite positive electrode in all the experiments presented in this manuscript.

A. 3. Characterization of graphite used for negative electrode of LIC

Two kinds of graphite materials from Superior Graphite (USA) were compared: SLC1512P (S_{BET} = 1.3 m^2/g, particle size 5 – 20 μm) and SLC1520P (S_{BET} = 1.0 m^2/g and particle size 10 – 30 μm). The X-ray diffraction patterns of these two materials were taken with Philips PW3050/60 diffractometer in Θ – Θ configuration with a monochromatic radiation CuKα = 1.5405 Å. The Figure 93 shows the characteristic lines of the hexagonal structure (H) together with lines of a rhombohedric phase (inset from 2Θ = 40° to 50° in Figure 93 (R) appearing during manufacturing of the materials [222]. Both graphites are developed for LIBs application and their particles display a "potato" shape, as shown by the SEM images as insets in Figure 93.

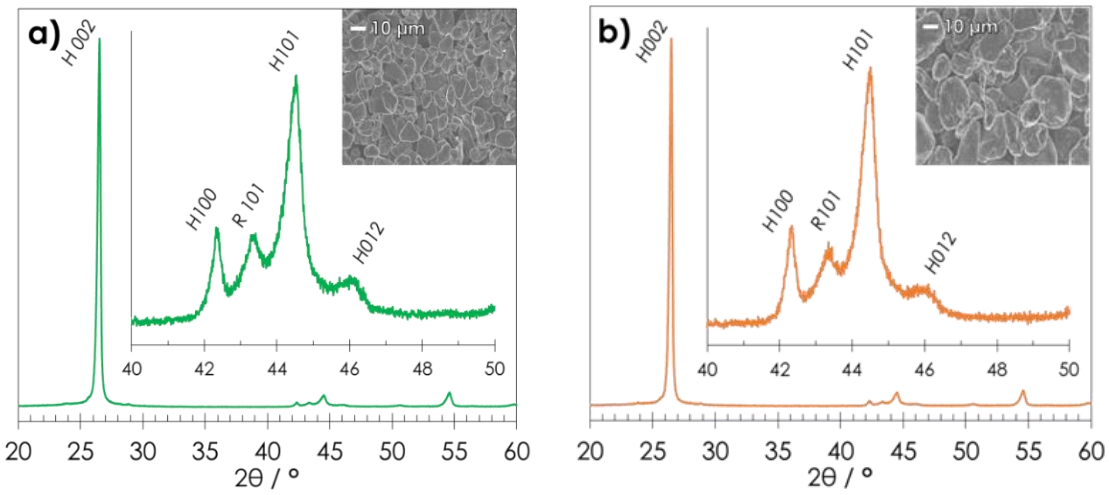

Figure 93 X-Ray diffractograms of graphite a) SLC1512P and b) SLC1520P with monochromatic radiation CuKα= 1.5405 Å. The insets are SEM pictures at magnification 1000x performed with a Merlin FE-SEM (Zeiss).

For making electrodes, an ink was prepared by mixing 91 or 87 wt.% SLC1512P or SLC1520 graphite, 8 wt.% PVdF 5130 binder (Solvay) dispersed in 1-methyl-2-pyrrolidinone (using a 5 wt.% PVdF solution in NMP, 99.5% anhydrous, Sigma Aldrich) and 1 or 5 wt.% Super C65 (Imerys) with a homogenizer T10 (IKA) at 12000 rpm for 15 minutes. Additional amount of NMP was introduced during mixing to adjust the viscosity of ink. Then, the ink was spread on copper foil treated on one side (Copper-Invar-Copper, thickness of 20 μm, Schlenk) with use of an automatic film applicator (Elcometer 4340)

and a doctor blade add-on with gap size adjusted. NMP was then evacuated from the coatings by natural evaporation under fume hood at 70 °C overnight and further under vacuum at 120 °C for 15 h. The electrochemical testing was performed in El-Cell cells where metallic lithium was used as a counter and reference electrode, and the electrolyte was 1 mol/L $LiPF_6$, EC:DMC. Figure 94 a – d shows the galvanostatic reduction (intercalation)/ oxidation(deintercalation) of the graphite SLC1512P at C/20 and C/5 with different amounts of Super C65. The increase of Super C65 (S_{BET} = 62 m^2/g) amount from 1 wt.% to 5 wt.% enables to reduce the ohmic drop, but at the same time the development of the solid electrolyte interphase (S.E.I.) characterized by the irreversible capacity is much higher, which can be further detrimental for the cycle performance of the cells [180, 223].

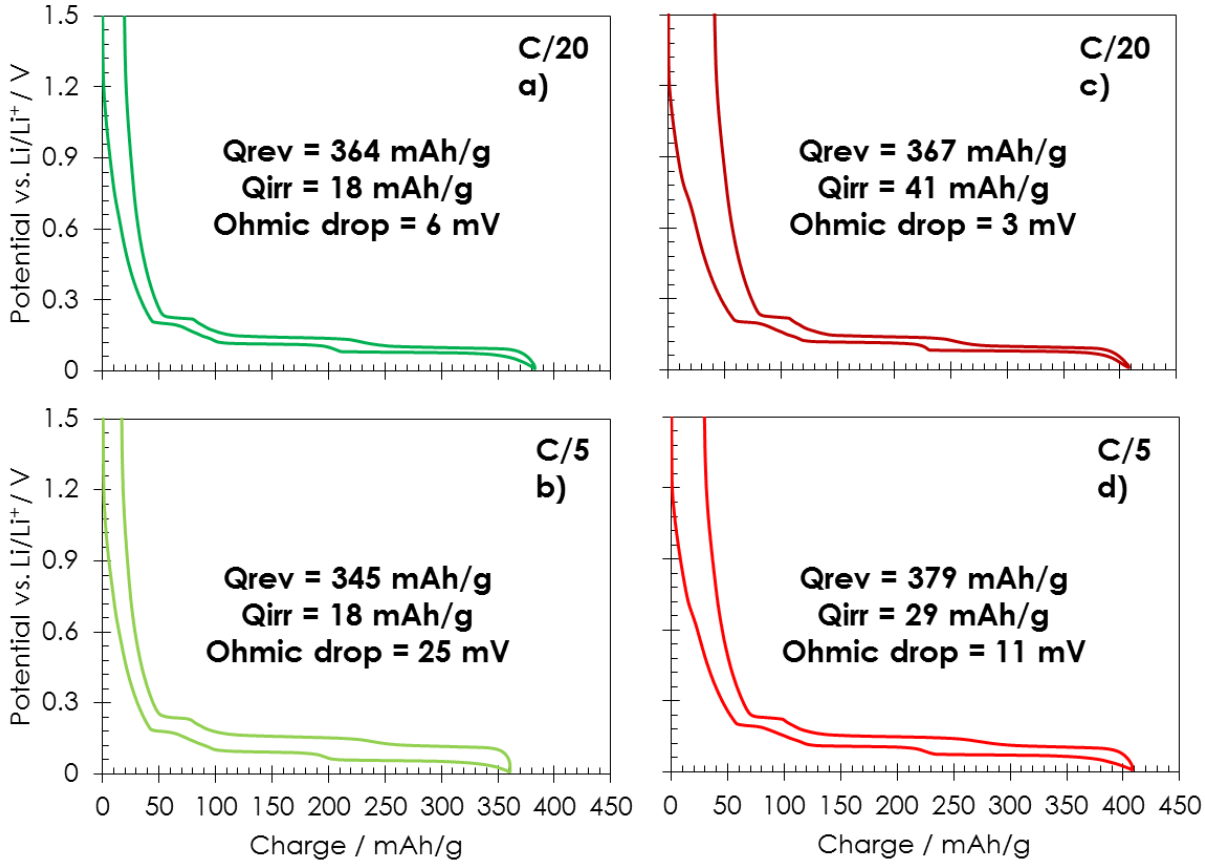

Figure 94 Lithium electrochemical intercalation/deintercalation in SLC1512P: a – b) electrodes with 1% of Super C65 and c – d) electrodes with 5% of Super C65.

Electrodes with 91 wt.% of graphite, 8 wt.% binder PVdF 5130 (Solvay) and 1 wt.% of Super C65 (Imerys) are then compared in Figure 95a-b for SLC1512P and Figure 95a–b for SLC1520P. Since the ohmic drop during the change of polarization sign is slightly lower for the SLC1512P graphite, this material will be selected for further experiments in LIC cells.

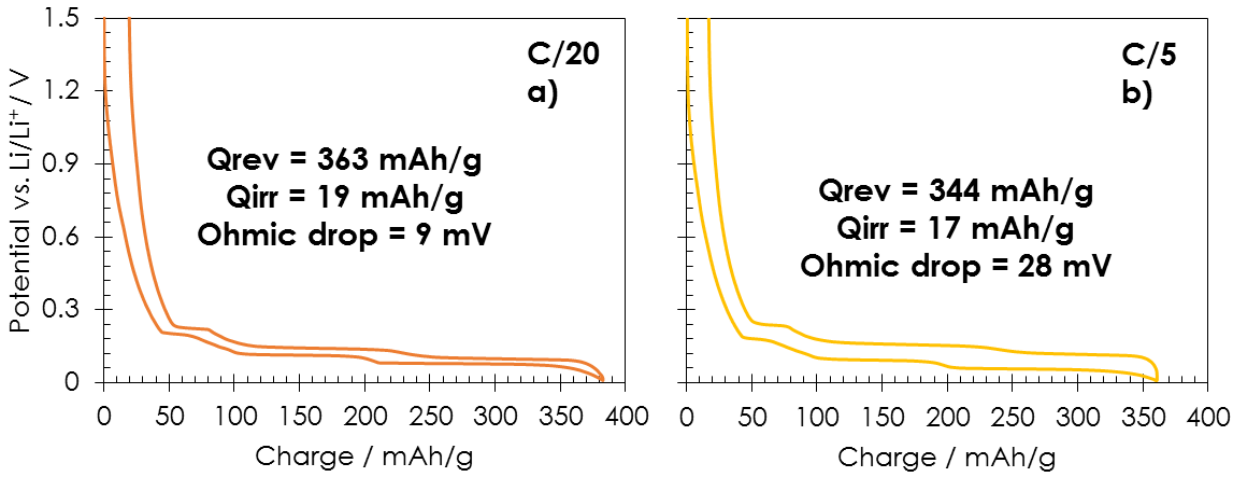

Figure 95 Lithium electrochemical intercalation/deintercalation in SLC1520P at) C/20 and b) C/5.

A. 4. Electrodes preparation

A. 4.1. Self-standing composite (sacrificial material + AC) electrodes with poly(tetrafluoroethylene) - PTFE binder

Since some of the investigated materials (Li_5AlO_4, Li_6ZnO_4, Li_8ZrO_6, Li_5ReO_6 and Li_2DHBCN) are sensitive to moisture, it was necessary to fabricate the electrodes with special precautions. Before to do such, AC and Super C65 were mixed in air atmosphere together with PTFE (60 wt.% dispersion in water, Aldrich) in 1/1 volume ratio water/isopropanol solution in order to reach the following composition of the solid mixture after evaporation of the liquid phase: 66.7 wt.% of AC, 25 wt.% of Super C65 and 8.3 wt.% of PTFE. The liquids were evaporated at 100 °C under fume-hood, and the solid was further dried in vacuum stove under vacuum at 120 °C for 12 h.

For the materials which were sensitive to contact with air, the dried solid was transferred in a glove–box, where it was mixed with an appropriate amount of sacrificial lithium source in

10-20 mL of n-heptane so as to reach the final composition of the solid mixture: 40 wt.% AC YP80F, 40 wt.% sacrificial lithium source, 15 wt.% Super C65 and 5wt.% of PTFE. For materials non sensitive to air, mixing was done under fume hood in same proportions with use of n-hexane. After natural evaporation of excess n-heptane (or n-hexane), the wet mass was placed in a mortar to get dough which was rolled to form approximately 250 μm thick sheet. Electrodes with diameter 16 mm were cut from the sheet with use of hollow punchers and placed in a Büchi glass oven where they were dried under vacuum at 120 °C for 12 h.

A. 4.2. Composite coated electrodes with poly(vinylidene fluoride) - PVdF binder

In case of composite positive electrodes, PVdF was used as binder only with lithium nickel oxide. For preparing the AC/LNiO composite electrode, an ink was prepared by mixing 25 wt.% of AC (YP 80F), 55 wt.% of lithium nickel oxide, 5 wt.% PVdF 5130 binder (Solvay) dispersed in 1-methyl-2-pyrrolidinone (using a 5 wt.% PVdF solution in NMP, 99.5% anhydrous, Sigma Aldrich) and 15 wt.% of Super C65; mixing was realized with a homogenizer T10 (IKA) at 12000 rpm for 15 minutes. Depending on the mass of the components, additional NMP was introduced during mixing in order to reduce the viscosity. The obtained ink was spread on the surface of an aluminum foil (thickness 35 μm , etched on both sides, Blue Solutions) with use of an automatic film applicator (Elcometer 4340) and a doctor blade add-on with adjusted gap size. NMP was then evacuated from the coating by natural evaporation under fume hood at 70 °C overnight and further under vacuum at 120 °C for 15 h. Any changes in this procedure are given in the main text.

A.5. Electrochemical cell and electrochemical conditions

For all the investigations, an El-Cell (Figure 96a) type of cell was used. It is composed of (Figure 96b): 1) stainless steel bracket, 2) golden spring which applies a constant and reproducible load on the piston, 3) stainless steel cover with jack 2 mm, 4) polyethylene (PE) o-ring ensuring tightness of the cell, 5) stainless steel piston resistant to corrosion in aprotic media, 6) polyether ether ketone (PEEK) sleeve guarantees that the electrodes are in central position and avoids short circuiting of the cell, 7) reference electrode, 8) stainless steel base, 9) cell stack. In case of two electrode investigations the reference electrode 7) is

replaced by PTFE plunger, and the separator was from Whatman GF/A glassy fiber with a thickness of 230 µm and a diameter of 18 mm.

The cell stack in the PEEK sleeve (6) is described in more details in Figure 96c where: 9a) positive electrode (its composition is given in the each chapter), 9b) glassy fiber separator with thickness 1550 µm, 9c) lithium pin used as a reference electrode and 9d) graphite electrode composed of 91 wt.% SLC1512P graphite (Superior Graphite), 8% PVdF 5130 binder (Solvay), and 1% Super C65 conductive additive (Imerys).

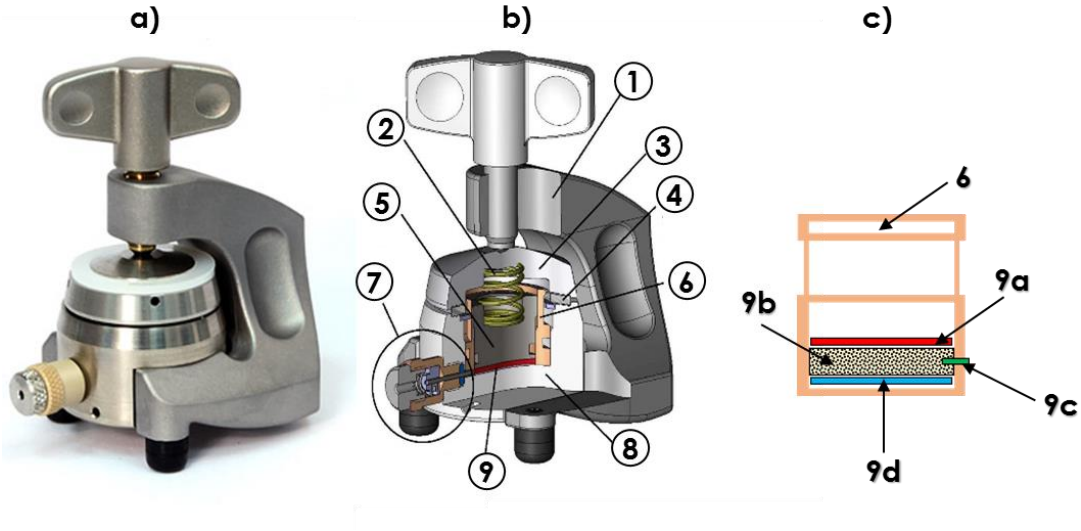

Figure 96 a) general view of El-Cell 3-electrode cell, b) technical view of the components of El-Cell cell, c) cell stack described in details.

In the experiments described in this thesis, the irreversibility of lithium extraction was determined in two electrode cell with glassy fiber separator (Whatman GF/A, diameter 18 mm and thickness 230 µm); a lithium disk (diameter 16 mm) was used as a counter and reference electrode; the electrolyte was 1 mol/L $LiPF_6$ in EC:DMC (vol. ratio 1:1). The experiments were performed at C/20 and C/10 (where C represents the theoretical capacity of the investigated material) in the potential range from 2.0 to 4.5 V vs. Li/Li^+ (unless not indicated otherwise in the main text).

The pre-lithiation of graphite was realized in a three electrode cell with lithium pin (diameter 0.8 mm) used as reference electrode; the separator was glassy fiber from El-Cell

with diameter 18 mm and thickness 1550 µm; the electrolyte was 1 mol/L $LiPF_6$ in EC:DMC (vol. ratio 1:1). The pre-lithiation was realized at C, C/5, C/10 or C/20 (theoretical capacity of graphite 372 mAh/g) with potential limits of 0.1 and 4.5 V vs. Li/Li^+ for the negative and positive electrode, respectively (unless not indicated otherwise in the main text). Once one of the limits was reached, the system was cycled galvanostatically in the voltage limits given in the main text. In some cases where different current rates were used during S.E.I. formation and intercalation of graphite, the information is added in the main text as example for the *in-situ* XRD studies.

A. 6. Characterization of lithiated metal oxides

A. 6.1. X-Ray Diffraction (XRD) analyses were done with Philips PW3050/60 diffractometer in Θ – Θ configuration with a monochromatic radiation CuKα = 0.15405 nm at 40 kV and 40 mA. The samples were pressed inside the cavity of a stainless steel frame; the excess of powder was removed with either glass or razor blade as shown in Figure 97 a - b.

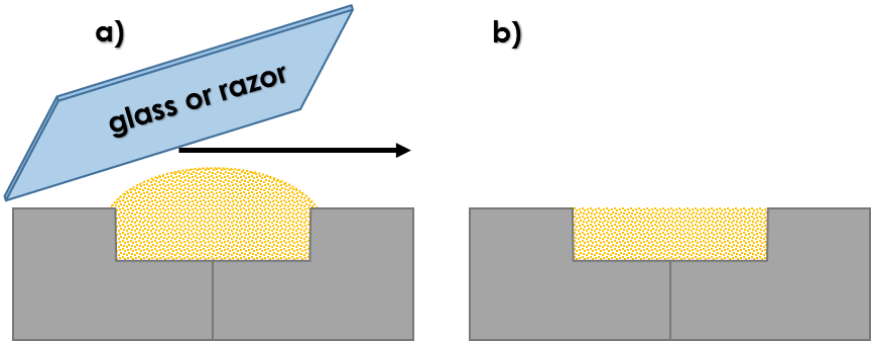

Figure 97 a) Preparation of the samples for XRD investigations with b) even and well packed material.

The data were stored on a computer with X'Pert Data collector software and then processed with FullProf Suit software version for calculating the crystal lattice parameters by Rietveld refinement. The R_{WP} parameter compares the difference in the position of all of the points for the calculated and experimental profiles. The smaller the difference between the positions of the points (preferably points are overlapping), the smaller the value of R_{WP}.

A. 6.2. Electrochemical cell used for *in-situ* XRD studies

Figure 98 a and b represents the cell construction. The upper part of the cell is its "positive" side and it is composed of a stiff, outer ring of diameter 5 cm and a hole of 2 cm behind which a metallic beryllium Be window (thickness of 200 μm and diameter 4 cm) is placed. A self-standing electrode made of wt.% AC YP80F, 40 wt.% Li_5ReO_6, 15 wt.% Super C65 and 5wt.% of PTFE was placed behind the Be window, which acts as a metallic current collector. As we wanted to investigate potential values higher than 3.5 V vs. Li/Li^+, a thin (3–4 μm) aluminum foil was placed between the Be window and the electrode material to protect Be from oxidation. This part of the cell was attached to the main body and sealing was realized with a rubber o-ring in contact with the Be window by tightening with six stainless steel screws. A cylindrical plunger shown in Figure 98 as A, B and C is used as the "negative" part of the cell. A spring was used to proper adjust the mechanical pressure within the cell. The incident X-ray beam penetrates through the Be window of the upper part and hits positive electrode. The cell was assembled inside an argon filled glove-box (MBraun) with less than 1 ppm of O_2 and H_2O, using a glassy fiber separator (Whatman GF/D, thickness 670 μm) soaked with 1 mol/L $LiPF_6$ in EC:DMC (vol. 1:1, 99.9% battery grade, Solvionic, H_2O < 20 ppm, 10.3 mS/cm at 20 °C).

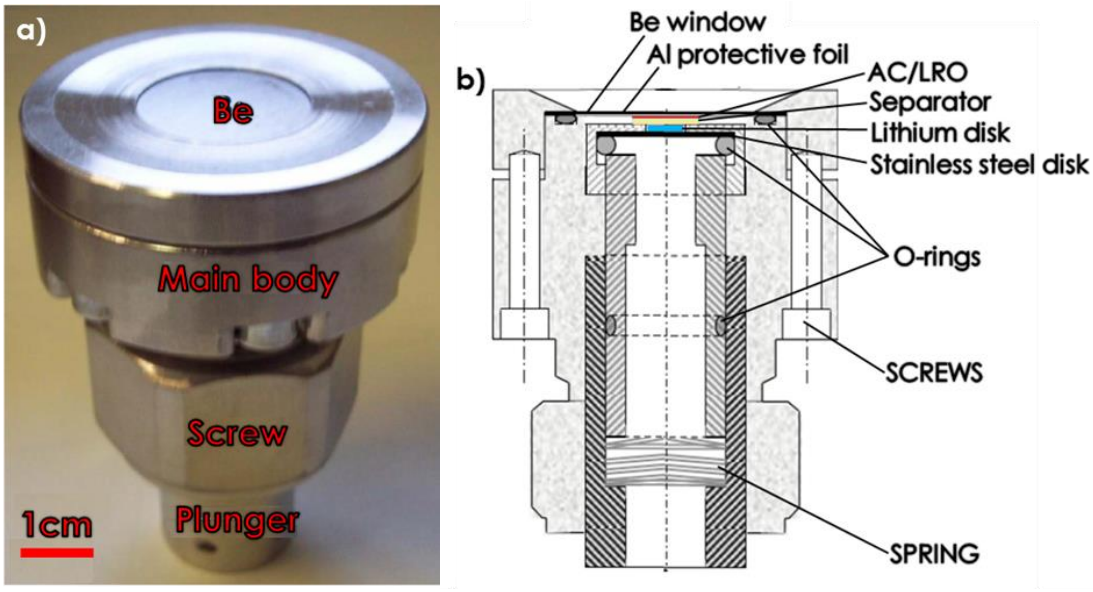

Figure 98 a) In-situ XRD electrochemical cell; b) technical description of the cell [224].

A. 7. Techniques used for the characterization of lithiated organic compounds

A. 7.1. Fourier Transform Infra-Red (FTIR) spectrometry: a Brüker Vertex 70 equipment was used in the wave number range from 4000 cm^{-1} to 400 cm^{-1}. KBr pellets were prepared to record the KBr spectra.

A. 7.2. Nuclear Magnetic Resonance (NMR) studies were conducted with a spectrometer Bruker AVANCE 500 MHz. Deutered methanol MeOD was used as a solvent and internal standard for chemical shifts.

A. 7.3. Differential Scanning Calorimetry (DSC) was done with DSC204 Phoenix 204 (Netzch) apparatus, where the protective gas was Nitrogen (N_2) of analytical purity. The material (4 mg) was placed in a closed aluminum crucible and an empty crucible was used as a reference. The samples were heated/cooled at 10 °C/min in the temperature range from 25 to 400 °C.

A. 7.4. Scanning Electron Microscopy (SEM) was performed with a Merlin FE-SEM (Zeiss) at different magnifications with voltage 15 kV.

A. 8. Chemicals and materials presented in the main text

- 1-Methyl-2-pyrrolidinone NMP (Sigma Aldrich, anhydrous, 99.5%)
- 2-isopropanol (POCH, CZDA, ODCZ. FP)
- 3,4-Dihydroxybenzonitrile DHBCN (Sigma Aldrich, 97%)
- Activated carbon YP80F (Kuraray)
- Aluminum (III) oxide Al_2O_3 (Sigma Aldrich puriss., ≥98% Al_2O_3 basis)
- Aluminum foil etched on both sides thickness 35 μm (BlueSolutions)
- Binder Poly(tetrafluoroethylene) PTFE (Sigma Aldrich, 60 wt % dispersion in H_2O)
- Binder Poly(vinylidene fluoride) PVdF 5130 (Solvay)

- Conductive agent multiwall carbon nanotubes MWCNT (Sigma Aldrich, O.D. × L 6-9 nm × 5 μm, >95% (carbon))
- Conductive agent Super C65 (Imerys, S_{BET} = 62 m^2/g)
- Copper foil treated on one side CIC/Copper Invar Copper thickness 25 μm (Schlenk)
- Electrolyte 1 mol/L lithium hexafluorophosphate dissolved in ethylene carbonate and dimethyl carbonate in the volumetric ratio 1:1 referred to as 1 mol/L $LiPF_6$ in EC:DMC (vol. 1:1) (Solvionic, 99.9% battery grade, H_2O < 20 ppm, 10.3 mS/cm at 20 °C)
- Graphite SLC1512P (Superior Graphite)
- Lithium carbonate Li_2CO_3 (Sigma Aldrich, purum ≥99%)
- Lithium hydride LiH (Sigma Aldrich, powder, −30 mesh, 95%)
- Lithium peroxide Li_2O_2 (Sigma Aldrich, technical grade, 90%)
- Nickel (II) oxide NiO_2 (Sigma Alrich, nanopowder, <50 nm particle size (TEM), 99.8% trace metals basis)
- Rhenium Re (Sigma Aldrich, powder, 99.995% trace metals basis)
- Separator cellulose thickness 25 μm (BlueSolutions)
- Separator glassy fiber:
    - Separator for 2 ELE configuration Whatman GF/A thickness 230 μm (Whatman)
    - Separator for 3 ELE configuration El-Cell thickness 1550 μm (El-Cell)
- Triplex foil, thickness 150 μm (BlueSolutions)
- Zinc (II) oxide ZnO (Sigma Aldrich, puriss. p.a., ACS reagent, ≥99.0%)
- Zirconium (IV) oxide ZrO_2 (Sigma Aldrich, powder, 5 μm, 99% trace metals basis)

REFERENCES

[1] S. H. Mohr, J. Wang, G. Ellem, J. Ward, D. Giurco; „Projection of world fossil fuels by country" *Fuel* 141 (2015) 120–135
[2] N. A. Utamaa, A. M. Fathonia, M. A. Kristiantoa, B.C. McLellanb „The end of fossil fuel era: supply-demand measures through energy efficiency" *Procedia Environmental Sciences* 20 (2014) 40 – 45
[3] H.E. Becker, U.S. Patent 2 800 616 (General Electric) (1957)
[4] D.I. Boos, U.S. Patent 3 536 963 (to Standard Oil, SOHIO) (1970)
[5] T.C. Murphy, R.B. Wright, R.A. Sutula, in: F.M. Delnick, D. Ingersoll, X. Andrieu, K. Naoi (Eds.), Electrochemical Capacitors II, Proceedings, vols. 96–25, The Electrochemical Society, Pennington, NJ, 1997, p. 258.
[6] H. von Helmholtz, „Über einige Gesetze der Verteilung elektrischer Ströme in körperlichen Leitern, mit Anwendung auf die thierisch-elektrischen Versuche," *Ann. Phys.Chem.*, 89 (1853) 211–233
[7] B.E. Conway, „Electrochemical Supercapacitors: Scientific Fundamentals and Technological Applications," *Kluwer- Plenum*, New York, 1999
[8] D.L. Chapman, „A contribution to the theory of electrocapillarity," *Phil. Mag.*, 25 (1913) 475–-481
[9] O. Stern, „The Theory of the Electrolytic Double-Layer," *Zeit. Elektrochem.*, 30 (1924) 508–516
[10] D.C. Grahame, „The Electrical Double Layer and the Theory of Electrocapillarity," *Chem. Rev.*, 41 (1947) 441–501
[11] J.O'M. Bockris, M.A.V. Devanathan, K. Muller, „The structure of charged interfaces," *Proc. R. Soc. London, Ser. A*, 274 (1963) 55–79
[12] A.G. Pandolfo, A.F. Hollenkamp, „Carbon properties and their role in supercapacitors," *J. Power Sources*, 157 (2006) 11–-27
[13] Y. Gogotsi, S. Dimovski, J.A. Libera, „Conical crystals of graphite," *Carbon*, 40 (2002) 2263–2267
[14] S.G. Lee, K.H. Park, W.G. Shim, M.S. Balathanigaimani, H. Moon, „Performance of electrochemical double layer capacitors using highly porous activated carbons prepared from beer lees," *J. Ind. Eng. Chem.*, 17 (2011) 450–454
[15] S.-E. Chun, J.F. Whitacre, „Investigating the role of electrolyte acidity on hydrogen uptake in mesoporous activated carbons," *J. Power Sources*, 242 (2013) 137–140
[16] T.E. Rufford, D. Hulicova-Jurcakova, Z. Zhu, G.Q. Lu, „Nanoporous carbon electrode from waste coffee beans for high performance supercapacitors," *Electrochem. Commun.*, 10 (2008) 1594–1597
[17] Z. Li, L. Zhang, B.S. Amirkhiz, X.H. Tan, Z.W. Xu, H.L. Wang, B.C. Olsen, C.M. Holt, D. Mitlin, „Carbonized chicken eggshell membranes with 3d architectures as high-performance electrode materials for supercapacitors," *Adv. Energy. Mater.*, 2 (2012) 431–437
[18] X. Li, C. Han, X. Chen, C. Shi, „Preparation and performance of straw based activated carbon for supercapacitor in non-aqueous electrolytes," *Microporous Mesoporous Mater.*, 131 (2010) 303–309
[19] L.G. Juntao Zhang, S. Kang, J. Jianchun, Z. Xiaogang, „Preparation of activated carbon from waste Camellia oleifera shell for supercapacitor application," *J. Solid State Electrochem.*, 16 (2012) 2179-2186

[20] R. Wang, P.Y. Wang, X.B. Yan, J.W. Lang, C. Peng, Q.J. Xue, „Promising porous carbon derived from celtuce leaves with outstanding supercapacitance and CO2 capture performance," *ACS Appl. Mater. Interf.,* 4 (2012) 5800–5806
[21] L. Wei, G. Yushin, „Electrical double layer capacitors with activated sucrose-derived carbon electrodes," *Carbon,* 49 (2011) 4830–4838
[22] D. Lozano-Castello, M.A. Lillo-Rodenas, D. Cazorla-Amoros, A. Linares-Solano, „Preparation of activated carbons from Spanish anthracite I. Activation by KOH," *Carbon,* 39 (2001) 741–749
[23] M. Molina-Sabio, F. Rodriguez-Reinoso, F. Caturla, M.J. Selles, „Porosity in granular carbons activated with phosphoric acid," *Carbon,* 33 (1995) 1105–1113
[24] F. Caturla, M. Molina-Sabio, F. Rodriguez-Reinoso, „Preparation of activated carbon by chemical activation with ZnCl2," *Carbon,* 29 (1991) 999–1007
[25] F. Derbyshire, M. Jagtoyen, M. Thwaites, „Activated carbons—production and applications: In Porosity in Carbons," *Halstead Press,* New York, 1995
[26] B.R. Puri, „Surface complexes on Carbon: Chemistry and Physics of Carbon," *Marcel Dekker,* New York, 1970
[27] P. Kleszyk, P. Ratajczak, P. Skowron, J. Jagiello, Q. Abbas, E. Frackowiak, F. Béguin, „Carbons with narrow pore size distribution prepared by simultaneous carbonization and self-activation of tobacco stems and their application to supercapacitors," *Carbon,* 81 (2015) 148-157
[28] E. Raymundo-Pinero, M. Cadek, F. Béguin, „Tuning carbon materials for supercapacitors by direct pyrolysis of seaweeds," *Adv. Funct. Mater.,* 19 (2009) 1032–1039
[29] R. E. Franklin, „Crystallite growth in graphitizing and non-graphitizing carbons," *Proc. Roy. Soc. A,* 209 (1951) 196–218
[30] J.F. Byrne, H. Marsh, „Origins and structure of porosity; Porosity in Carbons: Characterization and Applications," *Edward Arnold,* London, 1995
[31] F. Stoeckli, F. Kraehenbuehl, A. Lavenchy, V. Huber, J. Chim, „The physical and chemical characterization of active carbons by adsorption and immersion techniques," *Physique,* 81 (1984) 785–790
[32] P. J. F. Harris, „The physical and chemical characterization of active carbons by adsorption and immersion techniques," *Critical Rev. in Solid State and Mat. Sci.,* 30 (2005) 235–253
[33] C. Portet, P. L. Taberna, P. Simon, E. Flahaut, C. Laberty-Robert, „High power density electrodes for carbon supercapacitor applications," *Electrochim. Acta,* 50 (2005) 4174–4181
[34] N.L. Wu, S.Y. Wang, „Conductivity percolation in carbon-carbon supercapacitor electrodes," *J. Power Sources,* 110 (2002) 233–236
[35] C. Lastoskie, K. E. Gubbins, N. Quirke, Pore size distribution analysis of microporous carbons: a density functional theory approach, *J. Phys. Chem.,* 97 (1993) 4786–4796
[36] J. Chmiola, G. Yushin, R. Dash, Y. Gogotsi, „Effect of pore size and surface area of carbide derived carbons on specific capacitance," *J. Power Sources,* 158 (2006) 765–772
[37] H. Yamada, H. Nakamura, F. Nakahara, I. Moriguchi, T. Kudo, „Electrochemical Study of High Electrochemical Double Layer Capacitance of Ordered Porous Carbons with Both Meso/Macropores and Micropores," *J. Phys. Chem. C,* 111 (2007) 227-233

[38] G. Gryglewicz, J. Machnikowski, E. Lorenc-Grabowska, G. Lota, E. Frąckowiak, „Effect of pore size distribution of coal-based activated carbons on double layer capacitance," *Electrochim. Acta,* 50 (2005) 1197–1206.
[39] F. Stoeckli, A. Guillot, A. M. Slasli, D. Hugi-Cleary, „The comparison of experimental and calculated pore size distributions of activated carbons," *Carbon,* 40 (2002) 383–388.
[40] D. Lozano-Castello, D. Cazorla-Amoros, A. Linares-Solano, „Usefulness of CO_2 adsorption at 273 K for the characterization of porous carbons," *Carbon,* 42 (2004) 1231–1236.
[41] A.M. Puziy, O.I. Poddubnaya, A. Martınez-Alonso, F. Suarez-Garcıa, J. M. D. Tascon, „Characterization of synthetic carbons activated with phosphoric acid," *Appl. Surf. Sci.*, 200 (2002) 196–202.
[42] J. Jagiello, J.P. Olivier, „2D-NLDFT adsorption models for carbon slit-shaped pores with surface energetical heterogeneity and geometrical corrugation," *Carbon,* 55 (2013) 70–80
[43] E. Frąckowiak, „Carbon materials for supercapacitor application," *Phys. Chem. Chem. Phys.*, 9 (2009) 1774-1785
[44] C. Leon y Leon, L.R. Radovic, „Chemistry and Physics of Carbon: Interfacial chemistry and electrochemistry of carbon surfaces," *Marcel Dekker,* New York, 1994.
[45] Y. Zhu, S. Murali, W. Cai, X. Li, J. Won Suk, J. R. Potts, R. S. Ruoff, „Graphene and Graphene Oxide: Synthesis, Properties, and Applications," *Adv. Mater*., 22 (2010) 3906–3924
[46] A. K. Geim, P. Kim, „Carbon Wonderland," *Scientific American* 298 (2008) 90-97
[47] R. M. Reilly, „Carbon Nanotubes: Potential Benefits and Risks of Nanotechnology in Nuclear Medicine," *J Nucl Med,* 48 (2007) 1039-1042
[48] M. Pérez-Cabero, I. Rodríguez-Ramos, A. Guerrero-Ruíz, „Characterization of carbon nanotubes and carbon nanofibers prepared by catalytic decomposition of acetylene in a fluidized bed reactor," *J Catalysis,* 215 (2003) 305-309
[49] F. Béguin, E. Frąckowiak, „Carbons for Electrochemical Energy Storage and Conversion Systems," *CRC Press Taylor & Francis Group,* Boca Raton, 2010
[50] X. Zhang, X. Wang, L. Jiang, H. Wu, C.Wu, J. Su, „Effect of aqueous electrolytes on the electrochemical behaviours of super capacitors based on hierarchically porous carbon," *J. Power Sources*, 2016 (2012) 290-296
[51] A. Burke, „R&D considerations for the performance and application of electrochemical capacitors," *Electrochim. Acta,* 53 (2007) 1083-1091.
[52] M. Galiński, A. Lewandowski, I. Stępniak, „Ionic liquids as electrolytes," *Electrochim. Acta,* 51 (2006) 5567 – 5580
[53] F. Béguin, V. Presser, A. Balducci, E. Frąckowiak, „Carbons and Electrolytes for Advanced Supercapacitors,", *Adv. Mater.,* 26 (2014) 2219-2251
[54] B.E. Conway, „Double-layer and pseudo-capacitance types of electrochemical capacitors and their applications to the development of hybrid devices," *J. Solid State Electrochem.,* 7 (2003) 637–644
[55] J. Gamby , P. L. Taberna , P. Simon , J. F. Fauvarque , M. Chesneau , „Studies and characterisations of various activated carbons used for carbon/carbon supercapacitors" *J. Power Sources* 101 (2001) 109 – 116

[56] R. Kötz, M. Carlen, „Principles and applications of electrochemical capacitors," *Electrochim. Acta,* 45 (2000) 2483 – 2498
[57] M. Ue, „Mobility and Ionic Association of Lithium and Quaternary Ammonium Salts in Propylene Carbonate and γ-Butyrolactone," *J. Electrochem. Soc.,* 141 (1994) 3336 – 3342
[58] R. Kötz, M. Hahn, P. Ruch, R. Gallay, „Comparison of pressure evolution in supercapacitor devices using different aprotic solvents," *Electrochem. Comm*., 10 (2008) 359–362
[59] M. Arulepp, L. Permann, J. Leis, A. Perkson, K. Rumma, A. Jänes, E. Lust, „Influence of the solvent properties on the characteristics of a double layer capacitor,", *J. Power Sources,* 133 (2004) 320–328
[60] M. Ue, M. Takeda, M. Takehara, S. Mori, „Electrochemical Properties of Quaternary Ammonium Salts for Electrochemical Capacitors,", *J. Electrochem. Soc.,* 144 (1997) 2684 – 2688
[61] M. Ue, „Chemical Capacitors and Quaternary Ammonium Salts" *Electrochemistry,* 75 (2007) 565 – 572
[62] M. Ue , M. Takehara , Y. Oura , A. Toriumi , M. Takeda , „High sensitive detection of impurities in non-aqueous electrolyte solutions by a rotating disk electrode," *Denki Kagaku Electrochemistry,* 69 (2001) 458 – 461
[63] P. Wasserscheid, T. Welton, „Ionic Liquids in Synthesis," *Wiley-VCH,* Wienheim, 2008
[64] A. Balducci, R. Dugas, P. L. Taberna, P. Simon, D. Plée, M. Mastragostino, S Passerini, „High temperature carbon–carbon supercapacitor using ionic liquid as electrolyte," *J. Power Sources,* 165 (2007) 922 – 927
[65] M. Lazzari, F. Soavi, M. Mastragostino, „High voltage, asymmetric EDLCs based on xerogel carbon and hydrophobic IL electrolytes," *J. Power Sources,* 178 (2008) 490 – 496
[66] N. Handa, T. Sugimoto, M. Yamagata, M. Kikuta, M. Kono, M. Ishikawa, „A neat ionic liquid electrolyte based on FSI anion for electric double layer capacitor," *J. Power Sources,* 185 (2008) 1585 – 1588
[67] R. Kötz, M. Carlen, „Principles and applications of electrochemical capacitors," *Electrochim. Acta,* 45 (2000) 2483 – 2498
[68] N. Nanbu, T. Ebina , H. Uno, S. Ishizawa, Y. Sasaki, „Physical and electrochemical properties of quaternary ammonium bis(oxalato)borates and their application to electric double-layer capacitors," *Electrochim. Acta* 52 (2006) 1763 – 1770
[69] D. Weingarth , H. Noh , A. Foelske-Schmitz , A. Wokaun , R. Kötz , "A reliable determination method of stability limits for electrochemical double layer capacitors" *Electrochim. Acta,* 103 (2013) 119 – 124
[70] E. Frackowiak, Q. Abbas, F. Béguin, „Carbon/carbon supercapacitors," *J.Energy Chem.,* 22 (2013) 226 – 240
[71] V. Ruiz, R. Santamaria, M. Granda, C. Blanco, „Long-term cycling of carbon-based supercapacitors in aqueous media," *Electrochim. Acta,* 54 (2009) 4481 – 4486
[72] V. Khomenko, E. Raymundo-Piñero, F. Béguin, „A new type of high energy asymmetric capacitor with nanoporous carbon electrodes in aqueous electrolyte," *J. Power Sources,* 195 (2010) 4234 – 4241
[73] K. Fic, G. Lota, M. Meller, E. Frąckowiak, „Novel insight into neutral medium as electrolyte for high-voltage supercapacitors," *Energy Environ. Sci,* 5 (2012) 5842 – 5850

[74] Q. Gao, L. Demarconnay, E. Raymundo-Piñero, F. Béguin, „Exploring the large voltage range of carbon/carbon supercapacitors in aqueous lithium sulfate electrolyte," *Energy Environ. Sci.*, 5 (2012) 9611 – 9617
[75] P. Ratajczak, K. Jurewicz, P. Skowron, Q. Abbas, F. Béguin, „Effect of accelerated ageing on the performance of high voltage carbon/carbon electrochemical capacitors in salt aqueous electrolyte,", *Electrochim. Acta,* 130 (2014) 344 – 350
[76] Q. Abbas, P. Babuchowska, E. Frąckowiak, F. Béguin „High voltage AC/AC electrochemical capacitor operating at low temperature in salt aqueous electrolyte,", *J. Power Sources* IN PRESS doi:10.1016/j.jpowsour.2016.03.094
[77] D. Linden, T.B. Reddy, „Handbook of batteries," Third Edition, McGraw-Hill (2004)
[78] Z. Yang, J. Zhang, M.C.W. Kintner-Meyer, X. Lu, D. Choi, J.P. Lemmon, J. Liu, „Electrochemical Energy Storage for Green Grid," *Chem. Rev.* 111 (2011) 3577 – 3613
[79] F.F.C. Bazito, R.M. Torresi, „Cathodes for Lithium Ion Batteries: The Benefits of Using Nanostructured Materials," *J. Braz. Chem. Soc.* 17 (2006) 627 – 642
[80] K. Mizushima, P.C. Jones, P.J. Wiseman, J.B. Goodenough, „Li_XCoO_2 ($0<x<-1$): A new cathode material for batteries of high energy," *Mater. Res. Bull.* 15 (1980) 783 – 789
[81] J.B. Goodenough, K. Mizushima, T. Takada, „Solid-Solution Oxides for Storage-Battery Electrodes," *Jpn. J. Appl. Phys.* 19 (1980) 305 – 313
[82] B. Scrosati, J. Garche, „Lithium batteries: Status, prospects and future" *J. Power Sources* 195 (2010) 2419 – 2430
[83] M. Winter, J.O. Besenhard, M. Spahr, P. Novak, „Insertion Electrode Materials for Rechargeable Lithium Batteries," *Adv. Mater.* 10 (1998) 725 – 763
[84] P. Novák, K. Müller, S. V. Santhanam, O. Hass, „Electrochemically Active Polymers for Rechargeable Batteries," *Chem. Rev.* 97 (1997) 207–281
[85] P. Poizot, F. Dolhemb, „Clean energy new deal for a sustainable world: from non-CO_2 generating energy sources to greener electrochemical storage devices," *Energy Environ. Sci.*, 4 (2011) 2003 – 2019
[86] B. Peng, J. Chen, „Functional materials with high-efficiency energy storage and conversion for batteries and fuel cells," *Coordination Chemistry Reviews* 253 (2009) 2805 – 2813
[87] N. Douakha, M. Holzapfel, E. Chappel, G. Chouteau, L. Croguennec, A. Ott, B. Ouladdiaf, „Nuclear and Magnetic Structure of Layered $LiFe_{1-X}Co_XO2$ ($0\leq x\leq 1$) Determined by High-Resolution Neutron Diffraction," *J. Solid State Chem.* 163 (2002) 406 – 411
[88] H. Li, Z. Wang, L. Chen, X. Huang, „Research on Advanced Materials for Li-ion Batteries," *Adv. Mater* 21 (2009) 4593 – 4607
[89] G.G. Amatucci, J.M. Tarascon, L.C. Klein, „Cobalt dissolution in $LiCoO_2$-based non-aqueous rechargeable batteries," *Solid State Ionics* 83 (1996) 167 – 173
[90] J. Cho, C.S. Kim, S.I. Yoo, „Improvement of Structural Stability of $LiCoO_2$ Cathode during Electrochemical Cycling by Sol-Gel Coating of SnO_2," *Electrochem. Solid-State Lett.* 3 (2000) 362 – 365
[91] J. Cho, Y.J. Kim, B. Park, „Novel $LiCoO_2$ cathode material with Al_2O_3 coating for a Li ion cell," *Chem. Mater.* 12 (2000) 3788 – 3791
[92] H.J. Kweon, D.G. Park, „Surface Modification of $LiSr_{0.002}Ni_{0.9}Co_{0.1}O_2$ by Overcoating with a Magnesium Oxide," *Electrochem. Solid-State Lett.* 3 (2000) 128 – 130

[93] J. Cho, Y.J. Kim, T.J. Kim, B. Park, „Effect of Al_2O_3-Coated o-LiMnO2 Cathodes Prepared at Various Temperatures on the 55°C Cycling Behavior," *J. Electrochem. Soc.* 149 (2002) A127 – A132
[94] J.S. Kim, C.S. Johnson, J.T. Vaughey, S.A. Hackney, K.A. Walz, W.A. Zeltner, M.A. Anderson, M.M. Thackeray, „The Electrochemical Stability of Spinel Electrodes Coated with ZrO_2, Al_2O_3, and SiO_2 from Colloidal Suspensions," *J. Electrochem. Soc.* 151 (2004) A1755 – A1761
[95] E. Endo, T. Yasuda, A. Kita, K. Yamaura, K. Sekai, „A $LiCoO_2$ Cathode Modified by Plasma Chemical Vapor Deposition for Higher Voltage Performance," *J. Electrochem. Soc.* 147 (2000) 1291 – 1294
[96] G.G. Amatucci, A. Blyr, C. Sigala, P. Alfonse, J.M. Tarascon, „Surface treatments of $Li_{1+X}Mn_{2-X}O_4$ spinels for improved elevated temperature performance," *Solid State Ionics* 104 (1997) 13 – 25
[97] Y.K. Sun, J.M. Hun, S.T. Myung, S.W. Lee, K. Amine, „Significant improvement of high voltage cycling behavior AlF_3-coated $LiCoO_2$ cathode," *Electrochem. Commun.* 8 (2006) 821 – 826
[98] J.Y. Liu, N. Liu, Y. Bai, L.H. Shi, Z.X. Wang, L.Q. Chen, V. Hennige, A. Schuch, „Improving the Performances of $LiCoO_2$ Cathode Materials by Soaking Nano-Alumina in Commercial Electrolyte," *J. Electrochem. Soc.* 154 (2007) A55 – A63
[99] Y. Cho, Y.J. Kim, B. Park, „Novel $LiCoO_2$ Cathode Material with Al_2O_3 Coating for a Li Ion Cell," *Chem. Mater.* 12 (2003) 3788 – 3791
[100] R.A. Huggins, „Advanced Batteries: Materials Science Aspects,", Springer Science & Business Media, LLC (2009)
[101] D. Aurbach, K. Gamosky, B. Markovsky, G. Salitra, Y. Gofer, U. Heider, R. Oesten, M. Schmidt, „The Study of Surface Phenomena Related to Electrochemical Lithium Intercalation into Li_XMO_Y Host Materials (M = Ni, Mn)," *J. Electrochem. Soc.* 147 (2000) 1322 – 1331
[102] A. Rougier, P. Gravereau, C. Delmas, „Optimization of the Composition of the $Li_{1-Z}Ni_{1+Z}O_2$ Electrode Materials: Structural, Magnetic, and Electrochemical Studies," *J. Electrochem. Soc.* 143 (1996) 1168 – 1175
[103] B.V.R. Chowdari, G.V. Subbarao, S.Y. Chow, „The effects of sintering temperature and time on the structure and electrochemical performance of $LiNi_{0.8}Co_{0.2}O_2$ cathode materials derived from sol-gel method," *J. Solid State Electrochem.* 7 (2003) 456 – 462
[104] Y. Cho, G.B. Kim, H.S. Lim, C.S. Kim, S.Y. Yoo, „High-performance ZrO_2-coated $LiNiO_2$ cathode material," *Electrochem. Solid State Lett.* 4 (2001) A159 – A161
[105] I. Sadadone, C. Delmas, „$LiNi_{1-Y}Co_YO_2$ positive electrode materials: relationships between the structure, physical properties and electrochemical behaviour," *J. Mater. Chem.* 6 (1996) 193 – 199
[106] Z.Q. Yang, X. Sun, J. Mc Breen, „Structural changes and thermal stability: in situ X-ray diffraction studies of a new cathode material $LiMg_{0.125}Ti_{0.125}Ni_{0.75}O_2$," *Electrochem. Commun.* 2 (2000) 733 – 737
[107] K.K. Lee, K.B. Kim, „Electrochemical and Structural Characterization of $LiNi_{1-Y}Co_YO_2$ ($0 \leq Y \leq 0.2$) Positive Electrodes during Initial Cycling," *J. Electrochem. Soc.* 147 (2000) 1709 – 1717
[108] M.M. Thackeray, W.I.F. David, P.G. Bruce, J.B. Goodenough, „Lithium insertion into manganese spinels," *Mater. Res. Bull.* 18 (1983) 461 – 472

[109] M.M. Thackeray, P.J. Johnson, L.A. de Piciotto, P.G. Bruce, J.B. Goodenough, „Electrochemical extraction of lithium from $LiMn_2O_4$," *Mater. Res. Bull.* 19 (1984) 179 – 187
[110] S.T. Myung, S. Komaba, N. Kumagai, H. Yashiro, H.T. Chung, T.H. Cho, „ Nano-crystalline $LiNi_{0.5}Mn_{1.5}O_4$ synthesized by emulsion drying method," *Electrochim. Acta* 47 (2002) 2543 – 2549
[111] S.T. Myung, S. Komaba, N. Kumagai, „Enhanced Structural Stability and Cyclability of Al-Doped $LiMn_2O_4$ Spinel Synthesized by the Emulsion Drying Method," *J. Electrochem. Soc.* 148 (2001) A482 – A489
[112] B. Banov, Y. Todorov, A. Trifonova, A. Momchilov, V. Manev, „$LiMn_{2-X}Co_XO_4$ cathode with enhanced cycleability," *J. Power Sources* 68 (1997) 578 – 580
[113] M. Kaneko, S. Matsuno, T. Miki, M. Nakayama, H. Ikuta, Y. Uchimito, M. Wakihara, K. Kawamura, „Local Structural Studies of $LiCr_YMn_{2-Y}O_4$ Cathode Materials for Li-Ion Batteries," *J. Phys. Chem. B* 107 (2003) 1727 – 1733
[114] K. Amine, H. Tukamoto, H. Yasuda, Y. Fujita, „Preparation and electrochemical investigation of $LiMn_{2-X}Me_XO_4$ (Me: Ni, Fe, and x = 0.5, 1) cathode materials for secondary lithium batteries," *J. Power Sources* 68 (1997) 604 – 608
[115] J.H. Lee, J.K. Hong, D.H. Jang, Y.K. Sun, S.M. Oh, „Degradation mechanisms in doped spinels of $LiM_{0.05}Mn_{1.95}O_4$ (M=Li, B, Al, Co, and Ni) for Li secondary batteries," *J. Power Sources* 89 (2000) 7 – 14
[116] D. Guyomard, J.M. Tarascon, „New electrolyte compositions stable over the 0 to 5 V voltage range and compatible with the $Li_{1+X}Mn_2O_4$/carbon Li-ion cells," *Solid State Ionics* 69 (1994) 293 – 305
[117] D. Guyomard, J.M. Tarascon, *US Patent 5*, 192 (1993) 629
[118] A.K. Padhi, K.S. Nanjundaswamy, J.B. Goodenough, „Phospho-olivines as Positive-Electrode Materials for Rechargeable Lithium Batteries," *J. Electrochem. Soc.* 144 (1997) 1188 – 1194
[119] Z. Yang, J. Zhang, M.C.W. Kintner-Meyer, X. Lu, D. Choi, J. P. Lemmon, J. Liu, „Electrochemical Energy Storage for Green Grid," *Chem. Rev.* 111 (2011) 3577 – 3613
[120] S.Y. Chung, J.T. Bloking, Y.M. Chiang, „Electronically conductive phospho-olivines as lithium storage electrodes," *Nat. Mater.* 1 (2002) 123 – 128
[121] A. Goni, L. Lezama, A. Pujana, M.I. Arriortua, T. Rojo, „Clustering of Fe^{3+} in the $Li_{1-3X}Fe_XMgPO_4$ ($0<X<0.1$) solid solution," *Int. J. Inorg. Mater.* 3 (2001) 937 – 942
[122] N. Ravet, A. Abouimrane, M. Armand, „ From our readers: On the electronic conductivity of phospho-olivines as lithium storage electrodes," *Nat. Mater.* 2 (2003) 702
[123] Y. Hu, M.M. Doeff, R. Kostecki, R. Finones, „Electrochemical Performance of Sol-Gel Synthesized $LiFePO_4$ in Lithium Batteries," *J. Electrochem. Soc.* 151 (2004) A1279 – A1285
[124] A. Yamada, H. Koizumi, S.I. Nishimura, N. Sonoyama, R. Kanno, M. Yonemura, T. Nakamura, Y. Kobayashi, „Room-temperature miscibility gap in Li_XFePO_4," *Nat. Mater.* 5 (2006) 357 – 360
[125] P. Gibot, M. Casas-Cabanas, L. Laffont, S. Levasseur, P. Carlach, S. Hamelet, J.M. Tarascon, C. Masquelier, „Room-temperature single-phase Li insertion/extraction in nanoscale Li_XFePO_4," *Nat. Mater.* 7 (2008) 741 – 747

[126] Y.G. Wang, Y.R. Wang, E. Hosono, K.X. Wang, H. Zhou, „The Design of a $LiFePO_4$/Carbon Nanocomposite With a Core–Shell Structure and Its Synthesis by an In Situ Polymerization Restriction Method," *Angew. Chem. Int. Ed.* 47 (2008) 7461 – 7465
[127] P.P. Prosini, D. Zane, M. Pasquali, „Improved electrochemical performance of a $LiFePO_4$-based composite cathode," *Electrochim. Acta* 46 (2001) 3517 – 3523
[128] H. Chen, M. Armand, G. Demailly, F. Dolhem, P. Poizot, J.-M. Tarascon, „From Biomass to a Renewable $Li_XC_6O_6$ Organic Electrode for Sustainable Li-Ion Batteries," *ChemSusChem*, 1 (2008) 348 – 355
[129] H. Chen, M. Armand, M. Courty, M. Jiang, C. P. Grey, F. Dolhem, J.-M. Tarascon, P. Poizot, „Lithium Salt of Tetrahydroxybenzoquinone: Toward the Development of a Sustainable Li-Ion Battery," *J. Am. Chem. Soc*., 131 (2009) 8984 – 8988
[130] P. Poizot, F. Dolhem, „Clean energy new deal for a sustainable world: from non-CO_2 generating energy sources to greener electrochemical storage devices," *Energy Environ. Sci*., 4 (2011) 2003 – 2009
[131] Y. Morita, S. Nishida, T. Murata, M. Moriguchi, A. Ueda, M. Satoh, K. Arifuku, K. Sato, T. Takui, „Organic tailored batteries materials using stable open-shell molecules with degenerate frontier orbitals," *Nat. Mater*., 10 (2011) 947 – 951
[132] M. Yao, S.-I. Yamazaki, H. Senoh, T. Sakai, T. Kiyobayashi, „Crystalline polycyclic quinone derivatives as organic positive-electrode materials for use in rechargeable lithium batteries," *Mater. Sci. Eng*., 177 (2012) 483 – 487
[133] G. Milczarek, O. Inganas, „Renewable Cathode Materials from Biopolymer/Conjugated Polymer Interpenetrating Networks," *Science*, 335 (2012) 1468 – 1471
[134] Y. Liang, Z. Tao, J. Chen, „Organic Electrode Materials for Rechargeable Lithium Batteries," *Adv. Energy Mater*., 2 (2012) 742 – 769
[135] Y. Liang, Z. Tao, J. Chen, „Function-oriented design of conjugated carbonyl compound electrodes for high energy lithium batteries," *Chem. Sci*.,4 (2013) 1330 – 1337
[136] Y. Hanyu, Y. Ganbe and I. Honma, „Application of quinonic cathode compounds for quasi-solid lithium batteries," *J. Power Sources*, 221 (2013) 186 – 190
[137] T. Le Gall, H. R. Reiman, M. Grossel, J. R. Owen, „Poly(2,5-dihydroxy-1,4-benzoquinone-3,6-methylene): a new organic polymer as positive electrode material for rechargeable lithium batteries," *J. Power Sources* 119–121 (2003) 316 – 320
[138] X. Han, C. Chang, L. Yuan, T. Sun, J. Sun, „Aromatic Carbonyl Derivative Polymers as High-Performance Li-Ion Storage Materials," *Adv. Mater.*, 19 (2007) 1616 – 1621
[139] A.- L. Barrès, J. Geng, G. Bonnard, S. Renault, S. Gottis ,O. Mentré, C. Frayret, F. Dolhem, P. Poizot, „High-Potential Reversible Li Deintercalation in a Substituted Tetrahydroxy-p-benzoquinone Dilithium Salt: An Experimental and Theoretical Study," *Chem. Eur. J*. 2012, 18, 8800 – 8812
[140] W.A. Van Schalkwijk, B. Scrosati, Advances In Lithium-Ion Batteries, Kluwer Academic Publishers (2002)
[141] J.R. Dahn, T. Zheng, Y. Liu, J. S. Xue, „Mechanisms for Lithium Insertion in Carbonaceous Materials," *Science,* 270 (1995) 590 – 593
[142] Y.Liu, J. S. Xue, T. Zheng, J.R. Dahn, „Mechanism of Lithium Insertion in Hard Carbons Prepared by Pyrolysis of Epoxy Resins," *Carbon*, 34 (1996) 193 – 200
[143] H. Azuma, H. Imoto, S. Yamada, K. Sekai, „Advanced carbon anode materials for lithium ion cells,", *J. Power Sources,* 81 (1999) 1–7

[144] B. Guo, X. Wang, P. F. Fulvio, M. Chi, S.M. Mahurin, X.-G. Sun, S. Dai, „Soft-Templated Mesoporous Carbon-Carbon Nanotube Composites for High Performance Lithium-ion Batteries," *Adv. Mater.*, 23 (2011) 4661–4666
[145] E. Buiel, J.R Dahn, „Li-insertion in hard carbon anode materials for Li-ion batteries," *Electrochim. Acta* 45 (1999) 121–130
[146] M. Nagao, C. Pitteloud, T. Kamiyama, T. Otomo, K. Itoh, T. Fukunaga, K. Tatsumi, R. Kanno, „Structure Characterization and Lithation Mechanism of Nongraphitized Carbon for Lithium Secondary Batteries," *J. Electrochem. Soc.* 153 (2006) A914 – A916
[147] F. Béguin, F. Chevallier, C. Vix-Guterl, S. Saadallah, V. Bertagna, J. N. Rouzaud, E. Frackowiak, „Correlation of the irreversible lithium capacity with the active surface area of modified carbons," *Carbon* 43 (2005) 2160–2167
[148] T. Ohzuku, A. Ueda, N. Yamamoto, „Zero-Strain Insertion Material of $Li[Li_{1/3}Ti_{5/3}]O_4$ for Rechargeable Lithium Cells," *J. Electrochem. Soc.* 142 (1995)1431 – 1435
[149] E. Ferg, R.J. Gummow, A. Dekock, M.M. Thackeray, „Spinel Anodes for Lithium-Ion Batteries," *J. Electrochem. Soc.* 141 (1994) L147 – L150
[150] A.N. Jansen, A.J. Kahalan, K.D. Kepler, P.A. Nelson, K. Amine, D.W. Dees, D.R. Vissers, M.M. Thackeray, „Development of a high-power lithium-ion battery," *J. Power Sources* 81 (1999) 902 – 905
[151] G.-N. Zhu, H.-J. Liu, J.-H. Zhuang, C.-X. Wang, Y.-G. Wang, Y.-Y. Xia, „Carbon-coated nano-sized $Li_4Ti_5O_{12}$ nanoporous micro-sphere as anode material for high-rate lithium-ion batteries," *Energy Environ. Sci.* 4 (2011) 4016 – 4022
[152] C. Cheng, H. Liu, X. Xue, H. Cao, L. Shi, „Highly dispersed copper nanoparticle modified nano $Li_4Ti_5O_{12}$ with high rate performance for lithium ion battery," 120 (2014) 226–230
[153] G.B. Xu, W. Li, L.W. Yang, X. L. Wei, J. W. Ding, J.X. Zhong, P.K. Chu „Highly-crystalline ultrathin $Li_4Ti_5O_{12}$ nanosheets decorated with silver nanocrystals as a high-performance anode material for lithium ion batteries," 276 (2015) 247–254
[154] K. Naoi, S. Ishimoto, J.-I. Miyamotoad, W. Naoi, „ Second generation 'nanohybrid supercapacitor': Evolution of capacitive energy storage devices," *Energy Environ. Sci.* 5 (2012) 9363 – 9373
[155] K. Naoi, S. Ishimoto, Y. Isobe, S. Aoyagia, „High-rate nano-crystalline $Li_4Ti_5O_{12}$ attached on carbon nano-fibers for hybrid supercapacitors," *J. Power Sources* 195 (2010) 6250 – 6254
[156] P.G. Bruce, B. Scrosati, J.M. Tarascon, „Nanomaterials for Rechargeable Lithium Batteries," *Angew. Chem. Int. Ed.* 47 (2008) 2930 – 2946
[157] M. Winter, „The Solid Electrolyte Interphase The Most Important and the Least Understood Solid Electrolyte in Rechargeable Li Batteries," *Z. Phys. Chem.* 223 (2009) 1395 – 1406
[158] E. Peled, „The Electrochemical Behavior of Alkali and Alkaline Earth Metals in Nonaqueous Battery Systems – The Solid Electrolyte Interphase Model," *J. Electrochem. Soc.* 126 (1979) 2047 – 2051
[159] M. Arakawa, J. Yamaki, „The cathodic decomposition of propylene carbonate in lithium batteries," *J. Electroanal. Chem.* 219 (1987) 273 – 280
[160] M. Inaba, Z. Ogumi, „Up-to-date development of lithium-ion batteries in Japan," *IEEE Electr. Insul. M.* 17 (2001) 6 – 20

[161] P.B. Balbuena, Y. Wang, "Lithium Ion Batteries. Solid Electrolyte Interphase", *Imperial College Press* (2004)
[162] S.K. Jeong, M. Inaba, Y. Iriyama, T. Abe, Z. Ogumi, „Surface film formation on a graphite negative electrode in lithium-ion batteries: AFM study on the effects of co-solvents in ethylene carbonate-based solutions," *Electrochim. Acta* 47 (2002) 1975 – 1982
[163] M. Inaba, Y. Kawatate, A. Funabiki, S.K. JEong, T. Abe, Z. Ogumi, „STM study on graphite/electrolyte interface in lithium-ion batteries: solid electrolyte interface formation in trifluoropropylene carbonate solution," *Electrochim. Acta* 45 (1999) 99 – 105
[164] M. Winter, G.H. Wrodingg, J.O. Besenhard, W. Biberacher, P. Novak, „Dilatometric Investigations of Graphite Electrodes in Nonaqueous Lithium Battery Electrolytes," *J. Electrochem. Soc.* 147 (2000) 2427 – 2431
[165] Y. Ein-Eli, B. Markovsky, D. Aurbach, Y. Carmeli, H. YAmin, S. Luski, „The dependence of the performance of Li-C intercalation anodes for Li-ion secondary batteries on the electrolyte solution composition," *Electrochim. Acta* 39 (1994) 2559 – 2569
[166] A.N. Dey, „Lithium anode film and organic and inorganic electrolyte batteries," *Thin Solid Films* 43 (1977) 131 – 171
[167] D. Aurbach, M.L. Daroux, P.W. Faguy and E. Yeager, „Identification of Surface Films Formed on Lithium in Propylene Carbonate Solutions," *J. Electrochem. Soc.* 134 (1987) 1611 – 1620
[168] D. Aurbach, A. Zaban, A. Schecheter, Y. Ein-Eli, E. Zinigrad and B. Markovsky, „The Study of Electrolyte Solutions Based on Ethylene and Diethyl Carbonates for Rechargeable Li Batteries I . Li Metal Anodes," *J. Electrochem. Soc.* 142 (1995) 2873 – 2882
[169] D. Aurbach, „Review of selected electrode–solution interactions which determine the performance of Li and Li ion batteries," *J. Power Sources* 89 (2000) 206 – 218
[170] T. Yoshida, M. Takahashi, S. Morikawa, C. Ihara, H. Katsukawa, T. Shiratsuchi, J. Yamaki, „Degradation Mechanism and Life Prediction of Lithium-Ion Batteries," *J. Electrochem. Soc.* 153 (2006) A576 – A582
[171] K. Edström, M. Herstedt, D.P. Abraham, „A new look at the solid electrolyte interphase on graphite anodes in Li-ion batteries," *J. Power Sources* 153 (2006) 380 – 384
[172] D. Alliata, R. Kotz, P. Novak, H. Siegenthaler, „Electrochemical SPM investigation of the solid electrolyte interphase film formed on HOPG electrodes," *Electrochem. Commun.* 2 (2000) 436 – 440
[173] E. Peled, D. Golodnitsky, G. Ardel, „Advanced Model for Solid Electrolyte Interphase Electrodes in Liquid and Polymer Electrolytes," *J. Electrochem. Soc.* 144 (1997) L208 – L210
[174] A. Zaban, D. Aurbach, „Impedance spectroscopy of lithium and nickel electrodes in propylene carbonate solutions of different lithium salts A comparative study," *J. Power Sources* 54 (1995) 289 – 295
[175] A.M. Andersson, A. Henningson, H. Siegbahn, U. Jansson, K. Edström, „Electrochemically lithiated graphite characterised by photoelectron spectroscopy," *J. Power Sources* 119-121 (2003) 522 – 527
[176] A. Du Pasquier, F. Disma, T. Bowmer, A.S. Gozdz, G. Amatucci, J.M. Tarascon, „Differential Scanning Calorimetry Study of the Reactivity of Carbon Anodes in Plastic Li-Ion Batteries," *J. Electrochem. Soc.* 145 (1998) 472 – 477

[177] T. Zheng, A.S. Gozdz, G.G. Amatucci, „Reactivity of the Solid Electrolyte Interface on Carbon Electrodes at Elevated Temperatures," *J. Electrochem. Soc.* 146 (1999) 4014 – 4018
[178] H. Bryngelsson, M. Stjerndahl, T. Gustafsson, K. Edström, „How dynamic is the SEI?," *J. Power Sources* 174 (2007) 970 – 975
[179] C. Liebenow, M.W. Wagner, K. Lühder, P. Lobitz, J.O. Besenhard, „Electrochemical behaviour of coated lithium-carbon electrodes," *J. Power Sources* 54 (1995) 369 – 372
[180] W. Märkle, C. Y. Lu, and P. Novák, „Morphology of the Solid Electrolyte Interphase on Graphite in Dependency on the Formation Current," *J. Electrochemical Society* 158 (2011) A1478 – A1482
[181] S.S. Zhang, K. Xu, T.R. Jow, „EIS study on the formation of solid electrolyte interface in Li-ion battery," *Electrochim. Acta* 51 (2006) 1636–1640
[182] D. Aurbach, M.D. Levi, E. Levi, A. Schechter, „Failure and Stabilization Mechanisms of Graphite Electrodes," *J. Phys. Chem. B* 101 (1997) 2195 – 2206
[183] S.H. Kang, D.P. Abraham, A. Xiao, B.L. Lucht, „Investigating the solid electrolyte interphase using binder-free graphite electrodes," *J. Power Sources* 175 (2008) 526 – 532
[184] J.O. Besenhard, M. Winter, J. Yang, W. Biberacher, „Filming mechanism of lithium-carbon anodes in organic and inorganic electrolytes," *J. Power Sources* 54 (1995) 228 – 231
[185] Y. Ein-Eli, „A New Perspective on the Formation and Structure of the Solid Electrolyte Interface at the Graphite Anode of Li - Ion Cells," *Electrochem. Solid State Lett.* 2 (1999) 212 – 214
[186] M. Winter, J.O. Besenhard, M. Spahr, P. Nowak, „Insertion Electrode Materials for Rechargeable Lithium Batteries," *Adv. Mater.* 10 (1998) 725 – 763
[187] D. Aurbach, E. Zinigrad, Y. Cohen, H. Teller, „A short review of failure mechanisms of lithium metal and lithiated graphite anodes in liquid electrolyte solutions," *Solid State Ionics* 148 (2002) 405 – 416
[188] D. Aurbach, „Electrode–solution interactions in Li-ion batteries: a short summary and new insights," *J. Power Sources* 119 – 121 (2003) 497 – 503
[189] S. Mori, H. Asahina, H. Suzuki, A. Yonei, K. Yokoto, „Chemical properties of various organic electrolytes for lithium rechargeable batteries: 1. Characterization of passivating layer formed on graphite in alkyl carbonate solutions," *J. Power Sources* 68 (1997) 59 – 64
[190] D. Cericola, R. Kötz, „ Hybridization of rechargeable batteries and electrochemical capacitors: Principles and limits," *Electrochimica Acta* 72 (2012) 1 – 17
[191] G.G. Amatucci, „ Recent advances in lithium ion battery materials," *Electrochim. Acta* 45 (2000) 2461 – 2466
[192] G.G. Amatucci, F. Badaway, A.D. Pasquier, T. Zheng, „An Asymetirc Hybrid Nonaqueous Energy Storage Cell," *J. Electrochem. Soc.* 148 (2001) A930 – A939
[193] K. Naoi, Chapter 7 in Supercapacitors: Materials, Systems and Applications, F. Béguin, E. Frackowiak Eds., Wiley-VCH Verlag, Weinheim (2013)
[194] Y. Firouz, N. Omar, J.-M. Timmermans, P. Van den Bossche, J. Van Mierlo, „Lithium-ion capacitor – Characterization and development of new electrical model," *Energy* 83 (2015) 597 – 613
[195] Fuji Heavy Industry patents:
(a) N. Ando, S. Taguchi, Y. Hato, Organic electrolyte capacitor, EP1400996A1 (2002)

(b) S. Tasaki, N. Ando, M. Nagai, A. Shirakami, K. Matsui, Y. Hato, Lithium ion capacitor, WO 2006/112068 (2006)
(c) N. Ando, K. Kojima, S. Tasaki, H. Taguchi, T. Fujii, Y. Hato, C. Marumo, Organic electrolyte capacitor, US2007/0002524A1 (2007)
(d) H. Tanizaki, N. Ando, Y. Hato, Lithium-ion capacitor, EP1914764A1 (2007)
[196] T. Aida, K. Yamada, and M. Morita, „An Advanced Hybrid Electrochemical Capacitor That Uses a Wide Potential Range at the Positive Electrode," *Electrochem. Solid state Lett* 9 (2006) A534 – A536
[197] T. Aida, I. Murayama, K. Yamada, M. Morita, „Improvement in Cycle Performance of a High-Voltage Hybrid Electrochemical Capacitor," *Electrochem. Solid state Lett.* 10 (2007) A93 – A96
[198] JM Energy Company patents:
(a) Y. Naoshi, C. Takashi, O. Kazuyoshi, H. Kuniyasu, Lithium-ion capacitor, WO2012063545A1 (2012)
(b) T. Makoto, M. Chiaki, Lithium-ion capacitor, JP2009059732A (2009)
[199] A. Burke, presented in part at Advanced Automotive & Industrial Battery Conference, Mainz/ Germany, January, 2016
[200] http://www.jmenergy.co.jp/
[201] V. Khomenko, E. Raymundo-Piñero, F. Béguin, „High-energy density graphite/AC capacitor in organic electrolyte," *J. Power Sources* 177 (2008) 643 – 651
[202] C. Decaux, G. Lota, E. Raymundo-Piñero, E. Frackowiak, F.Béguin, „Electrochemical performance of a hybrid lithium-ion capacitor with a graphite anode preloaded from lithium bis(trifluoromethane)sulfonimide-based electrolyte," *Electrochimica Acta* 86 (2012) 282 – 286
[203] M.-S. Park, Y.-G. Lim, J.-H. Kim, Y.-J. Kim, J. Cho and J.-S. Kim, „A Novel Lithium-Doping Approach for an Advanced Lithium Ion Capacitor," *Adv. Energy Mater.* 1 (2011) 1002 – 1006
[204] M.-S. Park, Y.-G. Lim, J.-W. Park, J.-S. Kim, J.-W. Lee, J. H. Kim, S. X. Dou and Y.-J. Kim, „Li_2RuO_3 as an Additive for High-Energy Lithium-Ion Capacitors," *J. Phys. Chem. C*, 117 (2013) 11471 – 11478
[205] M.-S. Park, Y.-G. Lim, S. M. Hwang, J. H. Kim, J.-S. Kim, S. X. Dou, J. Cho and Y.-J. Kim, „Scalable Integration of Li_5FeO_4 towards Robust, High-Performance Lithium-Ion Hybrid Capacitors," *ChemSusChem* 7 (2014) 3138 – 3144
[206] Y.-G. Lim, D. Kim, J.-M. Lim, J.-S. Kim, J.-S. Yu, Y.-J. Kim, D. Byun, M. Cho, K. Cho, M.-S. Park, „Anti-fluorite Li_6CoO_4 as an alternative lithium source for lithium ion capacitors: an experimental and first principles study," *J. Mater. Chem. A*, 3 (2015) 12377 – 12385
[207] S. Kumagai , T. Ishikawa, N. Sawa, „Cycle performance of lithium-ion capacitors using graphite negative electrodes at different pre-lithiation levels," *Journal of Energy Storage* 2 (2015) 1 – 7
[208] E. Frąckowiak, S. Gautier, H. Gaucher, S. Bonnamy, F. Béguin, „Electrochemical storage of lithium multiwalled carbon nanotubes," *Carbon* 37 (1999) 61–69
[209] I. D. Ralstrick, C. Ho, R. A. Hugglns, „Lithium ion conduction in Li_5AlO_4, Li_5GaO_4 and Li_6ZnO_4," *Mat. Res. Bull*., 2 (1976) 953-958

[210] E. H. P. Cordfunke, R. R. Van der Laan, G. P. Wyers, „The heat capacities and derived thermophysical properties of Li_2ZrO_3 and Li_8ZrO_6 at temperatures from 0 to 1000 K," *J. Chem. Thermodynamics*, 24 (1992) 1251 – 1256
[211] https://materialsproject.org/
[212] E. Frackowiak, S. Gautier, H. Gaucher, S. Bonnamy, F. Béguin, „Electrochemical storage of lithium multiwalled carbon nanotubes," *Carbon* 37 (1999) 61–69
[213] S. Kirklin, M. K. Y. Chan, L. Trahey, M. M. Thackeray, C. Wolverton, „High-throughput screening of high-capacity electrodes for hybrid Li-ion–Li–O_2 cells,"*Phys. Chem. Chem. Phys.*, 16 (2014) 22073 – 22082
[214] L. R. Morss, E. H. Appelman, R. R. Gerz, D. Martin-Rovet, „Structural studies of Li_5ReO_6, Li_4NpO_5 and Li_5NpO_6 by neutron and X-ray powder diffraction," *J. Alloys and Comp.,* 203 (1994) 289 – 295
[215] W. H. Davenport, V. Kollonitsch, C. H. Kline, „ Advances in rhenium catalysts," *Ind. Eng. Chem.*, 60 (1968) 10 – 19
[216] P. Jezowski, K. Fic, O. Crosnier, T. Brousse, F. Béguin, „Use of sacrificial lithium nickel oxide for loading graphitic anode in Li-ion capacitors," *Electrochimica Acta* 206 (2016) 440 – 445
[217] D. Shanmukaraj, S. Grugeon, S. Laruelle, G. Douglade, J.-M. Tarascon, M. Armand, „Sacrificial salts: Compensating the initial charge irreversibility in lithium batteries," *Electrochem. Comm.* 12 (2010) 1344 – 1347
[218] W. Cai, H.Wang, D. Sun, Q. Zhang, X. Yao, M. Zhu, „Destabilization of $LiBH_4$ dehydrogenation through H^+–H^- interactions by cooperating with alkali metal hydroxides,", *RSC Adv.*, 4 (2014) 3082–3089
[219] A.-L. Barr, J. Geng, G. Bonnard, S. Renault, S. Gottis , O. Mentr, C. Frayret, F. Dolhem, P. Poizot „High-Potential Reversible Li Deintercalation in a Substituted Tetrahydroxyp-benzoquinone Dilithium Salt: An Experimental and Theoretical Study,", *Chem. Eur. J.*, 18 (2012) 8800 – 8812
[220] Y. Gogotsi, P. Simon, „Where Do Batteries End and Supercapacitors Béguin?,", *Science* 343 (2011) 1210 – 1211
[221] R. Kötz, M. Carlen, „Principles and applications of electrochemical capacitors," *Electrochim. Acta*, 45 (2000) 2483 – 2498
[222] C. M. Ghimbeu, C. Decaux, P. Brender, M. Dahbi, D. Lemordant, E. Raymundo-Piñero, M.Anouti, F. Béguin, C. Vix-Guterla, „Influence of Graphite Characteristics on the Electrochemical Performance in Alkylcarbonate LiTFSI Electrolyte for Li-Ion Capacitors and Li-Ion Batteries," *J. Electrochemical Society*, 160 (2013) A1907 – A1915
[223] P. Jezowski, K. Fic, O. Crosnier, T. Brousse, F. Béguin, „Use of sacrificial lithium nickel oxide for loading graphitic anode in Li-ion capacitors," *Electrochim. Acta* 206 (2016) 440 – 445
[224] J. B. Leriche, S. Hamelet, J. Shu, M. Morcrette, C. Masquelier, G. Ouvrard, M. Zerrouki, P. Soudan, S. Belin, E. Elkaïm, and F. Baudelet, „An Electrochemical Cell for *Operando* Study of Lithium Batteries Using Synchrotron Radiation," *J. Electrochem. Soc.* 157 (2010) A606 – A610

SCIENTIFIC ACHIEVEMENTS

1. PUBLICATIONS IN INTERNATIONAL JOURNALS:

1.1 Jeżowski P., Fic K., Crosnier O., Brousse T., Béguin F., *Electrochimica Acta,* Vol. 206 (2016) 440–445

IF: 4.721

1.2 Jeżowski P., Grzeszkowiak M., Nowicki M., Czajka R., Béguin F. *Journal of Power Sources,* Vol. 279, 555–562 (2015)

IF: 6.098

2. ORAL PRESENTATIONS:

2.1 **P. Jeżowski**, K.Fic, O. Crosnier, T. Brousse, E.Frąckowiak, F. Béguin
Hybridization as a clue to develop high energy supercapacitors
The Second Polish-French Forum of Science and Innovation
08.06.2016 Kraków, Poland

2.2 **P. Jezowski**, O. Crosnier, T. Brousse, F. Béguin
New materials for in-situ pre-lithiation of the graphite anode in lithium ion capacitor
66th Annual Meeting of the International Society of Electrochemistry
04 - 09.10.2015 Taipei, Taiwan
„Best oral presentation" by International Society of Electrochemistry

2.3 **P. Jeżowski**, K. Fic, O. Crosnier, T. Brousse, F. Béguin
Lithium metal oxides designed for pre-lithiation of graphite anode in lithium-ion capacitor
4th edition of the International Symposium on Enhanced Electrochemical Capacitors - ISEE'Cap15
08 – 12.06.2015 Montpellier, France

2.4 **P. Jeżowski**, K. Fic, O. Crosnier, T. Brousse F. Béguin
New pre-lithiation strategies of the graphite anode in lithium-ion capacitors
16th Topical Meeting of the International Society of Electrochemistry
22. - 26.03.2015 Angra dos Reis, Brasilia

2.5 **P. Jeżowski**, K. Fic, O. Crosnier, T. Brousse, F. Béguin
New pre-lithiation strategies of the graphite anode in lithium-ion capacitors
COST Action MP1004 Winter Seminar - Latest Developments in Electrochemical Capacitors
29 - 31.01.2015 Poznan, Poland

2.6 P. Ratajczak, **P. Jeżowski**, F. Béguin
Performance improvement of AC/AC capacitors in aqueous medium through modification of the current collector/active material interface
65th Annual Meeting of the International Society of Electrochemistry
31.08 - 05.09.2014 Lausanne, Switzerland

Lithium-ion capacitors based on in-situ pre-lithiation of the graphite electrode from a composite positive electrode

2.7 **P. Jeżowski**, K. Fic, O. Crosnier, T. Brousse, F. Béguin
Use of Sacrificial Oxide for Pre-lithiation of Graphitic Anode in Li-Ion Capacitors
COST Action MP1004 - Hybrid Energy Storage Devices and Systems for Mobile and Stationary Applications
08 - 10.12.2014 Tel Aviv, Israel

2.8 P. Ratajczak, **P. Jeżowski**, P. Skowron, K. Jurewicz, F. Béguin
Design and development of AC/AC supercapacitors in salt aqueous electrolyte
Winter seminar - Latest Developments in Electrochemical Capacitors
15 - 18.12.2013 Tartu, Estonia

2.9 F. Béguin, P. Ratajczak, P. Kleszyk, **P. Jeżowski**, Q. Abbas, P. Skowron, K. Fic, E. Frąckowiak
Strategies for enhancing the performance of carbon-based supercapacitors
VII International Scientific and Technical Conference – Carbon Materials & Polymer Composites
13 - 16.11.2012, Ustroń – Jaszowiec, Poland

2.10 P. Ratajczak, **P. Jeżowski**, K. Jurewicz, G. Lota, E. Frąckowiak, F. Béguin
Influence of supercapacitors operating conditions on their performance in aqueous electrolyte
COST Action MP1004 - Hybrid Energy Storage Devices and Systems for Mobile and Stationary Applications
01 - 03.10.2012 Kayseri, Turkey

3. POSTER PRESENTATIONS:

3.1 **P. Jeżowski,** O. Crosnier, T. Brousse and F. Béguin
Cathode materials designed for pre-doping of the graphite anode in lithium ion capacitor
6th International Conference on Carbon for Energy Storage/Conversion and Environment Protection CESEP' 2015
18 – 22.10.2015, Poznań, Poland

3.2 **P. Jeżowski** and F. Béguin
Activated carbon electrode expansion during EDL charging in various salt aqueous electrolytes
66th Annual Meeting of the International Society of Electrochemistry
04 - 09.10.2015, Taipei, Taiwan

3.3 **P. Jeżowski**, M. Grzeszkowiak, M. Nowicki, R. Czajka, F. Béguin
Chemical etching of stainless steel surface for performance enhancement of electrochemical capacitors in aqueous electrolyte
4th edition of the International Symposium on Enhanced Electrochemical Capacitors, ISEE'Cap15
08 – 12.06.2015, Montpellier, France
Poster was awarded

Lithium-ion capacitors based on in-situ pre-lithiation of the graphite electrode from a composite positive electrode

3.4 **P. Jeżowski**, T. Brousse, C. Ramirez-Castro, E. Frąckowiak, F. Béguin
Lithiated oxides as positive electrode additives for lithium ion capacitors
3rd International Symposium on Enhanced Electrochemical Capacitors - ISEECap2013
03 - 07.06.2013 Taormina, Italy

4. SHORT SCIENTIFIC MISSIONS:

Scientific stay at L'Institut des Matériaux Jean Rouxel de Nantes, France during which I developed the knowledge and skills about "Synthesis and characterization of novel materials applicable in lithium ion capacitors (LIC)"

Dates of stay:

01.06 – 10.07.2015

01.10 – 29.10.2014

30.09 – 01.11.2013

05.11 – 01.12.2012

5. PARTICIPATION IN SCIENTIFIC PROJECTS:

5.1 ECOLCAP

Project *Development of high performance and ECOLogically friendly superCAPacitors for energy management* realized in frame of the WELCOME program, funded by the Polish Foundation for Science (FNP) and European Union.

2014-2015; ***scientific-research assistant***

2012-2014; ***project realization assistant***

2011-2012; ***msc. stipend***

5.2 LIDER

Project *High power and high energy electrochemical capacitor* realized in frame of LIDER program, funded by National Center for Research and Develpoment (NCBiR)

2013-2015; ***scientific-research assistant***

5.3 POLONIUM

Polonium project 31438NH supported by The French embassy in Poland and the French "Ministère des affaires étrangères et du développement international" as well as Polish Ministry of Science and Higher Education in Poland are also greatly acknowledged for supporting this work.

2013-2015; ***researcher***

ABSTRACT

The lithium-ion capacitor (LIC) is a hybrid device which combines a redox battery-like negative electrode, with an electrical double-layer (EDL) positive one generally made from activated carbon, using a lithiated electrolyte, for example, $LiPF_6$ in EC:DMC. Owing to this construction, LICs can operate at a voltage up to 4.0 V, displaying much higher energy density (ca. 40 Wh/kg) than traditional electrical double-layer capacitors (EDLCs). However, before operating a LIC, it is necessary to pre-lithiate the graphite electrode in order to form at least the second stage graphite intercalation compound (GIC) LiC_{12}. In currently available industrial LICs, this is done by using an auxiliary metallic lithium electrode. This additional electrode complicates the construction, and in addition, the remaining lithium can be further the cause of safety hazards linked to short-circuits and thermal runaway. Therefore alternative strategies have been investigated.

The first one uses a concentrated solution of the lithium salt from which lithium ions are intercalated into graphite; consequently, the concentration and conductivity of the electrolyte decrease, which reduces the power of the LIC. The second strategy implements a composite positive electrode composed of activated carbon and a sacrificial lithium source, such as for example a lithium metal oxide; in this case, there is no depletion of electrolyte concentration. Unfortunately, for the oxides investigated until now, the lithium extraction potential is relatively high, which leads to unwanted oxidation of the electrolyte at the positive electrode during the graphite pre-lithiation step. In addition, the remaining dead mass in the positive electrode contributes to a reduction of the specific energy of the system. The objective of the PhD thesis dissertation is to optimize this elegant strategy by designing and implementing new sacrificial materials characterized by a very high irreversible capacity (to reduce their proportion in the positive electrode) and a low potential of lithium extraction (to prevent from electrolyte oxidation on the positive electrode). The manuscript is divided into 5 chapters.

The first chapter is a literature review presenting EDLCs, lithium-ion batteries (LIBs) and the state-of-the-art on LICs. For each system, the principles of energy storage, the most often used electrode materials, and the main advantages and disadvantages of the device are discussed. Special attention is focused on activated carbon (which is common for EDLCs and the positive electrode of LICs) and on graphite which is the negative electrode both in

LIC and LIB. The factors influencing the S.E.I. formation on graphite, as well as lithium intercalation are summarized. Also, the positive electrode materials of LIBs are carefully considered, as they have a comparable role in LIC with a sacrificial material, apart that lithium extraction is expected to be irreversible. Special attention is paid to the different methods for graphite pre-lithiation, and their pros and cons are discussed.

Chapter II aims at establishing the optimal electrochemical conditions for S.E.I. formation and graphite pre-lithiation, using $Li_{0.65}Ni_{1.35}O_2$ (LNiO) already know in the literature for its irreversible character of lithium extraction at relatively low potential ca. 4.2 V vs. Li/Li^+. Electrochemical techniques such as cyclic voltammetry (CV) and galvanostatic charge/discharge with potential limitation (GCPL), with metallic lithium electrode as counter and reference electrode, were used to carefully investigate the irreversibility of lithium extraction from LNiO. Due to the relatively low irreversible capacity of 120 mAh/g, the positive electrode of the LIC had to contain at least 55 wt.% of LNiO (the rest was 25 wt.% of activated carbon, 15 wt.% of conductive agent and 5 wt.% of binder) to forecast fabricating the second stage LiC_{12}. This could be realized by using a high current during the S.E.I. formation. The resulting LIC exhibited a stable performance during 1800 cycles in the operational voltage range from 2.2 to 3.8 V. However due to the relatively high amount of LNiO in the positive electrode, the specific energy of the LIC is only slightly higher than for an EDLC.

As the amount of extracted lithium ions from LNiO was relatively small, more lithium rich materials (with a high theoretical capacity of around 900 mAh/g) as lithiated aluminum (Li_5AlO_4), zinc (Li_6ZnO_4) and zirconium (Li_8ZrO_6) oxides were investigated in chapter III. However, for all of those materials, electrochemical studies by CV and GCPL have shown that a high potential around 4.6 V vs. Li/Li^+ is required to reach an irreversible capacity ca. 400 mAh/g. Since the low conductivity of these oxides appeared as one of the possible causes of this fair performance, we have decided to ball milling lithium zinc oxide (Li_6ZnO_4) together with conductive agents as carbon black (Super C65), multiwalled carbon nanotubes MWCNT-p (treated at high temperature to remove the remaining catalyst) or Super C65 + MWCNT-p mixture. With the later mixture, the irreversible capacity of Li_6ZnO_4 was enhanced to ca. 500 mAh/g at the potential of 4.5 V vs. Li/Li^+.

The assembled LIC cell in which the amount of Li_6ZnO_4 was reduced to 40 wt.% and the amount of activated carbon increased to 40 wt.% allowed to fabricate the LiC_6 graphite intercalation compound, without exceeding the potential of 4.5 V vs. Li/Li^+ for the positive electrode. However, the corresponding LIC cells demonstrated a very poor cycle life, even when restricting the voltage range dramatically. Despite the presence of MWCNT-p in the positive electrode, the resistance of the latter is still very high. We believe that it is probably related to the high band gap (around 5 eV) of this oxide.

Therefore, Chapter IV introduces lithium rhenium oxide (Li_5ReO_6) as potential low band gap (ca. 2.2 eV) material, with a relatively high theoretical capacity of 423 mAh/g. Contrary to the materials described in Chapter III, no additional processing by ball milling with conductive agents was necessary to reach practically an irreversible capacity of 410 mAh/g at 4.3 V vs. Li/Li^+. The AC/Li_5ReO_6 positive electrode was used to form the S.E.I., either at C/20 or C, and the intercalation into graphite was realized in both cases at C/20. Owing the thinner and more homogeneous layer when forming the S.E.I. at C, the LIC could perform easily 4000 charge/discharge cycles in the voltage range 2.2 – 4.1 V without any fade of capacitance. The specific energy of the LIC with AC/ Li_5ReO_6 positive electrode is almost four times higher than a conventional symmetric EDLC operating at 2.7 V with electrodes composed of the same activated carbon in an organic electrolyte.

The last chapter (Chapter V) proposes to use a renewable lithiated organic molecule, e.g., 3,4 – dihydroxybenzonitryl dilithium salt (Li_2DHBCN) as the internal source of lithium ions in the composite positive electrode. All lithium could be irreversibly extracted (irreversible capacity of 360 mAh/g) at very low potential ca. 3.2 V vs. Li/Li^+, which means that the electrolyte cannot be oxidized implementing this compound. A cell with 40 wt.%. of Li_2DHBCN in the positive AC electrode demonstrated 4 times higher energy density than an EDLC and an excellent cycle life (more than 5000 cycles) in the voltage range 2.1 – 4.0 V. For the first time, we demonstrated the possible realization of a pouch LIC with sacrificial Li_2DHBCN in the positive electrode. The performance of this device is analysed in the manuscript and research directions for its optimization are discussed.

STRESZCZENIE

Kondensator litowo-jonowy (ang. *lithium-ion capacitor* (LIC) to urządzenie hybrydowe do magazynowania energii elektrycznej. Pierwotna koncepcja kondensatora hybrydowego opiera się na wykorzystaniu procesu redoks zachodzącego na elektrodzie ujemnej (w tym przypadku interkalacja jonów litu w strukturę grafitu) oraz magazynowania ładunku w podwójnej warstwie elektrycznej (PWE) elektrody dodatniej, najczęściej wykonanej z węgla aktywowanego. Wykorzystanie procesu interkalacji jonów litu determinuje zastosowanie elektrolitu o charakterze organicznym, np. mieszaniny węglanów EC oraz DMC z solą litu ($LiPF_6$). Ze względu na swoją budowę, a dokładniej obszary potencjałów w których operują poszczególne elektrody, LIC może osiągać napięcie robocze około 4,0 V, przez co energia właściwa takiego układu jest o wiele większa (około 40 Wh/kg) niż dla tradycyjnych kondensatorów elektrochemicznych (ang. *electrical double-layer capacitor* (EDLC)). Jednak przed rozpoczęciem pracy cyklicznej, elektroda grafitowa musi zostać zainterkalowana w taki sposób, by osiągnąć co najmniej drugi stopień interkalacji i otrzymać interkalowany związek grafitu (ang. *graphite intercalation compound* (GIC)) o wzorze LiC_{12}. W większości LIC dostępnych na rynku proces interkalowania odbywa się przy użyciu dodatkowej (pomocniczej) elektrody wykonanej z metalicznego litu. Jednakże dodatkowa elektroda nie tylko komplikuje konstrukcję kondensatora - metaliczny lit pozostający w układzie po procesie interkalacji jest potencjalnie niebezpieczny, choćby z uwagi na możliwość zwarcia lub eksplozji układu. Z tego względu zaproponowano i zbadano inne możliwe metody interkalacji elektrody grafitowej, które nie wymagają zastosowania metalicznego litu jako źródła jonów dla procesu interkalacji.

Pierwsza z metod wykorzystuje stężone roztwory soli litu, z których jony litu są interkalowane w strukturę grafitu. Wadą tej metody jest malejące stężenie i przewodnictwo elektrolitu, co w konsekwencji prowadzi do spadku mocy LIC.

Druga z metod wykorzystuje dodatnią elektrodę kompozytową składającą się z węgla aktywowanego oraz związku będącego źródłem jonów litu, jak np. litowane tlenki metali przejściowych. Ponieważ źródłem jonów dla procesu interkalacji jest materiał elektrody, nie dochodzi do obniżenia stężenia elektrolitu. Niestety, litowane tlenki metali które zostały zbadane dotychczas, charakteryzują się wysokim potencjałem ekstrakcji atomów litu, co w konsekwencji prowadziło do utleniania elektrolitu na elektrodzie dodatniej w trakcie

procesu interkalacji. Co więcej, materiał tlenkowy pozostający w masie elektrody dodatniej po nieodwracalnej ekstrakcji atomów litu jako masa nieaktywna powoduje obniżenie energii właściwej układu.

Celem pracy doktorskiej było zoptymalizowanie metody interkalacji z wykorzystaniem elektrod kompozytowych poprzez zsyntetyzowanie nowych materiałów elektrodowych posiadających wysoką wartość tzw. pojemności nieodwracalnej (w celu obniżenia zawartości litowanego tlenku w kompozycie) oraz niską wartość potencjału przy której następuje ekstrakcja litu (tak by uniknąć utlenienia elektrolitu na elektrodzie dodatniej). Tekst rozprawy podzielony jest na 5 rozdziałów.

Rozdział pierwszy to przegląd literatury dotyczący EDLC, ogniw litowo-jonowych (ang. *lithium-ion batteries*, LIB) oraz nowoczesnych LIC. Każdy z systemów opisano pod kątem mechanizmów magazynowania energii, najczęściej używanych materiałów elektrodowych i elektrolitów oraz przedyskutowano ich główne wady i zalety. Uwagę skoncentrowano przede wszystkim na węglu aktywowanym (często stosowanym jako materiał elektrodowy zarówno w EDLC oraz jako elektroda dodatnia w LIC) a także graficie będącym elektrodą ujemną w LIC i LIB. Streszczono czynniki wpływające na proces interkalacji oraz formowanie warstwy pasywnej S.E.I. na powierzchni elektrody grafitowej. Opisano również materiały stosowane jako elektroda dodatnia w LIB z uwagi na ich podobną rolę w LIC, z zastrzeżeniem, że ekstrakcja w LIC powinna zachodzić w sposób nieodwracalny. Szczególną uwagę poświęcono różnym metodom interkalowania grafitu z uwzględnieniem ich zalet i wad.

Rozdział drugi dotyczy opracowania optymalnych warunków formowania S.E.I. oraz interkalowania grafitu przy pomocy $Li_{0.65}Ni_{1.35}O_2$ (LNiO), tj. materiału już znanego w literaturze ze względu na jego nieodwracalny charakter ekstrakcji litu przy stosunkowo niskim potencjale 4,2 V wzgl. Li/Li^+. Badania elektrochemiczne takie jak woltamperometria cykliczna (ang. *cyclic voltammetry* (CV)) i galwanostatyczne ładowanie/wyładowanie (ang. *galvanostatic charge/discharge with potential limitation* (GCPL)) z użyciem metalicznego litu jako elektrody przeciwnej i odniesienia zostały zastosowane do dokładnego określenia nieodwracalności procesu ekstrakcji z LNiO. Ze względu na stosunkowo niską pojemność nieodwracalną procesu ekstrakcji litu (120

mAh/g), elektroda dodatnia w LIC musiała zawierać co najmniej 55 $\%_{wag.}$ LNiO (a także 25 $\%_{wag.}$ węgla aktywowanego, 15 $\%_{wag.}$ czynnika przewodzącego i 5 $\%_{wag.}$ lepiszcza) aby osiągnąć drugi stopień interkalacji grafitu (LiC_{12}). Pożądane parametry uzyskano poprzez zastosowanie dużych gęstości prądu w trakcie formowania S.E.I. Uzyskany w ten sposób LIC charakteryzował się stabilną pracą cykliczną, tj. 1800 cykli przy napięciu pracy 2,2 do 3,8 V. Ze względu na stosunkowo dużą ilość LNiO w składzie elektrody dodatniej, gęstość energii takiego układu była niewiele większa od wartości uzyskiwanych dla EDLC.

Ze względu na stosunkowo małą ilość litu ekstrahowanego z LNiO, w następnym etapie badań wykorzystano materiały zawierające dużą liczbę atomów litu (z dużą pojemnością teoretyczną, tj. około 900 mAh/g) – litowane tlenki glinu (Li_5AlO_4), cynku (Li_6ZnO_4) czy cyrkonu (Li_8ZrO_6). Wyniki tych badań zostały opisane w rozdziale trzecim. Dla wszystkich wymienionych materiałów, badania elektrochemiczne jak CV i GCPL wykazały, że ekstrakcja atomów litu zachodzi przy wysokim potencjale około 4,6 V wzgl. Li/Li^+, a ich pojemność nieodwracalna bliska jest wartości 400 mAh/g. Niskie przewodnictwo tych tlenków określono, jako jedną z przyczyn takiego zachowania elektrochemicznego, dlatego też zadecydowano o mechanicznym zmieleniu tlenku cynkowo-litowego (Li_6ZnO_4) wraz z materiałami poprawiającymi przewodnictwo takimi jak sadza (Super C65), wielościenne nanorurki węglowe (ang. *multiwalled carbon nanotubes*, MWCNT). Należy zaznaczyć, że materiał został oczyszczony z pozostałości katalizatora w wysokiej temperaturze). Materiał zmielony z mieszaniną środków przewodzących charakteryzował się wartością pojemności nieodwracalnej około 500 mAh/g przy potencjale około 4,5 V wzgl. Li/Li+. W skonstruowanym LIC zawartość Li_6ZnO_4 została obniżona do 40 $\%_{wag.}$. Tym samym zwiększono zawartość węgla aktywowanego do 40 $\%_{wag.}$, co pozwoliło na osiągnięcie pierwszego stopnia interkalacji elektrody grafitowej (LiC_6). Potencjał elektrody dodatniej w tym układzie nie przekroczył wartości 4,5 V wzgl. Li/Li^+. Niestety, układ ten charakteryzował się umiarkowaną trwałością cykliczną, nawet przy ograniczonym napięciu pracy. Pomimo zastosowania MWCNT w składzie elektrody dodatniej, jej oporowy charakter był widoczny w czasie pracy cyklicznej układu. Prawdopodobnie jest to związane z dużą wartością przerwy energetycznej (blisko 5 eV) dla każdego z trzech litowanych tlenków.

W rozdziale czwartym przedstawiono tlenek litowo-renowy (Li_5ReO_6). Związek ten został wybrany ze względu na jego małą wartość przerwy energetycznej 2,2 eV oraz wysoką pojemność teoretyczną, wynoszącą 423 mAh/g. W przeciwieństwie do materiałów przedstawionych w rozdziale trzecim, żadna dodatkowa obróbka materiału jak mielenie w młynie kulowym nie była konieczna w celu osiągnięcia nieodwracalnej pojemności praktycznej na poziomie 410 mAh/g przy potencjale 4,3 V wzgl. Li/Li^+. Elektroda dodatnia AC/Li_5ReO_6 została wykorzystana do formacji S.E.I. przy użyciu prądu C/20 lub 1C. Interkalacja grafitu w obu przypadkach zachodziła w reżimie C/20. Ze względu na wytworzenie znacznie cieńszej i bardziej jednolitej warstwy w trakcie formowania S.E.I. w reżimie 1C, praca cykliczna LIC osiągała minimum 4000 cykli ładowania/wyładowania w zakresie napięcia 2,2 – 4,1 V. Zastosowanie elektrody dodatniej AC/Li_5ReO_6 pozwoliło na osiągnięcie niemal czterokrotnie wyższych wartości gęstości energii niż dla symetrycznych układów EDLC osiągających napięcia 2,7 V w elektrolicie organicznym z elektrodami wykonami z tego samego węgla aktywowanego.

Ostatni rozdział (piąty) opisuje możliwość zastosowania odnawialnych litowanych związków organicznych np.: sól litowa 3,4–dihydrooksybenzonoitrylu (ang. 3,4–dihydroxybenzonitryl dilithium salt (Li_2DHBCN)) jako wewnętrznego źródła jonów litu w elektrodzie kompozytowej. Wszystkie atomu litu mogą być nieodwracalnie wyekstrahowane (nieodwracalna pojemność 360 mAh/g) przy bardzo niskim potencjale 3,2 V wzgl. Li/Li+, co oznacza, że nie ma niebezpieczeństwa utlenienia elektrolitu przy zastosowaniu tego związku. Układ w którym dodatnia węglowa elektroda kompozytowa składała się z Li_2DHBCN 40 $\%_{wag.}$ przedstawia bardzo stabilną pracę cykliczną (więcej niż 5000 cykli) w zakresie napięcia pracy 2,1 – 4,0 V. Po raz pierwszy przedstawiono konstrukcję LIC z zastosowaniem Li_2DHBCN jako źródła atomów litu w elektrodzie dodatniej w postaci ogniwa kieszonkowego (ang. *pouch cell*). Wydajność tego układu została przenalizowana i skomentowana. Przedstawiono i omówiono także możliwe kierunki optymalizacji parametrów pracy tego układu.